

AN EXPERIMENTAL INVESTIGATION OF CONTROLS ON
CARBONATE DIAGENETIC TEXTURES AND MINERALOGY

by

JOYCE E. WATT

December, 1987

A THESIS SUBMITTED FOR THE DEGREE OF DOCTOR OF PHILOSOPHY
OF THE UNIVERSITY OF LONDON

Dept. of Geology
Imperial College
LONDON

This thesis is dedicated to all of my family
without whose support
the work would never have been done.

ABSTRACT

To simulate the early diagenesis of carbonates, experiments have been conducted at 183-200^o C and 5-11 MPa hydrostatic pressure for periods of up to six weeks using Recent oolitic and skeletal sands in the presence of natural seawater, SO₄²⁻-reduced seawater and freshwater. Textural, mineralogical and chemical changes occurred in the sediments with partial dissolution of aragonite and precipitation of calcite. The composition of the calcite varied but most contained less than 10 mole % MgCO₃, up to 1.6 mole % SrCO₃ and 2 mole % SO₄²⁻. Pore water chemistry also changed. The pore fluid mMg²⁺/mCa²⁺ was reduced to less than 1 during the first two weeks and the mSr²⁺/mCa²⁺ increased.

Granular-bladed and equant cement crystals were generated. Equant crystals have been found where nucleation rates were lowered due to higher pore fluid mMg²⁺/mCa²⁺ or lower rates of supply of Ca²⁺ and CO₃²⁻. There is no evidence that the morphology of cement crystals is controlled by the pore fluid mMg²⁺/mCa²⁺ as proposed by Folk (1974). Organic matter may act as a nucleation site for CaCO₃.

Secondary porosity was created in coated grain cortices. Where a high proportion of the cortex was composed of micritic and organic lamellae only those composed of aragonitic needles were removed. Partial infilling of these

by single calcite crystals occurred, retaining the outline of the lamellar structure. Wider pore spaces were created where there were fewer micrite/organic lamellae, these were partially infilled by irregular mosaics of sparry calcite.

Near the grain edges of peloids, a small amount of microporosity was created but most of the micrite which reacted underwent neomorphism. Most aragonite bivalve and gastropod fragments were unaltered although neomorphic alteration of some occurred. Aragonite dissolution was significantly retarded by dissolved SO_4^{2-} in the pore fluids.

ACKNOWLEDGEMENTS

This research programme was made possible by an award from the Natural Environment Research Council. Support in the field was given by the Department of Geology, University of Kuwait and the author gratefully acknowledges the help of all in the department, especially Prof. and Mrs. D. Almond, Dr. A Gunitalaka and Prof. D.J. Shearman.

Many thanks are also due to my supervisors, Dr. P.R. Bush and Dr. J. Ferguson for their many hours of help, especially during the writing up stage of the thesis. Also, Mr. B. Clark for designing and maintaining the experimental equipment used and for his help in operating it.

The staff of Applied Geochemistry are thanked for carrying out some of the analytical work. Also other members of the technical staff of Imperial College, especially Nick Morton for preparing the final plates.

My family have played an especially important role in this work. I would like to thank my parents for years of support, both personal and financial, also my sister, Wilma and brother-in-law, John. My husband, Ewan Neilson, is also especially thanked, for keeping me 'normal' throughout writing up, for his unending patience and for helping putting the thesis together.

LIST OF CONTENTS

	<u>PAGE NO.</u>
ABSTRACT	1
ACKNOWLEDGEMENTS	3
LIST OF CONTENTS	4
LIST OF FIGURES	12
LIST OF PLATES	15
LIST OF TABLES	17

PART I - INTRODUCTION AND EXPERIMENTAL METHOD

CHAPTER 1 - INTRODUCTION TO THE STUDY	19
1.1 EARLY EXPERIMENTAL WORK	19
1.2 LITERATURE REVIEW	23
1.2.1 Studies of Natural Diagenesis	23
1.2.2 Experimental Studies	28
1.3 AIM OF STUDY	36
1.4 THESIS PRESENTATION	36
CHAPTER 2 - EXPERIMENTAL METHODS, MATERIALS AND DESIGN AND ANALYTICAL PROCEDURE	38
2.1 INTRODUCTION	38
2.2 EXPERIMENTAL MATERIALS AND METHODS	38
2.2.1 Preparation of Materials	38
2.2.2 Experimental Procedure	41
2.3 EXPERIMENTAL DESIGN	49
2.3.1 Investigation of the Response of Seawater to the Experimental Conditions	50
2.3.2 Investigation of the Sediments	50
2.3.3 Physical Experimental Conditions	51

	<u>PAGE NO.</u>
2.3.4 Pilot Experiments	53
2.4 ANALYTICAL PROCEDURE	53
2.4.1 Petrography	54
2.4.2 Mineralogy	55
2.4.3 Geochemistry of Pore Fluids	60
2.4.4 Organic Matter	63
<u>PART II - RESULTS</u>	
CHAPTER 3 - INVESTIGATION OF THE EFFECT OF DIFFERENCES IN EXPERIMENTAL MATERIALS	64
3.1 INTRODUCTION	64
3.2 EVOLUTION OF SEAWATER DURING THE EXPERIMENTS	65
3.3 "AnalaR" ARAGONITE	71
3.4 GENERALISED PATTERN OF EXPERIMENTAL DIAGENESIS	71
3.5 SEDIMENTS COLLECTED FROM DIFFERENT LOCALITIES AND ENVIRONMENTS	73
3.5.1 Textural Variation	74
3.5.2 Pore Fluid and Cement Crystal Chemistry	96
3.6 INVESTIGATION OF SEDIMENTS	121
3.6.1 Sediment Composition	122
3.6.2 Grain Size	134
3.6.3 Organic Matter	146
CHAPTER 4 - INVESTIGATION OF THE EFFECT OF CHANGES IN THE EXPERIMENTAL CONDITIONS	158
4.1 INTRODUCTION	158
4.2 EFFECT OF TIME	158
4.2.1 Textural Development	159

	<u>PAGE NO.</u>
4.2.2 Cement Crystal Chemistry	168
4.2.3 Summary	174
4.3 EFFECT OF TEMPERATURE	176
4.4 EXPERIMENTS CONDUCTED AT DIFFERENT LEVELS OF HYDROSTATIC PRESSURE	178
4.4.1 Textural Development	178
4.4.2 Pore Fluid and Cement Crystal Chemistry	182
4.4.3 Summary	188
4.5 EFFECT OF NON-SAMPLING OF THE PORE FLUIDS	189
 CHAPTER 5 - EXPERIMENTS USING PORE FLUIDS OTHER THAN SEAWATER	 192
5.1 INTRODUCTION	192
5.2 SULPHATE REDUCED SEAWATER	193
5.2.1 Textural Development	193
5.2.2 Pore Fluid and Cement Crystal Chemistry	196
5.2.3 Summary	199
5.3 FRESHWATER	200
5.3.1 Textural Development	201
5.3.2 Pore Fluid and Cement Crystal Chemistry	202
5.3.3 Summary	205
 CHAPTER 6 - GEOCHEMISTRY OF THE REPLACEMENT FABRICS	 207
6.1 INTRODUCTION	207
6.2 SOLUTION CAVITY FILL CALCITE	208
6.3 NEOMORPHIC SPAR	211
6.4 EXAMPLE OF SHELL FRAGMENT REPLACED BY BOTH NEOMORPHIC SPAR AND SOLUTION CAVITY FILL CALCITE	220
6.5 SUMMARY	222

PART III - DISCUSSION AND CONCLUSIONS

CHAPTER 7 - FACTORS AFFECTING CEMENT CRYSTAL NUCLEATION AND MORPHOLOGY	224
7.1 INTRODUCTION	224
7.2 CONTROLS ON THE MORPHOLOGY OF THE CALCITE CEMENT CRYSTALS	225
7.2.1 Effect of Mg^{2+} Concentration of the Precipitating Fluids on Crystal Morphology	225
7.2.2 Effect of CO_3^{2-} Concentration of the Precipitating Fluids on Crystal Morphology	228
7.3 CHEMICAL CONTROLS ON THE NUCLEATION RATE OF CRYSTALS DURING EXPERIMENTS	232
7.3.1 Effect of Mg^{2+} in Controlling the Nucleation Rate	232
7.3.2 Effect of the Supply of Ions Through Aragonite Dissolution on the Nucleation Rate	234
7.3.3 Summary	236
7.4 PHYSICAL CONTROLS ON THE NUCLEATION RATE DURING THE EXPERIMENTS	238
7.4.1 Effect of Grain Substrate	238
7.4.2 Effect of Organic Matter	244
7.5 GEOLOGICAL SIGNIFICANCE	254
CHAPTER 8 - CONTROLS ON THE COMPOSITION OF THE CEMENTING PHASE	259
8.1 INTRODUCTION	259

	<u>PAGE NO.</u>
8.2 PHASES CONTAINING SIGNIFICANT AMOUNTS OF MgCO ₃	259
8.2.1 Cement containing more than 50 mole % MgCO ₃	260
8.2.2 Cement Containing 30-50 mole % MgCO ₃	261
8.2.3 Cement Containing less than 30 mole % MgCO ₃	262
8.2.4 Mineralogy of the Cementing Phase	262
8.3 CONTROLS ON THE MgCO ₃ , SrCO ₃ and SO ₄ ²⁻ CONTENTS OF THE CEMENT PHASE	268
8.3.1 Factors Affecting the MgCO ₃ Content	268
8.3.2 Effect of SO ₄ ²⁻ on Dolomite Precipitation	278
8.3.3 Summary	279
8.3.4 Factors Affecting the SrCO ₃ Content	280
8.3.5 Correlation Between MgCO ₃ and SrCO ₃	285
8.3.6 SO ₄ ²⁻ Content of Cement	286
8.4 GEOLOGICAL SIGNIFICANCE	288
 CHAPTER 9 - CREATION OF SECONDARY POROSITY AND FACTORS AFFECTING ARAGONITE DISSOLUTION	 290
9.1 INTRODUCTION	290
9.2 OCCURRENCES OF SECONDARY POROSITY	291
9.2.1 Coated Grains - Oomoldic Porosity	291
9.2.2 Micritic Carbonate and Peloids	295
9.2.3 Shell Fragments	296
9.2.4 Summary	297
9.3 FACTORS AFFECTING THE DISSOLUTION RATE OF ARAGONITE	298

	<u>PAGE NO.</u>
9.3.1 Effect of Grain Type	298
9.3.2 Effect of Grain Size	299
9.3.3 Effect of Pore Fluid Composition	301
9.4 GEOLOGICAL SIGNIFICANCE	307
CHAPTER 10 - CONTROLS ON THE DEVELOPMENT OF REPLACEMENT FABRICS - TEXTURE AND COMPOSITION	310
10.1 INTRODUCTION	310
10.2 SOLUTION CAVITY FILL CALCITE	311
10.2.1 Coated Grains	311
10.2.2 Shell Fragments	316
10.2.3 Composition of the Solution Cavity Fill Calcite	316
10.2.4 Age of the Solution Cavity Fill Calcite	317
10.3 NEOMORPHIC SPAR	319
10.3.1 Shell Fragments	319
10.3.2 Micritic Carbonate	324
10.3.3 Composition of the Neomorphic Spar	326
10.4 GEOLOGICAL SIGNIFICANCE	329
CHAPTER 11 - SUMMARY AND CONCLUSIONS	333
11.1 INTRODUCTION	333
11.2 FACTORS AFFECTING THE DISSOLUTION OF ARAGONITE	334
11.2.1 Effect of Grain Type	334
11.2.2 Effect of Grain Size	335
11.2.3 Effect of Dissolved SO_4^{2-} in the Pore Fluids	335
11.3 PRECIPITATION OF CEMENT	336
11.3.1 Effect of Organic Matter on Nucleation	336

	<u>PAGE NO.</u>
11.3.2 Controls on Cement Morphology	337
11.3.3 Cement Crystal Chemistry	339
11.4 REPLACEMENT OF GRAINS	341
11.4.1 Solution Cavity Fill Calcite	341
11.4.2 Neomorphism	342
11.5 CONCLUSIONS AND SUGGESTIONS FOR FURTHER WORK	343
REFERENCE LIST	346
APPENDIX I - PORE FLUID DATA	369
APPENDIX II - DESCRIPTION OF SEDIMENTS	383
APPENDIX III - LIST OF EXPERIMENTS AND EXPERIMENTAL CONDITIONS	393
APPENDIX IV - MICROPOROBE DATA	396
APPENDIX V - X-RAY DIFFRACTION DATA	414
APPENDIX VI - LIST OF TERMS USED AND FOLD-OUT OF ABBREVIATIONS	418

LIST OF FIGURES

<u>FIGURE NO.</u>		<u>PAGE NO.</u>
2.1	Schematic diagram of the experimental unit with one pressure cell, thermostatically controlled oven, screw pressure valve and water supply.	42
2.2	Schematic diagram of the experimental unit with four pressure cells, a thermostatically controlled heating chamber, constant pressure pump and water supply.	43
2.3	Simplified cross-section of pressure cell.	46
2.4	Schematic diagram showing the source of secondary and back-scattered electrons from a specimen surface.	56
2.5	Schematic diagram of the Inductively Coupled Plasma	60
2.6	Plot of original and rerun values for mMg^{2+}/mCa^{2+} and mSr^{2+}/mCa^{2+} pore fluid ratios for experiment 34/4.	61
3.1	Depletion in magnesium, calcium and sulphur levels (ppm) from that of seawater during experiment 34/1.	66
3.2	Evolution of seawater in terms of mMg^{2+}/mCa^{2+} and mSr^{2+}/mCa^{2+} pore fluid ratios.	69
3.3	Evolution of pore fluids from the composition of seawater during experiments using (A) sediment BSO (B) sediment ADEO, (C) sediment AKSO, (D) sediment AKDO and (E) Shark Bay Ooids.	98 and 101
3.4	Mole % $MgCO_3$ and $SrCO_3$ contained in cement crystals precipitated during experiments using sediment BSO.	104
3.5	Mole % SO_4^{2-} contained in cement crystals precipitated using sediment BSO.	106
3.6	Mole % $MgCO_3$ and $SrCO_3$ contained in cement crystals precipitated using sediment ADDO.	107
3.7	Mole % SO_4^{2-} contained in cement crystals precipitated using sediment ADDO.	108
3.8	Mole % $MgCO_3$ and $SrCO_3$ contained in cement crystals precipitated using sediment ADBO.	109
3.9	Mole % SO_4^{2-} contained in cement crystals precipitated using sediment ADBO.	110
3.10	Mole % $MgCO_3$ and $SrCO_3$ contained in cement crystals precipitated using sediment AKSO.	111

3.11	Mole % SO_4^{2-} contained in cement crystals precipitated using sediment AKSO.	112
3.12	Mole % MgCO_3 and SrCO_3 contained in cement crystals precipitated using sediment AKDO	113
3.13	Mole % SO_4^{2-} contained in cement crystals precipitated using sediment AKDO.	115
3.14	Mole % MgCO_3 and SrCO_3 contained in cement crystals precipitated using Shark Bay Ooids.	117
3.15	Mole % SO_4^{2-} contained in cement crystals precipitated using Shark Bay Ooids.	118
3.16	Evolution of pore fluids from the composition of seawater during experiments investigating the effect of the composition of the sediments. (30/1-4)	128
3.17	Depletion in Mg^{2+} (ppm) from the original level of seawater. Experiments 30/1-4.	129
3.18	Mole % MgCO_3 and SrCO_3 contained in the cement crystals precipitated in experiments 30/1-3.	131
3.19	Mole % SO_4^{2-} contained in the cement crystals precipitated during experiments 30/1-3.	132
3.20	Evolution of pore fluids from the composition of seawater during experiments investigating the effect of grain size. Experiments 28/1-4.	141
3.21	Depletion in Mg^{2+} (ppm) from the original composition of seawater during experiments 28/1-4.	142
3.22	Mole % MgCO_3 and SrCO_3 contained in cement crystals precipitated during experiments 28/1-4.	143
3.23	Mole % SO_4^{2-} contained in cement crystals precipitated during experiments 28/1-4.	144
2.24	Evolution of pore fluids from the composition of seawater during experiments investigating the effect of organic matter. Experiments 32/1-4.	152
3.25	Mole % MgCO_3 and SrCO_3 contained in cement crystals precipitated during experiments 32/1-4.	154
3.26	Mole % SO_4^{2-} contained in cement crystals precipitated during experiments 32/1-4.	155
4.1	Mole % MgCO_3 and SrCO_3 contained in cement crystals precipitated during aborted and short term experiments.	170
4.2	Mole % SO_4^{2-} contained in cement crystals precipitated during aborted and short term experiments,	171

4.3	Evolution of pore fluids from the composition of seawater during experiments 3686, 4086 and 4186, investigating the effect of hydrostatic pressure.	183
4.4	Mole % MgCO_3 and SrCO_3 contained in cement crystals precipitated during experiments 3686, 4086 and 4186.	186
4.5	Mole % SO_4^{2-} contained in the cement crystals precipitated during experiments 3686, 4086 and 4186.	187
4.6	Mole % MgCO_3 and SrCO_3 contained in the cement crystals precipitated during experiments 18/1 and 37/1.	190
4.7	Mole % SO_4^{2-} contained in the cement crystals precipitated during experiments 18/1 and 37/1.	190
5.1	Evolution of pore fluids in terms of $\text{mMg}^{2+}/\text{mCa}^{2+}$ and $\text{mSr}^{2+}/\text{mCa}^{2+}$ ratios of experiment 2985 from that of the SO_4^{2-} -reduced seawater.	197
5.2	Mole % MgCO_3 and SrCO_3 in cement crystals precipitated during experiments 2985 and 2185.	198
5.3	Mole % SO_4^{2-} contained in cement crystals precipitated during experiments 2985 and 2185.	198
5.4	Evolution of pore fluids in terms of $\text{mMg}^{2+}/\text{mCa}^{2+}$ and $\text{mSr}^{2+}/\text{mCa}^{2+}$ ratios from the composition of freshwater during experiment 3186.	203
5.5	Mole % MgCO_3 and SrCO_3 contained in the cement crystals precipitated during experiments 3186.	204
5.6	Mole % SO_4^{2-} contained in the cement crystals precipitated during experiment 3186.	205
6.1	Mole % MgCO_3 and SrCO_3 contained in unaltered non-skeletal aragonite and solution cavity fill calcite.	209
6.2	Mole % SO_4^{2-} contained in unaltered non-skeletal aragonite and solution cavity fill calcite.	210
6.3	Mole % MgCO_3 and SrCO_3 contained in the skeletal aragonite and neomorphic spar.	212
6.4	Mole % SO_4^{2-} contained in the skeletal aragonite and the neomorphic spar.	213
7.1	Geometric comparison of carboxyl group and carbonate anion.	248
7.2	Highly idealised illustration of the interaction of carboxyl groups with calcite surface.	248

8.1	X-ray diffraction (XRD) traces for the sediments collected at the end of experiments 3586 and 3886.	265
8.2	Plot of average $MgCO_3$ content of cement crystals precipitated during experiments using each sediment type against daily mean mMg^{2+}/mCa^{2+} pore fluid ratio.	271
8.3	Evolution of the pore fluids from the composition of seawater during experiments using (A) sediment BSO, (B) sediment ADBO, (C) sediment AKSO, (D) sediment AKDO and (E) Shark Bay Ooids. Baker and Kastner's (1981) stability fields for magnesite, dolomite and calcite have been superimposed.	273 and 274
8.4	Plot of average $SrCO_3$ content of cement crystals precipitated during experiments using each sediment type against daily mean mSr^{2+}/mCa^{2+} pore fluid ratio.	282
9.1	Data showing the aragonite-calcite equilibrium curve as a function of temperature and pressure.	291
10.1	Average mole % $MgCO_3$ and $SrCO_3$ contained in the cement precipitated during experiments using each sediment type, solution cavity fill calcite and neomorphic spar.	318

LIST OF PLATES

<u>PLATE NO.</u>		<u>PAGE NO.</u>
2.1	Experimental equipment and sediments on removal from pressure cells.	45
3.1	Anhydrite lath in sediment.	70
3.2	Experiments using Bahaman Subtidal Ooids.	75
3.3	Experiments using Abu Dahbi Dune Ooids.	78
3.4	Experiments using Abu Dhabi Beach Ooids.	82
3.5	Secondary electron 3-D images of cement crystals.	83
3.6	Experiments using Al-Khiran Subtidal Ooids.	87
3.7	Experiments using Al-Khiran Subtidal Ooids.	88
3.8	Experiments using Al-Khiran Dune Ooids.	90
3.9	Experiments using Shark Bay Ooids.	93
3.10	Investigation of sediment composition.	124
3.11	Investigation of sediment composition.	125
3.12	Investigation of sediment composition.	126
3.13	Investigation of sediment grain size.	136
3.14	Investigation of sediment grain size.	137
3.15	Investigation of the effect of organic matter.	148
3.16	Investigation of the effect of organic matter.	150
4.1	Experiment 2485, experimental time 7 days.	160
4.2	Experiment 2585, experimental time 15 days.	162
4.3	Experiment 2685, experimental time 21 days.	164
4.4	Experiment 18/4, experimental time 26 days.	167
4.5	Mg-rich cement crystals.	169
4.6	Investigation of hydrostatic pressure.	179
4.7	Investigation of hydrostatic pressure.	180
5.1	Experiment 2986, SO_4^{2-} -reduced seawater	194

<u>PLATE NO.</u>		<u>PAGE NO.</u>
5.2	Experiments 2985 and 3186, SO_4^{2-} -reduced seawater and freshwater.	201
6.1	Replacement fabrics.	215
6.2	Replacement fabrics.	219
7.1	Optically continuous overgrowths.	241
9.1	Original and secondary porosity fabrics.	293
10.1	Replacement fabrics.	315
10.2	Unaltered shell fragments.	323
AP1	Original sediments.	389
AP2	Original sediments.	390

LIST OF TABLES

<u>TABLE NO.</u>		<u>PAGE NO.</u>
2.1	Point counted data for starting sediments in volume %.	40
2.2	Mineralogical composition of sediments (wt.%)	41
2.3	Minimum temperature at which cementation occurred at a given pressure.	52
3.1	Conditions for experiments run using sediments BSO.	74
3.2	Conditions for experiments run using sediment ADDO.	77
3.3	Conditions for experiments run using sediment ADBO.	81
3.4	Conditions for experiments run using sediment AKSO.	85
3.5	Conditions for experiments run using sediment AKDO.	89
3.6	Conditions for experiments run using Shark Bay Ooids.	92
3.7	MgCO ₃ and SrCO ₃ (mole %) levels of individual cement crystals (BSO).	105
3.8	MgCO ₃ and SrCO ₃ (mole %) levels of one cement crystal precipitated using sediment AKDO.	116
3.9	Summary of results for experiments conducted using the range of sediments available.	119
3.10	Grain size and surface area of sediments used in the experiment 28/1-4.	135
4.1	Experiments studying the early stages of textural and mineralogical development.	159
4.2	Differences in concentrations (ppm) of Mg ²⁺ , Ca ²⁺ and S ⁶⁺ in the first pore fluid sample from that of seawater in experiments 3686, 4086 and 4186.	184
6.1	EPMA (mole %) for relic gastropod shown in Plate 6.1A.	214
6.2	EPMA (mole %) for peloid shown in Plate 6.1B.	217
6.3	EPMA (mole %) for the grain shown in Plate 6.1C.	218
6.4	EPMA (mole %) for relic gastropod shown in Plate 6.2A.	218

<u>TABLE NO.</u>		<u>PAGE NO.</u>
6.5	EPMA (mole %) for the grain shown in Plate 6.2B.	220
6.6	EPMA (mole %) for the grains shown in Plate 6.1D.	221
7.1	Increase in Sr^{2+} (ppm) from the level of seawater during experiments 32/1-4.	253
8.1	Range of MgCO_3 (mole %) contents of cement precipitated during experiments using each sediment type.	260
8.2	Details of the occurrences of intermediate Mg-rich phases.	261
8.3	SrCO_3 content (mole %) of cement crystals precipitated at different temperatures using the same starting sediments.	283
9.1	Levels of Sr^{2+} and Ca^{2+} (ppm) in the pore fluids of experiments 2185 and 2985.	303

PART I

INTRODUCTION AND EXPERIMENTAL METHODS

CHAPTER 1 - INTRODUCTION TO THE STUDY

1.1 EARLY EXPERIMENTAL WORK

Work on this research program was started by Drs J. Ferguson and P. Bush at Imperial College in 1980 and the results of the preliminary experiments were published in 1981 (Ferguson et. al., 1981). These early experiments were designed to test the feasibility of simulating early diagenesis using Recent ooids. Two experiments were carried out using the equipment described in Chapter 2. One was conducted over a period of 3 months, the other over 6 months. The samples were held at constant temperatures (120 and 140°C respectively) and pressures (4.8 and 9.6 MPa respectively). Seawater was used as the initial pore fluid and mineralogical changes were noted in the sediments of both experiments although no large scale transformation of aragonite to calcite occurred. The most significant changes were observed in the 6 month experiment. Chemical changes also occurred in the organic matter contained within the sediments, a Type II evolutionary pathway being seen in the kerogen.

Over the next three years, thirteen experiments were

conducted (Ferguson et al., 1984). Temperatures between 120 and 210 °C were employed with pressures ranging between 4.8 and 9.6 MPa. These experiments ran for periods varying from 28 days to 7 calendar months. Gaseous and liquid phases were collected and analysed at the end of the experiments. The lowest temperature at which cementation occurred was at 140 °C (after 7 months).

Two forms of calcite precipitation were observed:

- (i) rim calcite cements were formed where Bahaman Subtidal Ooids had been used while
- (ii) replacement calcite fabrics formed in dune ooids from the Arabian Gulf, containing 7 or 8 times less organic matter.

This lead Ferguson et al. (1984) to conclude that the organic matter contained within the ooids not only protected the original aragonitic structure in the way described by Shearman et al. (1970) but that it also physically prevented or slowed the dissolution-precipitation process.

They also reported on the hydrocarbon phases generated during the experiments. This was a continuation of the work by Ferguson and Ibe (1981 and 1982) on the association between oolitic sediments and light hydrocarbons. The gas phase generated was found to consist predominantly of carbon dioxide and nitrogen but a small proportion (<0.01%) was composed of light hydrocarbons (C1-C5). Consideration of

the light hydrocarbons generated showed that the unsaturated members dominated. Analysis of the organic solvent extract and acid insoluble organic residues was also carried out.

During this time Goodman (1986) was also conducting similar studies at Imperial College although her interest lay primarily in the association between light hydrocarbons and base metal ore deposits, hosted in carbonates. She used the same experimental apparatus and ran 6 experiments employing the optimum conditions defined by Ferguson et al. (1984) of 200 °C and 6.9 MPa and experimental times of up to 10 weeks. Experiments were undertaken where solutions of lead and zinc salts were introduced into the seawater to see whether these would be precipitated out and, if so, where and in what form.

Possible controls on the experimental diagenetic reactions were also discussed. Two types of material had been used, detrital skeletal material and ooids. Both of these were from the Bahamas. Only the sediments composed of ooids were found to cement. Three factors were investigated as being potential controls on cementation:

- (i) the nature of the carbonate sediment,
- (ii) the grain size and
- (iii) the effect of organic matter.

Goodman (1986) suggested that as ooids have a higher packing

density than skeletal fragments, a greater surface area for the adsorption of Mg^{2+} from the pore fluids would be available in sediments composed of ooids. Less Mg^{2+} would be available as an inhibitor to calcite precipitation in the pore fluids and therefore allow cementation of the sample to proceed. Although the inhibiting effect of Mg^{2+} on the precipitation of calcite is not disputed and indeed is well documented (e.g. Berner, 1975 and Berner et al., 1978), Goodman's experimental study was limited and factors such as the actual availability of ions for cementation were not investigated. Differences in cementation or non-cementation were explained in terms of the Mg^{2+} levels in the pore fluids. Another explanation put forward for the lack of cement in samples composed of skeletal fragments was that because fewer grain contacts occurred in samples composed of skeletal fragments, fewer reaction sites were therefore present, hence no cement was observed. This would be a valid point in the vadose regime where water is held at grain contacts and reactions mainly take place at these points (e.g. the meniscus cement described by Dunham, 1971) but in the pressure cells, where conditions were totally saturated this is not likely to be the case. The differences observed when the effect of grain size was studied were also attributed to the surface area available for the adsorption of Mg^{2+} . One experiment was carried out to test the effect that organic matter had on the reaction rate by placing a piece of blue-green algal mat in a

sandwich of ooids. No effect on the reactions was observed.

The position had therefore been reached where it was possible to simulate the fabrics produced by the early diagenesis of carbonates. Interest had mainly concentrated on whether cementation did or did not occur. Different forms of cement had not yet been generated. A more detailed study was therefore initiated and the results and conclusions of that study are presented in this thesis.

1.2 LITERATURE REVIEW

1.2.1 Studies of Natural Diagenesis

An exceptionally large body of literature exists on the early diagenesis of carbonates based on studies of Quaternary carbonates.

Significant contributions were made in the 1960's by Friedman (1964, 68) and Gavish and Friedman (1969) in developing the concepts of marine and freshwater diagenesis. The late 1960's and 1970's saw the development of the concept of the diagenetic environment with contributions coming from authors such as Matthews (1967, 68), Land (1970,

71, 73 a and b) and Folk (1974). In these early studies, it was recognised that there appeared to be a link between diagenetic texture and environment. Many detailed petrographic studies followed e.g. those by Schroeder (1972), Steinen (1974), Harrison (1975), Logan (1974), Harris (1978), Picha (1978) and Halley and Harris (1979). Good summaries can be found in Folk (1973, 74), Matthews (1974), Bathurst (1975, 80) and Longman (1980). Longman's paper is one which summarises many of the concepts of earlier papers. It is therefore briefly summarised here.

Longman (1980) reports four major diagenetic environments:

- (1) Marine Phreatic
- (2) Meteoric Vadose
- (3) Meteoric Phreatic and
- (4) Mixing Zone.

- (1) Marine Phreatic.

This is divided (ibid.) into two zones:

- (i) the stagnant zone - where there is little or no water circulation. The result of diagenesis in this zone is limited with little cementation occurring except in skeletal micropores and no leaching or alteration of aragonitic or high-Mg calcite grains.
- (ii) the active zone - where water is being continually pumped through the sediment by waves, tides or currents. The typical product of this diagenetic environment is a high

degree of cementation by random aragonite needles which form isopachous fringes, often with polygonal boundaries. Botryoidal aragonite, micritic Mg-calcite and isopachous fibrous Mg-calcite are also common cementing phases.

(2) Meteoric Vadose

In the vadose environment, fresh water is held at points of grain contact. Extensive solution occurs due to the undersaturated nature of the pore fluids with respect to CaCO_3 , aragonite is preferentially removed to high-Mg calcite producing moldic and vuggy porosity. The CaCO_3 , derived through the dissolution of aragonite and high-Mg calcite, is locally reprecipitated as a meniscus or pendant low-Mg calcite cement consisting of crystals with an equant morphology. The effects of diagenesis are limited and most of the intergranular, primary porosity is preserved, little secondary porosity being created.

(3) Meteoric Phreatic

Longman divides this environment into 3 zones:

(i) zone of solution - this occurs just below the meteoric vadose zone where the further development of moldic and/or vuggy porosity is found.

(ii) the active zone- some leaching continues but the zone is characterised by rapid cementation by equant low-Mg calcite crystals which coarsen in size towards the pore centres. Primary and secondary porosity is infilled by

equant calcite and the resultant rock shows little porosity. (iii) the stagnant zone - little further cementation or leaching occurs. The zone is characterised by the continued stabilisation of high-Mg calcite and by the neomorphism of aragonite to calcite with some preservation of original textures.

(4) Mixing Zone

This marks the boundary between the marine and freshwater environments with the pore fluid being a mixture of both i.e. brackish. Diagenesis in this zone is poorly understood mainly because examples are rare due to the narrowness of the zone, migration of the zone during rainfall or sea-level changes and the relatively stagnant nature of the water.

This zone however may be of great importance in the diagenetic processes of dolomitisation. The "Dorag" model of Badiozamani (1973) is a well known mixing-zone dolomitisation model. It is based on the assumption that the replacement of calcite by dolomite will proceed preferentially in waters undersaturated with respect to calcite but supersaturated with respect to dolomite. Badiozamani (1973) showed that although this applies to neither seawater nor freshwater, it does to mixtures of the two. Hardie (1987, p.169) however points out that Badiozamani's (ibid.) model is based on the solubility of ordered dolomites and that many Holocene dolomites are more

soluble, less ordered and Ca-rich. Other examples of Quaternary dolomites which are interpreted as being generated in the mixing zone are Land (1973 a, b and Ward and Halley, 1985).

As a result of these studies, the products of diagenesis in Quaternary limestones are well understood. Process models based on recent systems are now frequently applied to ancient sequences in order to unravel their diagenetic history (Wilkinson et. al., 1984). Over the last 10-15 years however, many workers (e.g. Folk, 1974; Sandberg, 1975, 83; Mackenzie and Pigott, 1981; Wilkinson et. al., 1982, 84) have suggested that diagenetic models based purely on Quaternary sequences may be inadequate. This is based on evidence which suggests that through geological time primary precipitation of CaCO_3 from seawater may have oscillated between precipitation of aragonite and calcite (e.g. Sandberg, 1975, Tucker, 1984). This has been attributed to changes in the $p\text{CO}_2$ of seawater (Mackenzie and Pigott, 1981; Sandberg, 1983 and Tucker, 1984).

Also, although the products of early diagenesis appear to fit conveniently into diagenetic environments, significant deviations from these patterns exist, as pointed out by Given and Wilkinson (1985). For example, equant high-Mg calcite cements have been found in the marine environment in different localities such as Belize (James and Ginsburg,

1979) and Eniwetok atoll (Warme and Schneiderman, 1983). Similarly, in the freshwater environment, whisker low-Mg calcite cements have been found (e.g. Longman, 1980).

Most diagenetic studies conducted in the 1980's have tended to look at the processes of diagenesis in carbonates of all ages. They have concentrated on particular aspects of diagenesis such as cementation (e.g. Schneiderman and Harris, 1985; Given and Wilkinson, 1985 and Meyers, 1987) and the factors controlling the early creation of porosity (e.g. Evans and Ginsburg, 1987). Processes of replacement and the chemical stabilisation of grains have also been studied (e.g. Sandberg and Hudson, 1983; Bruni and Wenk, 1985; Martin et. al., 1985 and Al-Assam and Veizer, 1986). The conclusions of many of these papers are considered in Chapters 7-10 of this thesis. There has also been an increasing number of experimental studies into the various aspects of carbonate diagenesis.

1.2.2 Experimental Studies

(1) Cementation

One of the earliest experimental studies, is that by Robertson et al. (1962). A constant load was applied to carbonate samples which were held in porous cylinders. Pressures of 30 to 500 psi (0.2 - 3.4 MPa) and temperatures

of 30 to 450 °C were employed. The experiments lasted for 1 hour to 4 days. The sediments which were used were peletal limemuds and muddy peletal sands of clay and silt sized fraction. Robertson et al. (ibid.) found that at higher temperatures, cementation was initiated and that the aragonitic sediments were partially converted to calcite. This was an important step in the study of the experimental simulation of carbonate diagenesis. Unfortunately no further results were published although the authors realised the potential of the experiments in the study carbonate diagenesis.

Ten years later, Thorstenson et al. (1972) published the results of a study which simulated vadose and phreatic cementation of skeletal sands. The experiments involved solution and precipitation as a function of variable CO₂ pressure, employing the use of CO₂-charged distilled water to leach a sample of carbonate sand. What they produced was a well cemented calcarenite with textures similar to those found in nature. A continuation of the work by Thorstenson et al. can be found in Badiozamani et al. (1977) where the results of experiments, also designed to simulate the cementation of carbonates are published. Various conditions of temperature, solution composition and physical environment of cementation resulted in the formation of cements similar to those found in nature. They concluded that they could distinguish between cements formed:

- (i) in NaCl solutions,
- (ii) fresh water,
- (iii) seawater,
- (iv) at various temperature and
- (v) in the phreatic and vadose environment.

To produce an adequate amount of cement for analysis, however, Badiozamani et al. (1977) found that the distilled water, synthetic seawater and NaCl solutions had to be initially equilibrated with one atmosphere of CO_2 , drained through a column of carbonate sand to achieve saturation with respect to CaCO_3 and then flushed through a second column of carbonate sand in which precipitation of calcite took place. The use of synthetic solutions, increased concentration of CO_2 and increased saturation of CaCO_3 all done outside the experimental charge, would all add uncertainties when studying the processes of diagenesis.

The effect of Mg^{2+} on the precipitation of aragonite and calcite was studied experimentally by Berner (1975) and Berner et al. (1978). Dissolved Mg^{2+} in seawater was found to have no effect on the seeded precipitation of aragonite but was found to severely retard the seeded precipitation of calcite. This demonstrated one of the controls that pore fluid composition can have on cementation.

Further controls on the composition of carbonate cements have also been recently investigated by Burton and Walter

(1987). Laboratory experiments were carried out (*ibid.*) to investigate the relative growth rates of calcite, high-Mg calcite and aragonite in seawater as functions of temperature (5, 25 and 37 °C) and of the carbonate ion concentration (2.5 to 15 times supersaturated with respect to calcite). Their study showed that the well documented shift towards the precipitation of lower mole % Mg calcite and the decrease in the abundance of aragonite cements with increasing oceanic depth and latitude could be attributed largely to lower temperatures and not the CO_3^{2-} concentration as suggested by Given and Wilkinson (1985).

Another area of investigation regarding carbonate cements has been that into the distribution coefficients for Sr and Mg in calcite and aragonite. If the factors which determine the distribution coefficient of each could be determined e.g. the pore fluid composition or the temperature of formation, then a powerful tool would be available for unravelling the diagenetic history of rocks. The results of experimental studies (e.g. Holland et al., 1964; Kinsman and Holland, 1969, Katz et al., 1972; Thorstenson and Plummer, 1977; Lorens, 1981; Baker et al., 1982 and Lahann and Siebert, 1982). However, the results of experimental studies have been conflicting and they are discussed in detail in Chapter 8.

(2) Formation of Secondary Porosity and Alteration of Biogenic Grains

Donath et. al. (1980) simulated the creation of secondary porosity during burial diagenesis by imposing conditions equivalent of about 10,000 ft. (axial pressure of 10,150 psi (70 MPa), lateral confining pressure of 8,700 psi (60 MPa) and a pore fluid pressure of 5,800 psi (40 MPa)). Samples of Mississippian oolitic limestone (low-Mg calcite) were tested using the pressure conditions outlined above and CO₂-charged water was passed through the sediment. They found that oomoldic porosity could be generated in this way and that the secondary porosity that was generated was fabric selective.

Experimental studies into the relative stability of biogenic grains have been conducted by Walter and Morse (Walter, 1985; Walter and Morse, 1985). The paper by Walter (1985) summarises the results of an experimental investigation into the dissolution rates of various biogenic carbonates and evaluates the roles that mineralogy, grain microstructure and solution saturation state play in determining the relative stability of aragonite and magnesian calcite during the dissolution phase of diagenesis. The dissolution experiments were performed in seawater and meteoric type solutions using crushed samples of different skeletal grain types composed of calcite, aragonite and magnesian calcite

at common grain sizes (37-125 microns). The kinetics of these dissolution experiments were reported by Walter and Morse (1985).

Land (1967) was the first to experimentally study the stabilisation of skeletal grains. The reactions, using aragonitic and high-Mg calcite shell fragments, were conducted in hydrothermal bombs (5 ml capacity) at 285 °C using distilled water. Aragonitic inversion was found to produce coarse grained equigranular mosaics while high-Mg calcites underwent incongruent dissolution to produce calcite plus a solution enriched in Mg^{2+} .

Turner et al. (1986) investigated the mechanism of alteration of high-Mg calcite to low-Mg calcite by conducting dissolution runs at 35 and 70 °C with distilled water saturated with 3 and 100% CO_2 . Changes in the biogenic high-Mg calcites were monitored by calculating mMg^{2+}/mCa^{2+} ratios in the solid and by studying the isotopic shifts. Differences in the microstructure of the grains appeared to control the changes in chemical and isotopic composition.

The importance of using natural material in experiments studying diagenetic reactions has been emphasised by the recent work of Bishoff et al. (1987). In this experimental study, the relative stabilities of synthetic and biogenic

high-Mg calcite in aqueous solution were investigated. Biogenic samples were found to be less stable than synthetic phases of similar Mg concentrations. This difference in stability was attributed to a greater variation in chemical and physical heterogeneities in biogenic samples. Bishoff et al. (ibid., p.1413) concluded that "only the results of synthetic dissolution experiments should be used to model the thermodynamic behaviour of the magnesian calcite solid-solution. The results for synthetic phases however, may not be appropriate to use for interpreting diagenetic reaction pathways for magnesium calcites in modern sediments." This stresses the importance of using natural materials in experimental diagenetic studies.

(4) Dolomitisation

Land (1967) also experimentally studied the process of dolomitisation. This was done by reacting weighed amounts of high-Mg calcites in stainless steel bombs with solutions of known Ca^{2+} and Mg^{2+} concentration near 300°C . He found that dolomitisation was speeded by:

- (i) increased instability of the reactant,
- (ii) increased Ca and Mg concentration in the solution,
- (iii) increased $m\text{Mg}^{2+}/m\text{Ca}^{2+}$ ratio of the solution,
- (iv) increased solid/solution ratio and
- (v) increased temperature.

Another study on dolomitisation is that by Baker and Kastner (1981). The dolomitisation of aragonite and calcite was studied by conducting hydrothermal reactions at 200 °C using seawater. Baker and Kastner (ibid.) found that the dolomitisation of CaCO_3 was not controlled primarily by the $\text{mMg}^{2+}/\text{mCa}^{2+}$ ratio of the precipitating fluids but by the dissolved concentration of SO_4^{2-} . They found that SO_4^{2-} severely retarded the precipitation of dolomite.

A comprehensive review of current views on the controls on dolomite precipitation can be found in Hardie (1987).

(5) Compaction

Interest has also been shown in compaction studies because of the link between compaction and the reduction of primary porosity. Examples can be found in Fruth et al. (1966), Bhattacharyya and Friedman (1979, 84) and Shinn and Robbin (1983). Textural features similar to those found in nature such as grain interpenetration, crushing and faulting were noted. Bhattacharyya and Friedman (1979) showed that where a high proportion of mud was contained in the sediment, the effect of compaction was greatly reduced.

1.3 AIM OF STUDY

The experiments conducted during this study used natural, largely unmodified sediments and fluids. The need for increasing the $p\text{CO}_2$ as in the studies by Thorstenson et al., (1972) was unnecessary because of the inherent instability of aragonite under the conditions employed (see section 9.1). The slightly lower pH of the seawater used (see section 2.2.1 (1)) also would have helped initiate the reactions. Diagenesis could therefore proceed through a dissolution-precipitation mechanism which produced fabrics identical to many of those seen in nature. The aim of the study was therefore to investigate the factors which controlled the generation of these fabrics during the experiments and to see if any parallels could be drawn with those which operate in the natural environments, i.e. to investigate the processes of diagenesis.

1.4 THESIS PRESENTATION

The thesis is presented in three parts. The first, of which this chapter is a part, comprises the introduction to the study and descriptions of the materials and methods which were employed. The results of the study are presented in the second part. However, much of the raw data can be found in the Appendices which are at the back of this volume. The third part of the thesis contains discussions on

cementation (morphology and composition of the crystals), aragonite dissolution and the creation of secondary porosity and the processes of replacement. In each case, the geological significance of the experimental results is considered. The conclusions of the study are presented in the final chapter.

CHAPTER 2 - EXPERIMENTAL METHODS, MATERIALS AND DESIGN AND ANALYTICAL PROCEDURE

2.1 INTRODUCTION

This chapter gives details of the methods and the objectives of the experiments. The first section describes the actual experimental methods. The second section discusses the experimental design while the last gives details of the analytical procedure and techniques that have been carried out and used in the collection of the data presented in this thesis.

2.2 EXPERIMENTAL MATERIALS AND METHODS

2.2.1 Preparation of Materials

(1) Liquids

Most of the experiments were carried out using seawater and a quantity was collected for this purpose from the English Channel in an opaque polythene container. On collection, following the methods previously established by Ferguson et al. (1984), the seawater was slightly acidified (20 mls 10% HCl per gallon) to kill off and prevent the further growth

of bacteria and other organisms. This would account for the slightly lower pH value of 7.1 (see Appendix I) when compared to average values of 7.8 - 8.2 (e.g. Drever, 1982). Prior to storage, the water was filtered in the laboratory using membrane filters (pore size 0.45 μm) to remove most of the suspended material.

Pilot experiments using SO_4^{2-} -reduced seawater and freshwater were also conducted. The SO_4^{2-} was removed from the seawater by adding a calculated amount of barium chloride. This precipitated the sulphate as barium sulphate and left an equivalent amount of chloride ions in solution. The freshwater (rainwater) used was collected in the north of Scotland. This again was filtered prior to storage but was not acidified. Both solutions had a lower pH than the seawater.

Elemental analyses and pH values of all liquids used can be found in Appendix I.

(2) Solids

Material for the experimental work was obtained from deposits of Recent sediments from four areas:

- (i) the Bahamas,
- (ii) Abu Dhabi,
- (iii) Kuwait and

	BSO	ADDO	ADBO
Coated grains	64.5	69.2	79.8
Peloids	35.5	30.8	16.8
Shell fragments	tr	tr	3.1
Quartz grains	0.0	0.0	tr
Feldspar	0.0	0.0	tr
Dolomite	0.0	0.0	0.0

	AKSO	AKDO	SBSO	SBDO
	60.9	60.0	57.6	70.1
	28.8	36.8	31.2	20.7
	8.2	2.4	9.2	6.0
	1.2	tr	2.7	2.3
	tr	tr	0.0	0.0
	0.0	0.0	0.0	tr

Table 2.1 - Point Counted Data for Starting Sediments in volume %. Less than 1 volume % denoted by 'tr'. BSO - Bahaman Subtidal Ooids, ADDO - Abu Dhabi Dune Ooids, ADBO - Abu Dhabi Beach Ooids, AKSO - Kuwait Subtidal Ooids, AKDO - Kuwait Dune Ooids, SBSO - Shark Bay Subtidal Ooids, SBDO - Shark Bay Dune Ooids.

(iv) Shark Bay, Western Australia.

These sediments are predominantly oolitic but contain varying proportions of skeletal carbonates and reworked grains from older formations (quartz, feldspar and dolomite) as shown in Table 2.1. Samples of purely skeletal carbonates were also collected from Kuwait. Mineralogical data are also given in Table 2.2. Detailed descriptions of these sediments can be found in Appendix II.

	ARAG	LMC	HMC	QTZ	FSP
BSO	96.4	1.6	2.0		
ADDO	97.6	0.6	1.8		
ADBO	80.0	9.0	5.0	5.0	1
AKSO	86.0	4.0	3.0	7.0	
AKDO	87.0	5.0	2.0	6.0	
SBSO	76.0	5.0	9.0	10.0	
SBDO	71.0	7.0	12.0	10.0	

Table 2.2 - Mineralogical composition of sediments from X-ray diffraction analysis. Values in wt.%. .

2.2.2 Experimental Procedure

Two experimental units using the same design of pressure cell but different modes of applying temperature and pressure were available. These are shown schematically in Figs. 2.1 and 2.2 and the laboratory is shown in Plate

SINGLE CELL

(schematic)

- ⊕ pressure dial
- ⊗ shut off valve
- sampling point

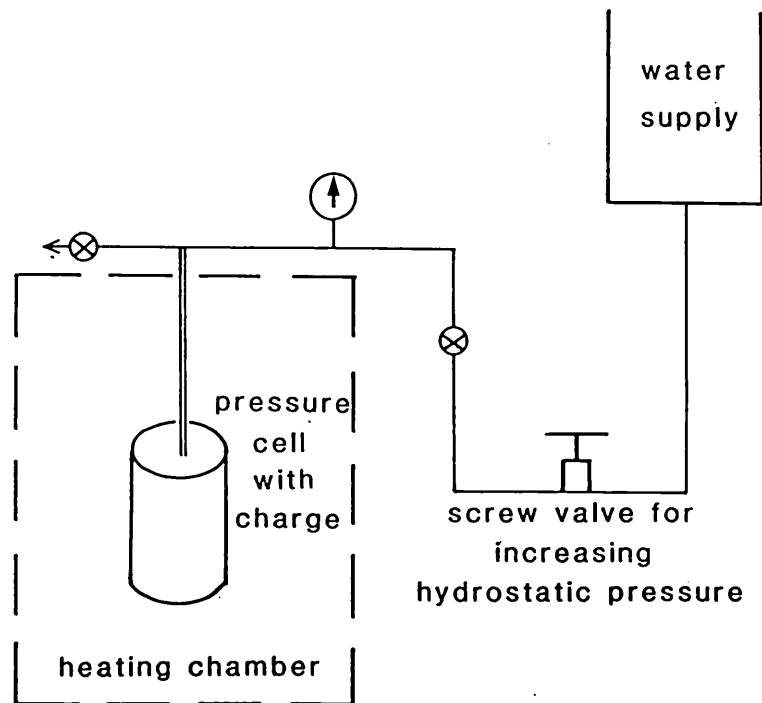


Fig. 2.1 - Schematic diagram of the experimental unit with one pressure cell, thermostatically controlled oven, screw pressure valve and water supply.

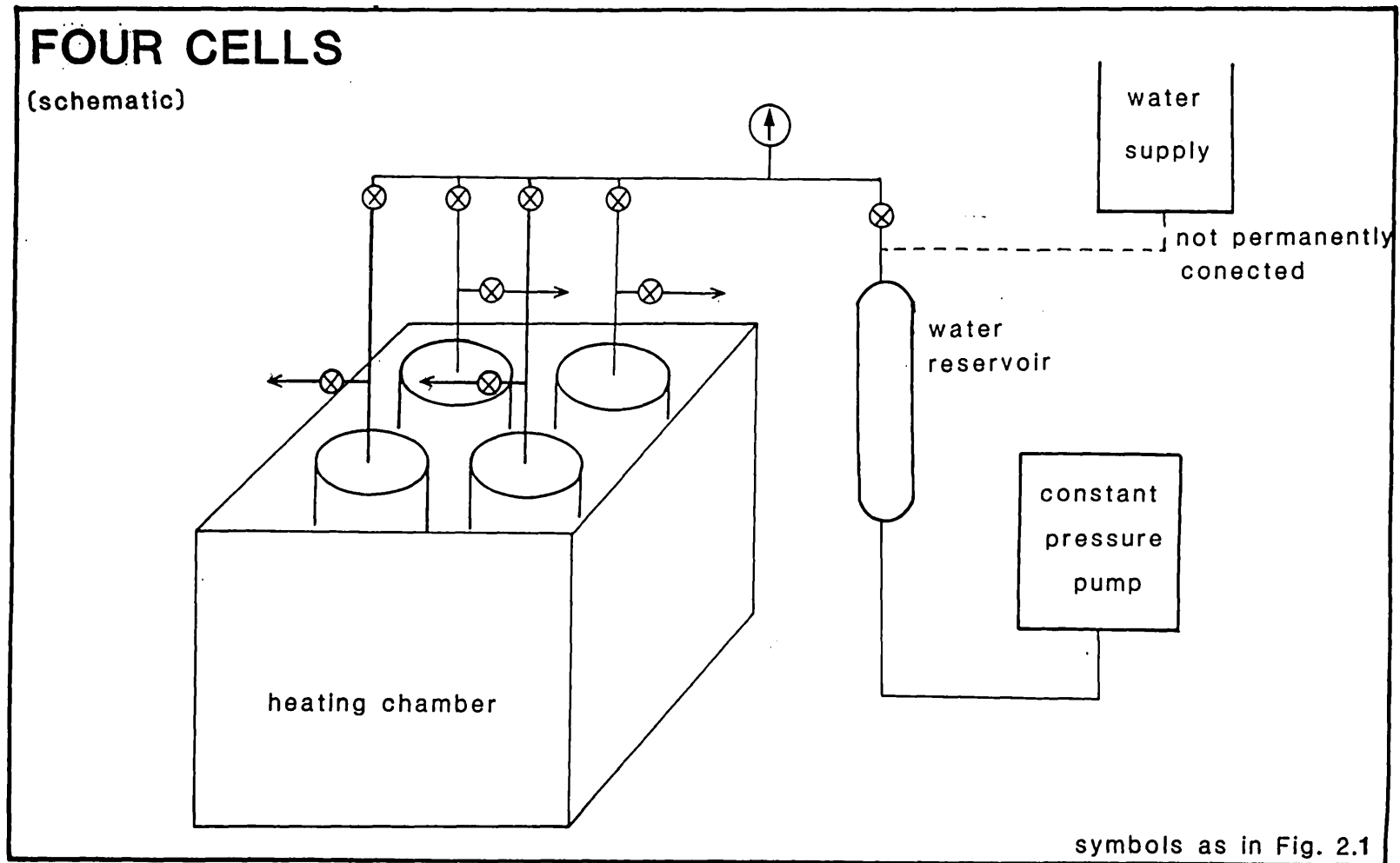


Fig. 2.2 - Schematic diagram of the experimental unit with four pressure cells, a thermostatically controlled heating chamber, constant pressure pump and water supply.

2.1 A. Fig. 2.1 shows a thermostatically controlled oven in which a maximum running temperature of $200 \pm 2^{\circ}\text{C}$ was employed. This oven accommodated 1 pressure cell (dimensions of inner chamber 52 mm diameter x 88 mm depth). Varying hydrostatic pressures from 5 to 11 MPa were employed using this cell. These pressures were achieved and maintained by the use of a screw valve. Fig. 2.2 shows a thermostatically controlled heating chamber which was run at $183 - 186 \pm 2^{\circ}\text{C}$. This chamber accommodated 4 pressure cells of a slightly smaller size than the one shown in Fig. 2.1 (dimensions of inner chamber 52 mm diameter x 53 mm depth). Hydrostatic pressure could be set and maintained at some predetermined level and maintained using a constant hydraulic pressure pump.

The basic design of the pressure cells is shown in Fig. 2.3 (larger cell) and Plate 2.1 B (smaller cell). The stainless steel cells allowed the experiments to be carried out at elevated temperatures (200°C maximum employed) and hydrostatic pressures (11 MPa maximum employed). Equivalent pressure units can be found in Appendix III.

PLATE 2.1 - EXPERIMENTAL EQUIPMENT AND SEDIMENTS ON REMOVAL
FROM PRESSURE CELLS

(A) Photomicrograph of experimental laboratory. The oven on the left had side houses the single pressure cell. The heating chamber in the far right hand corner houses the four pressure cells.

(B) Detail of the smaller of the experimental pressure cells. Scale bar 5 cm.

(C) Surface of the sediments on removal from the pressure cell. Calcite cement crystals bind sediment grains. Scale bar 0.25 mm.

PLATE 2.1



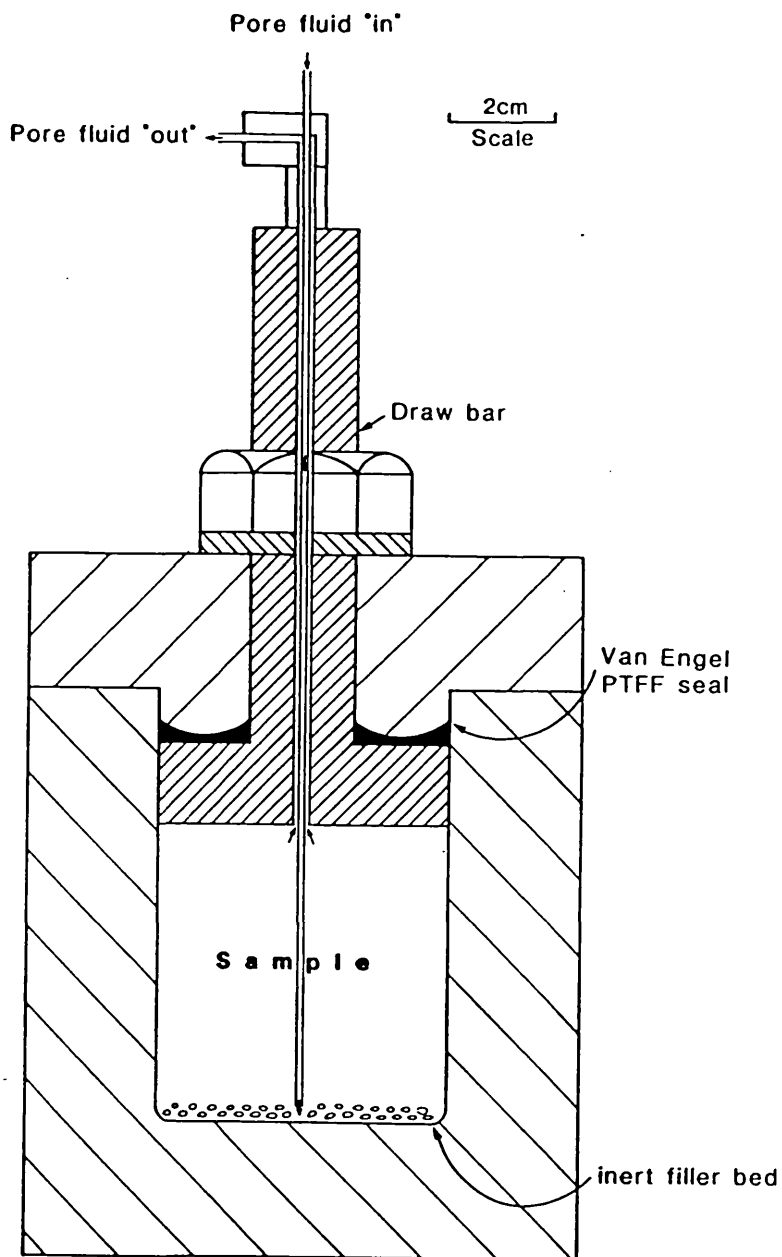


Fig. 2.3 - Simplified cross-section of pressure cell.

Samples of the unconsolidated carbonate grains, weighing approximately 50 gms (approximately 40 mm diameter x 20mm

depth) were placed in PTFE containers (modified PTFE beakers) and saturated with water. The PTFE containers with the water saturated samples were then placed in the pressure cells and the cells were topped up with water of the same composition as that in the PTFE container. The cell was then sealed.

The required experimental conditions of temperature and pressure were built up over a period of 12 hours. Once achieved, they were maintained for periods of one to six weeks depending on the requirements of the experimental design. The time was based on previous work by Ferguson et. al. (1984). Using a similar experimental procedure, they found that cementation occurred within four weeks with conditions of 180 °C and 96.5 bars and of 200 °C and 48.25 bars (pressures equivalent to 9.6 and 4.8 MPa respectively). During this present study, time periods of up to 6 weeks were employed as simulated diagenesis was found to proceed to a greater extent and in many cases the system reached apparent chemical equilibrium.

Using this equipment, temperature control was simple and successful but control of the hydrostatic pressure proved to be more difficult for two reasons:

(i) because of the reactions which occurred in the pressure cells. The main reactions affecting the hydrostatic pressure were the sediment volume change during the

aragonite-calcite transformation (8% volume increase) and the production of gases due to the breakdown of some of the organic matter (CO₂, nitrogen and minor quantities of light hydrocarbons, Ferguson et. al., 1984) and

(ii) because of the basic type of equipment used. The screw valve shown in Fig 2.1 was operated and controlled manually. Fluctuations in pressure therefore could not be continuously rectified.

To monitor the geochemical changes that occurred within the system, small fluid samples (2-4 ml) were collected at weekly intervals, resulting in a maximum of 5 volume % fluid substitution occurring at weekly intervals. All liquid samples were stored at 4 °C until they could be analysed. Analysis (see section 2.4.3 for technique) of the liquids was usually carried out within two days of collection. This meant that the chemical system was not entirely closed but was restricted. At the hydrostatic pressure maintained within the pressure cells, any gases generated were kept in solution. The fluids however were collected at a point in the system (see Figs. 2.1 and 2.2) which was at atmospheric pressure. At this point therefore the fluids separated into a gaseous and a liquid phase.

After the experiments had run for the required time, the pressure cells were cooled over a period of 12 hours, keeping the hydrostatic pressure above 3.5 MPa to prevent

the fluids from boiling. Once the cells were opened however, the fluid separated and any free gas escaped. The liquid phase was drained off. Some well cemented samples had to be cut from their PTFE containers while others, only partially cemented were easily removed. Plate 2.1 C shows the surface of a partially cemented sediment after its removal from the cell.

2.3 EXPERIMENTAL DESIGN

Initial studies by Ferguson et al. (1984) showed that the possibility of simulating the early diagenesis of carbonates using the equipment designed and built at Imperial College, existed. In these experiments a limited selection of oolitic carbonate sediments from the Bahamas and Abu Dhabi was used and various experimental conditions of time, temperature and pressure were investigated. Since that time, a selection of oolitic and skeletal samples were made available for the experimental work from Shark Bay and Kuwait. The response of all these sediments to the experimental conditions was therefore studied. 24 experiments were conducted. Various physical conditions were imposed and pilot experiments involving different types of fluids were also conducted. 18 of these were single cell experiments, run in the apparatus shown in Fig. 2.1 while the other 6 were run using the 4 cell apparatus shown in Fig. 2.2. A total of 42 samples were therefore tested and

studied. Details of these experiments are given in Appendix III.

2.3.1 Investigation of the response of seawater to the experimental conditions

To isolate reactions occurring due to the heating of seawater, one cell with no solid sample was run under standard time, temperature, pressure and pore fluid sampling conditions. The evolution of the pore fluid in response purely to the physical experimental conditions was studied. The results are presented in section 3.2.

2.3.2 Investigation of the sediments

A series of experiments were run under very similar physical conditions using seawater and sediment samples from all of the different collection areas. The results of these experiments (see section 3.5) were significant in that different textural diagenetic features were produced under the very comparable experimental conditions. Factors within the sediments obviously had an effect on diagenetically produced features such as cement morphology, replacement and neomorphic textures. The parameters which differed between sediment samples such as sediment composition, grain size and the amount of organic matter were therefore investigated (see results in section 3.6).

2.3.3 Physical experimental conditions

(1) Time

Although most experiments were run for 40-50 days (see Appendix III), the early stages in the development of the textures were studied in experiments that lasted for between 7-26 days. The results of these experiments can be found in section 4.2.

(2) Temperature and pressure

Ferguson et. al. (1984) have shown that the temperature at which experiments were run was vital in controlling the rate of reaction e.g. in 28 days, a sample run at 200 °C was found to have cemented while one run at 130 °C was not, hydrostatic pressure in both cases was identical.

Hydrostatic pressure also appeared to have some effect. The data presented in Table 2.3 from Ferguson et al. (1984) show that the higher the pressure, the lower was the temperature required for cementation to occur. Thus, temperature coupled with the level of hydrostatic pressure imposed had an effect on the rate of the diagenetic reaction.

Pressure (bars)	Minimum temp. at which cementation occurred (°C)
48.25	200
75.84	190
96.5	160

Table 2.3 - Minimum temperatures at which cementation occurred at a given pressure, Ferguson et. al., 1984.

Samples which were identical were therefore run under different pressures but identical temperature and sampling conditions to determine the effect of hydrostatic pressure on the diagenetic reactions. The results of these experiments can be found in section 4.4.

(3) Effect of fluid sampling

The effect of non-sampling of the pore fluids was also studied by comparing two experiments run under similar experimental conditions of time, temperature and pressure using the same sediment. The pore fluids of one experiment were sampled in the normal procedure, the pore fluids of the other were not. The results of these experiments can be found in section 4.5.

2.3.4 Pilot experiments

As well as the main areas of investigation into the possible control on the experimental diagenesis of sample type, temperature, hydrostatic pressure, time and the effect of pore fluid sampling, pilot experiments were conducted to study the effect of varying the pore fluid composition. The results of these experiments are reported in Chapter 5. These experiments gave interesting results but were not followed up because of a lack of time. It is suggested that further experimentation in this area would give valuable insight into the effects of pore fluid composition on diagenesis.

2.4 ANALYTICAL PROCEDURE

To obtain a full understanding of the diagenetic effects that occurred during the experiments, various types of data were obtained. These include:

- (1) The petrographic examination of the solid material using techniques such as standard optical microscopy, scanning electron microscopy (both secondary and back-scatter imaging) and a limited amount of transmission electron microscopy.
- (2) The mineralogical examination of the solid material using X-ray diffraction analysis.
- (3) The geochemical examination of the solid material using

microprobe analysis.

(4) The geochemical examination of the resulting pore fluids using inductively coupled plasma techniques.

2.4.1 Petrography

(1) Preparation of material

The partially lithified sediments were dried at room temperature on their removal from the pressure cells. They were then set in araldite containing a dark blue pigment and thin sectioned. Thin sections were ground to a thickness of 15 μm and polished. Samples of the original sediments were also impregnated and thin sectioned.

(2) Optical microscopy

The thin sections were examined using normal optical microscopes to determine the changes that had occurred in the sediments. Textural relationships between the original grains and diagenetically produced features such as cement, secondary porosity, replacement and neomorphic textures, were studied. Many of these features were easily seen and distinguished using this method and hence much of the petrographic observations were made using standard optical microscopy.

(3) Scanning electron microscopy (SEM)

Broken specimen surfaces were examined using the secondary mode of the JEOL 733 electron microscope. This gave a three dimensional image from which information about the cement crystal morphology could be obtained.

Small fragments of the samples were mounted on aluminium stubs with a silicon glue. Once dry, these were then coated with a thin layer of gold (around 200 \AA) to prevent electrostatic charging of the specimen surface while under examination in the SEM (Echelin, 1978).

(4) Back-scatter electron imaging (BSI)

Back-scattered electrons have a different source within the specimen to secondary electrons (see Fig. 2.4). While secondary electrons are emitted from the surface layer, back-scattered electrons come both from the surface and from beneath the surface within a volume of the material under examination. The energy intensity of these electrons is related to the mean atomic number of the crystal hence, areas of different mean atomic number i.e. chemistry or mineralogy, can be distinguished (Hall and Lloyd, 1981).

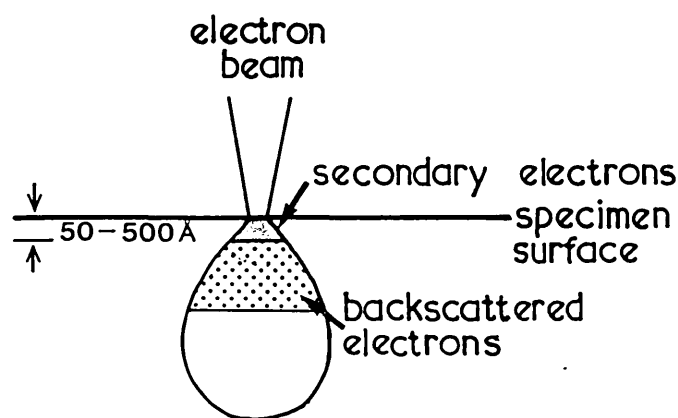


Fig. 2.4 - Schematic diagram showing the source of secondary and back-scattered electrons from a specimen surface.

The polished thin sections, covered with a thin film of carbon to prevent charging, were used for this method of examination. Back-scattered imaging proved particularly valuable when studying for example the difference in Mg content of the cements generated during the experiments. Minerals with a high mean atomic number appeared lighter than those with a low mean atomic number. Carbonates containing a high level of Mg^{2+} therefore appeared darker than low-Mg calcite or aragonite and could be easily and quickly identified.

(5) Transmission electron microscopy (TEM)

Significant levels of Sr^{2+} and SO_4^{2-} were contained in the calcite which was precipitated. To check whether these were present as a separate $SrSO_4$ phase or not, foils of the cement crystals of one experiment were prepared and studied

using the TEM. The author did not conduct any extensive study using the TEM and the work was carried out by Drs. K.H. Brodie and S.H. White. No detailed discussion of the technique is therefore presented.

2.4.2 Mineralogy

(1) X-ray Diffraction (XRD)

X-ray diffraction (XRD) was used primarily to determine the bulk mineralogy of the samples and to provide an indication of how much of the original aragonite had been converted to calcite. This provided a semiquantitative measure of the degree to which experimental diagenesis had proceeded. The Mg contents of the calcite however were not determined using this technique. The XRD method for determining the amount of Mg in the calcite lattice is based upon the d-spacing of the crystal lattice. As the precipitated calcite contains Sr^{2+} and SO_4^{2-} as well as Mg^{2+} as major trace elements, the calcite lattice d-spacing would have been affected making the method unreliable (Busenberg and Plummer, 1985).

Whole rock samples were ground to a fine powder (<2 μm) and mounted, dry, onto XRD cavity mounts. These were scanned and oscillated six times between 28 and 36 $^\circ 2\theta$ to obtain a reliable average peak height. Cobalt k_α radiation, a time

constant of 2 and a chart speed of $1^{\circ}2\theta/\text{minute}$ were employed. Variable count rates per second were used to achieve maximum on chart peak heights. Average peak height values were compared with peak height curves obtained for mixtures of known quantities of minerals using the data of Cuff (1972). The precision of this technique is $\pm 5-10\%$ and all data were used bearing this in mind.

(2) Microprobe Analysis

Geochemical data were collected using the JEOL 733 electron microscope (see sections 2.4.1 (3) and (4)) which has a microprobe facility. For this, the carbon-coated, polished thin sections were used with the machine in back-scatter image mode to assist in the location of suitable points for analysis. Energy-dispersive spectrometry (EDS) was used with livetimes of 300 seconds and a beam current necessary to achieve a counts per second rate of 1500-1600 on a cobalt standard. Pure CaCO_3 should have a cation oxide total of 56.03 (Schofield and Adams, 1986). Carbonates are particularly difficult to analyse using an electron microprobe because CO_3^{2-} can be driven off as CO_2 if the beam current is too high. Often due to operating difficulties, fluctuations in the beam current were noted. These were compensated for by frequently recalibrating with the cobalt standard. Because of these difficulties, many analyses were rejected. Cation oxide totals of 56.03 ± 3 were accepted.

However, there are occasions where analyses with cation oxide totals outside the stated range are used as they were the only source of data (e.g. those used in section 6.4). All data used are presented in Appendix IV together with the method for calculating the mole % values.

The accuracy of the microprobe for Mg^{2+} , Sr^{2+} and SO_4^{2-} was checked by analysing standards of MgO and SrSO_4 . The mean oxide total for each standard was 99.5 and 101.95 with standard errors on those means of 0.85% and 0.71% respectively. However, by using cation oxide totals of ± 3 , additional errors of up to $\pm 5\%$ have been incurred. The maximum error in mole % MgCO_3 is therefore $\pm 6.5\%$ and $\pm 8\%$ in mole % SrCO_3 and SO_4^{2-} . These are large errors, most calcite however contained less than 10 mole % MgCO_3 , 1.3 mole % SrCO_3 and 2 mole % SO_4^{2-} (see Appendix IV). Errors of up to 8% on those levels are much less than the spread of data encountered (see data in section 3.5.2 (2)). Also, in the Mg-rich phases, differences between 30-85 mole % MgCO_3 have been observed (see section 4.2), errors of up to 6.5 % will not remove or invalidate any differences observed. However, it is accepted that smaller errors would have been preferential and it is for this reason that the trends of the microprobe data only have been studied. In future studies, if detailed geochemical data were required, it would be advisable to use a secondary standard of calcite of known composition. Concentrations less than 1000 ppm are not

detectable using the microprobe (Schofield and Adams, 1986).

2.4.3 Geochemistry of pore fluids

All pH values for unused water samples were obtained using a standard pH meter, calibrated using buffer solutions with pH 4, 7 and 9. The meter was checked at regular intervals during measurements.

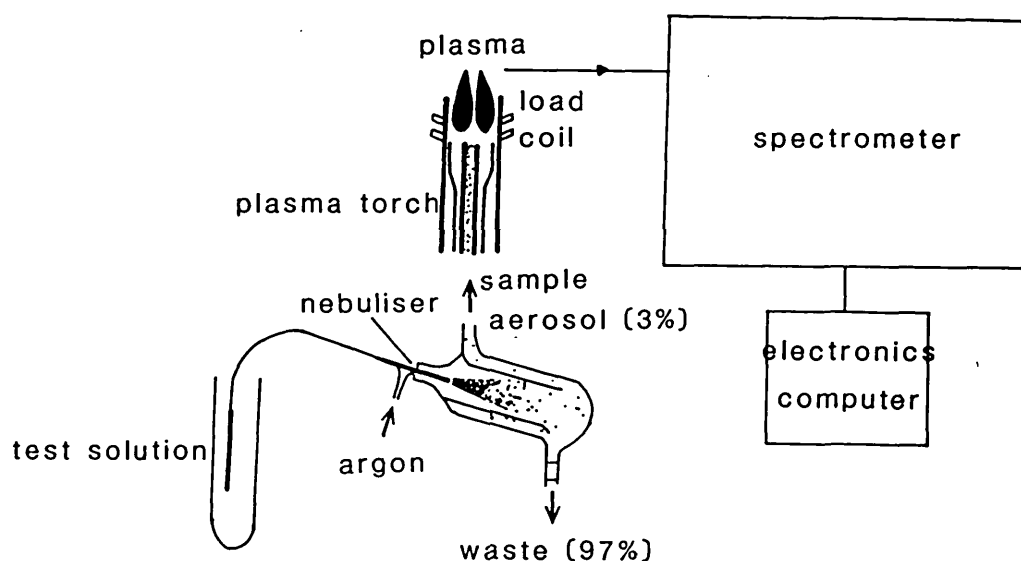


Fig. 2.5 - Schematic diagram of the Inductively Coupled Plasma (modified after Thompson and Walsh (1983)).

Pore fluid samples were analysed using inductively coupled plasma spectrometry (ICPS). This employs a conventional spectroscopic technique, but with the addition of a unique emission source - the inductively coupled plasma. Fig. 2.5

shows the basic principals of the equipment. Fluid samples are mixed with argon gas in a nebuliser to form a very fine spray. This then passes through the plasma torch which is located in a 2 or 3 turn induction coil, carrying a very high frequency alternating current. This maintains ionisation and keeps the temperature at about 10,000K. Sample material passing through the plasma is completely ionised. Details of the equipment and technique are given in Thompson and Walsh (1983). All samples were analysed to give elemental concentrations of Mg, Ca, Sr and S. Pore fluid analyses are given in Appendix I.

(1) Precision of technique

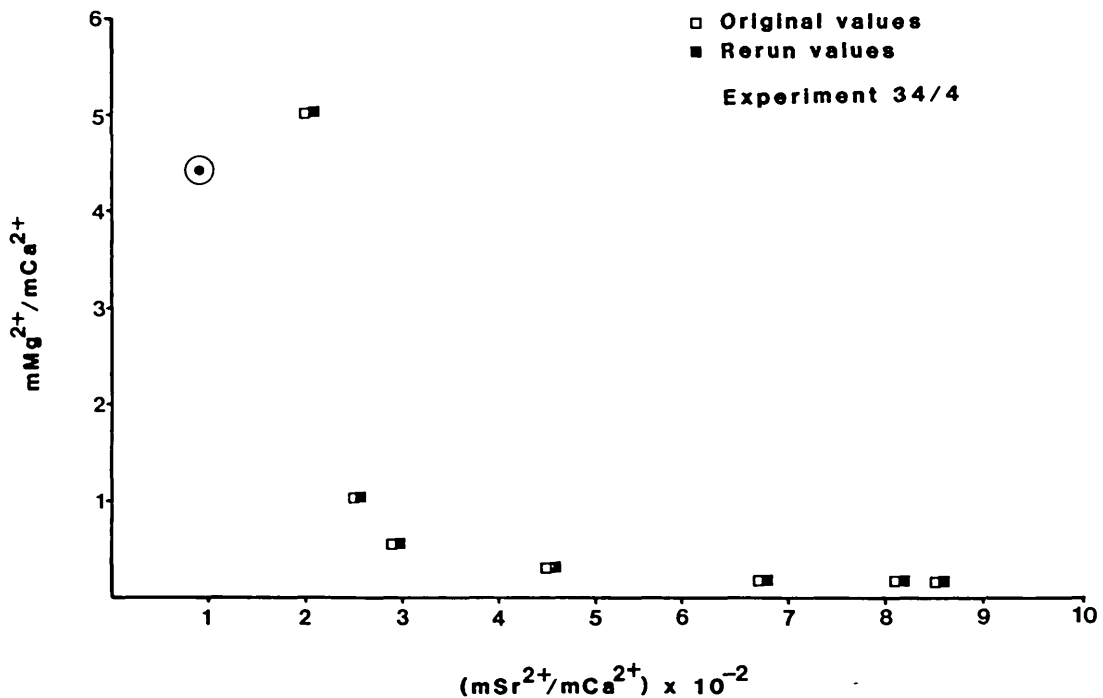


Fig. 2.6 - Plot of original and rerun values for mMg²⁺/mCa²⁺ and mSr²⁺/mCa²⁺ pore fluid ratios for experiment 34/4.

Thompson and Walsh (1983) give precision values for ICPS analysis as being around +/- 1 % but can occasionally be as high as +/- 5 % (lower precision). Analysis of the standard (see Appendix I) showed that the standard errors of Mg^{2+} , Ca^{2+} , Sr^{2+} and S^{6+} were 0.24%, 0.28%, 0.22% and 0.41% respectively. As a check on the precision of the technique, the pore fluids of samples from experiment 34/4 were rerun two months after they were first analysed, the results are shown in Fig. 2.6. No significant difference in the molecular ratios were noted.

(2) Data handling

Although elemental concentrations (i.e. ppm) relative to the starting liquid were used in a few cases (e.g. to study the precipitation of anhydrite from seawater, see section 3.2 or the uptake of Mg^{2+} , see Fig. 3.21), study of the geochemical data in this way proved to be unhelpful. The trends observed were much less consistent when compared to those obtained using mMg^{2+}/mCa^{2+} and mSr^{2+}/mCa^{2+} ratios. The latter have therefore been used except in the few cases where use of ppm values helped clarify the results. Both elemental and molecular ratio data however have been presented in Appendix I.

2.4.4 Organic matter

Total organic carbon (TOC) analyses were carried out on all starting sediments using a Perkin Elmer 240C elemental analyser. The reproducibility of this technique however was found to be very poor possibly because of the tendency of Recent organic matter to be broken down on treatment with acid (e.g. Byres et. al., 1978; Van Iperen and Helder, 1985) and the results were therefore not used.

PART II - RESULTS

CHAPTER 3 - INVESTIGATION OF THE EFFECT OF DIFFERENCES IN EXPERIMENTAL MATERIALS

3.1 INTRODUCTION

Preliminary investigations by Ferguson et al. (1984) and Goodman (1986) showed that the differences in the diagenetic fabric which were produced (i.e. the cementation and replacement of grains), were linked, in some way, to the nature of the carbonate sediments that were used as starting materials for the experiments. Ferguson et al. (1984) attributed major differences in the replacement fabric to the amount of organic matter that was contained within the sediment grains. Goodman (1986) attributed differences in the extent of cementation to the ability of the sediments to remove Mg^{2+} from the pore fluids by the adsorption of Mg onto the grain surfaces.

It was therefore considered necessary to experiment with a range of calcium carbonate sediments, predominantly composed of coated grains but with a variety of other carbonate and non-carbonate grains (see Appendix II for full descriptions of the sediments used). The causes of the differences in the diagenetic textures generated, could then perhaps be more fully understood. It was also considered necessary to study the reactions which occurred during the heating of the seawater under pressure in the absence of any sediment, so

that the effect of this could then be separated from reactions involving both sediment and seawater. To check the effect that the experimental conditions had on pure aragonite, one experiment was also carried out using "AnalaR" aragonite as this material had no complicating factors such as grain structure or organic matter (which could provide a source of CO₂ to drive the reactions).

This chapter reports on the results of experiments studying reactions involving:

- (1) seawater only
- (2) seawater and "AnalaR" aragonite and
- (3) seawater together with sediment samples from different depositional environments and of different composition.

3.2 EVOLUTION OF SEAWATER DURING THE EXPERIMENTS

One experiment (34/1) was conducted, to study the reactions that occurred during the heating under pressure of seawater alone under experimental temperature conditions of 183 +/- 2 °C and pressures of 7.65 MPa (s.d. 0.74 MPa).

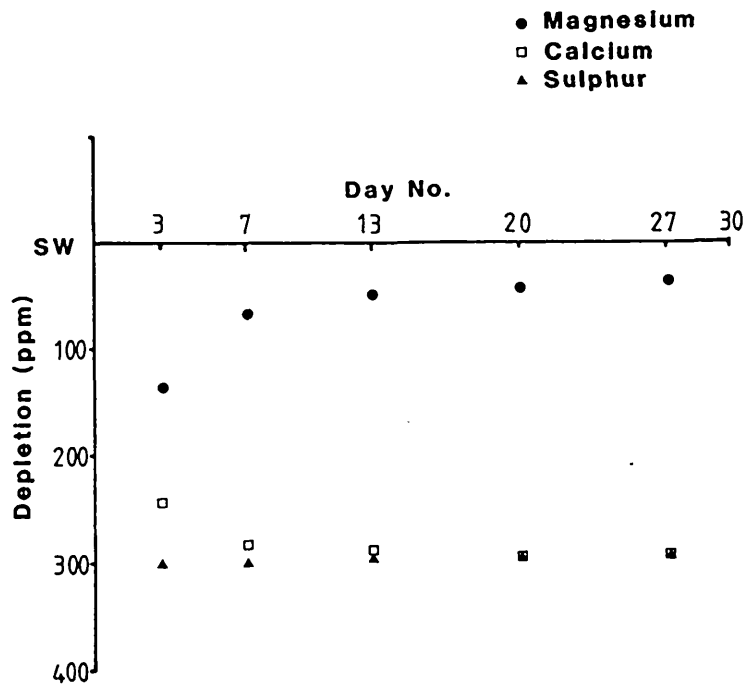


Fig. 3.1 - Depletion in magnesium, calcium and sulphur levels (ppm) from that of seawater (SW) during experiment 34/1.

The chemical evolution of the pore fluid over 30 days experimental time, is shown in Figs. 3.1 and 3.2. The results indicate that anhydrite (CaSO_4) and some sort of magnesium oxysulphate as found by Bishoff and Seyfried (1978), precipitated. The following calculations show how much of each phase was precipitated from 80 mls of seawater.

Phases precipitated at the beginning of the experiment:

From Fig. 3.1, it can be seen that 300 ppm S^{6+} was removed from pore fluids therefore

$$\left[\frac{(16 \times 4) + 32.06}{32.06} \right] \times 300 = 898.8 \text{ ppm } \text{SO}_4^{2-} \text{ was removed.}$$

In molecular terms

$$\begin{aligned} \text{SO}_4^{2-} \text{ removed} &= 898.8/96.06 \\ &= 9.4 \text{ millimoles} \end{aligned}$$

250 ppm Ca^{2+} was also removed from pore fluids, therefore

$$\begin{aligned} \text{Ca}^{2+} \text{ removed} &= 250/40.08 \\ &= 6.2 \text{ millimoles} \end{aligned}$$

i.e. a maximum of 6.2 millimoles of CaSO_4 was initially precipitated from approximately 80 mls of seawater which is in close agreement with the data in Bishoff and Seyfried (1978) where 6.8 millimoles of CaSO_4 was found to precipitate from 100 mls of seawater at 200°C. An excess of 3.2 millimoles of SO_4^{2-} was therefore removed from the fluids at the beginning of the experiments.

Bishoff and Seyfried (1978), in their calculations, attributed the removal of Mg^{2+} and excess SO_4^{2-} , to the precipitation of " MgSO_4 " and " $\text{Mg}(\text{OH})_2$ " phases. Following their method of calculation, Fig. 3.1 shows that 135 ppm Mg^{2+} was also initially removed from the pore fluids.

$$\begin{aligned} \text{i.e. } & 135/24.32 \text{ millimoles Mg}^{2+} \\ & = 5.6 \text{ millimoles Mg}^{2+} \end{aligned}$$

Assuming precipitation of 3.2 millimoles "MgSO₄", using all the available SO₄²⁻, an excess of 2.4 millimoles Mg²⁺ was removed from the seawater, suggesting that the "Mg(OH)₂" phase found to have been precipitated by Bishoff and Seyfried (1978) may also have been precipitated in this case, although Bishoff and Seyfried (ibid.) found it to be precipitated only at temperatures greater than 300 °C. Bishoff and Seyfried (1978) found unidentified crystals at the end of their experiments which "presumably are a single phase that represents the combined "MgSO₄" and "Mg(OH)₂" components inferred from the composition of the solution" (ibid., p.845). They called this phase a magnesium oxysulphate. The gradual increase of Mg²⁺ and S⁶⁺ in solution during the experiment suggests that the Mg phase precipitated may have been relatively unstable, whereas the continued decrease in the amount of Ca²⁺ in solution suggests further precipitation of CaSO₄.

At the end of the experiment, when the cells cooled down, the bulk composition of the seawater returned to near that at the start of the experiment (see Fig.3.2), indicating a high rate of dissolution of the precipitated phases on cooling of the solution. Sufficient anhydrite has been found in other experiments for it to be analysed and

identified but no magnesium oxysulphate has been identified.

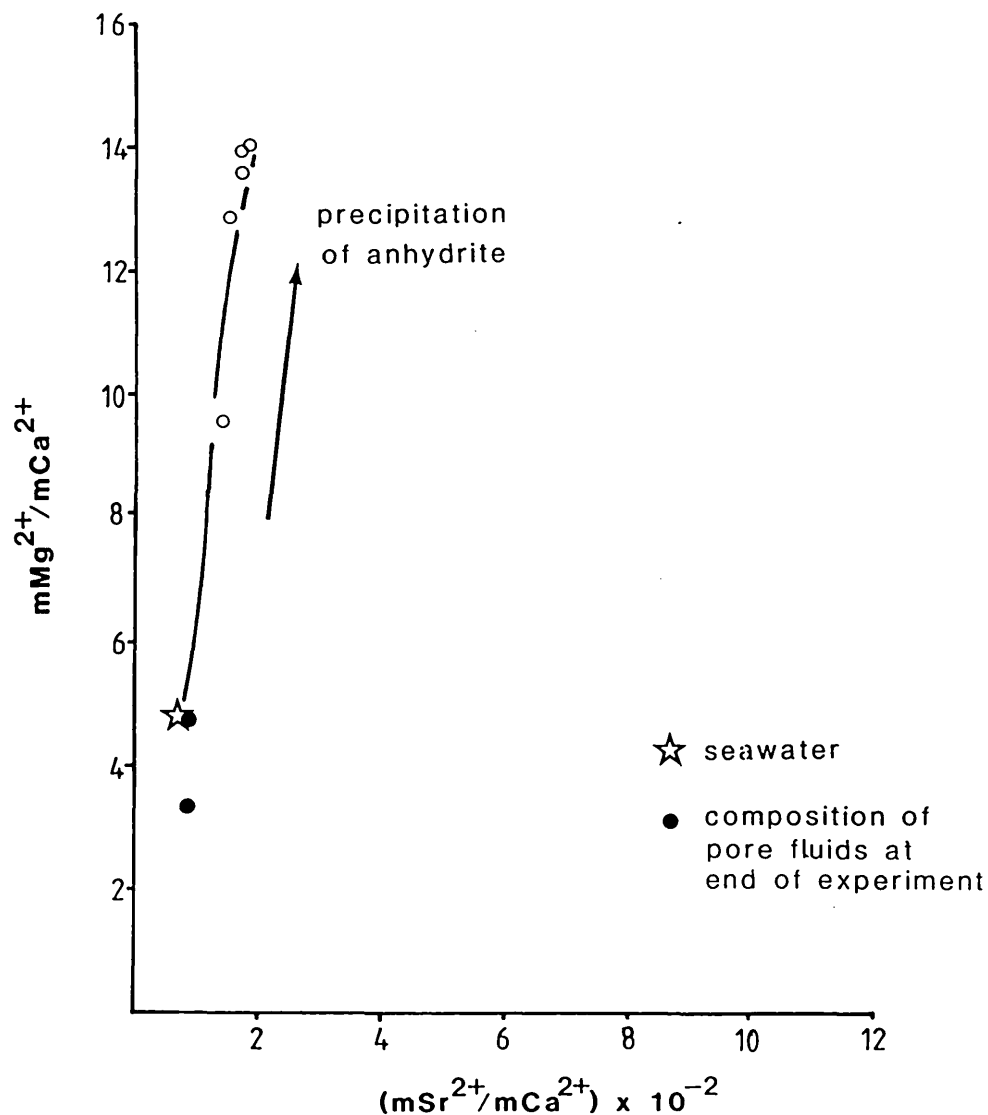


Fig. 3.2 - Evolution of seawater (34/1) in terms of $\text{mMg}^{2+}/\text{mCa}^{2+}$ and $\text{mSr}^{2+}/\text{mCa}^{2+}$ pore fluid ratios.

The anhydrite usually occurred only on sediment surfaces and lining the walls of the experimental cell and PTFE container but occasionally it has been found within the sediment. Plate 3.1 shows such an occurrence. The relationship between the sediment grains, anhydrite lath and cement

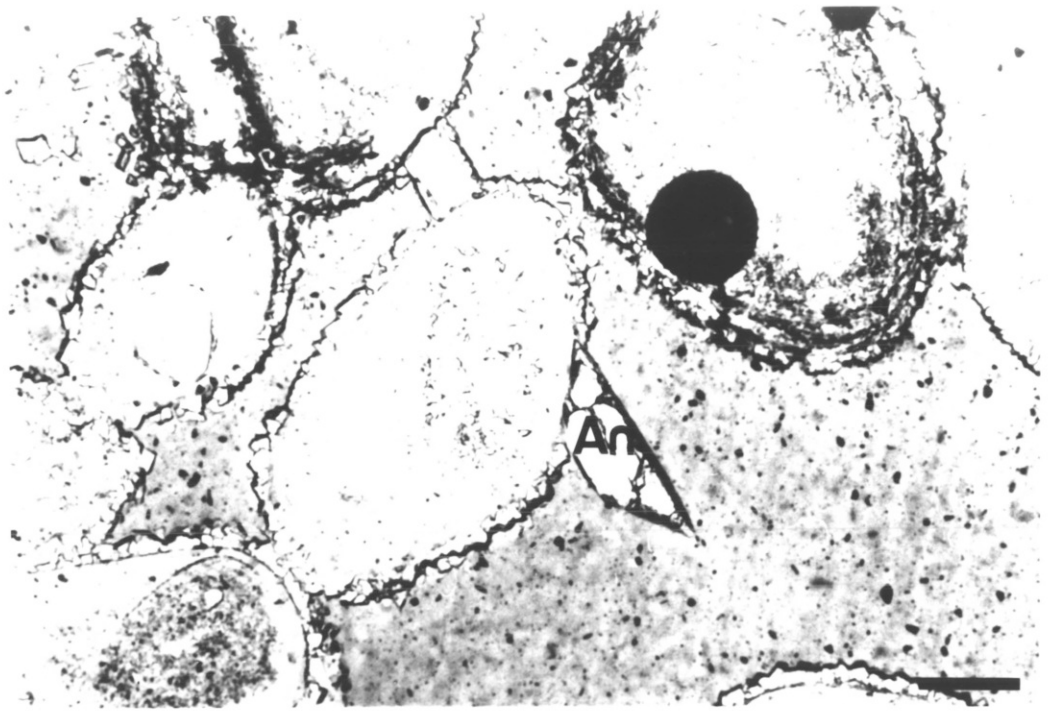


PLATE 3.1

Anhydrite lath within the partially lithified sediment. Anhydrite (An) predates the fringe of calcite cement which surrounds the grain edge on which no anhydrite is present.

Experiment 34/4. PPL. Scale bar 50 μm .

crystals confirm that it is of an early origin.

3.3 "AnalaR" ARAGONITE

One experiment (34/2) was conducted using very fine "AnalaR" aragonite powder (produced by Hopkins and Williams Ltd (BDH Chemicals)) to study the effects of the elevated temperature/pressure seawater system on pure aragonite. No source of CO₂ was present within the solid material in the form of organic matter (although a small amount of dissolved organic matter was likely to have been present in the seawater). The change in the solid is therefore attributed to the temperature/pressure conditions of the experiment. XRD analysis of the resultant material showed that the aragonite was totally converted to calcite (see Appendix V). It is however noted that the very fine aragonite precipitated from concentrated solutions, such as that used here, reacts extremely rapidly when compared to natural material (Land, 1967).

3.4 GENERALISED PATTERN OF EXPERIMENTAL DIAGENESIS

The general pattern of reaction which occurred during the experiments will be briefly outlined, so that the detailed results of the experiments can be studied in terms of their individuality.

In the first few days of the experiments, anhydrite (CaSO_4) precipitated from the seawater and possibly a magnesium oxysulphate phase as shown in section 3.2.1. This precipitate was accompanied or succeeded by the dissolution of aragonite and the precipitation of calcite. These processes are shown by an increase in the pore fluid $\text{mSr}^{2+}/\text{mCa}^{2+}$ ratio and a decrease in the $\text{mMg}^{2+}/\text{mCa}^{2+}$ ratio respectively.

When the cell was opened, originally unconsolidated sediments were found to be either partially or completely cemented. XRD results (see Appendix V) indicate levels of aragonite dissolution ranging from 0 to 100% depending on the experiment. Typical levels of aragonite dissolution in sediment samples were approximately 10 - 30%.

Petrographic observation showed a wide range of experimentally generated fabrics. Cement crystals of different sizes and morphologies were observed. Originally aragonitic grains had undergone dissolution forming either moldic porosity which, in some cases, was partially infilled by calcite or, had undergone neomorphism, resulting in irregular mosaics of sparry calcite.

Geochemically, a variety of cement compositions were found. Typically the cement phase was either a low-Mg calcite or a high-Mg calcite with less than 10 mole % MgCO_3 . However, in

some cases, cement crystals were found to contain up to 84 mole % MgCO_3 . All replacement phases were composed of low-Mg calcite.

3.5 SEDIMENTS COLLECTED FROM DIFFERENT LOCALITIES AND ENVIRONMENTS

As noted in section 2.2.1, starting materials were available from four locations:

- (1) the Bahamas,
- (2) Abu Dhabi,
- (3) Kuwait and
- (4) Shark Bay.

Seven sediment types were available and full descriptions are given in Appendix II. Experiments were conducted using all of these sediments. After the experiments had been run, the samples from the different areas were found to display differences in petrographic textures, particularly in cement morphology. Variations in the chemical evolution of the pore fluids and crystal compositions were also noted.

At the outset of the research program, the effect that variations in the physical conditions of the experiments, such as pressure and pore fluid sampling frequency, would have on the reactions, were not fully appreciated. All sediments were therefore rerun later under identical

experimental conditions using the four cell apparatus (see section 2.2.2). The petrographic differences that were initially observed were found still to exist and hence the results of all experiments are discussed. A complete list of the experiments conducted and the experimental conditions employed can be found in Appendix III.

3.5.1 TEXTURAL VARIATION

(1) Bahaman Subtidal Ooids (BSO).

Expt. No.	Time(days)	Temp.(°C)	Press.(MPa)	
			μ	σ
1685	45	186	6.2	1.05
30/1	43	183	7.8	1.09
34/3	37	183	7.7	0.74
4086	50	200	6.9	0.68

Table 3.1 - Conditions for experiments run using the sediment BSO.

Bahaman Subtidal Ooids (BSO) were used as starting sediments in experiments 1685, 30/1, 34/3 and 4086. The conditions under which these were run are given in Table 3.1.

Fluctuations in the hydrostatic pressure within the experimental cell occurred for the reasons given in section 2.2.2, the mean value (μ) and its standard deviation (σ) are

PLATE 3.2 - BAHAMAN SUBTIDAL OOIDS

(A) Experiment 1685 - Isopachous fringes of granular-bladed cement crystals surround sediment grains. A wider cement fringe is observed surrounding the peloid. The overlay shows where lamellar secondary porosity (oomoldic) has been created and infilled. Neomorphic spar has partially replaced areas of the micritic peloid (see overlay). PPL. Scale bar 20 μm .

(B) Experiment 4086 - Isopachous fringes of granular-bladed cement crystals surround grains. A cluster of cement crystals (C), resembling the form of an algal filament, is observed in the sediment pore space. Secondary porosity (oomoldic) has been created in the cortex of the coated grain (see overlay) while micro-porosity has been created in the peloid. Some of the micritic carbonate has been replaced by neomorphic spar (N). PPL. Scale bar 50 μm .

(C) Experiment 34/3 - Detail of cement crystals (C) on an algal filament which is protruding from the grain surface. PPL. Scale bar 20 μm

(D) Experiment 1685. Detail of grain in which the oomoldic porosity has been infilled by solution cavity fill calcite retaining the original structure of the coated grain cortex (see overlay). Some areas of unfilled secondary porosity remain. Micro-porosity is observed in the micritic peloid. Isopachous fringes of granular-bladed cement crystals surround grains. PPL. Scale bar 50 μm .

OVERLAY KEY

Areas outlined - oomoldic porosity

Areas stippled - micro-porosity

Areas shaded - replacement fabrics

PLATE 3.2

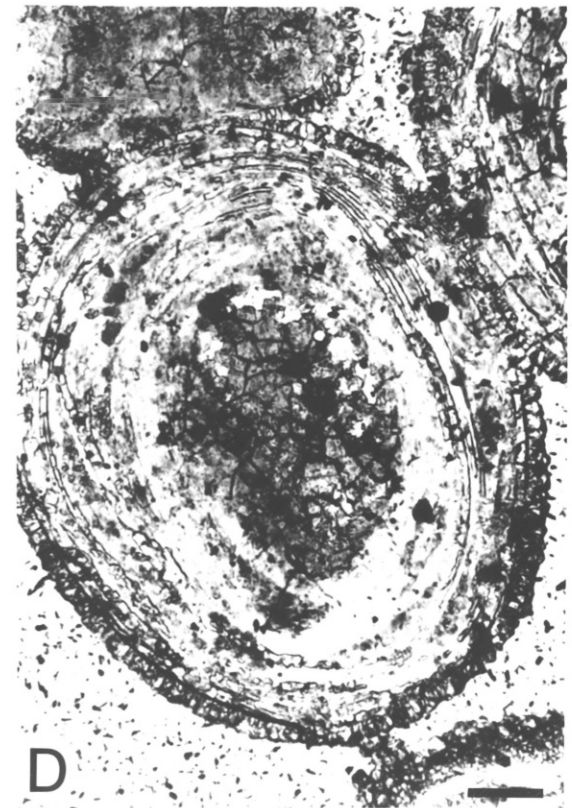
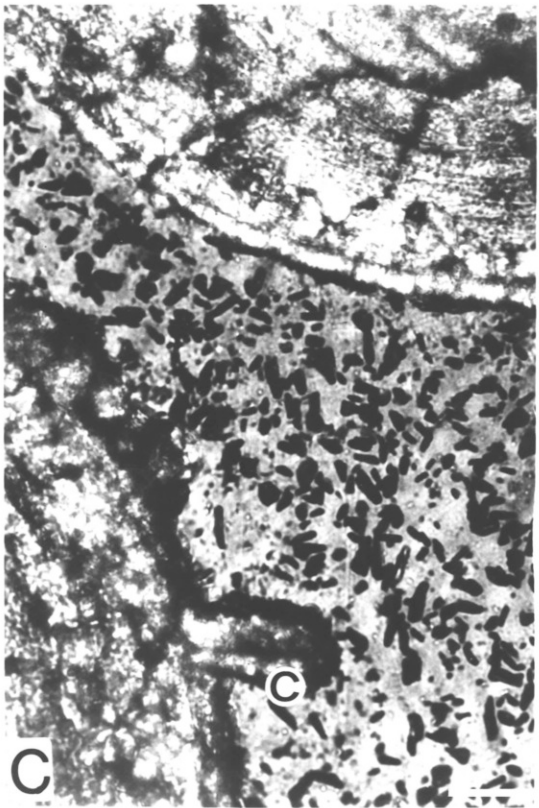
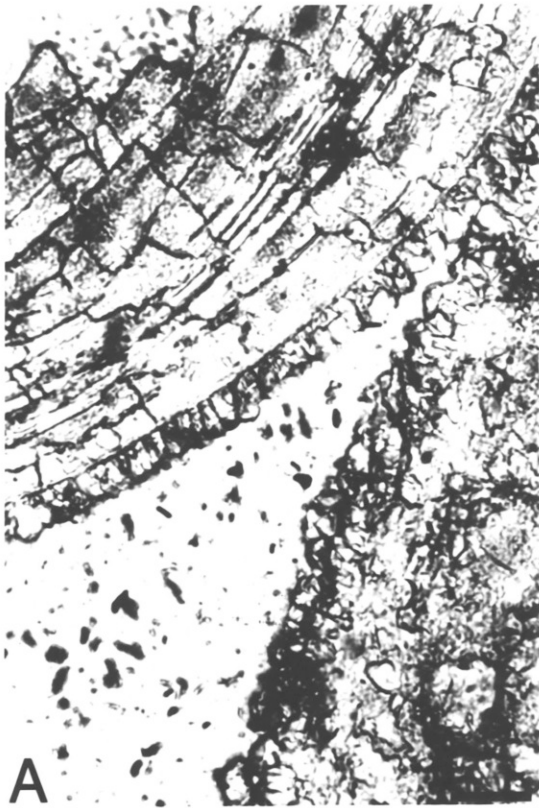
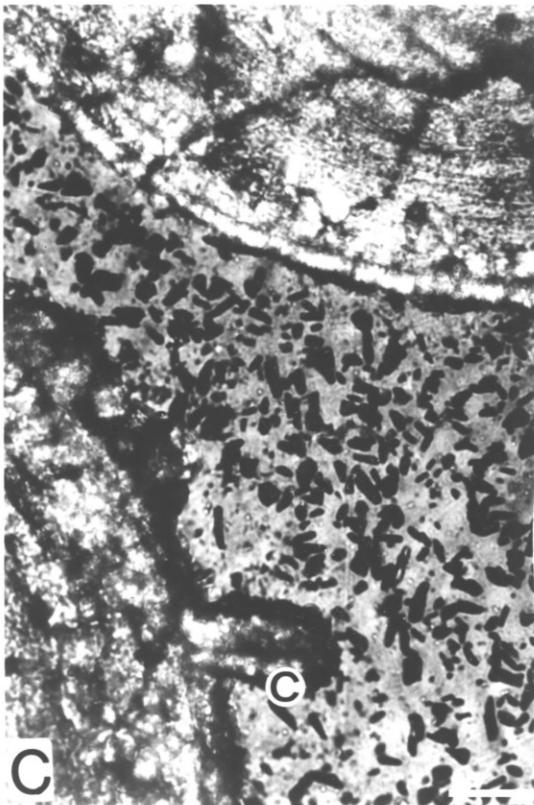


PLATE 3.2



therefore given in Table 3.1.

Cement: At the end of each experiment, all samples of sediment BSO, were found to show an identical form of cement, an isopachous fringe of small granular-bladed crystals (see Plate 3.2 A-D). SEM observation shows these crystals to be of a 'baton' type morphology (see Plate 3.5). The average width of this isopachous fringe is 10 μm , ranging from 6 - 20 μm . Coated grains typically display a cement fringe of single crystal width but micritic peloids show several layers of cement crystals (see Plate 3.2 A and D). Occasionally cement crystal clusters are found in association with organic filaments (see Plate 3.2 B and C).

Secondary porosity: Oomoldic porosity has been created in the cortices of coated grains by the dissolution of aragonitic lamellae (see Plate 3.2 B). Micritic peloids are also affected by dissolution with the development of microporosity (see Plate 3.2 B and D).

Replacement: Solution cavity fill calcite is found in some of the oomoldic porosity. This typically mimics the original lamellae (see Plate 3.2 A and D). Some micritic aragonite has been replaced by neomorphic spar where small crystals larger than the original micrite (typically less than 10 μm in diameter), are observed (see Plate 3.2 A and B).

XRD data (see Appendix V) can only be used in the broadest sense as it is only correct to +/- 5-10%. In experiments using sediment BSO, 10-25% of the original aragonite was removed.

(2) Abu Dhabi Dune Ooids (ADDO)

Abu Dhabi Dune Ooids (ADDO) were used as the starting sediments in experiments 18/1 and 37/1. The conditions under which these were run are given in Table 3.2.

Expt.No.	Time(days)	Temp.(°C)	Press.(MPa)	
			μ	σ
18/1	47	183	6.9	N/D
37/1	47	183	7.9	1.3

Table 3.2 - Conditions for experiments run using sediment ADDO.

Cement: The partially lithified sediments which were collected at the end of both experiments show an identical form of cement, an isopachous fringe of small granular-bladed crystals as shown in Plate 3.3 A-C. The width of this fringe is typically 7 - 9 μm where a single layer of crystals are present. The cement is similar to

PLATE 3.3 - ABU DHABI DUNE OIDS

(A) Experiment 37/1 - Isopachous fringes of granular-bladed cement crystals. Peloids show the development of several layers of cement crystals (C) while coated grains show only one layer. Oomoldic porosity has been created in the cortices of coated grains with micro-porosity being created in the micritic (see overlay). A small amount of the oomoldic porosity has been infilled by lamellar calcite (see overlay). Neomorphic spar (N) partially replaces micritic carbonate. PPL. Scale bar 50 μm .

(B) Experiment 37/1 - Several layers of granular cement crystals are observed on the peloid while one layer of cement crystals only is observed on the coated grain. PPL. Scale bar 20 μm .

(C) Experiment 18/1 - The cortex of the central grain has been replaced by solution cavity fill calcite (R). Areas of secondary porosity remain between the replacement calcite and the original micritic nucleus (P). All grains are surrounded by an isopachous fringe of bladed cement crystals. PPL. Scale bar 50 μm .

(D) Experiment 37/1 - Detail of neomorphic spar (N) replacing micrite. PPL. Scale bar 20 μm .

OVERLAY KEY

Areas outlined - oomoldic porosity

Areas stippled - micro-porosity

Areas shaded - lamellar calcite

PLATE 3.3

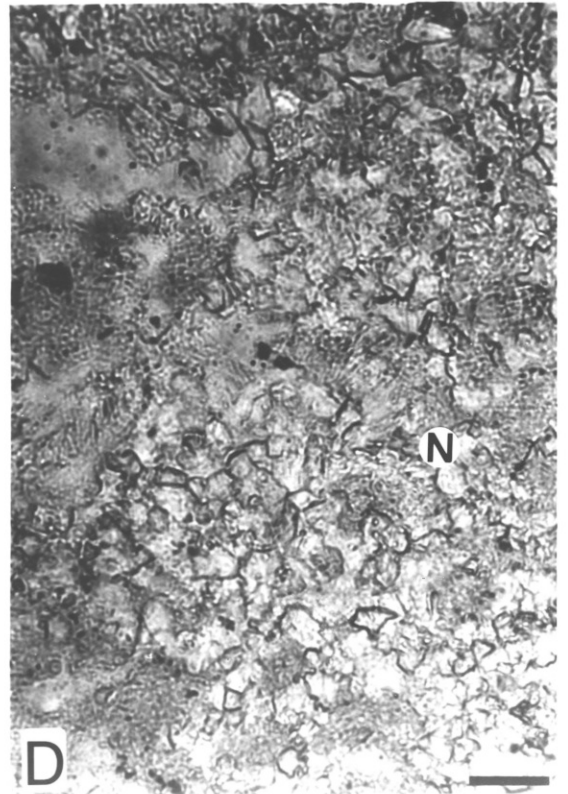
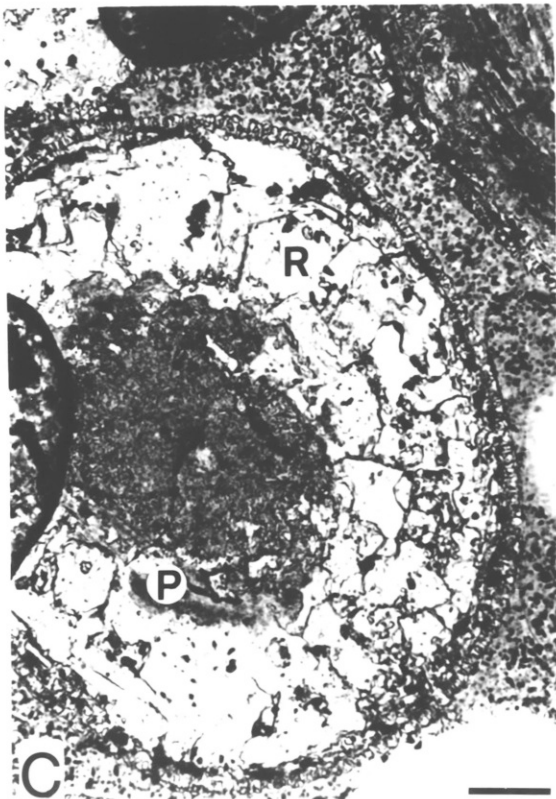
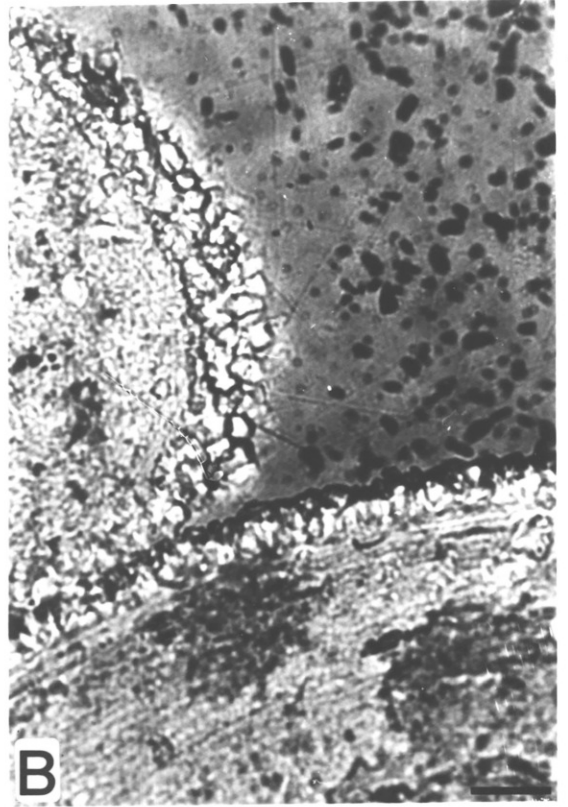
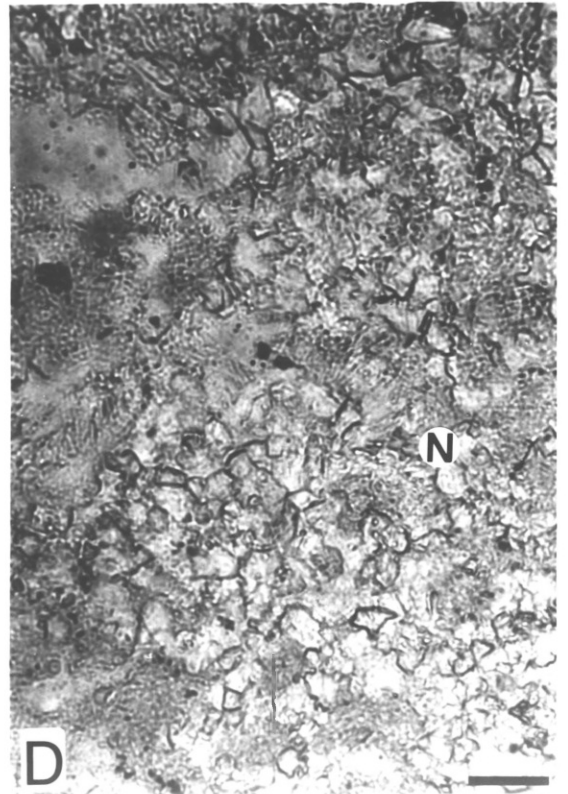
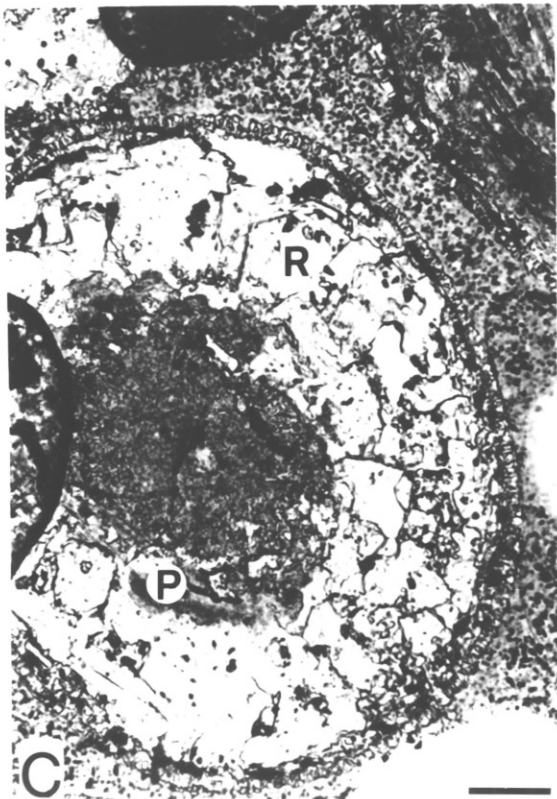
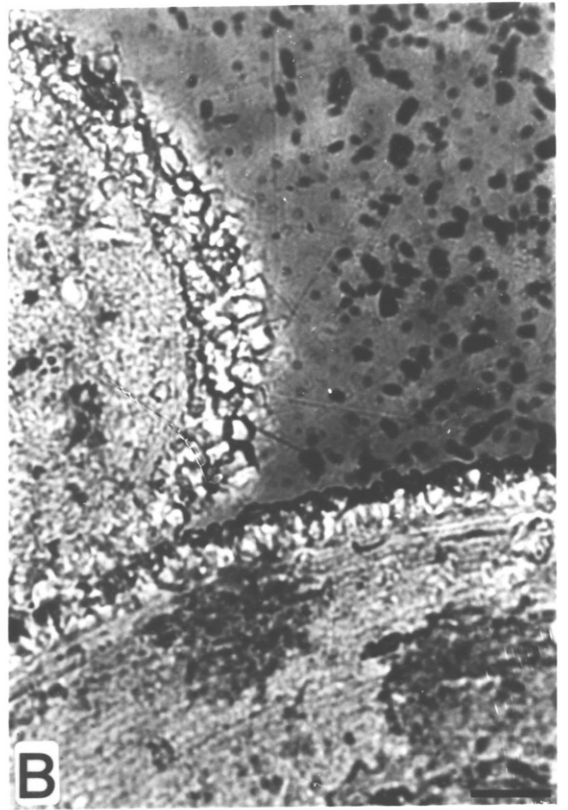


PLATE 3.3



that generated using sediment BSO. Coated grains show the development of a single layer of cement crystals while peloids show the development of multiple layers of cement crystals (see Plate 3.3 B).

Secondary Porosity: Oomoldic porosity has been created in the cortices of coated grains by the dissolution of aragonite lamellae (see Plate 3.3 A) while micro-porosity has been created in micritic peloids (see Plate 3.3 A). Both of these types of porosity are similar to those observed in experiments using sediment BSO.

Replacement Textures: The infilling of oomoldic porosity by solution cavity fill is well developed and takes two forms. The most common form is where the original lamellar cortices of coated grains have been partially replaced by calcite retaining the original outline of the grain (similar to that observed in the partially lithified sediment BSO, see Plate 3.3 A). The second form has developed where the solution cavity was sufficiently large to be filled by sparry calcite as shown in Plate 3.3 C. Neomorphic spar (typically less than 10 μm diameter) has been found replacing micritic peloids, where patches of calcite larger than the original micritic aragonite, are observed (see Plate 3.3 A and D).

All diagenetic textures generated are therefore very similar

to those found in experiments where sediment BSO was used. XRD data however showed that 20-25% of the original aragonite was removed, slightly more in experiments using sediment BSO.

(3) Abu Dhabi Beach Ooids (ADBO)

Abu Dhabi Beach Ooids (ADBO) were used as the starting sediments for experiments 1785 and 37/2. The conditions under which these were run are given in Table 3.3.

Expt. No.	Time(days)	Temp.(°C)	Press.(MPa)	
			μ	σ
1785	47	186	6.0	0.7
37/2	47	183	7.9	1.3

Table 3.3 - Conditions for experiments run using sediment ADBO.

Cement: The partially lithified sediments from both experiments display a cement fabric which is composed of equant crystals (see Plate 3.4 A and B), very different from those previously described from experiments using sediments BSO and ADDO. SEM observation show these crystals to be of a rhombohedral morphology, similar to those precipitated using sediment SBO (see Plate 3.5). The size of these

PLATE 3.4- ABU DHABI BEACH OOIDS

(A) Experiment 1785 - Continuous and discontinuous fringes of equant cement crystals surround sediment grains. Clusters of cement crystals are associated with areas of organic matter (OM). Secondary porosity (P) has been created in the cortices of coated grains and micro-porosity in areas of micrite. An anhydrite lath (An) is observed in the sediment pore space. Back-scatter electron image. Scale bar 50 μm .

(B) Experiment 37/2 - An irregular mosaic of neomorphic calcite (N) replaces the cross-lamellar structure of an aragonitic shell fragment (A). Areas of oomoldic porosity and micro-porosity are also seen. Areas of original aragonite occur between some of the neomorphic spar. Isolated, equant cement crystals occur along the grain edge. XP. Scale bar 20 μm .

(C) Experiment 37/2 - Detail of fabric shown in Plate 3.4 B. Note how the neomorphic spar (N) and the skeletal aragonite (A) interfinger. XP. Scale bar 20 μm .

(D) Experiment 1785 - Detail of neomorphic calcite (N) replacing an aragonitic shell fragment (A). This is not the same grain as featured in Plate 3.4 (B) or (C). The aragonite and calcite boundaries interfinger but the boundaries between spar crystals are much straighter. XP. Scale bar 50 μm .

PLATE 3.4

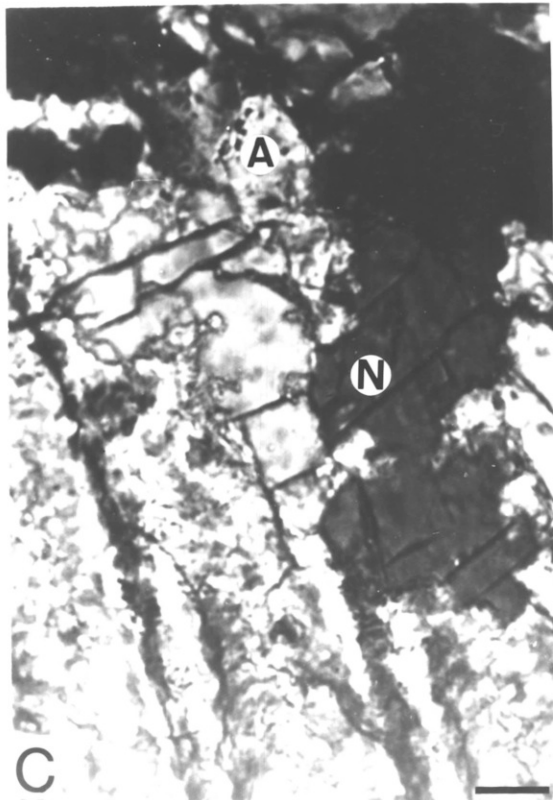
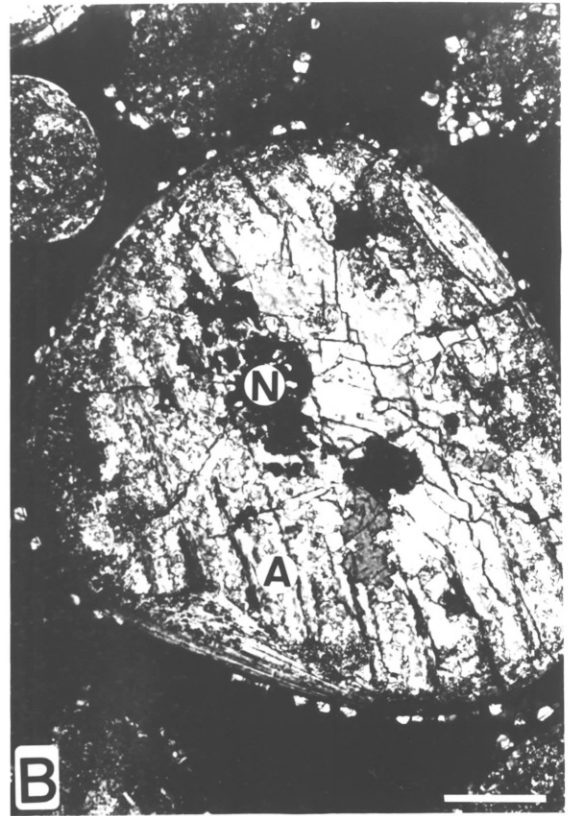
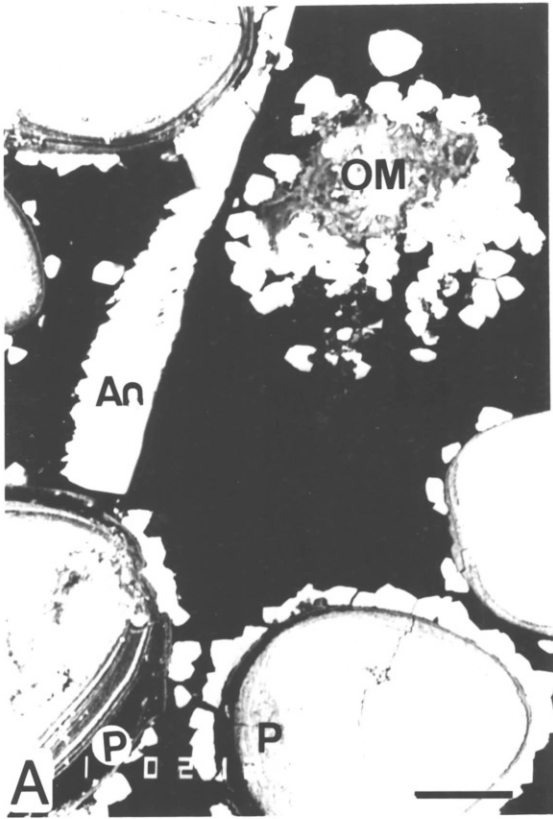


PLATE 3.5 - SECONDARY ELECTRON 3-D IMAGES OF CEMENT
CRYSTALS

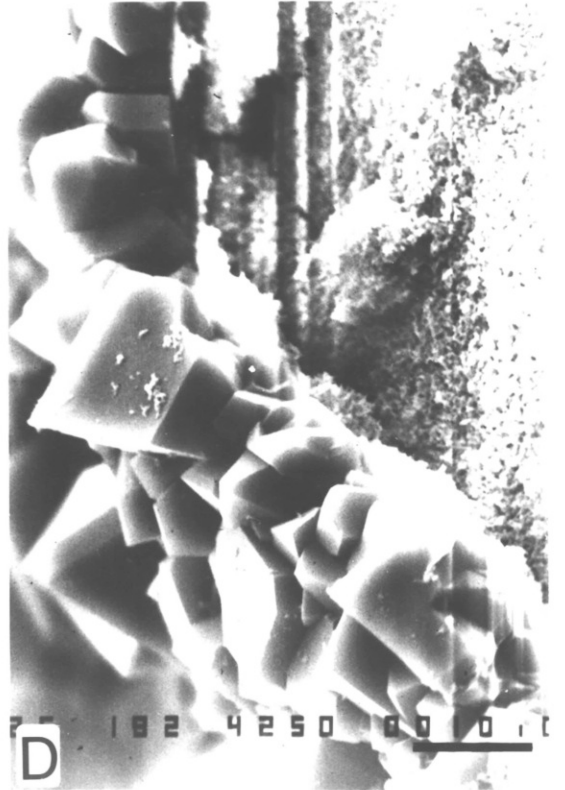
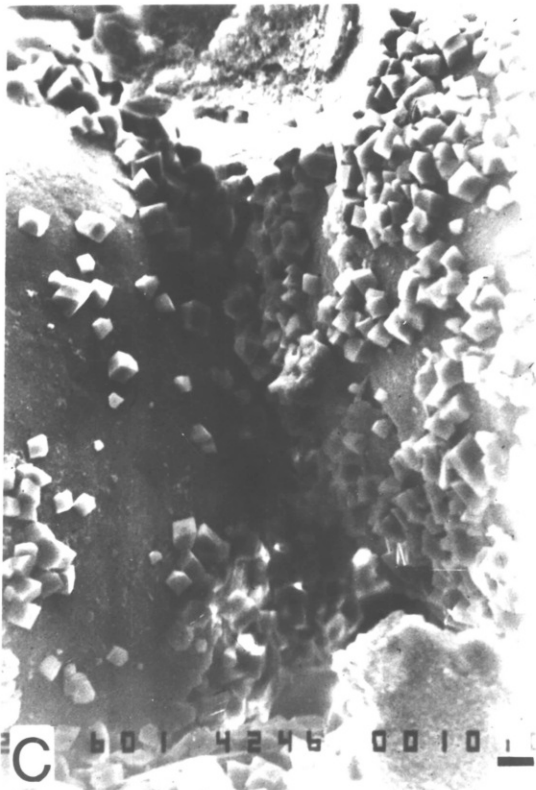
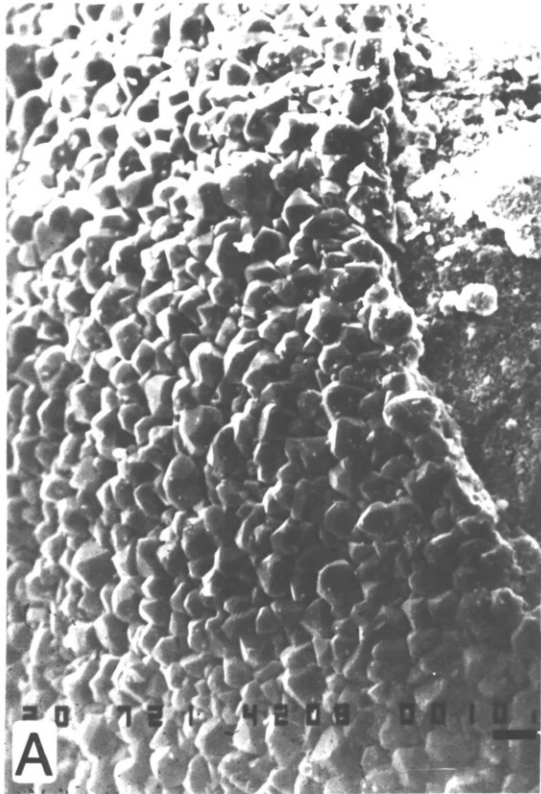
(A) Experiment 1685 - Isopachous layer of granular-bladed cement crystals on sediment grain. The cement crystals are tightly packed leaving little room in which further growth sideways could occur. Scale bar 10 μm .

(B) Experiment 1685 - Detail of isopachous cement crystals. In 3-D, these crystals show a 'baton' type of morphology. Scale bar 10 μm .

(C) Experiment 1584 - Equant cement crystals. The isolated nature of the crystals is clearly shown. More rhombohedral crystal faces are developed than in the granular-bladed fabric. Scale bar 10 μm .

(D) Experiment 1584 - Detail of equant crystals. These crystals form a more continuous fringe than those shown in Plate 3.5 C. Scale bar 10 μm .

PLATE 3.5



crystals ranges from about 7 μm to 30 μm , with an average of 15 μm . They are much larger than the crystals generated in the granular-bladed fabric and form discontinuous rims. Clusters of cement crystals on organic matter are common (see Plate 3.4 A).

Secondary porosity: The creation of pore space is limited when compared to experiments using sediments BSO and ADDO. Where found, it takes the form of oomoldic porosity (see Plate 3.4 A) with a small amount of micro-porosity developed in micritic peloids (see Plate 3.4 A and B).

Replacement Textures: Solution cavity fill of oomoldic porosity is limited (see Plate 3.4 A). Most replacement in these sediments is of a neomorphic origin, in particular of shell fragments (which are more abundant than in sediments BSO and ADDO). Plate 3.4 B and C shows the results of neomorphic replacement of an aragonitic shell fragments. The cross-lamellar structure of the shell fragments (A) has been partially replaced by an irregular mosaic of sparry calcite crystals (N). Areas of aragonite exist between the neomorphic crystals and all phase boundaries are very irregular (see Plate 3.4 C). Plate 3.4 D shows the results of neomorphism in a shell fragment from experiment 1785. The boundary between the original aragonite (A) and the neomorphic spar (N) is irregular but the boundaries between the neomorphic spar crystals are much straighter when

Compared to those in Plate 3.4 B and C. The neomorphic crystals shown in Plate 3.4 D are also much larger than those in Plate 3.4 C.

XRD aragonite conversion data show that a significantly smaller amount of the original aragonite has been removed (<5%) when compared to sediments BSO and ADDO (10-25% and 20-25% respectively) which correlates with the lack of secondary porosity, generated through the dissolution of aragonite.

(4) Kuwait Subtidal Ooids (AKSO)

Kuwait Subtidal Ooids (AKSO) were used as the starting sediment in experiments 2185, 32/1 and 37/3. The conditions under which these were run are given in Table 3.4.

Expt.No	Time(days)	Temp.(°C)	Press.(MPa)	
			μ	σ
2185	38	186	11	2.3
32/1	40	183	7.4	1.2
37/3	47	183	7.9	1.3

Table 3.4 - Conditions for experiments run using sediment AKSO.

Cement: The cement fabric that has been developed on the grains of these sediments is found to be a mixture of granular-bladed and equant (see Plate 3.6 A) crystal morphologies, varying from grain to grain. The cement crystals form isopachous fringes (approximately 12 μm in width on sediment grains). Differences in the cement type is shown in Plate 3.6 B where the occurrence of a bladed cement fringe is seen on a bivalve shell fragment (B) while a coated grain displays a cement fringe of granular-equant crystals (G). Plate 3.7 C shows an inner layer of granular cement (G) overgrown by larger equant crystals (C). Optically continuous overgrowths of calcite (O) are observed on echinoid fragments (see Plate 3.6 A)

Secondary Porosity: The typical development of oomoldic porosity is observed where cortical aragonite has been dissolved from coated grains (see Plate 3.6 A and 3.7 A) and micro-porosity has been created in micritic carbonate (see Plate 3.7 A and B). Occasional shell fragments also display the effects of dissolution (see Plate 3.7 A and B). In these cases certain zones of the shell structure have been exploited as shown in Plate 3.7 B but such examples are unusual.

Replacement Textures: Replacement fabrics are found to be

PLATE 3.6 - AL-KHIRAN SUBTIDAL OIDS

(A) Experiment 37/3 - Isopachous fringes of bladed, granular and equant cement crystals (C) surround sediment grains. Discontinuous calcite overgrowths (O) grow in optical continuity off echinoderm fragments. A considerable amount of secondary porosity has been created in the sediment (P). PPL. Scale bar 100 μm .

(B) Experiment 2185 - The morphology of the cement crystals varies from grain to grain. A bladed cement fringe (B) grows off the substrate of a bivalve fragment while granular-equant cement crystals (G) surround a coated grain. PPL. Scale bar 50 μm .

(C) Experiment 2185 - An irregular mosaic of neomorphic spar (N) totally replaces the structure of a gastropod shell fragment. PPL. Scale bar 100 μm .

PLATE 3.6

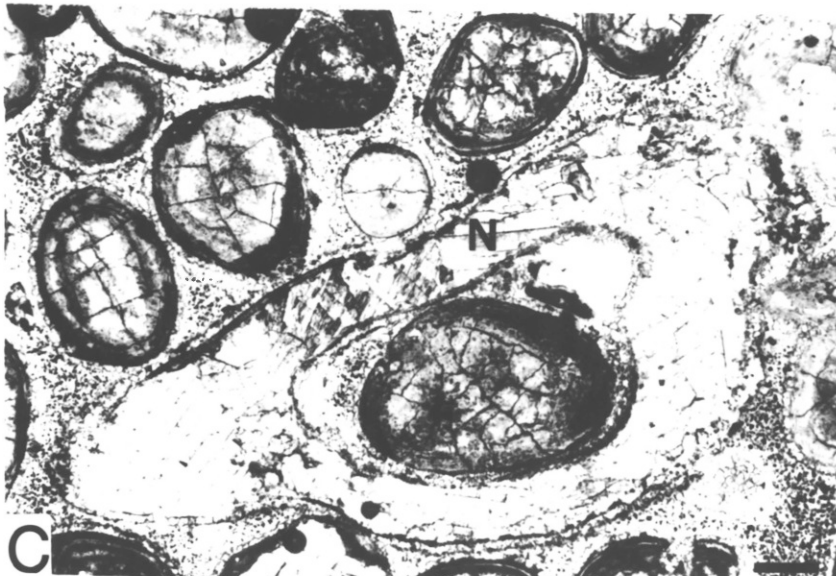
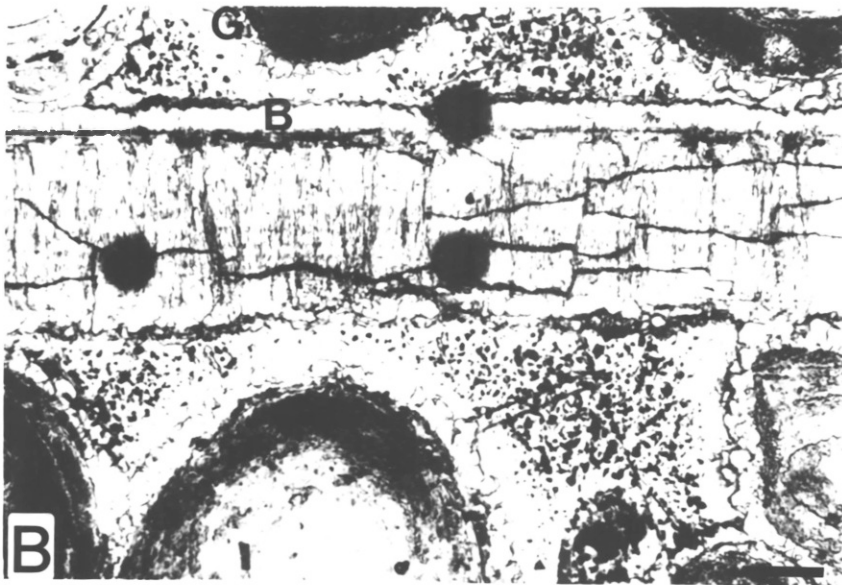
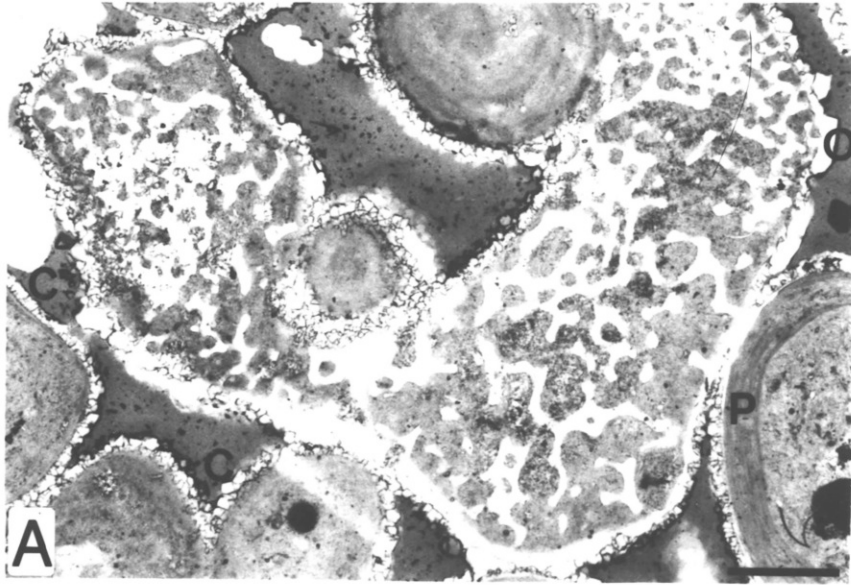


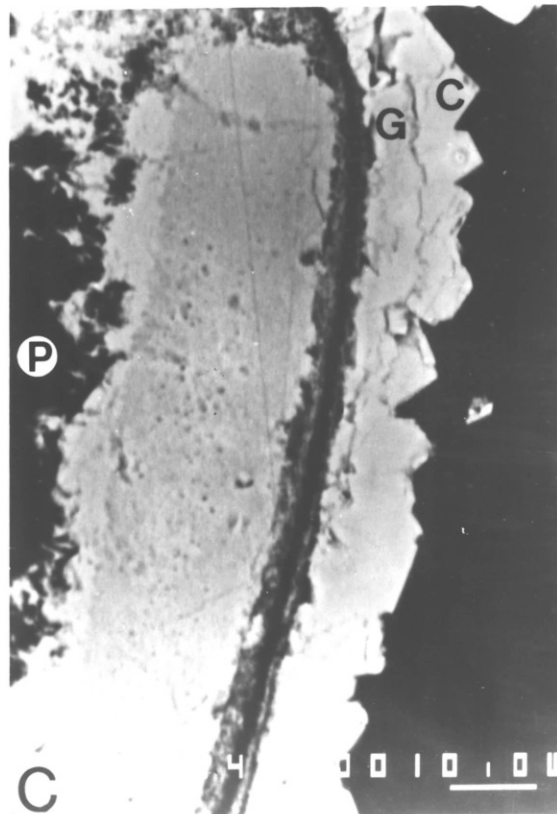
PLATE 3.7 - AL-KHIRAN SUBTIDAL OIDS

(A) Experiment 2185. Isopachous fringes of bladed, granular and equant cement crystals surround sediment grains. A considerable amount of secondary porosity has been created particularly in the cortices of coated grains (see grains in top and bottom right hand corners). Micro-porosity has been created in the bottom right hand grain by the removal of micrite. Some secondary porosity has also been created by the dissolution of skeletal aragonite (A) and has been partially infilled by solution cavity fill calcite (R). Back-scattered secondary electron image. Scale bar 100 μm .

(B) Experiment 37/3 - The structure of an aragonite shell fragment has been exploited during dissolution. Micro-porosity (P) has also been created in the micrite. Back-scattered secondary electron image. Scale bar 10 μm .

(C) Experiment 37/3 - Outer fringe of equant cement crystals (C) overlies an inner granular-bladed fringe (G). Secondary porosity (P) has been created by the removal of aragonite. Back-scattered secondary electron image. Scale bar 10 μm .

PLATE 3.7



predominantly neomorphic in origin (see Plate 3.6 C).

Replacement of grains by solution cavity fill calcite is however observed. Plate 3.7 A shows a shell fragment (A) undergoing dissolution to form secondary porosity which has been partially infilled by solution cavity fill calcite (R).

XRD data show that 10-25% of the original aragonite has been removed.

(5) Kuwait Dune Ooids (AKDO)

Kuwait Dune Ooids (AKDO) were used as the starting sediments in experiments 2085 and 37/4. The conditions under which these were run are given in Table 3.5.

Expt.No.	Time(days)	Temp.(°C)	Press.(MPa)	
			μ	σ
2085	42	186	7.6	1.4
37/4	47	183	7.9	1.3

Table 3.5 - Conditions for experiments run using sediment AKDO.

Cement: In this set of experiments, the cement that has been precipitated on the grains is composed of isopachous rims of bladed-granular cement crystals (see Plate 3.8 A-D). The width of these fringes varies from 9 to 18 μm with the

PLATE 3.8 - AL-KHIRAN DUNE OOIDS

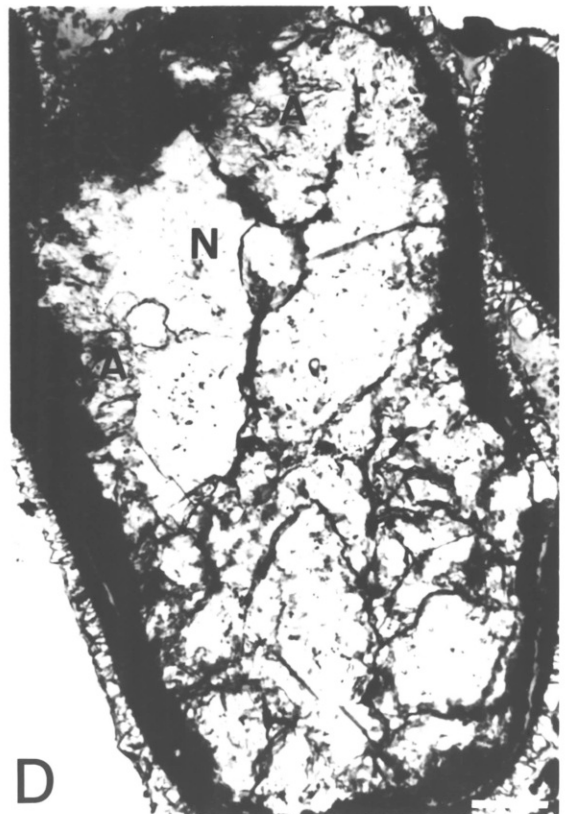
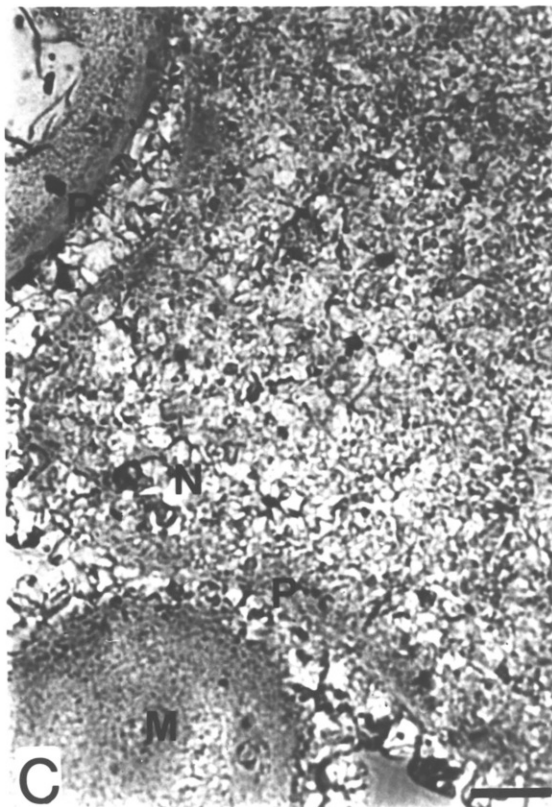
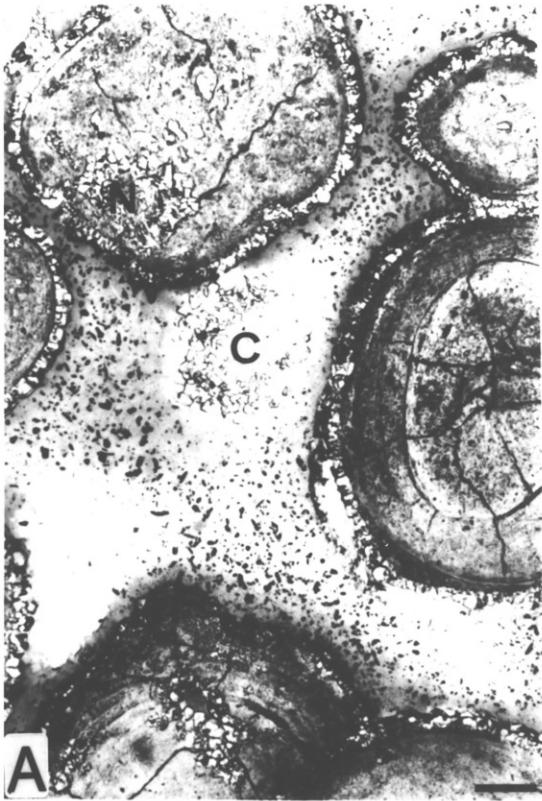
(A) Experiment 37/4 - An isopachous fringe of granular-bladed cement crystals surround each sediment grain. A cluster of cement crystals (C) is observed in the sediment pore space. Neomorphic spar (N) replaces some of the original micrite. PPL. Scale bar 50 μm .

(B) Experiment 37/4 - An isopachous fringe of granular-bladed cement crystals surround each sediment grain. Note how cement crystals are clustered in the bored surfaces of a coated grain (C). The secondary porosity created in the cortices of coated grains (P) can be clearly observed in the middle grain. PPL. Scale bar 50 μm .

(C) Experiment 37/4 - Detail showing areas of secondary porosity (P) and neomorphic spar (N) which replaces micrite. Microporosity is present in some of the original micritic grains (M). PPL. Scale bar 20 μm

(D) Experiment 2085 - Shell fragment almost totally replaced by neomorphic spar (N). Areas of relic aragonite (A) remain. PPL. Scale bar 50 μm .

PLATE 3.8



widest cement fringes being found on peloids. Cement clusters are again observed (see Plate 3.8 A)

Secondary Porosity: Oomoldic porosity is very well developed (see Plate 3.8 B and C), with small amounts of micro-porosity being developed in micrite (see Plate 3.8 C).

Replacement Textures: Replacement textures are limited with no large scale infilling of the oomoldic porosity which was generated (see Plate 3.8 A-C). Neomorphic calcite (N) replaces micrite (see Plate 3.8 A and C) while shell fragments are occasionally observed to be replaced by irregular mosaics of neomorphic spar (see Plate 3.8 D). Relic aragonite structures within the neomorphic spar are very occasionally seen (see Plate 3.8 D).

XRD data shows that 20-40% of the original aragonite has been removed.

(6) Shark Bay Ooids (SBSO, SBDO and SBO)

Shark Bay Ooids were used as the starting sediments in experiments 1384, 3386 (SBSO); 1584 (SBDO) and 34/4 (SBO). The conditions under which these experiments were run are given in Table 3.6.

Expt.No	Time(days)	Temp.(°C)	Press.(MPa)	
			μ	σ
1384	30	186	9.8	1.4
3386	44	186	8.9	1.0
1584	31	186	6.6	1.2
34/4	37	183	7.7	0.7

Table 3.6 - Conditions for experiments run using Shark Bay Ooids.

Cement: The cement crystals generated in experiments using Shark Bay Ooids, are typically equant in morphology. These are shown in Plate 3.9 A-D. These crystals are often isolated, forming a discontinuous rim around grains (see Plate 3.9 D). SEM observation shows these crystals to be rhombohedral (see Plate 3.5). However, occasional rims of more granular-bladed crystals (C) are also observed (see Plate 3.9 C). Areas of organic matter and bored grain surfaces often display a thicker coating of smaller, granular cement crystals than other grains (see Plate 3.9 A and D). The width of this fringe varies from 15 - 50 μm but typically a single crystal layer of cement is around 20 μm in width (see Plate 3.9 B).

Secondary Porosity: Oomoldic porosity is very well developed as shown in Plate 3.9 A, B and D with small areas of micro-porosity (see Plate 3.9 B).

PLATE 3.9 - SHARK BAY OIDS

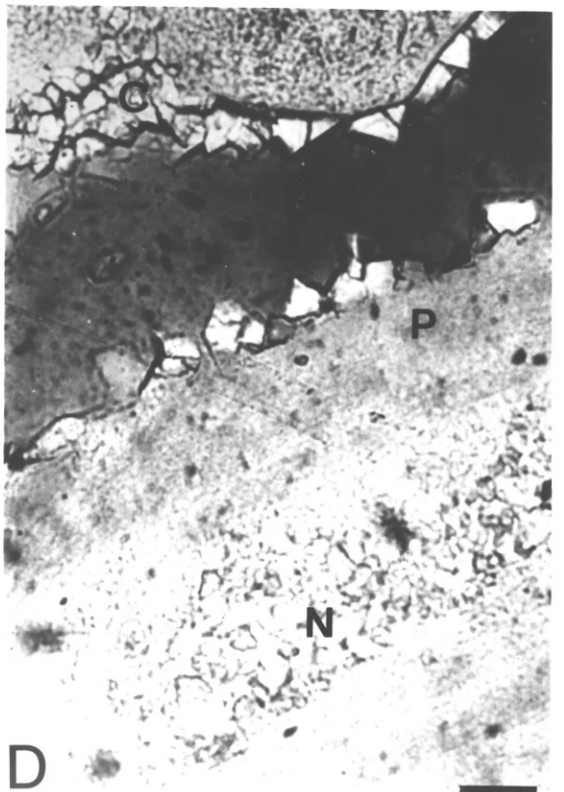
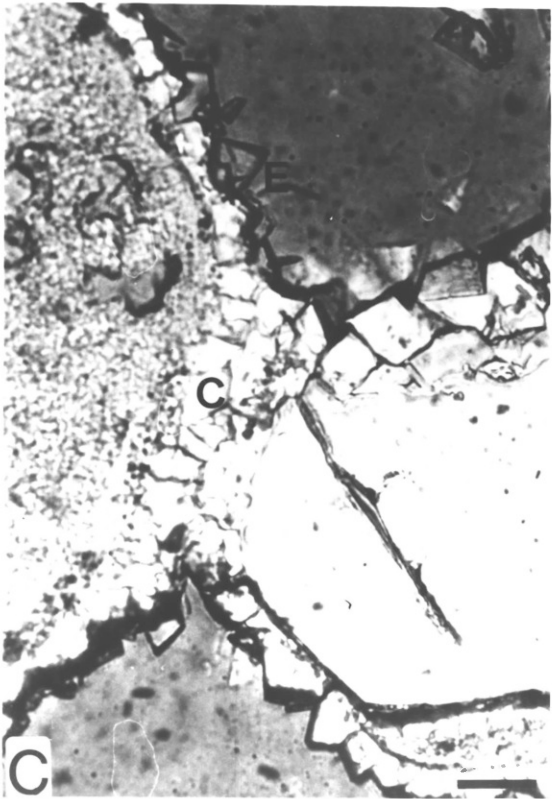
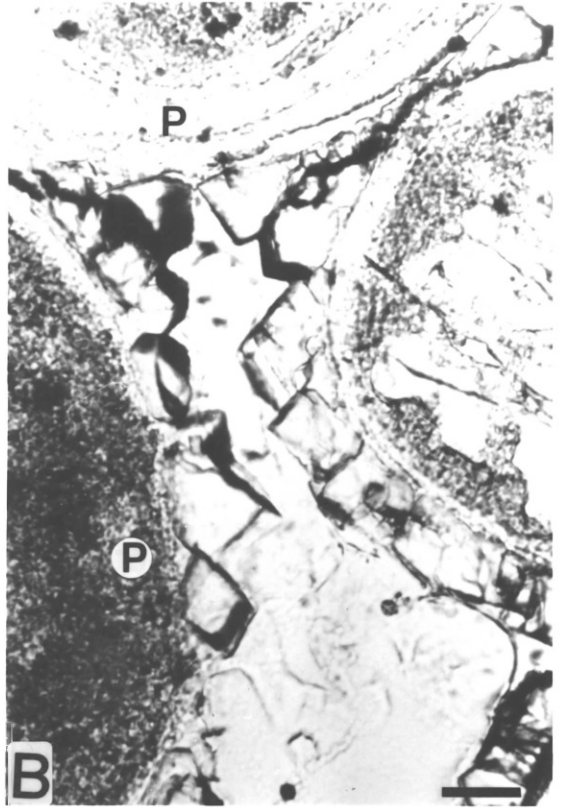
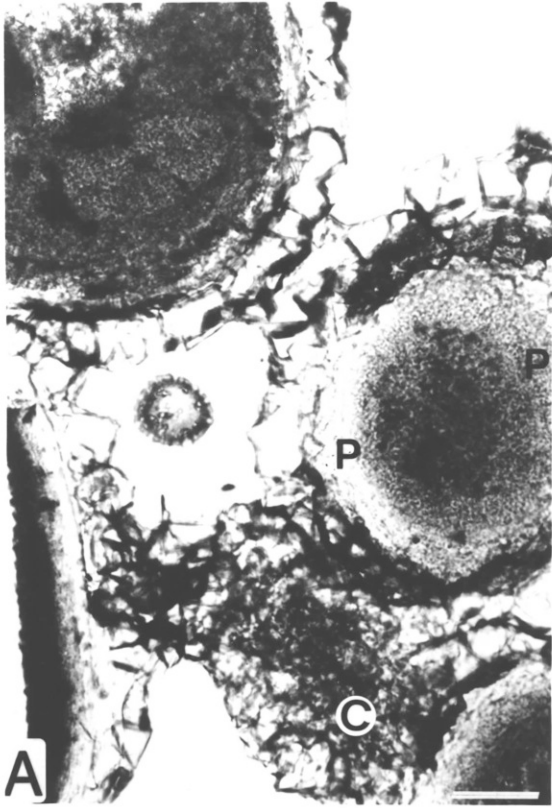
(A) Experiment 1584 - Equant cement crystals surround sediment grains. A cluster of cement crystals is observed in the sediment pore space (C). Secondary porosity (P) has been created in the cortices of coated grains and in micritic carbonate. PPL. Scale bar 75 μm .

(B) Experiment 1584 - Equant cement crystals surround sediment grains. Secondary porosity (P) has been created in the cortices of coated grains and in micrite. PPL. Scale bar 20 μm .

(C) Experiment 3386 - Right hand grain (quartz) displays a fringe of equant cement crystals while the left hand grain (peloid) displays a fringe which is composed of granular-bladed crystals (C) with an outer equant (E) layer. PPL. Scale bar 20 μm .

(D) Experiment 34/4 - Discontinuous rims of equant cement crystals surround grains. Clusters of granular crystals (C) occur in bored surfaces of grains. Secondary porosity (P) has been created in the cortices of coated grains with neomorphic spar (N) replacing some of the micrite. PPL. Scale bar 20 μm .

PLATE 3.9



Replacement Textures: Most of the secondary porosity which was created during the experiments remains unfilled. The replacement of micritic peloids by neomorphic spar, is the most common form of replacement (see Plate 3.9 D).

XRD data show that 0-25% of the original aragonite was removed.

(7) SUMMARY

Differences in diagenetic textures were observed between sediment types. Each sediment type however displayed the same type of textures when tested under a variety of experimental conditions of time, temperature and pressure although the degree of alteration was found to vary slightly.

(i) Cement Morphology.

Cement morphologies range between two end members.

(a) Granular-bladed cement crystals - these form an isopachous fringe of small crystals. The maximum width of this type of cement fringe is around 20 μm , typically 6 - 13 μm .

(b) Equant cement crystals - these are larger crystals than those in type (a). Individual crystals range from 10 - 30

μm across, typically 15-20 μm , with maximum cement fringe widths of 50 μm . This type of cement is formed by either a continuous or discontinuous layer of crystals.

Micritic peloids and areas of organic matter in all partially lithified sediments, often show multiple layer cement fabrics while coated grains typically display only one layer of cement crystals.

In most cases the partially lithified sediments are characterised by having a cement fabric of either type (a) or type (b) but variations in that fabric from grain to grain have been noted.

(ii) Intra-grain textures.

Each grain type is found to react differently.

(a) Coated grains - the aragonitic cortex of coated grains is greatly affected by dissolution in most cases. The secondary porosity (oomoldic) which is created is, in some cases, partially infilled by low-Mg calcite. The morphology of the crystals infilling the porosity depends on the size of the pore space being filled.

(b) Micritic peloids - some dissolution of the micritic aragonite is found to occur, forming micro-porosity.

Usually however, alteration of the original aragonite is marked by patches of neomorphic spar (calcite) often around

4-5 μm , with maximum sizes of around 10 μm .

(c) Aragonitic shell fragments - are either affected by dissolution forming secondary porosity or, more commonly, undergo neomorphism. Where they have reacted, the shell fragments have usually been totally replaced by neomorphic spar but intermediate stages are found. Original shell structures are found co-existing with the neomorphic spar and the two phases are separated by an alteration front of sub-micron size (below the resolution of normal optical microscopes).

3.5.2 PORE FLUID AND CEMENT CRYSTAL CHEMISTRY

In this section, the pore fluid chemical composition trends and the electron microprobe chemical analyses for cement crystals are presented. The cement crystals are likely to have been precipitated directly from the pore fluids while solution cavity fill and neomorphic spar phases because of the closeness of the sites of dissolution and precipitation, may have been influenced in their chemistry by the material which they replace. Any relationship which may exist between the fluids and solids will therefore be most easily seen using pore fluid and cement geochemical data. Analyses for solution cavity fill calcite and neomorphic spar, together with data for relic aragonitic and calcitic phases, are presented in Chapter 6.

(1) Pore Fluid Evolution

The evolution of the pore fluids for each group of experiments are shown in Fig. 3.3 (a)-(e). Each graph shows an overall decrease in the $m\text{Mg}^{2+}/m\text{Ca}^{2+}$ ratio due to the removal of Mg^{2+} from the pore fluids by the precipitation of cement and possibly a small amount of magnesium oxysulphate and possibly by the adsorption of Mg^{2+} onto grain surfaces (Berner, 1975). In most cases, the $m\text{Sr}^{2+}/m\text{Ca}^{2+}$ ratio increases continuously due to the dissolution of aragonite and hence release of Sr^{2+} . Experiment numbers marked by (eq) however indicate that the $m\text{Sr}^{2+}/m\text{Ca}^{2+}$ ratio for that experiment increased to an apparent maximum, after which the $m\text{Sr}^{2+}/m\text{Ca}^{2+}$ ratio decreased slightly.

(i) Bahaman Subtidal Ooids (Fig. 3.3(a))

Three apparent trends in the data are observed. The trends for experiments 30/1 and 34/3 are consistent. These were both run in the smaller of the two types of cell (see section 2.2.2) at 183°C . Experiments 1685 and 4086 however, were run in the larger cell at temperatures of 186°C and 200°C respectively. The shift in the $m\text{Sr}^{2+}/m\text{Ca}^{2+}$ ratio towards higher values at the beginning of experiment 1685 from that of 30/1 and 34/3, represents a relative increase in the

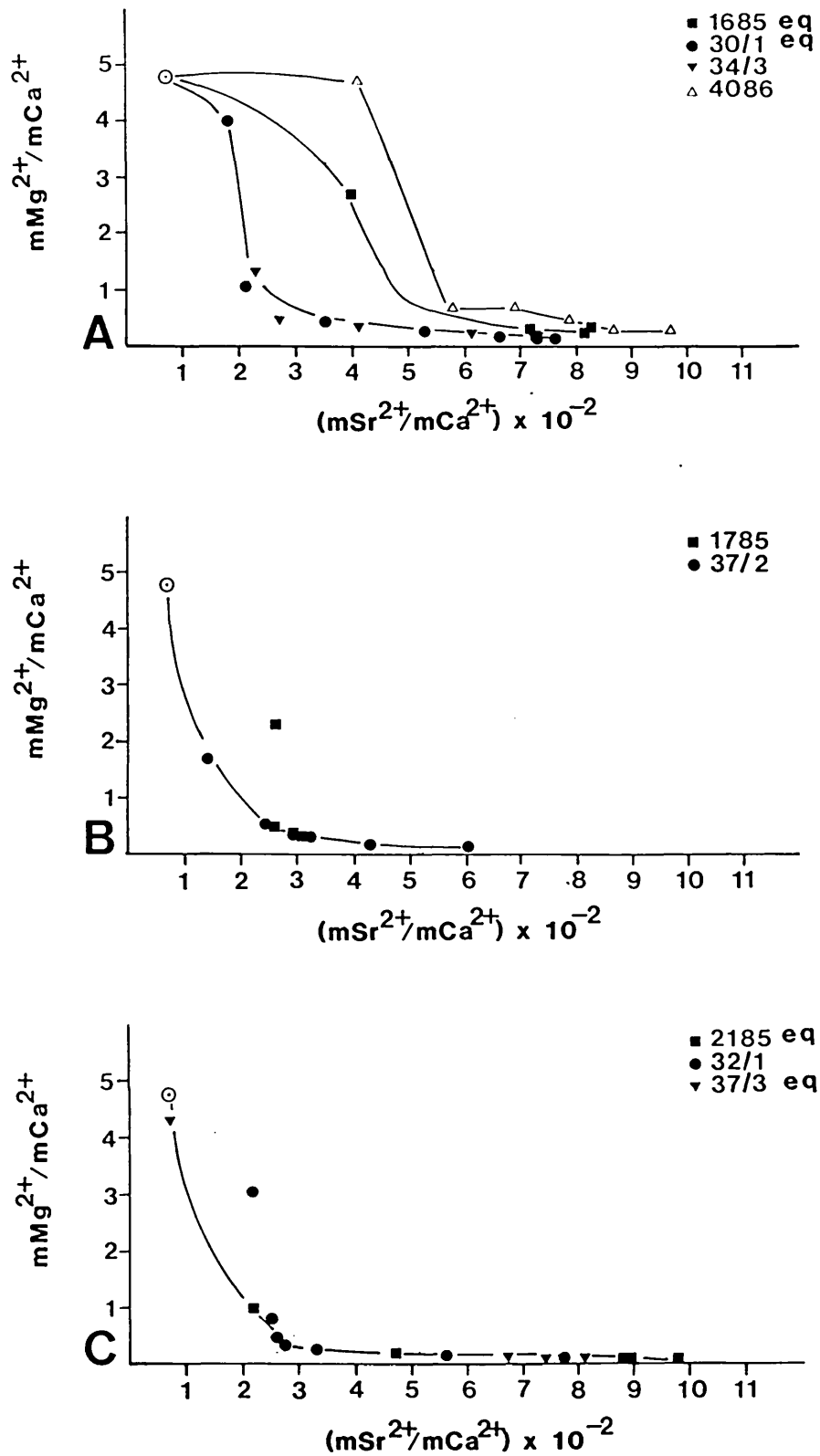


Fig. 3.3 - Evolution of pore fluids from the composition of seawater (⊙) during experiments using (A) sediment BSO, (B) sediment ADBO and (C) sediment AKSO.

level of Sr^{2+} in the pore fluid but that of 4086 represents a relative decrease in the level of Ca^{2+} (see Appendix I).

Although there is a relationship between temperature and the $\text{mSr}^{2+}/\text{mCa}^{2+}$ ratio, no relationship between the aragonite dissolution rate and temperature (in the range 183-200°C) is observed.

Each experiment run shows an initially high $\text{mMg}^{2+}/\text{mCa}^{2+}$ ratio which falls to less than 1 in the first two weeks of each experiment, and relatively high (see Table 3.9) final $\text{mSr}^{2+}/\text{mCa}^{2+}$ values (0.1 maximum).

(ii) Abu Dhabi Dune Ooids

Experiment 18/1 was part of a group of experiments designed to study the effect of not sampling the pore fluids (see further discussion in section 4.5). No pore fluid data are therefore available. Also, data are only available for the end of experiment 37/1. The maximum $\text{mSr}^{2+}/\text{mCa}^{2+}$ ratio observed was 0.082, at a $\text{mMg}^{2+}/\text{mCa}^{2+}$ ratio of 0.1 - 0.2.

(iii) Abu Dhabi Beach Ooids (Fig. 3.3(b))

One major trend is apparent in both experiments. Initially however, the pore fluids from experiment 1785 appear to deviate from that trend by having a higher $\text{mSr}^{2+}/\text{mCa}^{2+}$

ratio. Experiment 1785 was run at a slightly higher temperature (186 °C) than experiment 37/2 (183 °C), in the larger and smaller cells respectively which may account for the difference. When compared to Fig. 3.3(a), the amount of Sr^{2+} which was released, due to aragonite dissolution, appears to have been greatly reduced. The maximum $\text{mSr}^{2+}/\text{mCa}^{2+}$ ratio observed for 37/2 was 0.06, while that for 1785 was only 0.03 correlating with the low degree of aragonite dissolution noted in both the petrography of the solid and the XRD data (see 3.5.1). It should be noted that experiments 1785 and 37/2 each ran for 47 days, similar to those using sediment BSO (37 and 50 days). The difference in the degree of aragonite dissolution between the two types of sediment cannot be attributed to time but must have been caused by some internal factor in the sediment e.g. a higher proportion of shell fragments in sediment ADBO than in sediment BSO.

(iv) Kuwait Subtidal Ooids (Fig. 3.3(c)).

A similar, early pattern in the $\text{mSr}^{2+}/\text{mCa}^{2+}$ ratios to Fig. 3.3(b), can be seen in Fig. 3.3(c). In this case however, the deviation in the initial trend observed in experiment 32/1 from that of experiments 2185 and 37/3, cannot be correlated with differences in the temperature or the experimental cell in which the experiment was run. A lower sample weight was used in experiment 32/1 than in 37/3

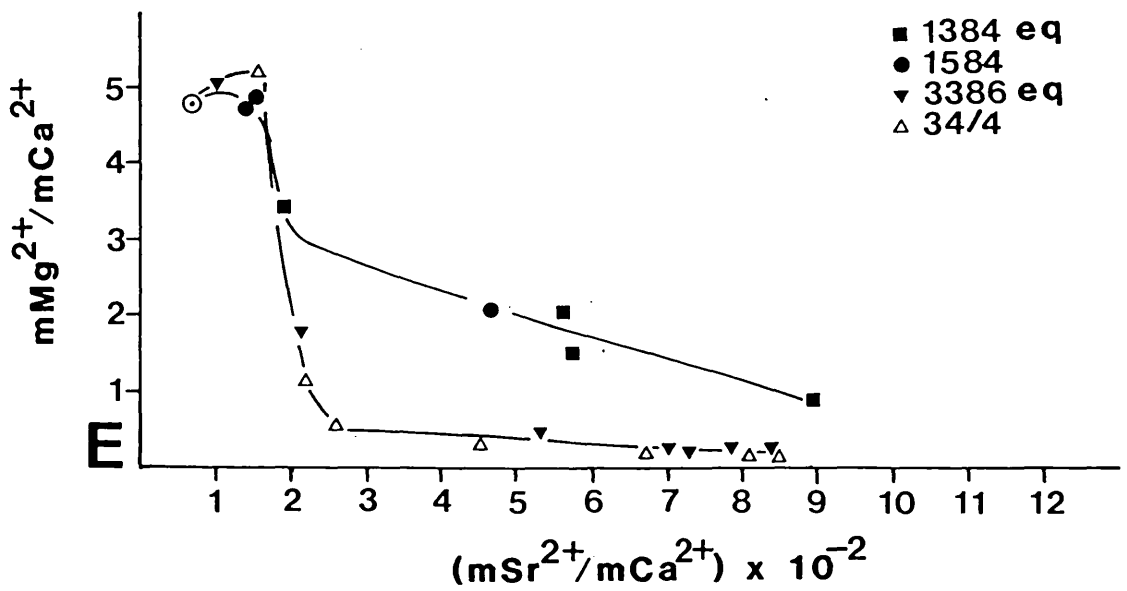
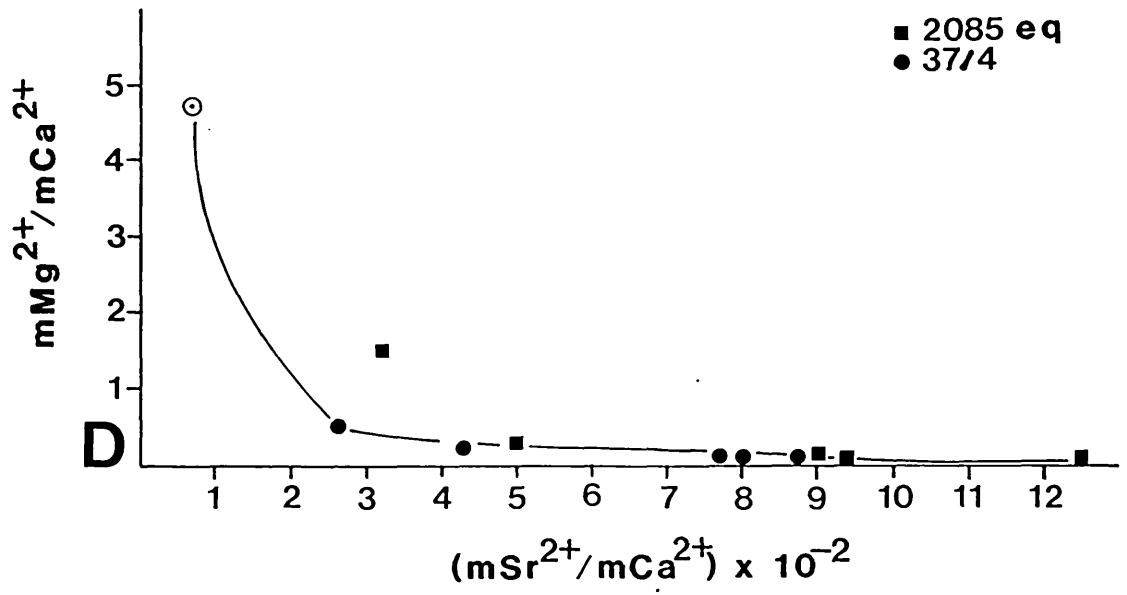


Fig. 3.3 - Evolution of pore fluids from the composition of seawater (⊙) during experiments using (D) sediment AKDO and (E) Shark Bay Ooids.

although both were conducted in the same experimental cell. If the sample weight-fluid ratio had affected the mSr^{2+}/mCa^{2+} ratio then one would have expected the pore fluids of experiment 37/3 to have a greater mSr^{2+}/mCa^{2+} ratio than that of experiments 37/3. A high final mSr^{2+}/mCa^{2+} ratio, similar to that for experiments using sediment BSO (see Fig.3.3(a)), is observed.

(v) Kuwait Dune Ooids (Fig. 3.3(d))

No data for the first pore fluid sample collected from experiment 37/4 are available. The early part of both trends can therefore only be inferred. The trends fall into the pattern observed in other data groups where a higher temperature correlates with a higher initial degree of Sr^{2+} input to the fluids via aragonite dissolution. In this particular group of experiments, an extremely high final value for the mSr^{2+}/mCa^{2+} ratio is observed reaching a maximum of 0.125.

(vi) Shark Bay Ooids (Fig. 3.3(e))

A very different pattern to any of the previous data sets is observed. All experiments are characterised by early mMg^{2+}/mCa^{2+} ratios higher than that of seawater (the starting fluid). After the first samples were collected,

the $m\text{Mg}^{2+}/m\text{Ca}^{2+}$ ratio for experiments 3386 and 34/4, was seen to drop very rapidly to typical levels of less than 1. In experiment 1384 and, in particular, 1584, the $m\text{Mg}^{2+}/m\text{Ca}^{2+}$ ratio remained very high when compared to all other data sets with minimum values of 1.2 and 2.1 respectively. Maximum $m\text{Sr}^{2+}/m\text{Ca}^{2+}$ ratios were around 0.08 to 0.09.

(2) Cement Crystal Chemistry

In the calcite (identified using XRD) cement crystals, there are significant amounts of the trace elements Mg^{2+} , Sr^{2+} , and S^{6+} . The molecular proportions of MgCO_3 and SrCO_3 and SO_4^{2-} in the calcite structure have been calculated by the method described in Appendix IV and the analyses used can also be found in Appendix IV.

(i) Bahaman Subtidal Ooids (Figs 3.4 and 3.5).

Fig.3.4 shows the relationship between the amount of MgCO_3 and SrCO_3 (mole %) held within the structure of the calcite cement. The composition of the cement varies both within each experiment and also between experiments. The cement precipitated in experiment 1685 appears to contain less MgCO_3 than that of experiment 30/1 while in experiment 4086, the composition of the cement, in terms of MgCO_3 , lies between

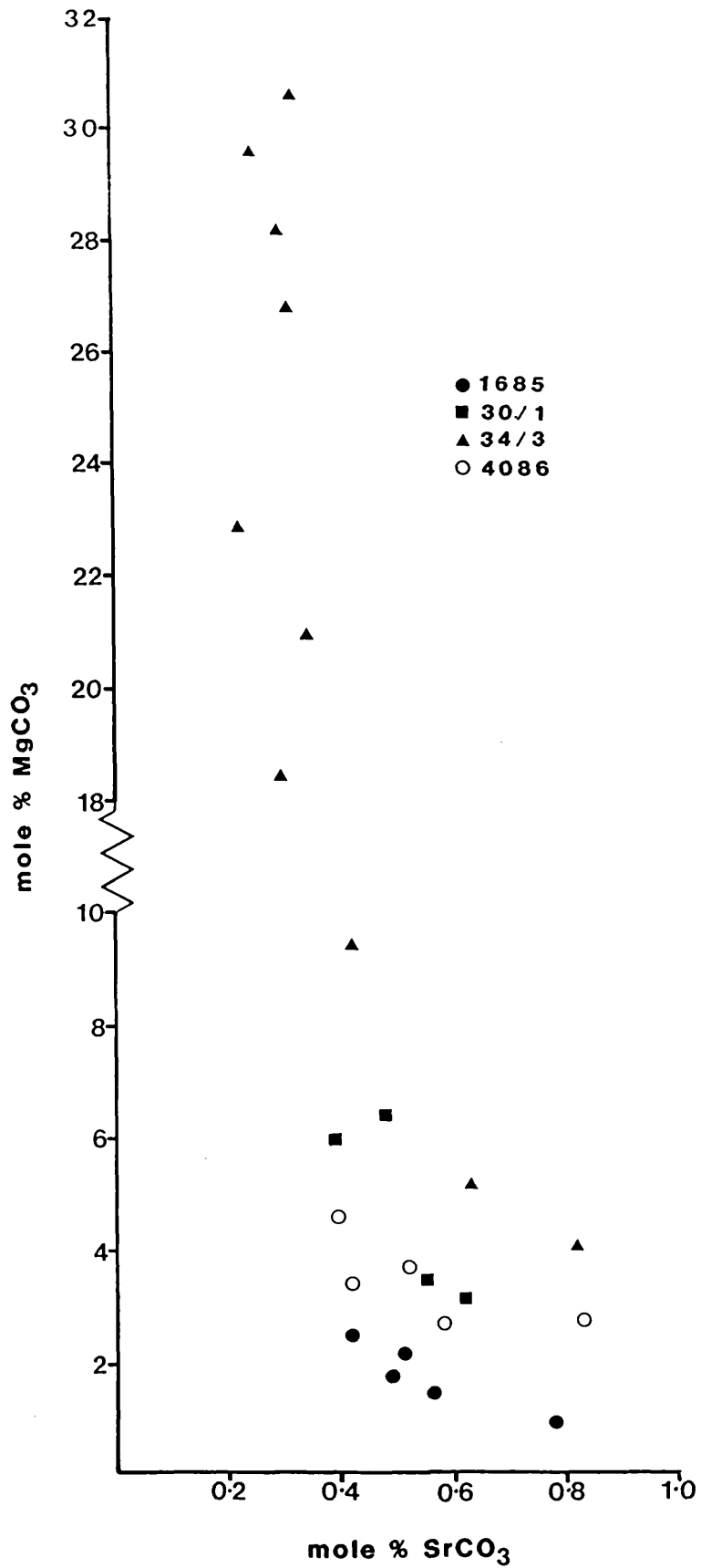


Fig. 3.4 - Mole % MgCO₃ and SrCO₃ contained in cement crystals precipitated during experiments using sediment BSO.

that of experiments 1685 and 30/1. The cement precipitated in experiment 34/3 however contains significantly more MgCO_3 than the cement in any of the others. On examination of the thin sections, the cement crystals precipitated in experiment 34/3, are very small (Plate 3.2 A and C). Small cement crystals have been found to be relatively enriched in MgCO_3 when compared to larger cement crystals (see section 4.2).

The levels of SrCO_3 found in the cement crystals do not display the same level of variation as the MgCO_3 content. A correlation between the two levels is noted however, the higher the MgCO_3 level of the calcite, the lower the SrCO_3 level.

Analyses through individual crystals (see Table 3.7) indicate that the base of the cement crystal is richer in MgCO_3 than the edge of the same crystal while the level of SrCO_3 display the opposite pattern. Two examples of this are given in Table 3.7.

Expt. No.	30/1		4086	
	MgCO_3	SrCO_3	MgCO_3	SrCO_3
Base	6.39	0.99	5.96	0.40
Edge	3.44	1.24	2.76	0.83

Table 3.7 - MgCO_3 and SrCO_3 (mole%) levels of individual cement crystals. (BSO).

This appears to correspond with the pattern of decreasing $m\text{Mg}^{2+}/m\text{Ca}^{2+}$ and increasing $m\text{Sr}^{2+}/m\text{Ca}^{2+}$ ratios with time observed in the pore fluids.

The precipitated cement phase has also been found to contain significant amounts of SO_4^{2-} . The levels of this are shown in Fig. 3.5. Values range from 0.4 - 1.4 mole % SO_4^{2-} (typically 0.75 - 1.4 mole %). Cement crystals were studied for differences between the bases and edges but no trend was observed.

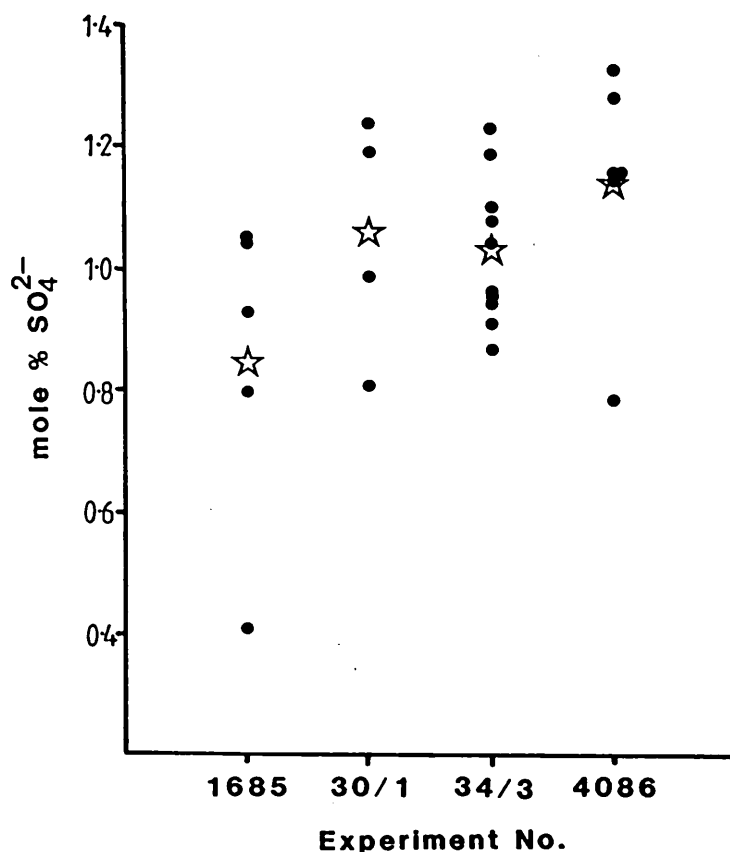


Fig. 3.5 - Mole % SO_4^{2-} contained in cement crystals precipitated using sediment BSO. Mean values (☆) have been shown.

(ii) Abu Dhabi Dune Ooids (Fig.3.6 and 3.7)

The composition of the cement precipitated in experiments using sediment ADDO varies slightly between experiments 18/1 and 37/1, but there is a considerable overlap in the analyses. The level of MgCO_3 varies from 2.4 to 7.2 mole % while that of SrCO_3 is found to vary from 0.38 to 0.87 mole %. The negative correlation between the amount of MgCO_3 and SrCO_3 also being found in this data set (see Fig 3.6).

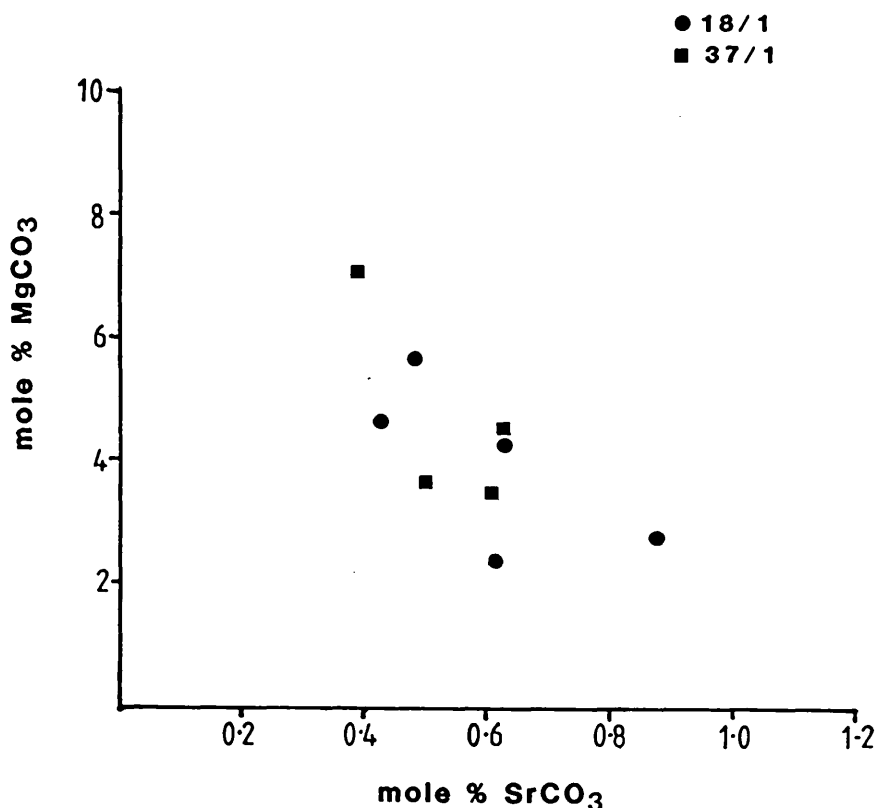


Fig. 3.6 - Mole % MgCO_3 and SrCO_3 contained in cement crystals precipitated using sediment ADDO.

Significant levels of SO_4^{2-} are also found in the cement precipitated during these experiments (see Fig. 3.7). The overall amount of SO_4^{2-} in the cement (range 0.5 - 1.35 mole

%) is similar to that of the cement crystals precipitated in experiments run using sediment BSO. The variation in the amount of SO_4^{2-} in the cement precipitated in experiment 18/1 is less than that found in 37/1.

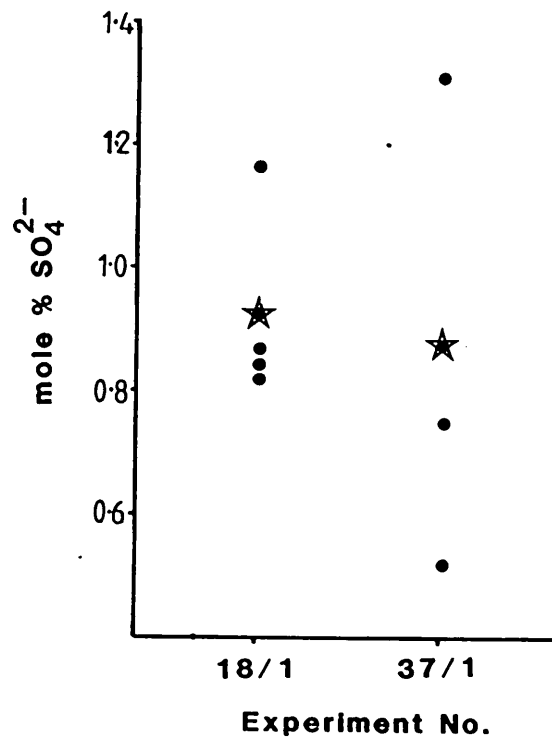


Fig. 3.7 - Mole % SO_4^{2-} contained in cement crystals precipitated using sediment ADDO. Mean values (\star) have been shown.

(iii) Abu Dhabi Beach Ooids (Figs. 3.8 and 3.9)

The cement precipitated in experiment 1785 shows a considerable variation in the amount of MgCO_3 contained within the calcite lattice (1 -12 mole % MgCO_3), see Fig. 3.8. Cores to cement crystals, enriched in Mg^{2+} , were

observed in the partially lithified sediment of this experiment and the data are presented in section 4.2. Generally, there appears to be a relatively high level of MgCO_3 associated with the cement. The level of SrCO_3 (0.2 - 0.8 mole %) is lower than in other data sets although it shows the same magnitude of variation. This correlates with the low levels of Sr^{2+} observed in the pore fluids (see Fig. 3.3 (b)) and the lower levels of aragonite dissolution observed (see section 3.5.1 (3)) when compared to those for experiments using sediments BSO and ADDO. The inverse correlation between MgCO_3 and SrCO_3 is again noted.

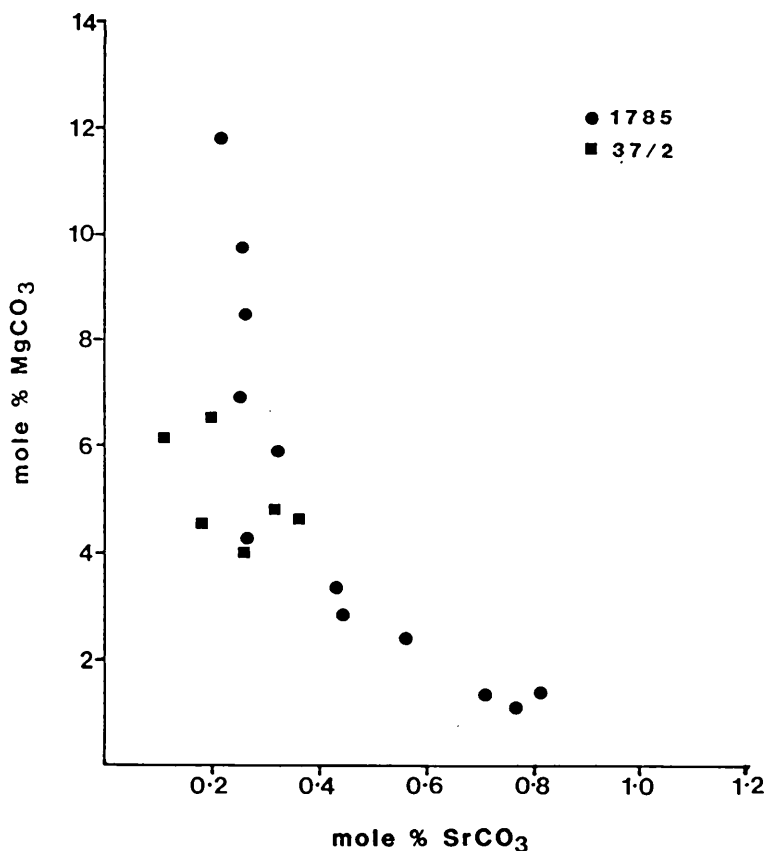


Fig. 3.8 - Mole % MgCO_3 and SrCO_3 contained in cement crystals precipitated using sediment ADBO.

The cement of experiment 37/2 shows a much less pronounced variation in composition with respect to MgCO_3 and SrCO_3 . The inverse correlation between the two phases however is apparent, also the relatively low level of SrCO_3 . The variation in both MgCO_3 and SrCO_3 is comparatively low when compared to those of experiment 1785.

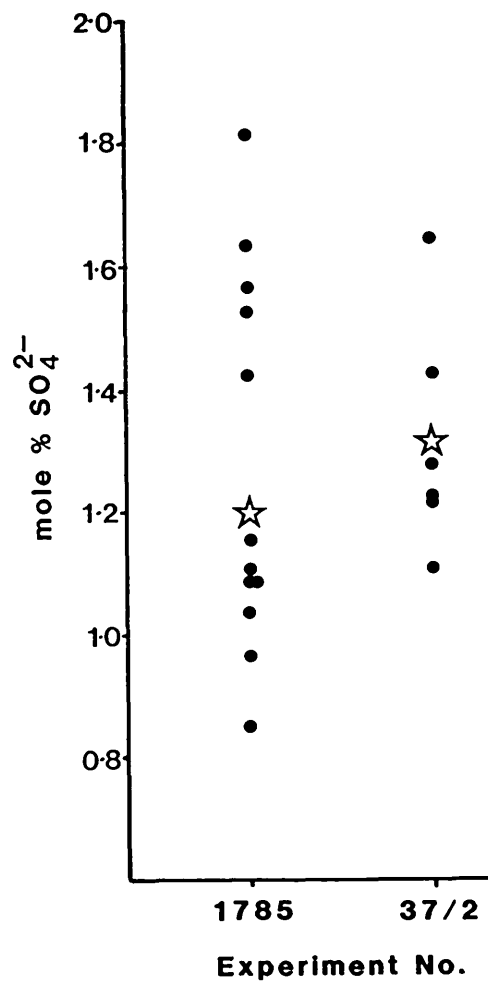


Fig. 3.9 - Mole % SO_4^{2-} contained in cement crystals precipitated using sediment ADBO. Mean values (\star) are shown.

Relatively high levels of SO_4^{2-} are present in the cement of both experiments (see Fig. 3.9). Although the data from the

cement precipitated in experiment 1785 show a larger variation of the SO_4^{2-} level (0.85 - 1.85 mole %) than that of experiment 37/2 (1.1 -1.7 mole %), this may not be significant in terms of the maximum analytical error (see section 2.4.2 (2)).

(v) Kuwait Subtidal Ooids (Figs. 3.10 and 3.11)

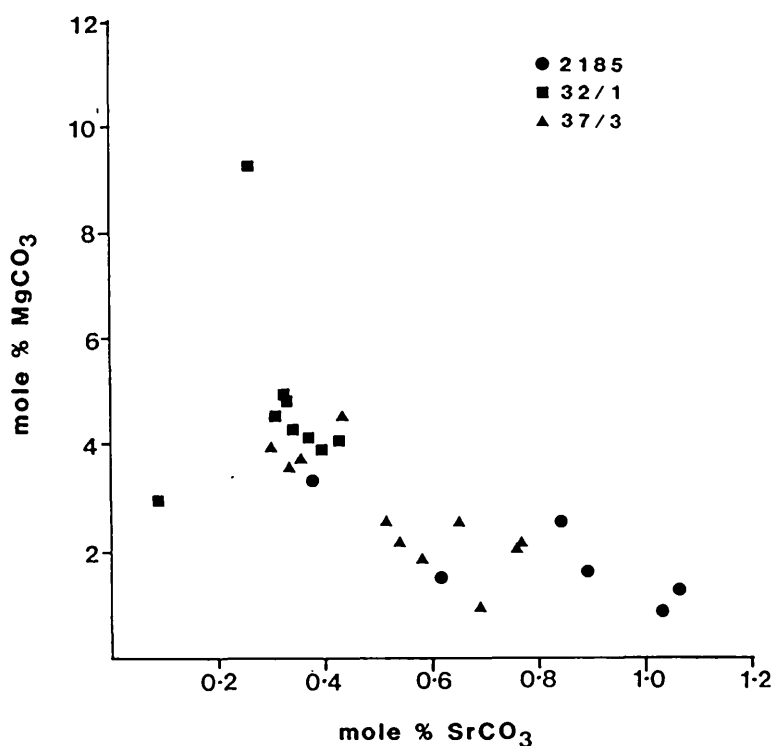


Fig. 3.10 - Mole % MgCO_3 and SrCO_3 contained in cement crystals precipitated using sediment AKSO.

Fig 3.10 shows that, with respect to MgCO_3 and SrCO_3 substitution in the calcite lattice, the cement precipitated in experiments 2185 and 32/1 fall into two distinct areas. The cement of 32/1 has relatively high levels of MgCO_3

(typically 4 - 5 mole %) and low levels of SrCO_3 (typically 0.3 - 0.5 mole %), while that of 2185 shows the opposite pattern i.e. lower levels of MgCO_3 (0.5 - 3.5 mole %) with high levels of SrCO_3 (0.35 - 1.05 mole %). The composition of the cement precipitated in experiment 37/3 lies between that of 32/1 and 2185 in terms of its MgCO_3 and SrCO_3 content. Again there is a negative correlation between the mole % MgCO_3 and SrCO_3 in the cement crystals.

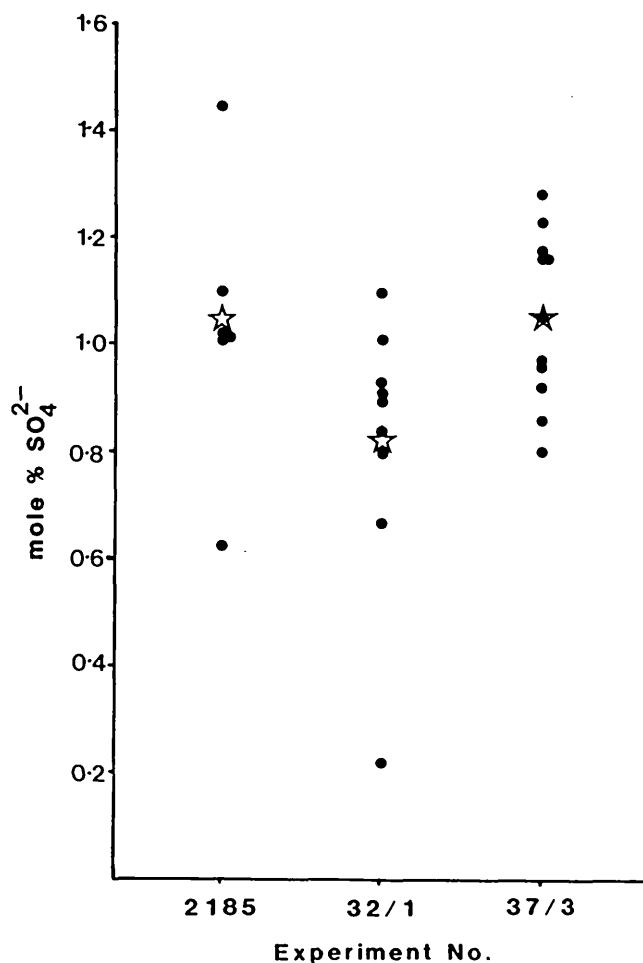


Fig. 3.11 - Mole % SO_4^{2-} contained in cement crystals precipitated using sediment AKSO. Mean values (\star) are shown.

Levels of SO_4^{2-} , similar to those found in the cement of experiments using sediments BSO and ADDO, are present in the cement precipitated using sediment AKSO (Fig. 3.11). The cement generated in all experiments show similar levels of SO_4^{2-} (generally 0.6 - 1.5 mole % SO_4^{2-}).

(vi) Kuwait Dune Ooids (Figs 3.12 and 3.13)

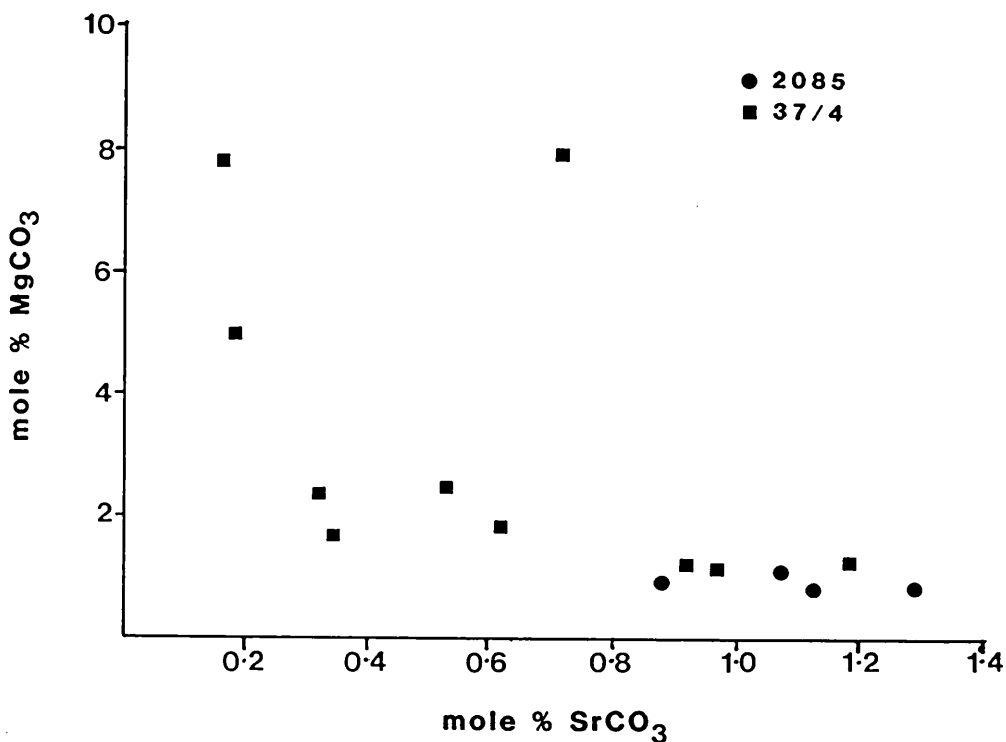


Fig. 3.12 - Mole % MgCO_3 and SrCO_3 contained within the cement precipitated during experiments using sediment AKDO.

Two very different compositional distributions are noted in this data set although again the negative correlation between MgCO_3 and SrCO_3 is seen. The cement precipitated in experiment 2085 shows a very restricted variation although few analyses are available. The MgCO_3 content of the cement

is around 1 mole % MgCO_3 with the SrCO_3 content being relatively high (0.85 - 1.3 mole %). The cement precipitated in experiment 37/4 on the other hand, shows an extreme level of variation in both the MgCO_3 level (0.5 - 8 mole %) and in the SrCO_3 level (0.15 - 1.2 mole %). More analyses are available however and may in part account for the differences in variation seen between the two experiments.

Within the MgCO_3 and SrCO_3 compositional distribution of the cement precipitated in experiment 37/4, three groups of data points are noticeable.

(a) High Mg content ($\text{MgCO}_3 > 4$ mole %) - these appear to have variable SrCO_3 contents, although it is possible, bearing in mind the inverse relationship between MgCO_3 and SrCO_3 in the cement, that the high value for SrCO_3 observed in one analysis, is a rogue value.

(b) Moderate Mg content (MgCO_3 1.5 - 3.3 mole %) - these have a moderate SrCO_3 level (0.3 - 0.65 mole %).

(c) Low Mg content (approximately 1 mole % MgCO_3) - these analyses show high levels of SrCO_3 (0.9 - 1.2 mole %).

The typical inverse relationship between MgCO_3 and SrCO_3 is apparent but it must be noted that these data groups do not correspond to early, mid and late parts of the cement crystals. A decrease in the MgCO_3 and an increase in SrCO_3 content of the cement crystals is observed with time as

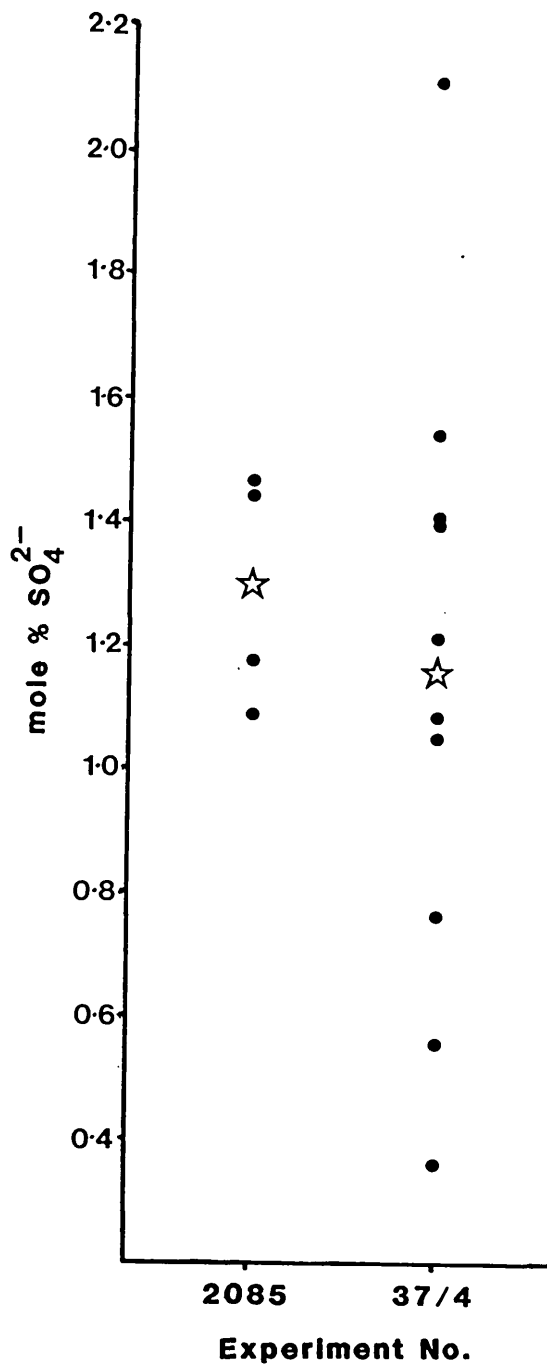


Fig. 3.13 - Mole % SO_4^{2-} contained in cement crystals precipitated during experiment using sediment AKDO. Mean values (☆) are shown.

shown in Table 3.8 in individual crystals but the early or late stages of all cement crystals do not show a uniformity in composition. In a case like this, where there is extreme overall variability, the variability is seen from crystal to crystal and not just through individual crystals.

	MgCO ₃	SrCO ₃
Centre	4.99	0.18
Edge	1.80	0.61

Table 3.8 - MgCO₃ and SrCO₃ levels (mole %) for the centre and edge of one cement crystal generated using the sediment AKDO.

The SO₄²⁻ data show the same general pattern of variability in the cement precipitated in experiments 2085 and 37/4 as the MgCO₃ and SrCO₃ data (see Fig 3.13) although the data set for 2085 is much smaller than for 37/4. The cement of experiment 2085 shows concentrations of SO₄²⁻ in the range 1.1 - 1.5 mole % with a low variation. The SO₄²⁻ content of the cement precipitated in experiment 37/4 however shows a very high level of variability, ranging from 0.35 - 2.15 mole %.

(vii) Shark Bay Ooids (Fig. 3.14 and 3.15)

The cement that was precipitated in each of the experiments using Shark Bay Ooids shows a very similar distribution of MgCO₃ and SrCO₃ (mole %). The cement of experiment 34/4

shows the greatest variation both in terms of MgCO_3 and SrCO_3 . The cement of the other three experiments (1384, 1584 and 3386) all show broadly similar distributions of SrCO_3 levels (0.45 - 1.3, 0.55 - 1.2 and 0.55 - 1.05 mole % respectively). The MgCO_3 contents of the cement precipitated in experiments 1384 and 3386 are very similar (1.0 - 2.5 mole %) while that of 1584 is slightly more variable with a higher upper limit (1 - 4 mole %).

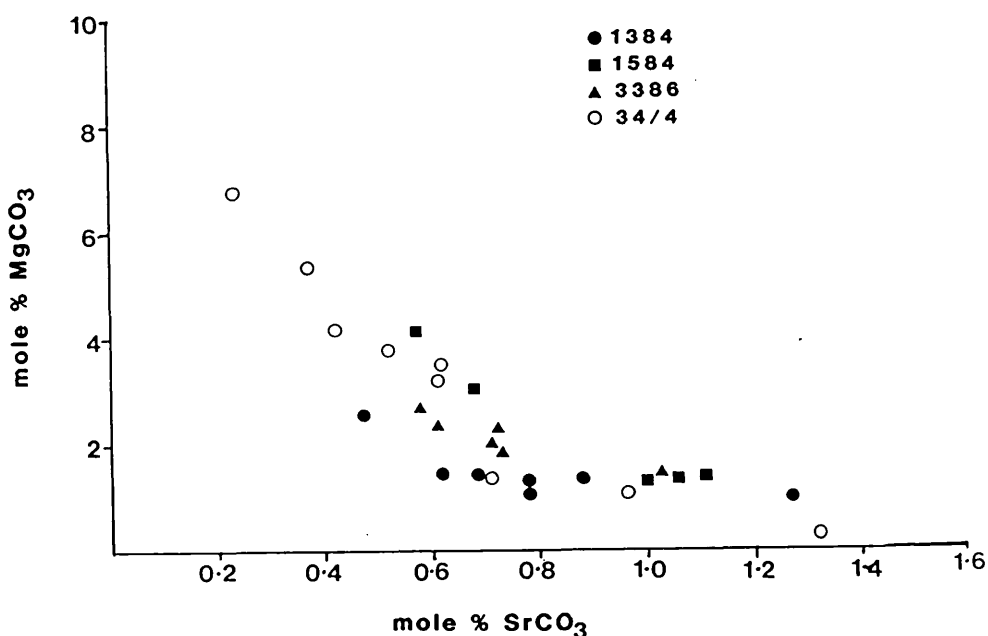


Fig. 3.14 - Mole % MgCO_3 and SrCO_3 contained in cement crystals precipitated using Shark Bay Ooids.

The level of SO_4^{2-} observed in these cement crystals tends to be variable and high (see Table 3.9). The cement crystals precipitated in experiments 1384 and 3386 show the least variability with levels of 1.25 - 1.8 and 0.95 - 1.4 mole % SO_4^{2-} respectively while that of experiments 1584 and 34/4

show very variable levels with both being in the range 0.5 - 1.9 mole % SO_4^{2-} .

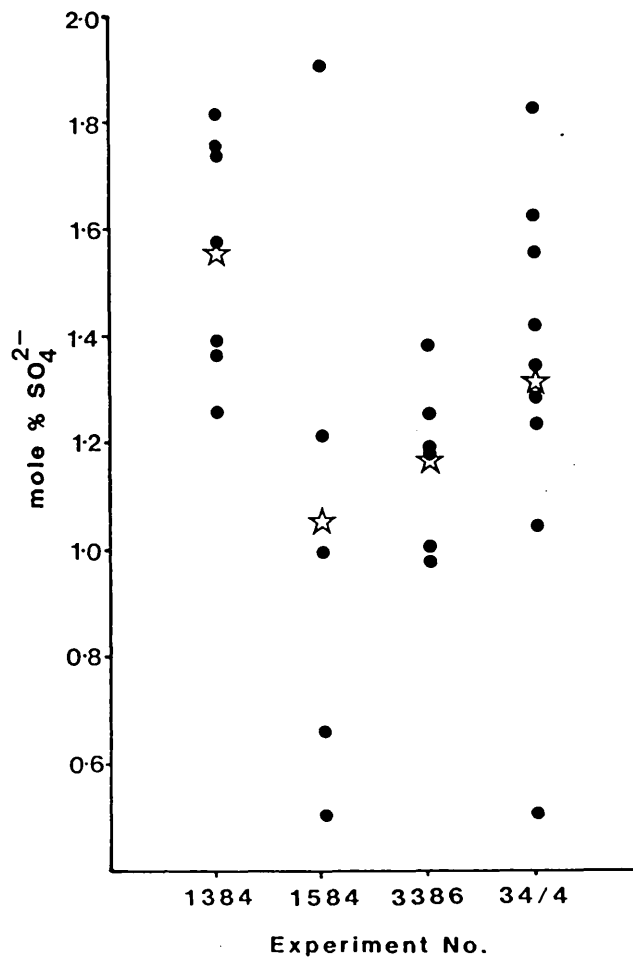


Fig. 3.15 - Mole % SO_4^{2-} contained in cement crystals precipitated using Shark Bay Ooids. Mean values (☆) are shown.

(3) SUMMARY

The experiments show broadly similar pore fluid evolution

Sediment Type	Predominant Cement Fabric	Wt.% Aragonite removed (XRD)	Maximum pore fluid mSr^{2+}/mCa^{2+}	mole% $MgCO_3$	Cement	
					mole% $SrCO_3$	mole% SO_4^{2-}
BSO	Granular-bladed	10-20	0.075 - 0.1	< 10 18-32	0.22 - 0.83	0.41 - 1.33
ADDO	"	20-25	0.08	< 8	0.38 - 0.88	0.52 - 1.32
ADBO	Equant	< 5	0.03 - 0.06	< 12	0.1 - 0.82	0.85 - 1.9
AKSO	Granular - bladed (equant)	10-25	0.08 - 0.1	< 10	0.09 - 1.06	0.22 - 1.45
AKDD	Granular-bladed	20-40	0.09 - 0.125	< 8	0.15 - 1.28	0.36 - 1.54
SBO	Equant	0-25	0.08 - 0.09	< 7	0.23 - 1.32	0.5 - 1.9

Table 3.9 - Summary of results for experiments conducted using the range of sediments available.

trends. In most cases there is an overall decrease in the $m\text{Mg}^{2+}/m\text{Ca}^{2+}$ ratio from 4.8 (the value of seawater used here) to less than 1 in the first two weeks of the experiment. In all cases the $m\text{Sr}^{2+}/m\text{Ca}^{2+}$ ratio either increases to a maximum, after which it drops slightly to what appears to be a chemical equilibrium or, continues to increase. Maximum $m\text{Sr}^{2+}/m\text{Ca}^{2+}$ levels in the pore fluids vary between sediment types.

One set of data (that obtained using Shark Bay Ooids) differs in that the early pore fluid samples show an increase in the $m\text{Mg}^{2+}/m\text{Ca}^{2+}$ ratio due to increased levels of Mg^{2+} when compared to that of seawater. Following this, the $m\text{Mg}^{2+}/m\text{Ca}^{2+}$ ratio in some of these experiments remained high. In these experiments, the largest equant crystal cement fabrics have been observed.

The final levels of $m\text{Sr}^{2+}/m\text{Ca}^{2+}$ in the pore fluids varied significantly, correlating with the levels of aragonite dissolution as suggested by XRD data (see Table 3.9) and petrographic observation. The set of data which showed the lowest final level of $m\text{Sr}^{2+}/m\text{Ca}^{2+}$ in the pore fluids also showed equant cement fabrics, and the lowest range of SrCO_3 levels (mole%) in the precipitated cement. The set of data which showed the highest final level of $m\text{Sr}^{2+}/m\text{Ca}^{2+}$ in the pore fluids on the other hand, displayed granular-bladed fabrics, the highest level of aragonite dissolution and the

highest levels of SrCO_3 (mole%) in the cement crystals.

The level of MgCO_3 observed in the cement appears to vary greatly. Smaller cement crystals (e.g. 34/3) show very high levels of MgCO_3 (in a few cases as high as 30 mole % MgCO_3) but no clear relationship between the pore fluids and the level of MgCO_3 in the cement was observed during these experiments.

3.6 INVESTIGATION OF SEDIMENTS

Although they had been subjected to similar experimental conditions, it was apparent that the different sediments had reacted in different ways. The fabrics which had been created showed similarities e.g. the creation of secondary porosity and the replacement textures produced, but the cement fabrics that had been generated varied significantly.

The sediments differed in several ways:

- (i) the composition of the sediments varied both in terms of grain composition and mineralogy (see Tables 2.1 and 2.2),
- (ii) the grain size of the sediments differed (see Appendix II) and
- (iii) the amount of organic matter associated with the sediments is likely to have differed (e.g. subtidal compared to dune ooids).

3.6.1 SEDIMENT COMPOSITION

The sediments that were used in the experiments described in section 3.5 were composed of different proportions of coated grains, peloids and shell fragments (see Table 2.1). The results presented in section 3.5.1 show that the cortical layers of coated grains were much more prone to dissolution than shell fragments (the majority of which were either stable or underwent insitu recrystallisation). It was therefore considered appropriate to experiment with sediment samples composed of coated grains and peloids only, shell fragments only and mixtures of known quantities of shell fragments and non-skeletal grains (coated grains and peloids). In these experiments it could be possible to study the effect that the sediment composition and hence the aragonite dissolution rate had on the diagenetic results if any.

Four experiments were run under identical time (43 days), temperature ($183 \pm 2^{\circ}\text{C}$), pressure (7.8 MPa, s.d. 1.1 MPa) and sampling conditions with sediments samples as follows:

- (i) 100% sediment BSO (30/1),
- (ii) 77% sediment BSO, 23% shell fragments (30/3),
- (iii) 67% sediment BSO, 33% shell fragments (30/2) and

(iv) 100% shell fragments (30/4).

Sediment BSO is composed primarily of coated grains (with micritic nuclei) and peloids (see Appendix II). Very few shell fragments (<1%) are found in the sediment. The shell fragments that were used were from a sample collected from a beach strandline in Kuwait (AKS4, see Appendix II).

(1) Textural Development

Cement: In this series of experiments the cement that was precipitated was predominantly of the granular-bladed morphology described in section 3.5.1. In the experiments in which samples of sediment BSO and mixtures of sediments BSO and AKS4 were used, cementation proceeded to varying degrees (see Plates 3.10 and 3.12). Cementation was patchy however. When the cells were opened, areas of coated grains and peloids were found to be very well cemented while areas consisting of a greater proportion of shell fragments were less well cemented. The sample consisting of 100 % shell fragments was not cemented. The average widths of the cement fringes that are observed on coated grains and peloids are (i) 100% coated grains 8 μm , (ii) 77% coated grains 10 μm and (iii) 66% coated grains 14 μm . Clusters of granular cement crystals are found in close association with organic filaments (see Plate 3.10 A-C).

PLATE 3.10 - INVESTIGATION OF SEDIMENT COMPOSITION

(A) Experiment 30/1 (100 % BSO) - An isopachous fringe of granular-bladed cement crystals surrounds sediment grains. Clusters of cement crystals (C) are observed protruding from grain surfaces resembling the form of algal filaments. Secondary porosity (P) has been created in grain cortices and in micrite. Neomorphic spar (N) is also found to replace some of the micrite. PPL. Scale bar 50 μ m.

(B) Experiment 30/1 - Clusters of cement crystals form irregular strings (C) resembling the form of algal filaments. PPL. Scale bar 50 μ m.

(C) Experiment 30/3 (77 % BSO, 23 % AKS4) - An isopachous fringe of granular-bladed cement crystals surrounds sediment grains. Several layers of cement crystals are observed on peloids and cement clusters (C) are again observed in the sediment pore spaces, similar to those in Plate 3.10 A and B. PPL. Scale bar 50 μ m.

(D) Experiment 30/3 - Secondary porosity (P) and neomorphic spar (N) replacing micrite, are observed. PPL. Scale bar 50 μ m.

PLATE 3.10

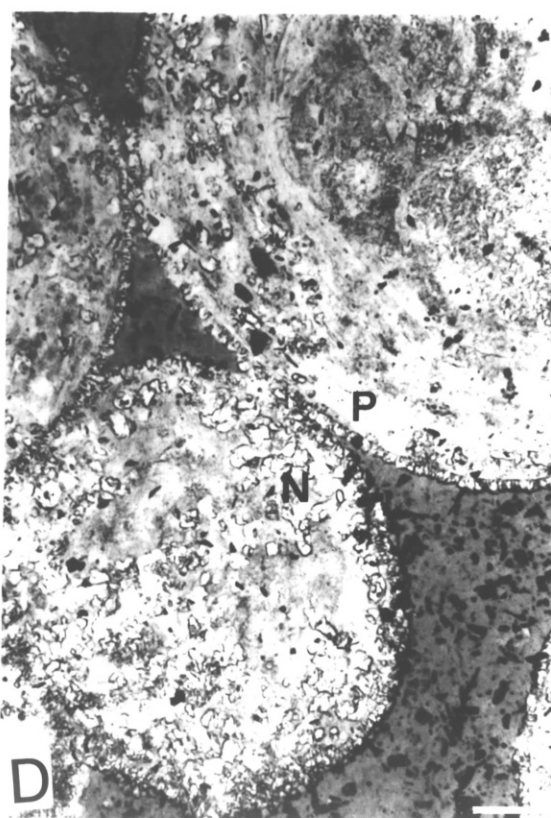
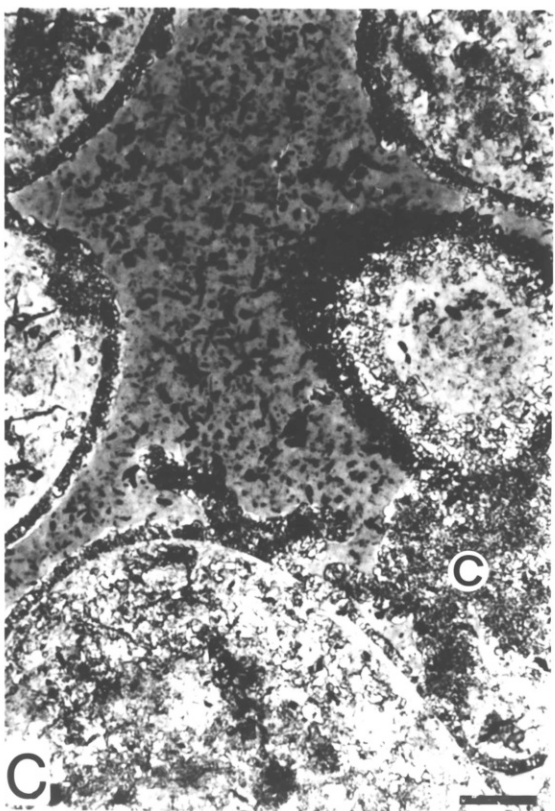
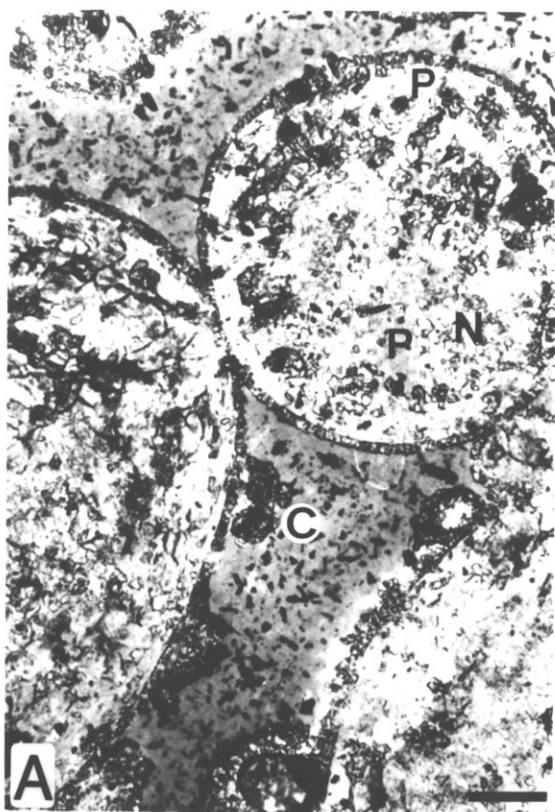


PLATE 3.11 - INVESTIGATION OF SEDIMENT COMPOSITION

(A) Experiment 30/3 (77 % BSO, 23 % AKS4) - Spired calcite overgrowth (O) grows off an echinoderm fragment. An isopachous fringe of granular-bladed cement crystals grow off a micritic peloid in which areas of vuggy micro-porosity (P) can be seen. PPL. Scale bar 50 μm .

(B) Experiment 30/3 - Echinoderm fragment with spired calcite overgrowth (O) which is in optical continuity. PPL. Scale bar 100 μm .

(C) Experiment 30/2 (66 % BSO, 34 % AKS4) - An isopachous fringe of granular-bladed cement crystals surrounds each sediment grain. The coated grain (top right hand corner) shows one layer of cement crystals only while uncoated grains show the development of several layers. PPL. Scale bar 50 μm .

(D) Experiment 30/2 - An isopachous fringe of granular-bladed cement crystals surrounds sediment grains except for the straight, broken edge of the grapestone (G) where a few, isolated equant cement crystals are observed. The creation of oomoldic and vuggy micro-porosity (P) is clearly observed. A limited amount of infilling of this by small, granular solution cavity fill calcite crystals (R), is observed. PPL. Scale bar 100 μm .

PLATE 3.11

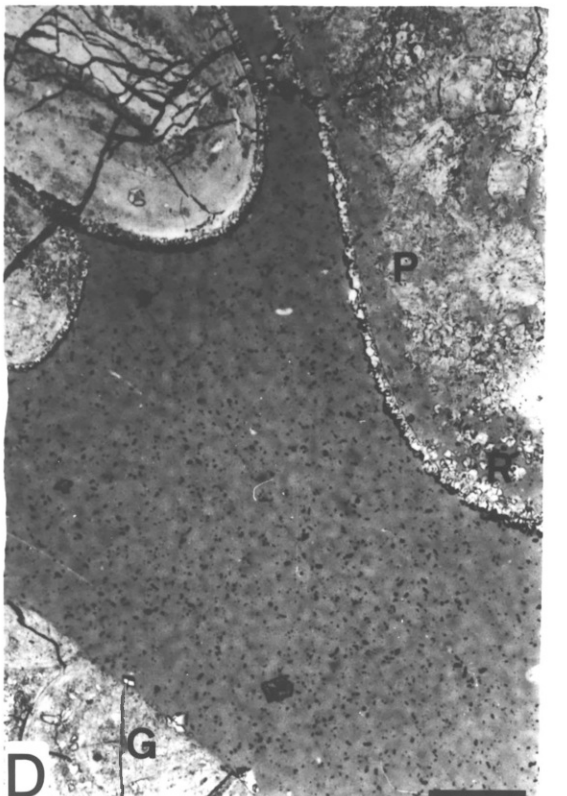
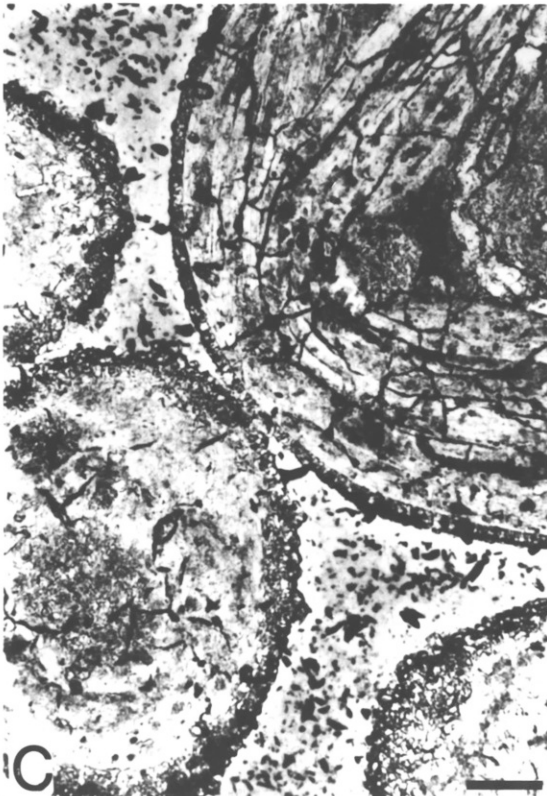
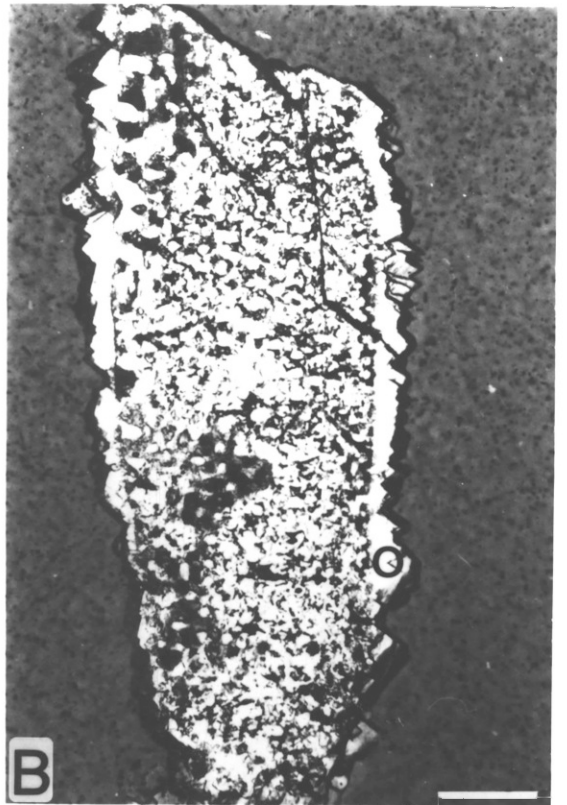
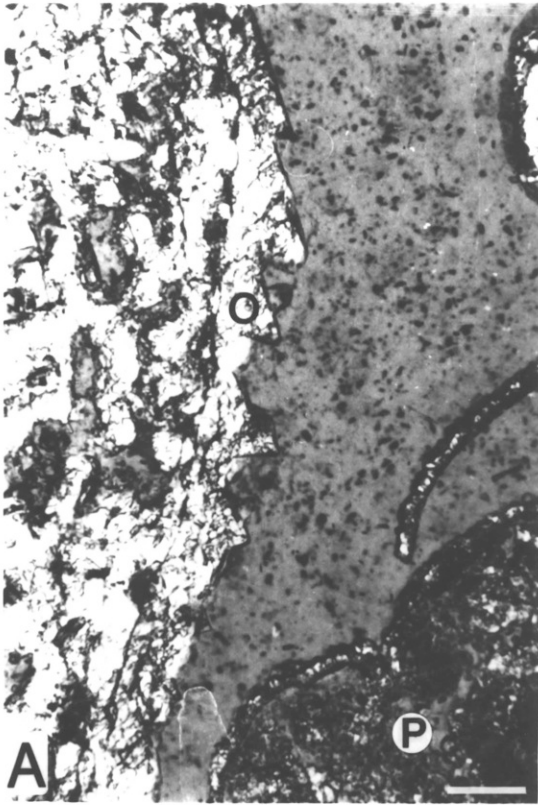


PLATE 3.12 - INVESTIGATION OF SEDIMENT COMPOSITION

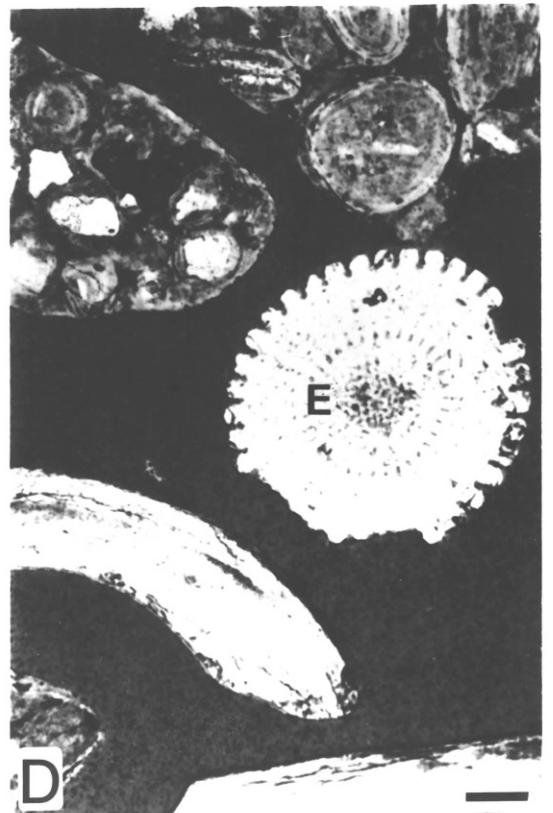
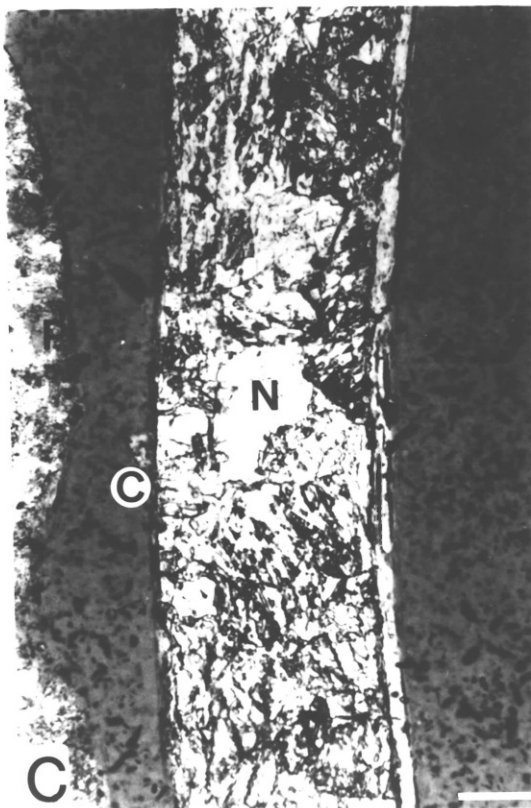
(A) Experiment 30/2 (66 % BSO, 34 % AKS4) - An isopachous fringe of granular-bladed cement crystals surrounds all grains except the quartz grain (Q) which shows a discontinuous fringe of granular-equant cement crystals. Secondary porosity (P) has been created predominantly in the cortices of coated grains. PPL. Scale bar 100 μm .

(B) Experiment 30/2 - A shell fragment, now totally replaced by neomorphic spar (N), had originally been partially coated. The aragonite cortex has been removed to form secondary porosity (P) and is fringed by a discontinuous rim of granular-bladed cement crystals. The cement fringe (C) which surrounds this grain is found mainly where the oomoldic porosity has been created. Other grains show the development of some cement but this is limited. Vuggy micro-porosity (P) has also been created in the coated grain to the right of the shell fragment. PPL. Scale bar 100 μm .

(C) Experiment 30/4 (100 % AKS4) - One isolated, equant cement crystal (C), is observed growing off the shell fragment which has been totally replaced by neomorphic spar (N). Small amounts of micro-porosity (P) have been created at the edge of the peloid to the left of the replaced shell fragment. PPL. Scale bar 20 μm .

(D) Experiment 30/4 - No cementation or alteration of the sediment is observed. No calcite overgrowth is observed on the echinoderm fragment (E). PPL. Scale bar 200 μm .

PLATE 3.12



In the partially lithified sediments, longitudinal sections of echinoderm fragments display spired overgrowths of calcite (see Plate 3.11 A and B). In the sample composed entirely of shell fragments, echinoderm fragments show no overgrowths (see Plate 3.12 D) and only very occasional equant cement crystals are observed (see Plate 3.12 C).

Secondary Porosity and Replacement: In the partially lithified sediments, secondary porosity was created taking the typical form of oomoldic porosity (Plates 3.10 A and 3.12 A) and micro-porosity which often forms vugs (see Plates 3.10 D, 3.11 A and D and 3.12 B). Any infilling of this secondary porosity has been very limited (see Plate 3.11 D). Neomorphic processes have however affected some of the shell fragments and an example of this is shown in Plate 3.12 C where an originally aragonitic bivalve fragment has been totally replaced by an irregular mosaic of sparry calcite.

XRD analysis shows that 10-15% of the original aragonite was removed from the sediment during the experiment using 100% sediment BSO, 15-20% in experiments using 77 and 66 % sediment BSO and 5-10 % in the experiment using 100% shell fragments.

(2) Pore Fluid Chemistry

For each experiment, the pore fluid samples were collected

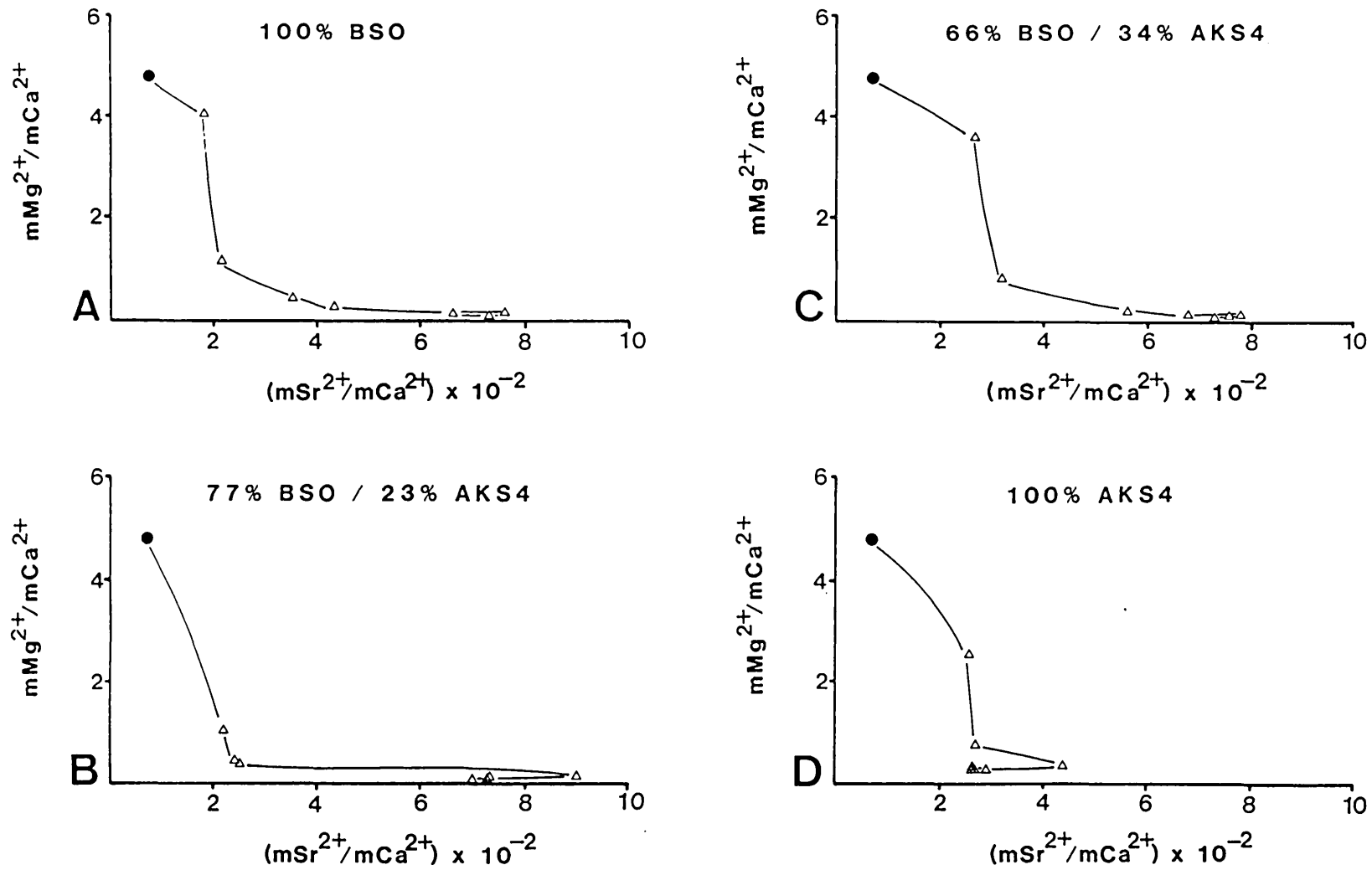


Fig. 3.16 - Evolution of pore fluids from the composition of seawater (●) during experiments investigating the effect of the composition of the sediments. (A) Experiment 30/1, (B) Experiment 30/3, (C) Experiment 30/2 and (D) Experiment 30/4.

on the same day, so the pore fluid evolution curves (see Fig. 3.16) can be directly compared.

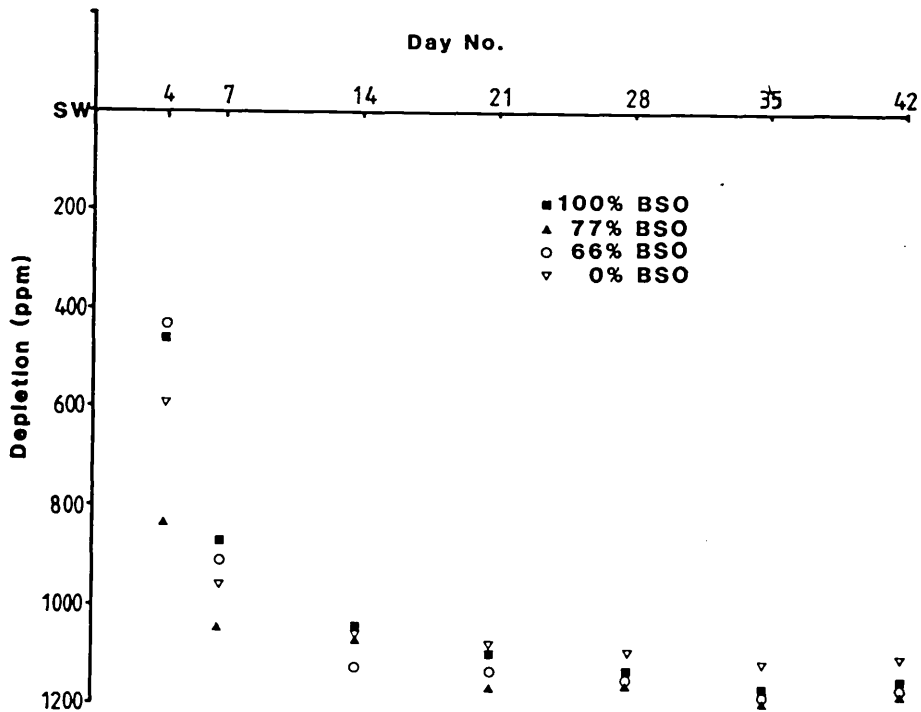


Fig. 3.17 - Depletion in Mg^{2+} (ppm) from the original level of seawater (SW) during experiments 30/1 (100% BSO), 30/3 (77% BSO), 30/2 (66% BSO) and 30/4 (100% AKS4).

If the initial drops in the mMg^{2+}/mCa^{2+} ratios of the pore fluids collected from each experiment involving coated grains are considered, then no correlation between that and the sediment composition is observed. A correlation is observed between the drop and the sample weight (see Fig. 3.16 and Appendix III) which may suggest that the sample weight and hence the available surface area controlled the removal of Mg^{2+} from the pore fluids. If the actual levels

of Mg^{2+} (ppm) in the pore fluids are considered (see Fig. 3.17) then it can be seen that this is not the case. The early decrease in the mMg^{2+}/mCa^{2+} ratios must be a function of both the level of Mg^{2+} and Ca^{2+} in the fluids. No apparent reason can therefore be found for the differences observed.

The initial increase in the mSr^{2+}/mCa^{2+} ratio increases with successively greater amounts of shell fragments in the sediment. The samples composed of 34 % and 100 % shell fragments showed the highest early mSr^{2+}/mCa^{2+} ratios, both being approximately 2.5×10^{-2} . The maximum mSr^{2+}/mCa^{2+} ratios observed in the pore fluids do not follow this pattern based on sediment composition. The highest maximum mSr^{2+}/mCa^{2+} ratio that was observed (9×10^{-2}) was found in the experiment which used the greatest sediment weight (see Appendix III) where the sediment contained coated grains. The maximum mSr^{2+}/mCa^{2+} ratio of the pore fluids therefore appeared to be partially dependent on the sample weight to pore fluid ratio. The maximum mSr^{2+}/mCa^{2+} ratio observed in the experiment using 100% shell fragments however, was much lower than in the other experiments (4.5×10^{-2} compared to $7.5 - 9 \times 10^{-2}$) indicating that sediment composition also had an effect. The decrease in the mSr^{2+}/mCa^{2+} ratio at the end of the experiments is due to a drop in the Sr^{2+} level of the pore fluids (see Appendix I). This is most likely to have been caused by a decrease in the output of Sr^{2+} via aragonite dissolution (i.e. slowing of the reactions) but continued

uptake of Sr^{2+} from the pore fluids by the precipitation of calcite containing significant levels of SrCO_3 (see section 3.6.1 (3) below).

(3) Cement Crystal Chemistry

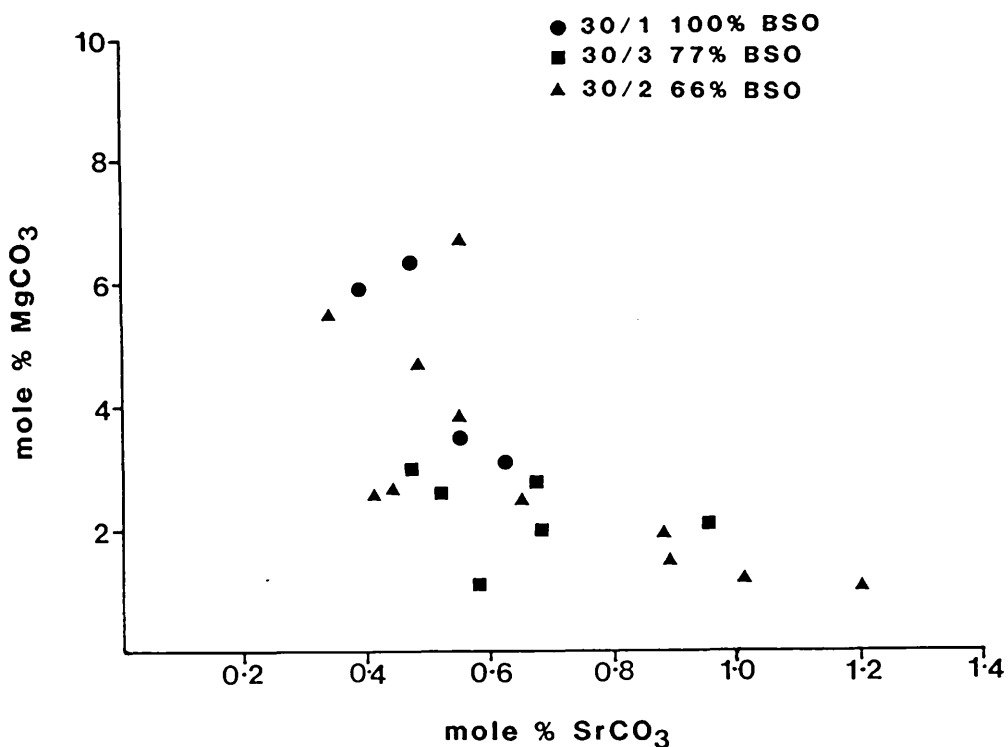


Fig. 3.18 - Mole % MgCO_3 and SrCO_3 contained in the cement crystals precipitated in experiments 30/1-3.

Fig. 3.18 shows the MgCO_3 and SrCO_3 composition of the cement phases precipitated in three experiments involving coated grains. The largest distribution of compositions is shown by the cell in which 66% coated grains were used (30/2). The composition of the cement precipitated in the other two experiments fall within this distribution although they themselves show slightly varying compositions. The

experiment using 100% BSO has a generally higher $MgCO_3$ content (3-7 mole%) and lower $SrCO_3$ (0.35 - 0.65 mole %) content than the experiment using 77% coated grains (1-4 and 0.45- 1 mole % respectively). No apparent correlation between the composition of the cement and that of the starting sediment is observed however.

The SO_4^{2-} levels observed in the cement crystals precipitated during the experiments are also very similar. The overall range is typically 0.7-1.5 mole% (see Fig. 3.19).

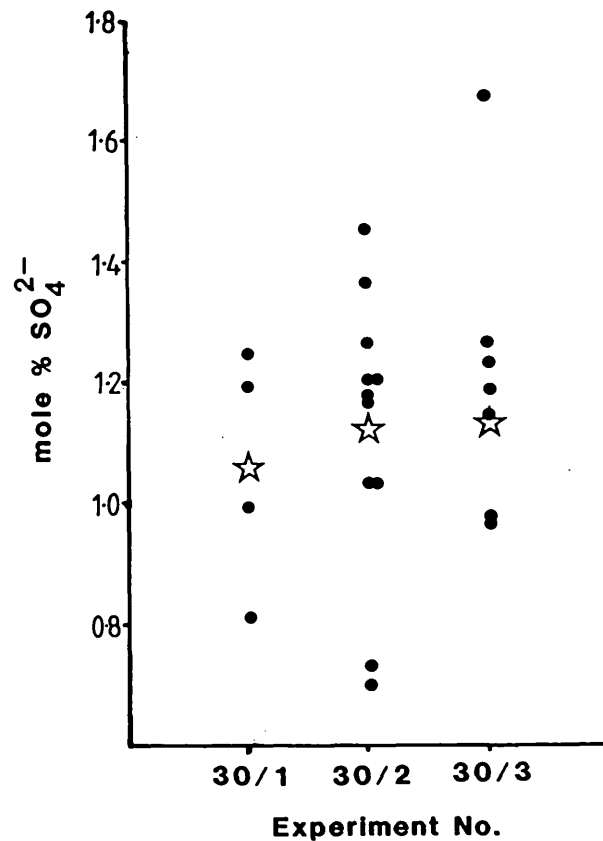


Fig. 3.19 - Mole % SO_4^{2-} contained in cement crystals precipitated during experiments 30/1 (100 % BSO), 30/2 (66% BSO) and 30/3 (77% BSO). Mean values are shown (☆).

(4) SUMMARY

No significant differences in the morphology of the cement crystals that were precipitated in this series of experiments were observed except on echinoderm fragments where optically continuous overgrowths of calcite were observed and in the experiment using shell fragments only where very occasional, isolated, equant cement crystals were noted.

In sediment samples composed of mixtures of sediments BSO and AKS4, areas of coated grains and peloids were cemented to a greater degree than areas of shell fragments. The width of the cement fringe on coated grains increased with a decrease in the proportion of coated grains but this is likely to have been the results of increasing cementation on coated grains and peloids. Clusters of granular cement crystals were found in association with organic matter. The composition of the cement precipitated was very similar in all experiments.

The initial decrease in the $\text{mMg}^{2+}/\text{mCa}^{2+}$ can be correlated with the initial sample weight in experiments using sediments containing coated grains. This however was not due to decreasing levels of Mg^{2+} and was likely to be caused by

complex reactions involving the precipitation of SO_4^{2-} phases from the seawater and the early precipitation of calcite and dissolution of aragonite. The experiment using 100% shell fragments does not follow this pattern. In the experiments containing mixtures of sediments BSO and AKS4, the greater the proportion of shell fragments the greater the early increase in the $\text{mSr}^{2+}/\text{mCa}^{2+}$ ratio. A correlation between sample weight and maximum $\text{mSr}^{2+}/\text{mCa}^{2+}$ ratios is observed with the greater the sample weight accompanying greater maximum $\text{mSr}^{2+}/\text{mCa}^{2+}$ ratios where the sediments contained coated grains. The sediment composed of shell fragments did not show this hence maximum $\text{mSr}^{2+}/\text{mCa}^{2+}$ ratios are likely to be a function of sediment type and weight.

3.6.2 GRAIN SIZE

One major factor which varied from sediment to sediment was the grain size (see Appendix II). Four experiments were therefore conducted under conditions of identical time (40 days), temperature ($183 \text{ C} \pm 2^\circ \text{C}$), pressure (8.4 MPa, s.d. 0.8 MPa) and sampling conditions, using a sample of sediment AKDO which was split into the size fractions given in Table 3.10. Table 3.10 also gives the external sediment surface area available for reaction in each experiment, calculated from the sample weight and average density of the sediment using the formula:

$$\text{surface area} = (3\text{wt})/r\rho$$

where

r = radius (cm)

wt = weight in grams

ρ = average density (gms/cc) based on the composition of each sediment sample

Expt. No	Grain size	Surface area (cm ²)
28/1	>0.42mm	<1212
28/2	0.42-0.35	2267-2644
28/3	0.35-0.25	2768 - 3835
28/4	<0.25	>3161

Table 3.10 - Grain size and surface area of sediments used in the experiments.

(1) Textural Development

Differences in the degree of alteration and, in particular the cement fabric generated in each experiment, have been observed.

Cement: The cement which has been precipitated in experiment 28/1 (grain size >0.42 mm), is predominantly of an equant-rhombic morphology (see Plate 3.13 A and B). The cement crystals are typically isolated, scattered along grain boundaries (see Plate 3.13 A). Clusters of crystals are seen on grain surfaces which have been bored by algae (see Plate 3.13 B). The maximum diameter of these crystals

PLATE 3.13 - INVESTIGATION OF SEDIMENT GRAIN SIZE

(A) Experiment 28/1 (grain size $> 0.42\text{mm}$) - Isolated equant cement crystals fringe sediment grains. Back-scattered electron image. Scale bar $100\ \mu\text{m}$.

(B) Experiment 28/1 - Isolated equant cement crystals fringe sediment grains except on bored surfaces where cement crystal clusters (C) are observed. Secondary porosity (P) is observed in the cortices of coated grains. Back-scattered electron image. Scale bar $100\ \mu\text{m}$.

(C) Experiment 28/2 (grain size $0.35\text{-}0.42\ \text{mm}$) - An isopachous fringe of granular-bladed cement crystals surround coated grains. Peloids show wider fringes (C). Secondary porosity (P) has been created in the grains but many of the irregular cavities (H) are holes which have been created during slide thin section preparation. Large crystals of neomorphic spar replace some of the original micrite. PPL. Scale bar $50\ \mu\text{m}$.

(D) Experiment 28/2 - An isopachous layer of granular-bladed cement crystals fringe coated grains while peloids display several layers of cement. Secondary porosity has been created in the cortices of coated grains (P) and in places is partially filled by granular solution cavity fill calcite crystals (R) which grow in from the grain edge. PPL. Scale bar $50\ \mu\text{m}$.

PLATE 3.13

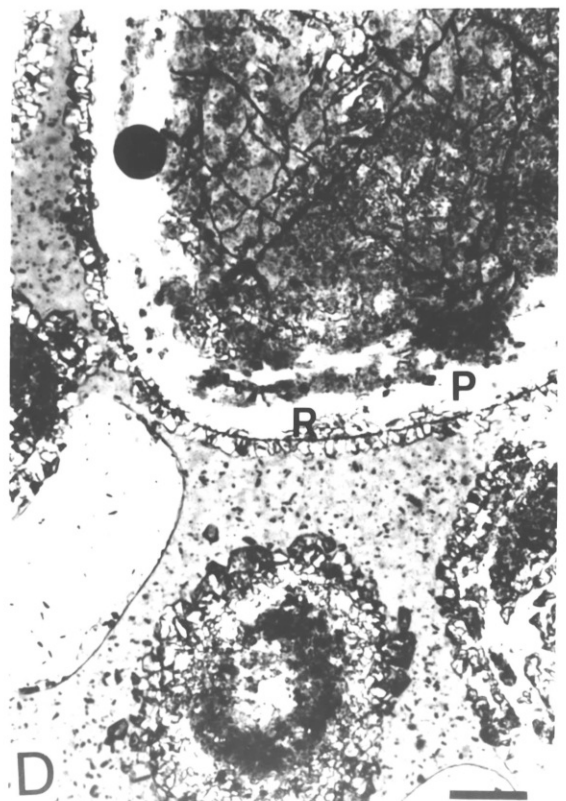
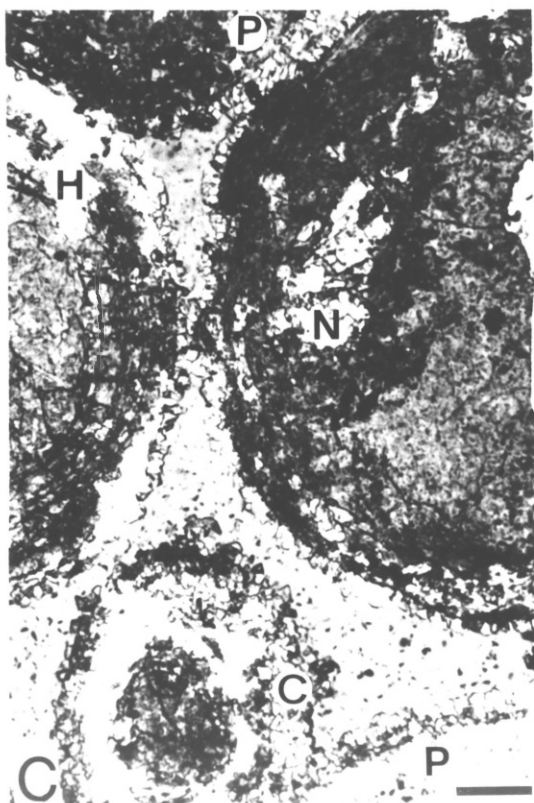
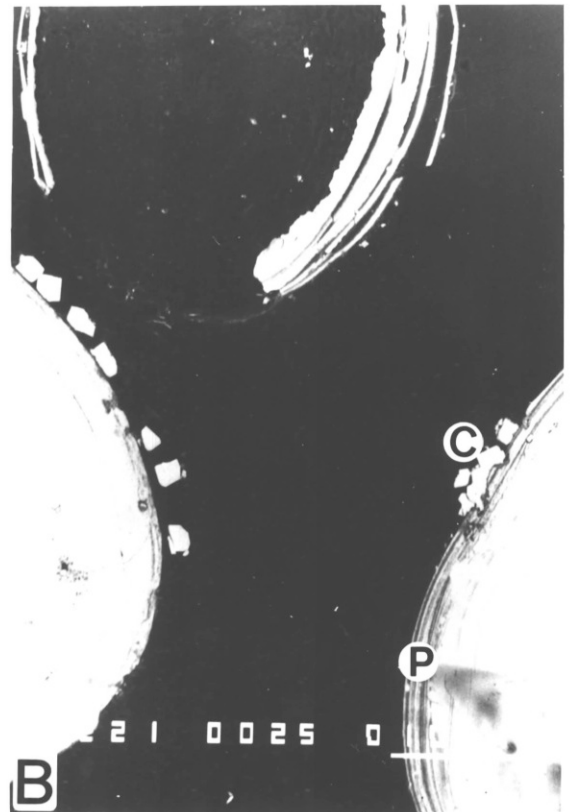
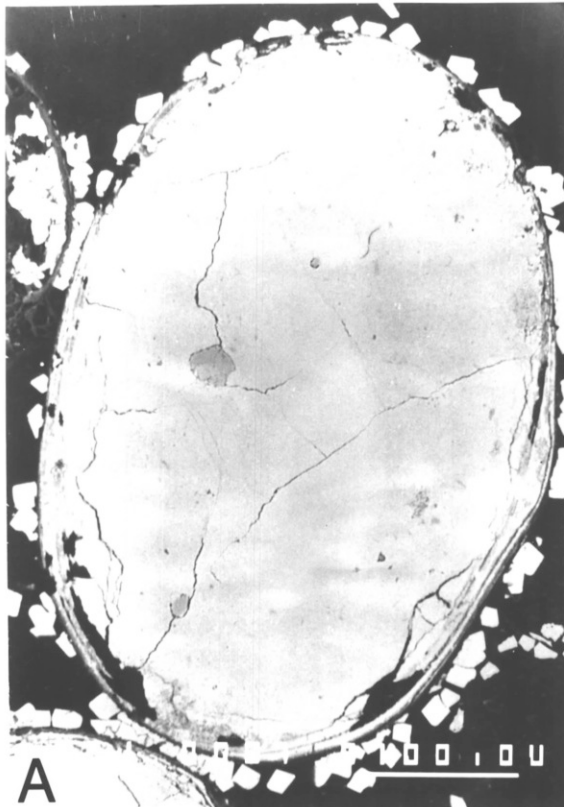


PLATE 3.14 - INVESTIGATION OF SEDIMENT GRAIN SIZE

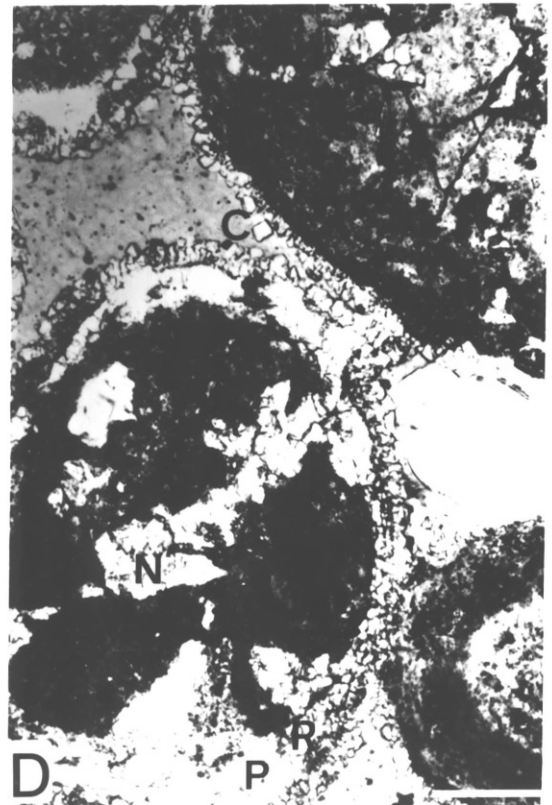
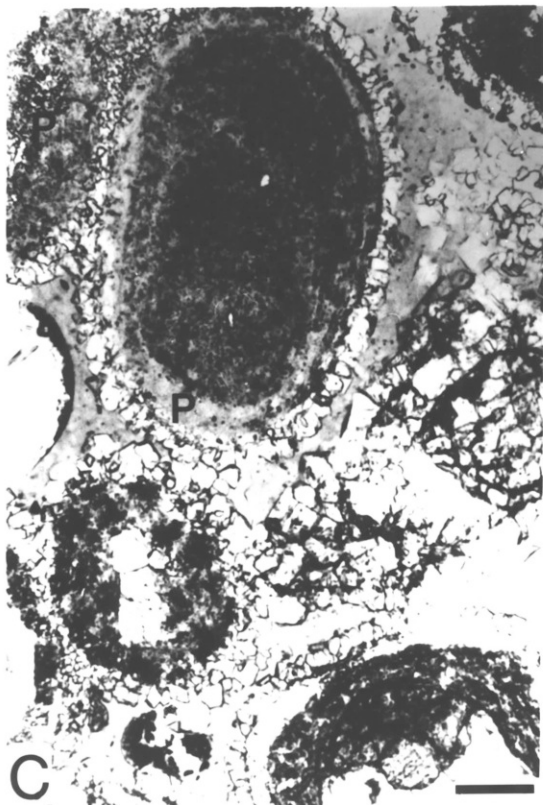
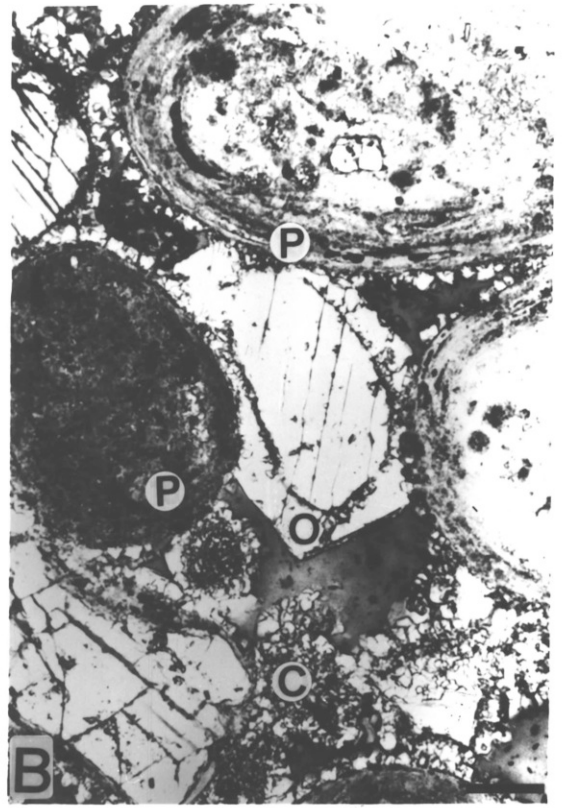
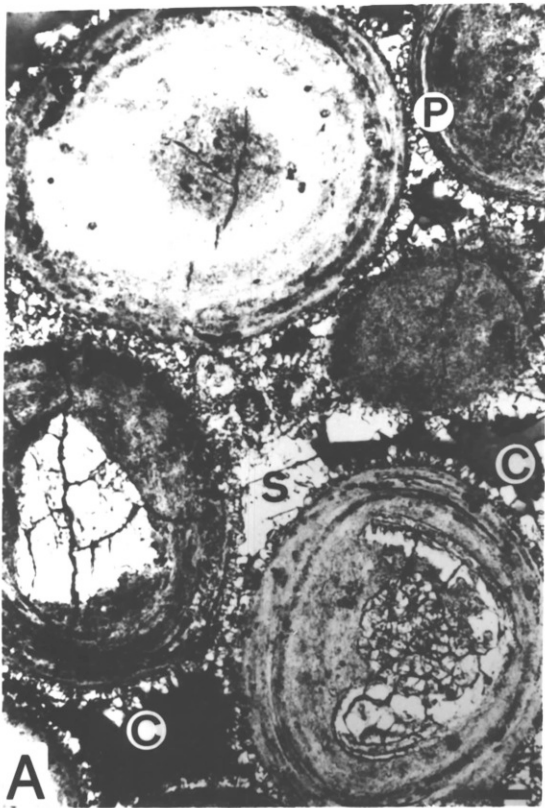
(A) Experiment 28/3 (grain size 0.25-0.35 mm) - Irregular fringes of granular, bladed and equant cement crystals surround sediment grains. Equant crystals tend to be found overgrowing an earlier granular-bladed fringe (C). Large, sparry calcite crystals (S) occlude areas of sediment pore space, enveloping earlier cement fringes. PPL. Scale bar 50 μ m.

(B) Experiment 28/3 - Irregular fringes of granular, bladed and equant cement crystals surround sediment grains. Clusters of cement crystals (C) are found in the sediment pore space. A calcite overgrowth (O) is observed on a grain composed of a single crystal of calcite. This grain was fringed by granular-bladed cement crystals prior to being enveloped in the later overgrowth. Secondary porosity is present in the cortices of coated grains and peloids. PPL. Scale bar 50 μ m.

(C) Experiment 28/4 (grain size < 0.25 mm) - Irregular fringes of granular, bladed and equant cement crystals surround sediment grains. Equant crystals are more abundant than in Plate 3.14 A and B. Secondary porosity (P) is well developed in coated grains and as microporosity in peloids (see grain in top left hand corner). PPL. Scale bar 50 μ m.

(D) Experiment 28/4 - Predominantly granular-bladed cement crystals fringe sediment grains with later equant cement crystals (C). Secondary porosity has been created in the cortices of coated grains (P) and is partially replaced by sparry solution cavity fill calcite crystals (R). Large crystals of neomorphic spar (N) replace the micrite of peloids. PPL. Scale bar 50 μ m.

PLATE 3.14



ranges from 9-22 μm , with an average of 15-16 μm .

The morphology of the cement generated in experiments 28/2 and 28/3 (see Plates 3.13 C and D and 3.14 A and B), is predominantly granular-bladed with later equant cement crystals. The cement precipitated during experiment 28/4 is also granular-bladed but with a significant proportion of equant crystals (see Plate 3.14 C and D). The widths of the fringes generated in each experiment are as follows:

(i) 28/2, minimum width of 8-10 μm (see Plate 3.13 C and D). Coated grains show the narrowest cement fringe with peloids displaying wider cement fringes.

(ii) 28/3, the minimum width of fringe observed is around 10-12 μm but many fringes are much wider than this (see Plate 3.14 A and B) being up to 20 μm wide on peloids. Clusters of cement crystals up to 80 μm in diameter (see Plate 3.14 B) and large sparry crystals (see Plate 3.14 A and B) in sediment pore spaces are common. An optically continuous overgrowth on a grain composed of a single calcite crystal is observed in Plate 3.14 B. This shows an early phase of granular cement crystals which are not in optical continuity with the grain and which are overgrown by the later optically continuous overgrowth.

In experiment 28/4, the minimum width of a single crystal fringe of cement crystals is around 15 μm (see Plate 3.14 C and D). Multiple layer cement fringes are also common (see

Plate 3.14 C), especially on uncoated peloidal grains, along with cement clusters (see Plate 3.14 C).

Secondary Porosity: Secondary porosity has been created to varying degrees by the dissolution of aragonite has occurred in all experiments to varying degrees. In experiment 28/1, a small amount of aragonite has been removed from the cortices of coated grains (see Plate 3.13 B).

Much more secondary porosity has been created in the other three experiments (see Plate 3.13 C and D and 3.14), particularly in experiments 28/3 and 28/4 (see Plate 3.14 A-D). Again, most of this has been created by the removal of cortical aragonite but a small amount of micro-porosity has been created by the removal of micritic aragonite.

Replacement Textures: Replacement of the secondary porosity created by aragonite dissolution is very limited. Some of the micritic nuclei of coated grains have been partially replaced by neomorphic sparry calcite (see Plates 3.13 C and 3.14 D) and solution cavity fill calcite is found to infill some of the secondary porosity in Plates 3.13 D and 3.14 D.

XRD analysis indicates that during experiment 28/1, less than 10% of the original aragonite was removed while approximately 10, 25 and 30 % was removed during experiments

28/2, 28/3 and 28/4 respectively.

This correlates with the degree of alteration observed petrographically. The sediment in experiments 28/3 and 28/4 show the most alteration (in terms of aragonite dissolution and calcite precipitation) while the sediment in experiment 28/1 shows only a small amount of change (isolated cement crystals and a small amount of secondary porosity).

Experiment 28/2 shows intermediate levels of cementation, secondary porosity and XRD aragonite conversion figures. An increase in the degree of reaction therefore accompanies a decrease in the grain size in sediments of the same type and composition.

(2) Pore Fluid Evolution

The pore fluid evolution curves present a complicated pattern (see Fig. 3.20). The early decrease in the mMg^{2+}/mCa^{2+} ratio of the pore fluids, does not correlate with either the grain size or perhaps more importantly, the total surface area available within the sediment. If the Mg^{2+} (ppm) data are considered (see Fig 3.21), then an increase in the early uptake of Mg^{2+} is observed with an increase in the available surface area i.e. decrease in grain size. External surface area therefore appears to affect the removal of Mg^{2+} from the pore fluids.

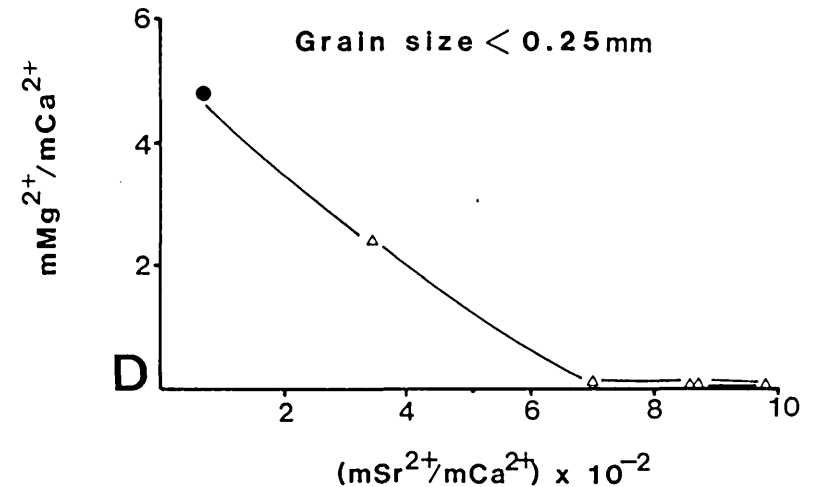
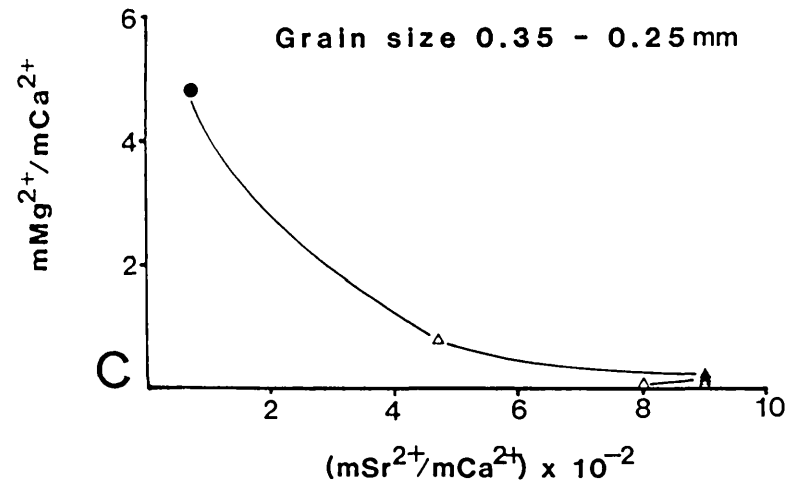
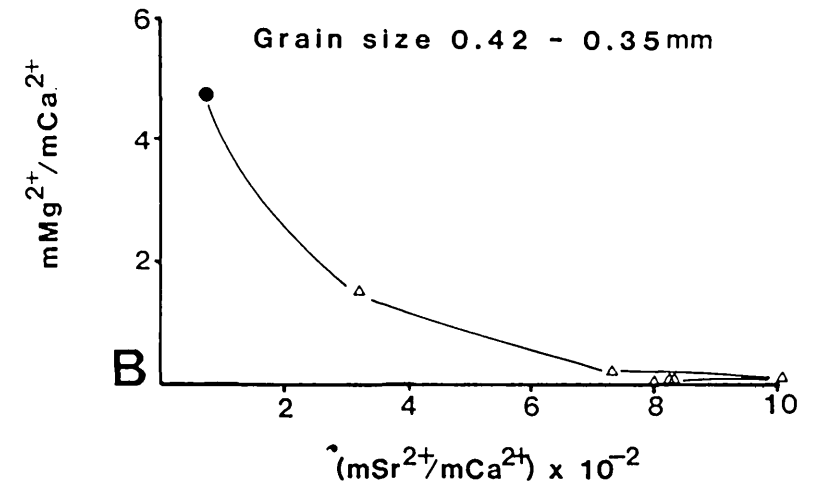
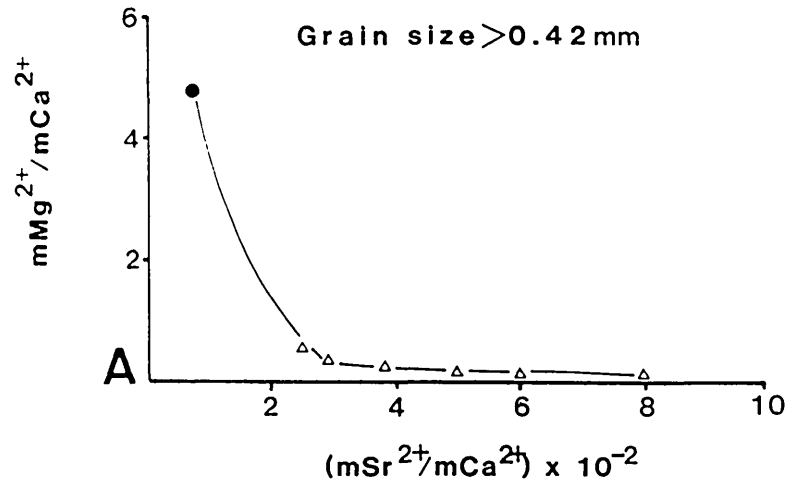


Fig. 3.20 - Evolution of pore fluids from the composition of seawater (●) during experiments investigating the effect of the sediment grain size. (A) Experiment 28/1, (B) Experiment 28/2, (C) Experiment 28/3 and (D) Experiment 28/4.

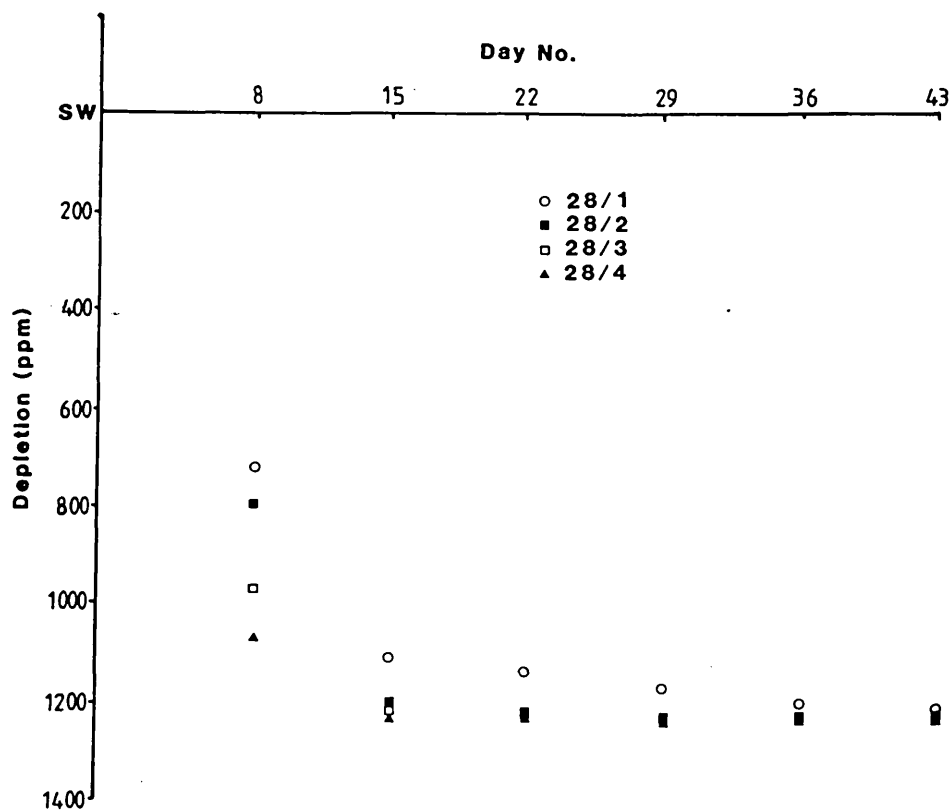


Fig. 3.21 - Depletion in Mg^{2+} (ppm) from the original composition of seawater (SW) during experiments 28/1-4.

An increase in the early mSr^{2+}/mCa^{2+} ratio is observed with an increase in the surface area available. The maximum mSr^{2+}/mCa^{2+} ratios of the pore fluids do not follow any definite pattern although the largest grain size (experiment 28/1) displays the lowest mSr^{2+}/mCa^{2+} ratio (8×10^{-2}) while maximum ratios of $9-10 \times 10^{-2}$ are found to characterise the pore fluids of the other experiments. The lowest maximum mSr^{2+}/mCa^{2+} ratio, observed in the pore fluids of experiment 28/1, correlates with both the restricted nature of the diagenetic fabrics (see Plate 3.13 A and B) and the low aragonite conversion factor obtained using XRD analysis

(>10%).

(3) Cement crystal chemistry

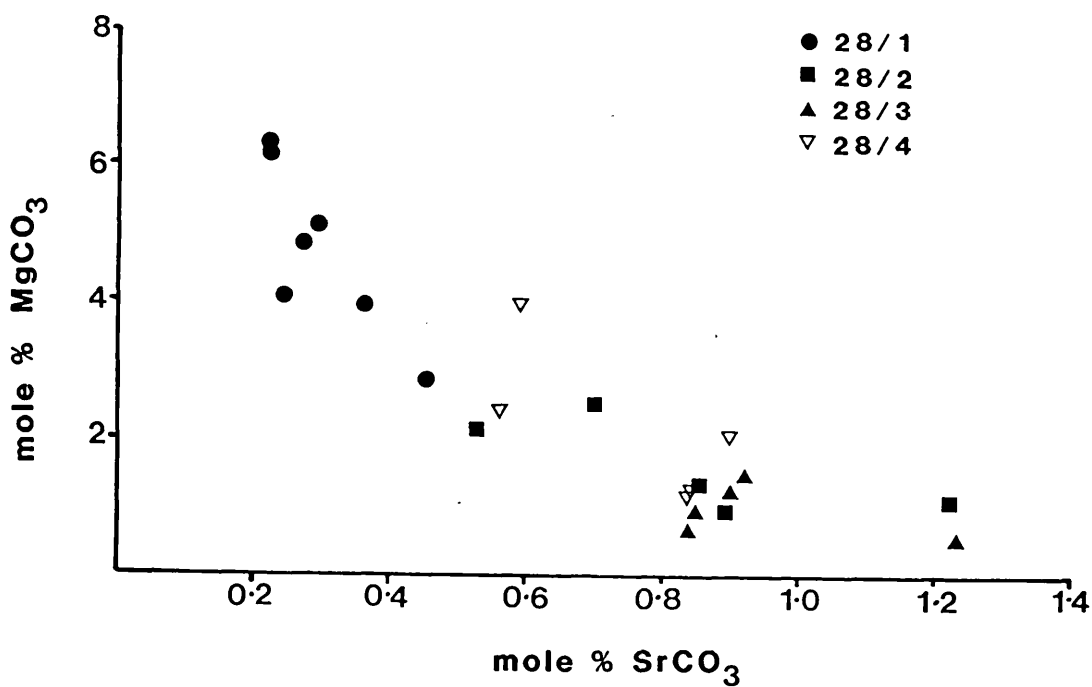


Fig. 3.22 - Mole % MgCO₃ and SrCO₃ contained in cement crystals precipitated during experiments 28/1-4.

The calcite cement which was precipitated in experiments 28/1, 28/2 and 28/3 show a progressive decrease in the amount of MgCO₃ contained within its structure and an increase in the SrCO₃ content (see Fig. 3.22). The cement precipitated in experiment 28/4 however displays a

composition, in terms of MgCO_3 and SrCO_3 , similar to that of experiment 28/2 except that the MgCO_3 content in this cement phase is slightly higher than that of experiment 28/2.

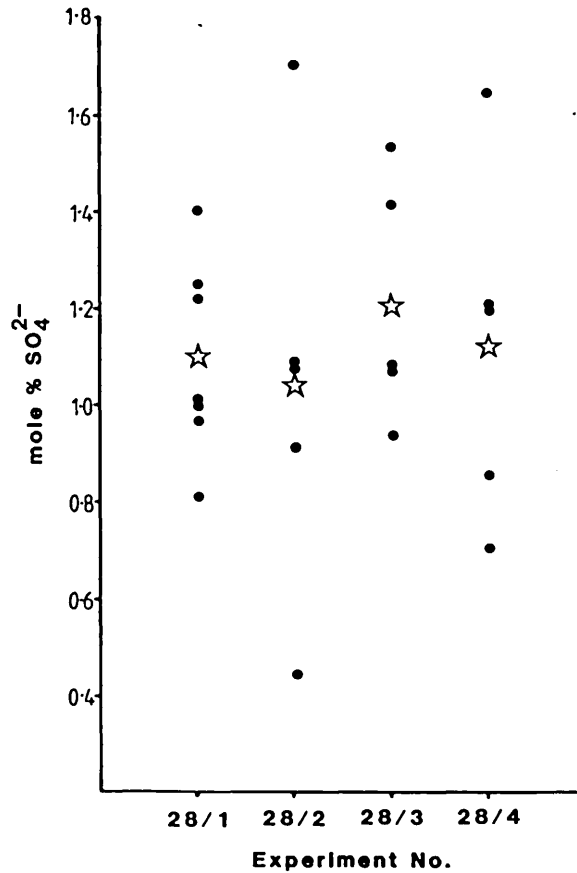


Fig. 3.23 - Mole % SO_4^{2-} contained in cement crystals precipitated during experiments 28/1-4. Mean values (☆) are shown.

The range of SO_4^{2-} levels within the calcite cement precipitated in each experiment is similar and all average values are around 1.0-1.2 mole % (see Fig. 3.23).

(4) SUMMARY

The grain size of the sediment used in the experiments was found to have the following effects.

(i) An increase in the degree of reaction (i.e. aragonite dissolution and calcite precipitation) accompanies a decrease in the grain size.

(ii) Where the degree of reaction is lowest i.e. the largest grains size, the cement fabric generated is of an equant morphology. All other experiments investigating grain size show cement crystals of a granular-bladed morphology.

(iii) An increase in the external sediment surface area correlates with an increase in the early removal of Mg^{2+} from the pore fluids although it does not directly affect the mMg^{2+}/mCa^{2+} ratio. An increase in the surface area also correlates with an early increase in the mSr^{2+}/mCa^{2+} ratio again indicating that external surface area is important in controlling the rate of the experimental diagenesis.

(iv) In sediments with a grain size greater than 0.25mm, a decrease in the $MgCO_3$ content and an increase in the $SrCO_3$ content of the cement crystals (mole%), is observed accompanying a decrease in the grain size. This accompanies the precipitation of a greater amount of cement and a

greater degree of aragonite dissolution. Sediments with a grain size less than 0.25 mm however show a cement composition of moderate $MgCO_3$ and $SrCO_3$ content when compared to the three experiments using sediments of a larger grain size.

3.6.3 ORGANIC MATTER

Another parameter which is likely to have varied between the sediments used, was the amount of organic matter associated with those sediments. Earlier results showed that often, cement was in close association with organic matter, either on algal filaments or grain surfaces bored by algae or on areas of organic matter which were found to be floating within the sediment pore spaces (see section 3.5.1).

The effect that the organic matter which covers the grains had on the precipitation of calcite cement crystals, was studied by taking two sets of sediments, one consisting of sediment AKSO and the other of sediment AKS4 (shell fragments). Each of the sediments were split into two parts, one being soaked in distilled water, the other in hydrogen peroxide. Effervescence of CO_2 (released during the breakdown of organic matter) had stopped in the sample of shell fragments (AKS4) soaked in H_2O_2 . However, a small amount of CO_2 was still being released from the sample of

sediment AKSO. This is probably because of the high level of internal organic matter in coated grains and peloids. Thereafter four experiments were conducted under identical time (40 days), temperature (183 C +/- 2°C), pressure (7.4 MPa, s.d. 1.2 MPa) and pore fluid sampling conditions, using the sediments as follows:

- (i) AKSO, soaked in distilled water (32/1),
- (ii) AKSO, soaked in hydrogen peroxide (32/2),
- (iii) AKS4, soaked in distilled water (32/3) and
- (iv) AKS4, soaked in hydrogen peroxide (32/4).

(1) Textural Development

(i) Kuwait Subtidal Ooids

Cement: The experiments run using sediment AKSO (32/1 and 32/2) both show the development of granular-bladed cement fabrics. Isopachous fringes of cement are observed in both experiments. The width of the cement fringes generated in experiment 32/1 is 8-15 μm (see Plate 3.15 A and B). The grains in experiment 32/2 (soaked in H_2O_2) are also coated by a layer of granular cement crystals but the cement fringes are generally restricted to a single layer and are often discontinuous (see Plate 3.15 C and D), narrower (around 6 μm) and more equant in character.

PLATE 3.15 - INVESTIGATION OF THE EFFECT OF ORGANIC
MATTER

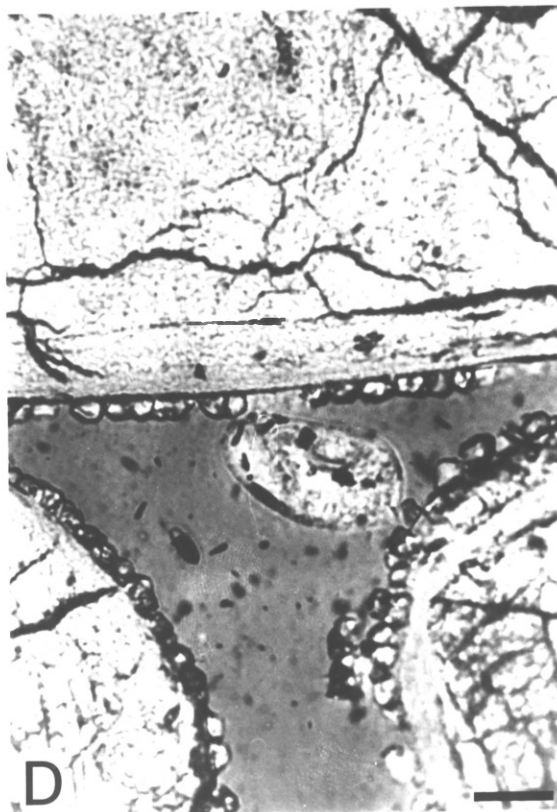
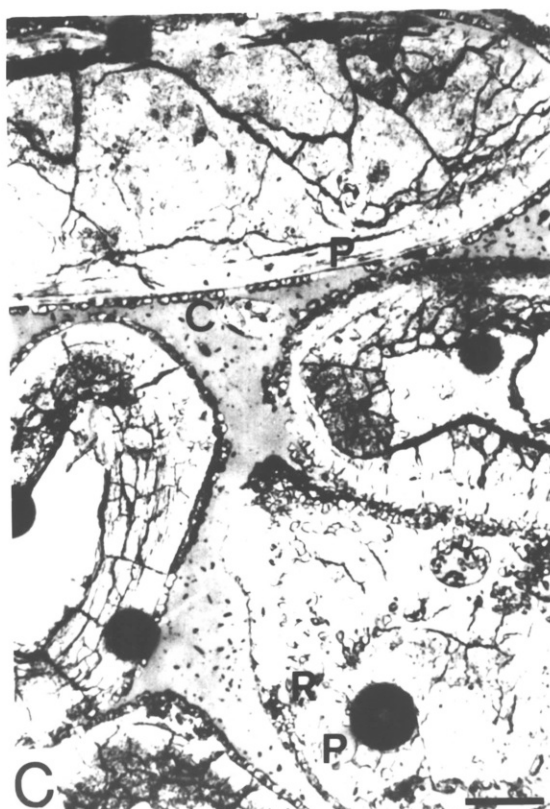
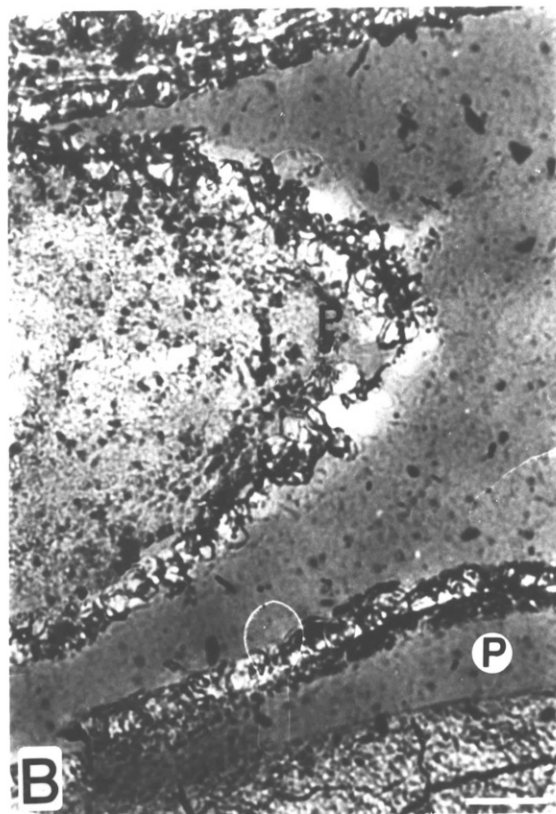
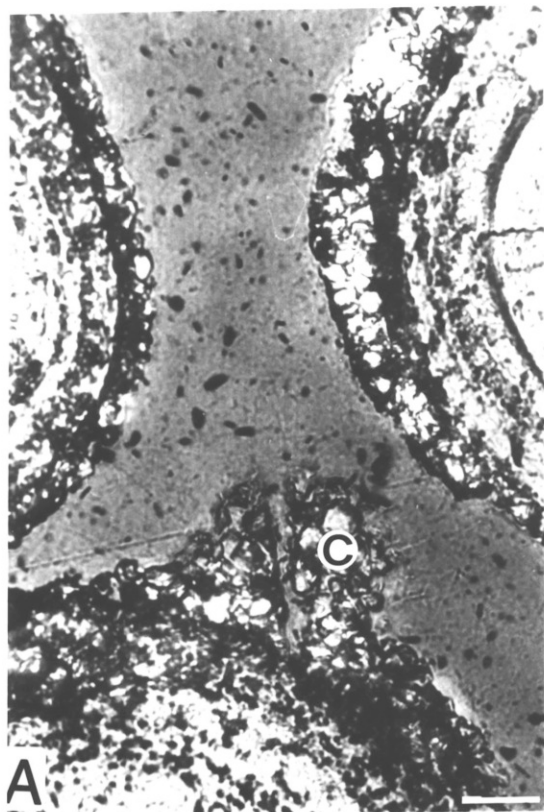
(A) Experiment 32/1 (AKSO) - Isopachous fringes of granular cement crystals surround sediment grains. A cluster of granular cement crystals (C) is observed with an empty central canal on the surface of a peloid. PPL. Scale bar 20 μm .

(B) Experiment 32/1 - Isopachous fringe of granular cement crystals surround sediment grains. Secondary porosity (P) has been created in the cortices of coated grains and in micritic peloids (micro-porosity). Scale bar 20 μm .

(C) Experiment 32/2 (AKSO soaked in H_2O_2) - Discontinuous fringes of granular-equant cement crystals (C) surround sediment grains. Secondary porosity (P) has been created in the cortices of coated grains and in micritic grains. Vuggy pore spaces are partially infilled by small granular, solution cavity fill calcite crystals (R). PPL. Scale bar 50 μm .

(D) Experiment 32/2 - Detail of the discontinuous and granular-equant nature of the cement crystal fringes. PPL. Scale bar 20 μm .

PLATE 3.15



Secondary Porosity: The sediment from experiment 32/1 shows the development of a greater amount of secondary porosity, via the dissolution of aragonite, than that from experiment 32/2 (c.f. Plate 3.15 B and C). Most of the porosity created is oomoldic with a small amount of vuggy and micro-porosity from the dissolution of micrite (see Plate 3.15 A-D).

Replacement Textures: The infilling of secondary porosity and replacement of grains has been limited. Small amounts of solution cavity fill calcite infilling vuggy porosity is observed (see Plate 3.15 C)

XRD analysis shows that during experiment 32/1, 10-15 % of the original aragonite was removed while less than 5 % was removed during experiment 32/2 (soaked in H₂O₂).

(ii) Kuwait Shell Fragments.

Cement: The sample of shell fragments, soaked in distilled water (experiment 32/3) shows the development of a limited amount of cement crystals (see Plate 3.16 A and B) on the few coated grains and peloids that are present. Using optical microscopy, the sediment soaked in hydrogen peroxide (32/4) appears to be devoid of cement crystals (see Plate 3.16 C and D). Any such crystals that are present in the

PLATE 3.16 - INVESTIGATION OF THE EFFECT OF ORGANIC
MATTER

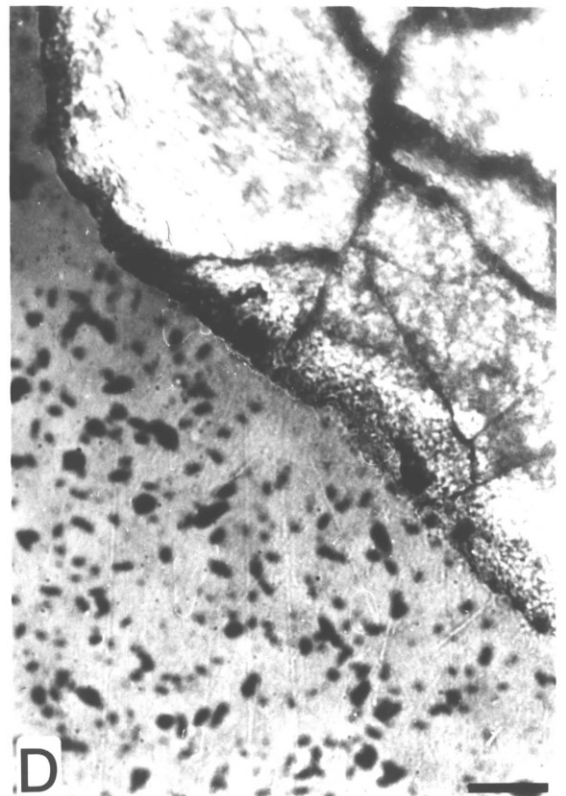
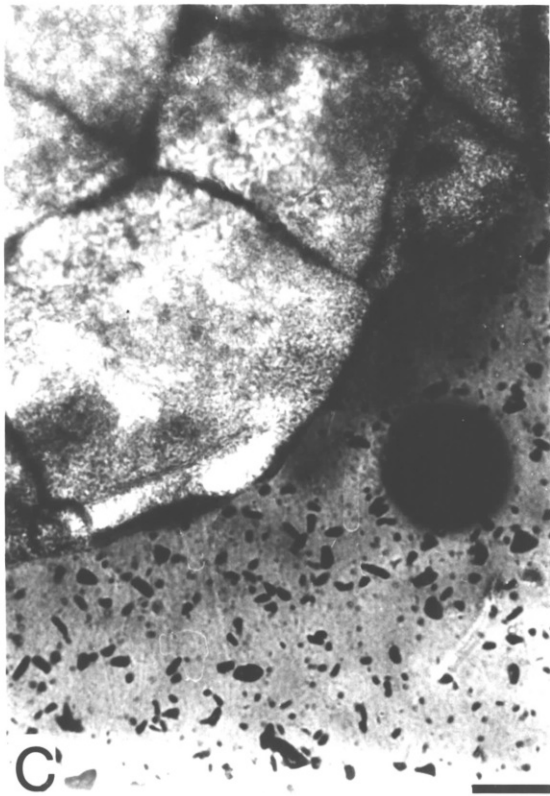
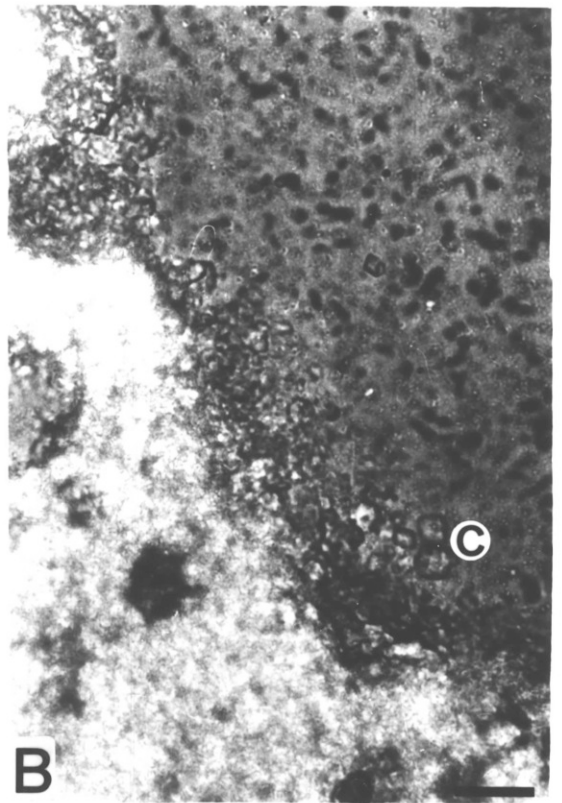
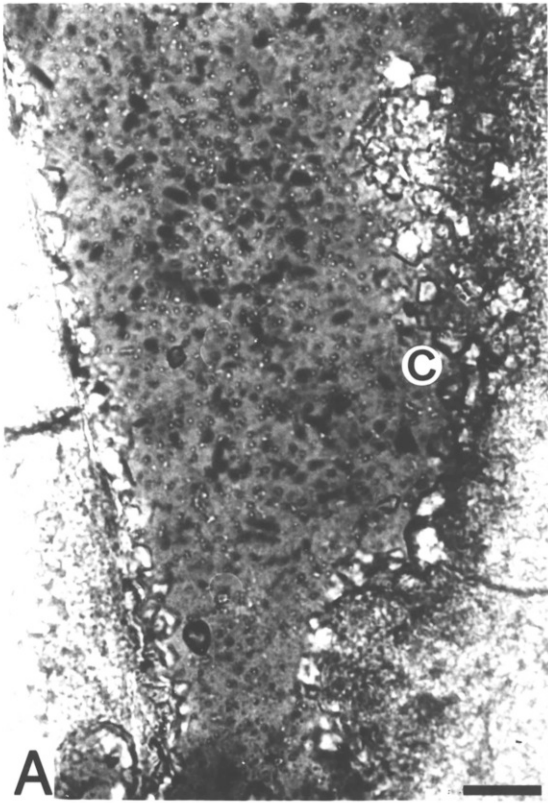
(A) Experiment 32/3 (AKS4) - Small cement crystals (C) are observed on the surfaces of a coated grain and peloid. PPL. Scale bar 20 μm .

(B) Experiment 32/3 - Small cement crystals (C) are observed on the surface of a peloid. PPL. Scale bar 20 μm .

(C) Experiment 32/4 (AKS4 soaked in H_2O_2) - Surface of a peloid devoid of cement crystals. PPL. Scale bar 20 μm .

(D) Experiment 32/4 - Surface of a peloid devoid of cement crystals. PPL. Scale bar 20 μm .

PLATE 3.16



partially lithified sediment, require the use of an electron microscope for their observation.

Secondary Porosity: Very little, if any, secondary porosity has been created in association with the shell fragments in experiment 32/3 and 32/4 (see Plate 3.16 A-D).

Replacement Textures: Replacement has been limited to a few shell fragments which have undergone neomorphism, where the original structure has been replaced by a mosaic of sparry calcite.

XRD analysis shows the same pattern observed in the experiments run using coated grains. The sediment soaked in hydrogen peroxide shows hardly any alteration whatsoever (0% aragonite dissolution), while the sediment of experiment 32/3 shows a small amount of aragonite dissolution (approximately 5 %).

(2) Pore Fluid Evolution

(i) Kuwait Subtidal Ooids

The pore fluid evolution curves (in terms of $\text{mMg}^{2+}/\text{mCa}^{2+}$ and $\text{mSr}^{2+}/\text{mCa}^{2+}$ ratios) for both experiments using coated grains (32/1 and 32/2) are very similar (see Fig. 3.24) irrespective of the latter being soaked in H_2O_2 .

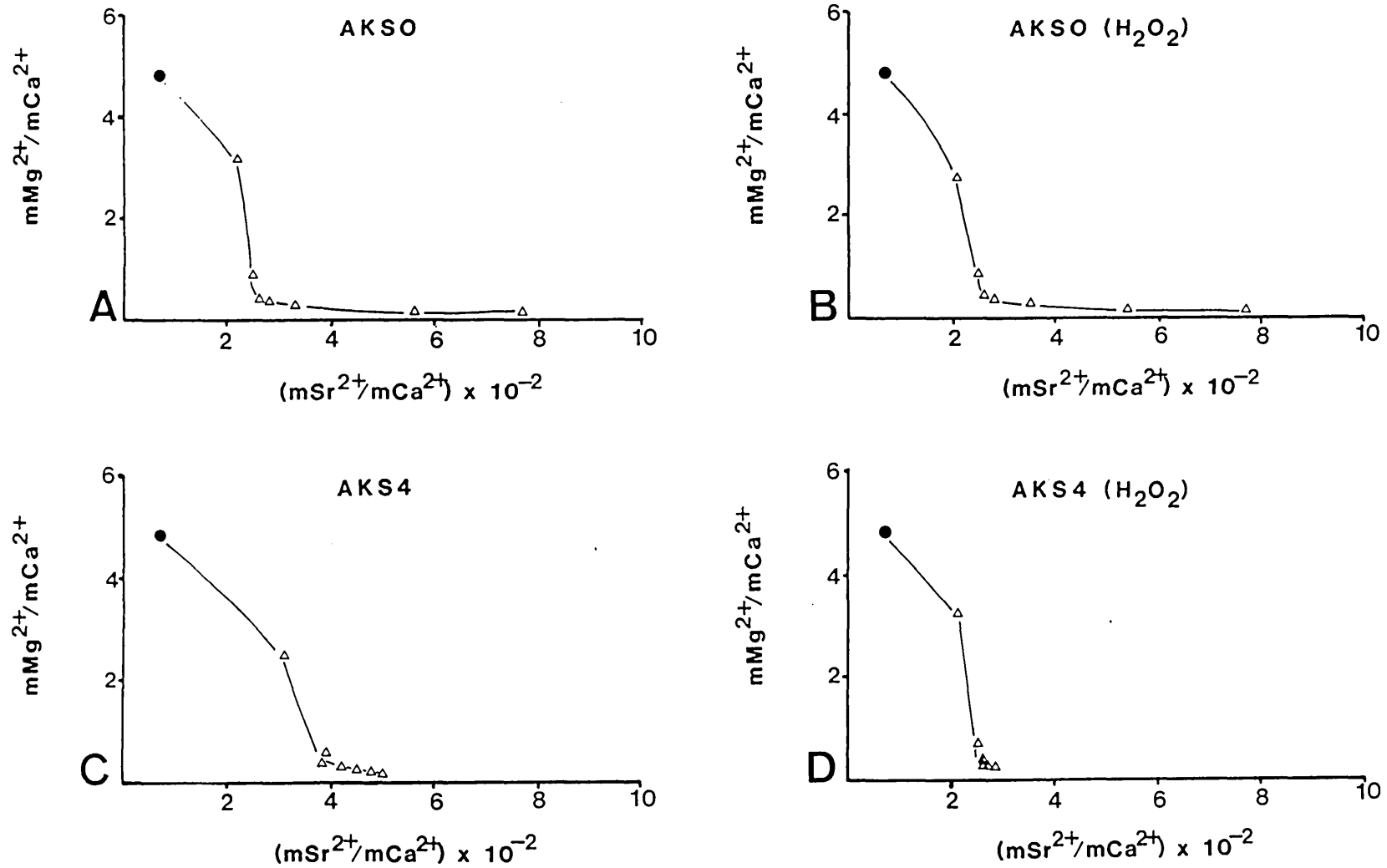


Fig. 3.24 - Evolution of pore fluids from the composition of seawater (●) during experiments investigating the effect of organic matter. (A) Experiment 32/2, (B) Experiment 32/2, (C) Experiment 32/3 and (D) Experiment 32/4.

(ii) Kuwait Shell Fragments

The evolution curves of the pore fluids during experiments 32/3 and 32/4 show significant deviations with respect to their $m\text{Sr}^{2+}/m\text{Ca}^{2+}$ ratios. This ratio increases much more in the experiment using shell fragments soaked in distilled water (maximum value 5×10^{-2}) than in the experiment using shell fragments soaked in hydrogen peroxide (maximum value of 3×10^{-2}).

(3) Cement Crystal Chemistry

(i) Kuwait Subtidal Ooids

The chemical distribution of the cement crystals precipitated in both experiments show a considerable overlap of their MgCO_3 and SrCO_3 contents (see Fig 3.25).

The MgCO_3 content on average, is slightly higher in the cement precipitated in experiment 32/1 than that in experiment 32/2 (soaked in H_2O_2) but both are typically in the range 2-5.5 mole %. The SrCO_3 content of the cement, on average, is slightly lower in experiment 32/1 than in experiment 32/2 (soaked in H_2O_2). The SrCO_3 content of the cement precipitated in experiment 32/1 ranges from being not significant to a maximum of 0.45 mole % while the SrCO_3

content of the cement precipitated in experiment 32/1 ranges from 0.15-0.65 mole %.

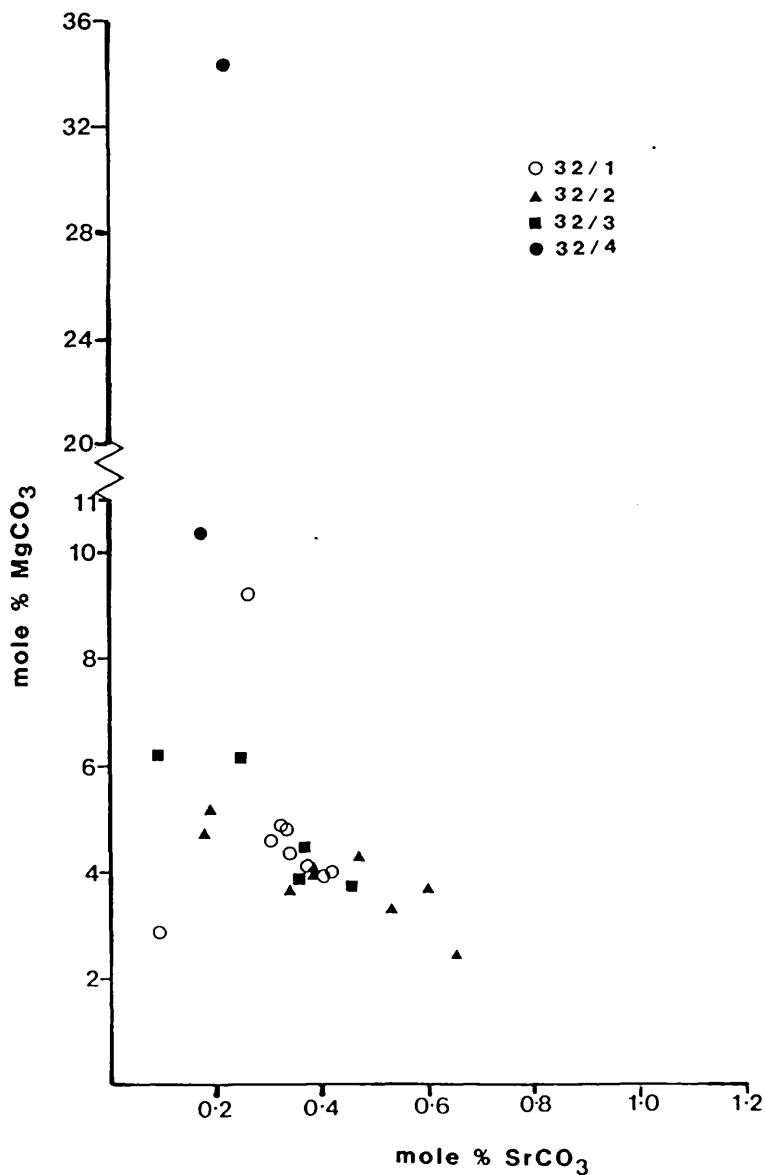


Fig. 3.25 - Mole % MgCO₃ and SrCO₃ contained in cement crystals precipitated during experiments 32/1-32/4.

The SO₄²⁻ contents of the cement crystals are also very similar in the cement precipitated in both experiments (see Fig. 3.26) with most analyses being in the range 0.65-1.3

mole %.

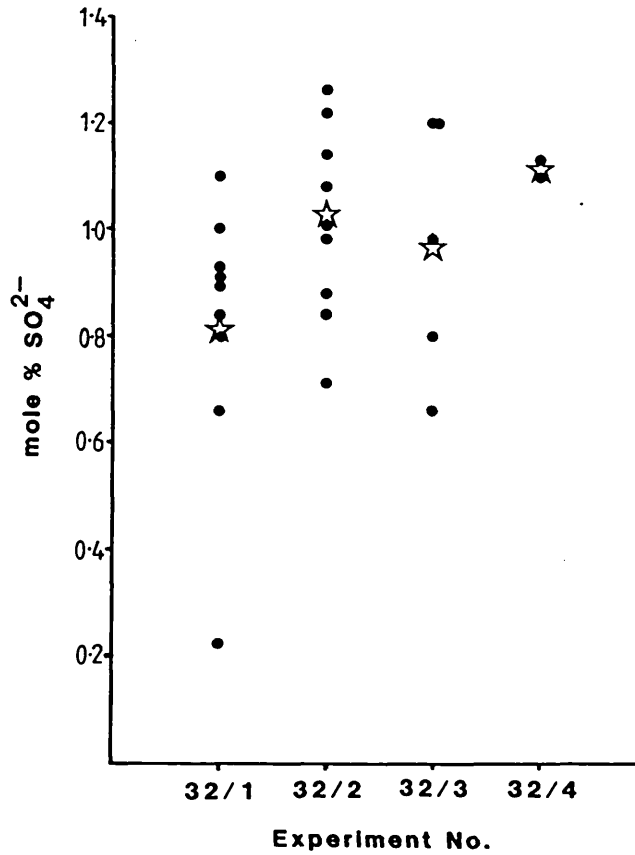


Fig. 3.26 - Mole % SO_4^{2-} contained in cement crystals precipitated during experiments 32/1-4. Mean values (\blacklozenge) are shown.

(ii) Kuwait Shell Fragments

The chemical distribution of the cement crystals precipitated in experiment 32/3 (AKS4), is very comparable to that of the cement precipitated in experiment 32/1 (AKSO). The range of MgCO_3 is slightly lower 3.5 - 6.5 compared to 4 - 9.5 mole %) and the range of SrCO_3 levels is almost identical from being not significant to 0.45 mole %.

The levels of SO_4^{2-} contained within the cement precipitated are also comparable to those of the cement precipitated in both experiments 32/1 and 32/2, being in the range 0.65 - 1.2 mole %.

Cement crystals in experiment 32/4 were very few in number. Two however, have been analysed and these show compositions which are comparable to small cement crystals which have been found in other experiments (see section 4.2). The MgCO_3 contents of these crystals are 10.4 and 34.4 mole % with SrCO_3 contents of 0.17 and 0.22 mole % respectively (see Fig. 3.24). The SO_4^{2-} contents of these crystals fall in the upper range of those observed for the cement crystals analysed in the other experiments i.e. 1.1 - 1.13 mole % (see Fig. 3.25).

(4) SUMMARY

Using sediment AKSO (coated grains), soaking in hydrogen peroxide had the following effects:

- (i) less cement was precipitated,
- (ii) the degree of alteration as measured by XRD was less and
- (iii) the chemistry of the cement phase varied slightly in that average MgCO_3 contents were slightly lower and SrCO_3

and SO_4^{2-} contents slightly higher than those precipitated in experiments using sediment AKSO which had not been soaked in hydrogen peroxide.

Soaking in hydrogen peroxide however did not significantly affect the composition of the pore fluids during the experiments.

Using sediment AKS4 (shell fragments), soaking in hydrogen peroxide had the following effects:

- (i) the precipitation of cement crystals was reduced,
- (ii) the degree of alteration as measured by XRD, was reduced,
- (iii) the small cement crystals that were precipitated showed a similar composition to small cement crystals found in other experiments, i.e. high MgCO_3 content 10 - 35 mole % and low SrCO_3 contents 0.17 - 0.22 mole %. SO_4^{2-} levels of 1.1 and 1.13 mole % were observed.
- (iv) lower $\text{mSr}^{2+}/\text{mCa}^{2+}$ ratios were observed in all pore fluid samples collected during the experiment.

CHAPTER 4 - INVESTIGATION OF THE EFFECT OF CHANGES IN THE EXPERIMENTAL CONDITIONS

4.1 INTRODUCTION

The experimental conditions which were varied during this part of the investigation were:

- (1) the length of time,
- (2) the temperature applied,
- (3) the hydrostatic pressure applied and
- (4) whether pore fluid sampling occurred or not.

Results relating to each of these are presented.

4.2 EFFECT OF TIME

Most experiments were run for between 40 - 50 days, during which time diagenesis proceeded to such an extent that processes of cement precipitation, the creation of secondary porosity, the infilling of that porosity and the replacement of grains could be studied (see section 3.5). However, several experiments were run for periods of less than 30 days so that processes involved in the the early development of these fabrics could be studied. Also several experiments had to be aborted because of hydrostatic pressure failure and although these are not directly comparable because of the loss of hydrostatic pressure, they nevertheless are of

interest when examining the very early stages of the experimental diagenesis.

Expt.No.	Sediment	Time(days)	
2485	ADBO	7] No pore fluid sampling
2585	ADBO	15	
2685	ADBO	21	
18/4	ADDO	26	
3586	BSO	Aborted day 4	
3886	BSO	Aborted day 3	

Table 4.1 - Experiments studying the early stages of textural and mineralogical development.

4.2.1 TEXTURAL DEVELOPMENT

(1) Fabrics Developed in Experiments of 7 to 26 Days
Duration (no fluid substitution)

Experiment 2485 (7 days)- No cement is found to have been precipitated during this experiment as shown in Plate 4.1 A and B. Petrographic examination (see Plate 4.1 B) shows that little, if any, of the original aragonite underwent dissolution and XRD data confirms this indicating that (much) less than 5 % of the aragonite went into solution.

The early stages of neomorphic alteration however, have been

PLATE 4.1 - EXPERIMENT 2485, EXPERIMENTAL TIME 7 DAYS

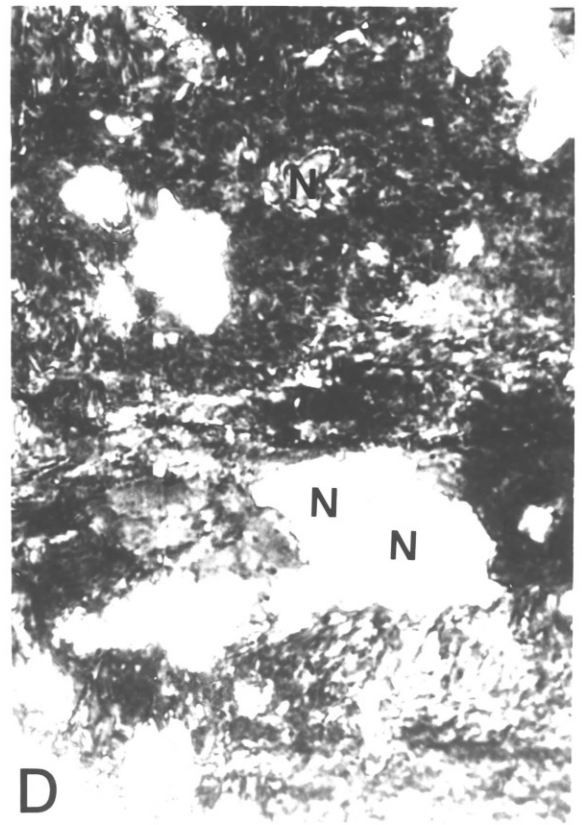
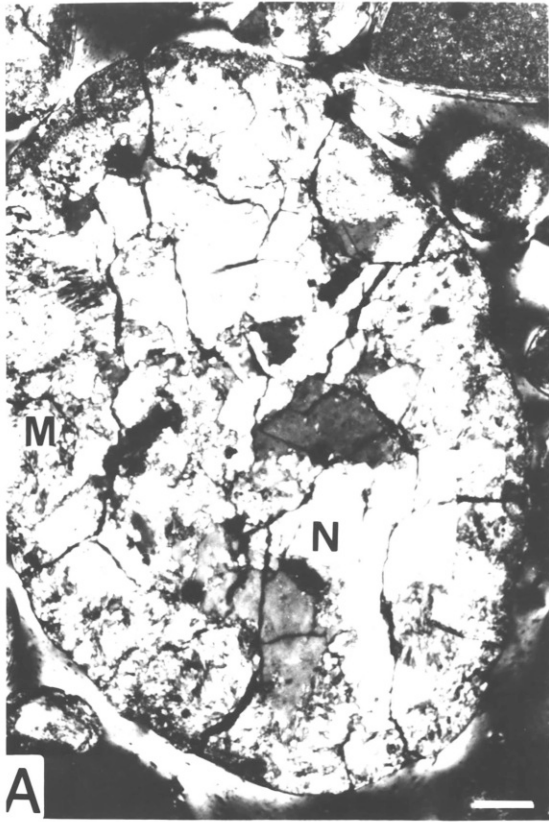
(A) Micritised grain which has undergone partial neomorphism. The boundaries between the neomorphic spar (N) and the original micrite (M) are irregular and narrow areas of original micrite are seen between spar crystals. XP. Scale bar 100 μm .

(B) Shell fragment nucleus to coated grain undergoing neomorphism. Neomorphic spar (N) begins as discrete areas in the original aragonite shell structure (A). Boundaries are irregular. Coated grains show no evidence of alteration retaining pseudo-uniaxial crosses. XP. Scale bar 100 μm .

(C) Detail of neomorphic spar (N) in grain shown in (B). XP. Scale bar 20 μm .

(D) Detail of neomorphic spar (N) in grain shown in (B). XP. Scale bar 20 μm .

PLATE 4.1



noted as shown in Plate 4.1. Plate 4.1 A shows a micritised grain in which areas of neomorphic spar (N) are observed. These areas of neomorphic spar are much larger than the spar which usually replaces micritic carbonate (see section 3.5.1). The patches of calcite spar have coalesced in certain areas forming an irregular mosaic. Plate 4.1 B shows a coated grain which has, as its nucleus, an aragonitic shell fragment. Patches of calcite spar (bright spots) are observed within the shell fragment, details of which are shown in Plate 4.1 C and D. Most of these areas of spar are composed of single crystals but some of the larger areas (see Plate 4.1 D) show the development of two or more crystals (N). All of these neomorphic spar crystals show irregular boundaries, both with the original aragonite and with each other. These areas are very variable in size as shown in Plate 4.1 A-D.

Experiment 2585 (15 days)- A small number of equant calcite crystals are observed surrounding grains (see Plate 4.2 A and B). These crystals range in size, up to a maximum of 8 μm in diameter but are usually around 5 μm . They are small when compared to the cement crystals shown in section 3.5.1(3) (average size 15 μm), which were generated using the same starting sediment and similar physical conditions of temperature and hydrostatic pressure but under longer experimental times. Plate 4.2 B shows how most of these early cement crystals are found in association with the

PLATE 4.2 - EXPERIMENT 2585, EXPERIMENTAL TIME 15 DAYS

(A) Unaltered coated grain (A) with pseudo-uniaxial cross. Isolated cement crystals are observed along grain edges (C). XP. Scale bar 50 μm .

(B) Small calcite cement crystals (C) are more frequently associated with peloids and broken surfaces of coated grains. The nucleus of the elongate coated grain has been almost totally replaced by neomorphic spar (N). The overlay shows where areas of original micrite exist. Areas of small neomorphic spar crystals replacing micrite are also shown on the overlay. XP. Scale bar 50 μm .

(C) Area of organic matter in the sediment pore space on which many calcite crystals have grown. XP. Scale bar 20 μm .

(D) Micritic peloid which has been partially replaced by neomorphic spar (N). The boundary between the micrite and calcite spar is irregular. Boundaries between spar crystals are also irregular. XP. Scale bar 50 μm .

OVERLAY KEY

Areas stippled - unaltered micrite

Areas outlined - neomorphic spar replacing micrite.

PLATE 4.2

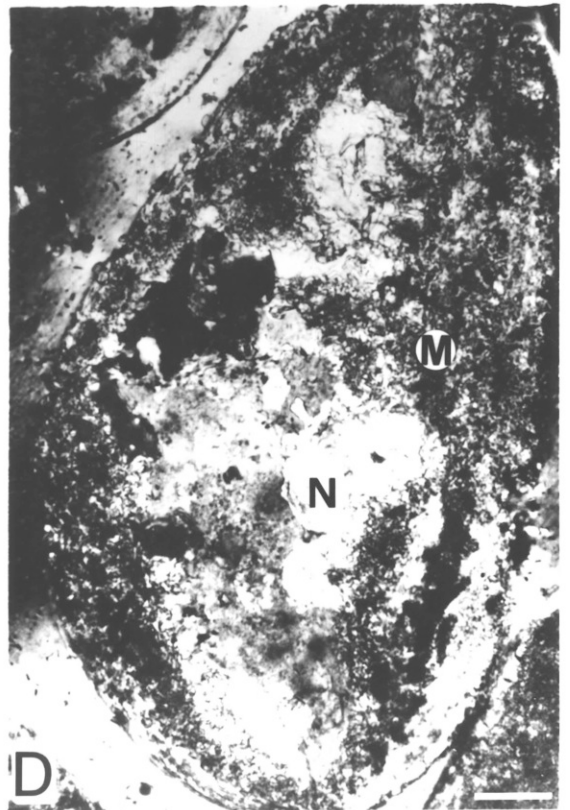
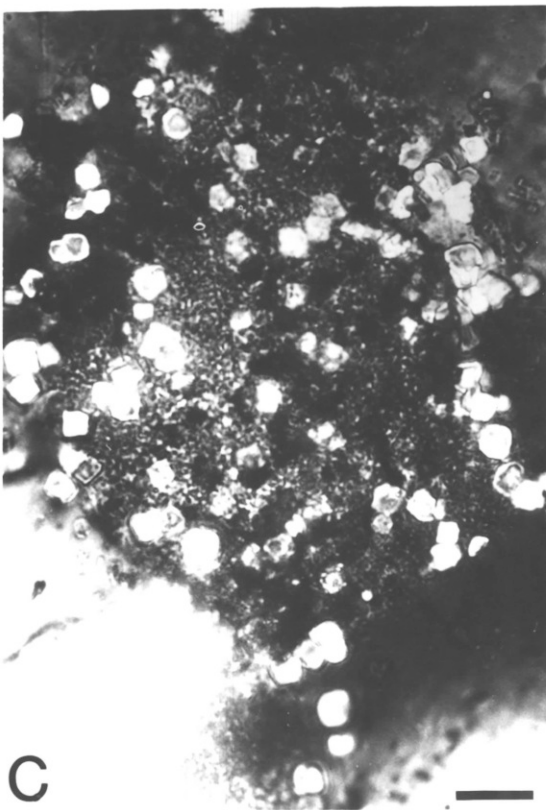
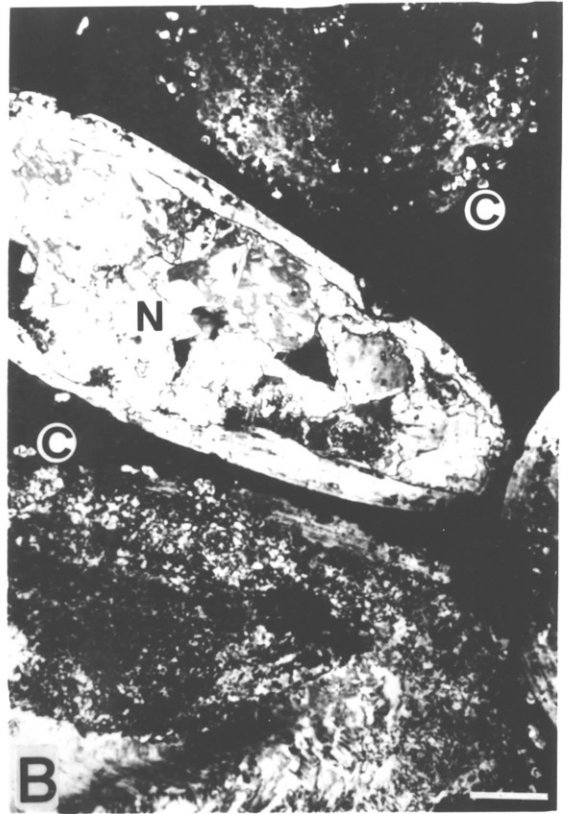
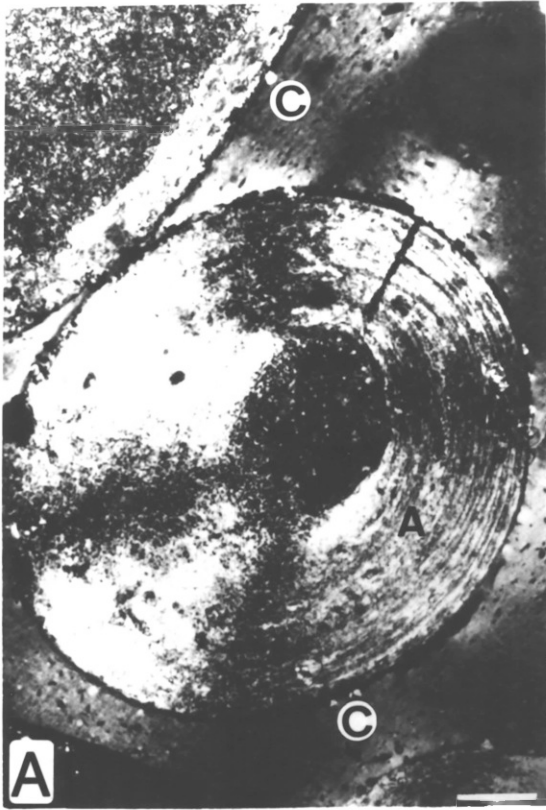
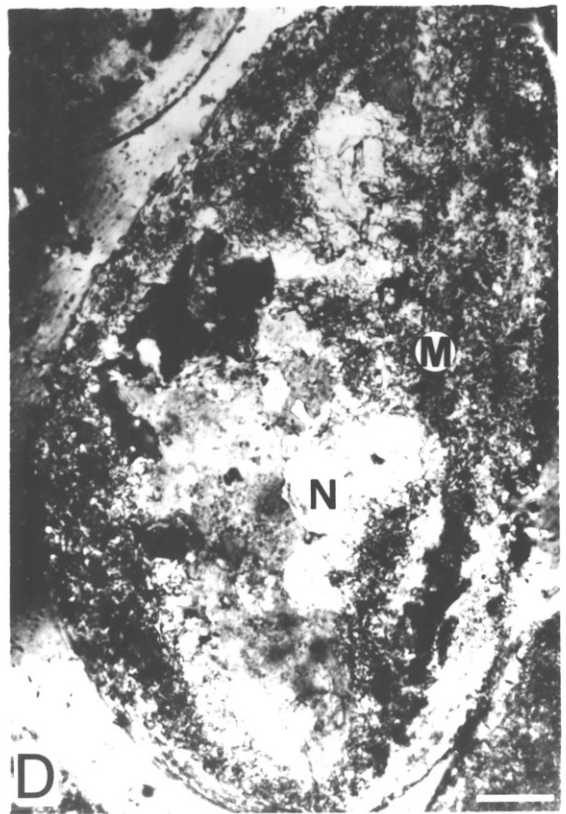
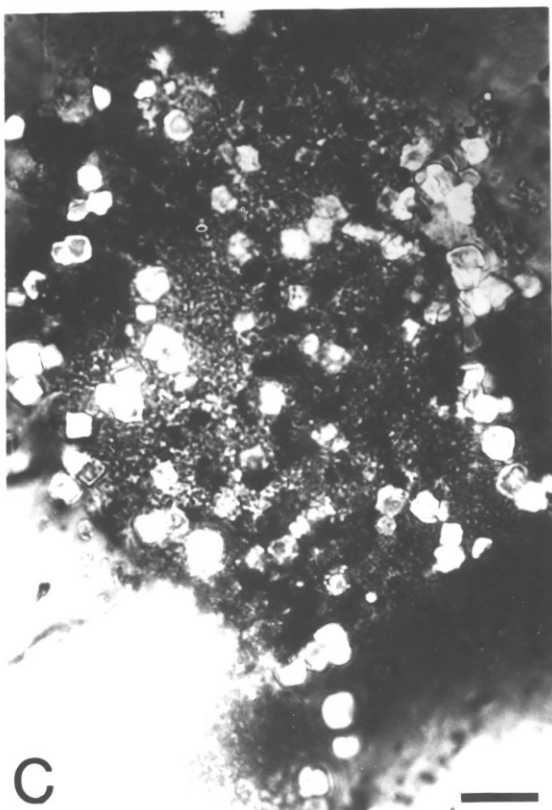
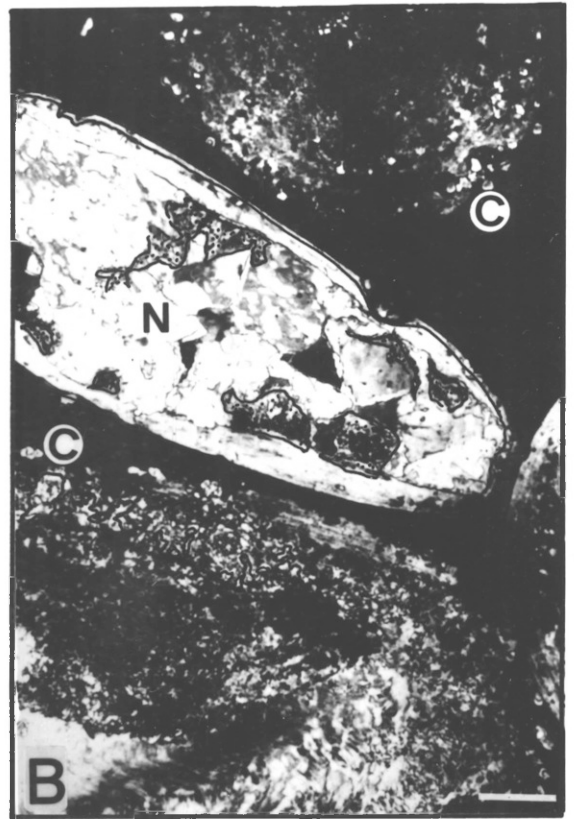
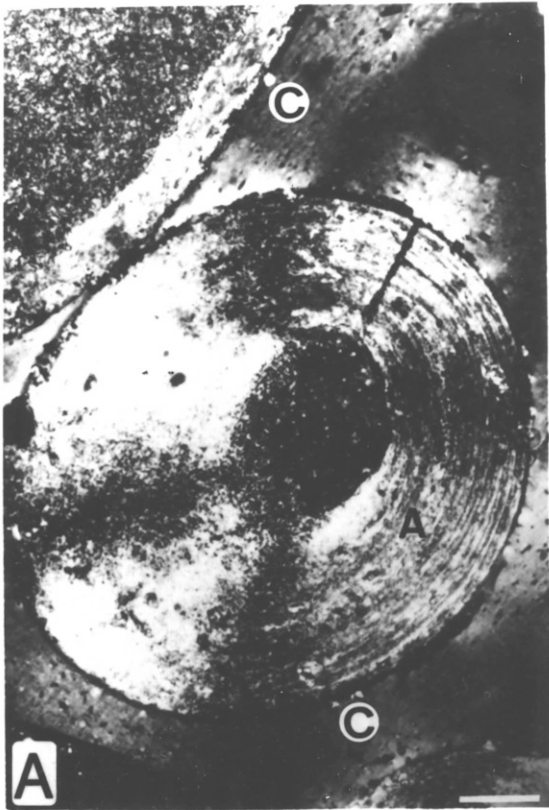


PLATE 4.2



irregular surfaces of micritic peloids. Many more crystals are observed in association with organic matter/micritic carbonate than on other sediment grains (see Plate 4.2 C).

Plate 4.2 A and B show that very little secondary porosity has been created. The coated grain shown in Plate 4.2 A with the thick cortex (A), still displays a pseudo-uniaxial cross, which is seen in modern, unaltered ooids (see Scholle, 1978, p.115). XRD analysis again shows that almost no aragonite has been removed (less than 5% - see Appendix V).

The results of neomorphism are much more advanced in the sediment of experiment 2585 when compared to material from experiment 2485. Plate 4.2 B shows a coated grain in which the nucleus has been almost totally replaced by an irregular mosaic of sparry, neomorphic calcite (N). Small areas of original micrite however exist (see overlay). Plate 4.2 D also shows a peloid in which a large proportion of the micrite has been replaced. The size of these neomorphic crystals are larger than those seen in the results presented in section 3.5.1. The crystal boundaries between the neomorphic spar (N) and the micrite (M) are very irregular often interfingering.

Experiment 2685 (21 days)- Slightly more calcite crystals are observed surrounding grains in the partially lithified

PLATE 4.3 - EXPERIMENT 2685, EXPERIMENTAL TIME 21 DAYS

(A) Isolated, equant cement crystals are observed on surfaces of coated grains (see overlay) but clusters of nuclei are observed on broken surfaces of peloids (C). The original aragonite cortices of coated grains (A) show no evidence of alteration. PPL. Scale bar 50 μm .

(B) A greater number of equant cement crystals are observed on broken surfaces of coated grains (C) than on smooth surfaces (see overlay). Much of the micritic nucleus of the left hand grain has undergone neomorphism resulting in a mosaic of small granular crystals (N). PPL. Scale bar 50 μm .

(C) Partially replaced grain. Overlay shows areas resembling neomorphic spar and solution cavity fill calcite. PPL. Scale bar 50 μm .

(D) Detail of the replaced grain shown in Plate 4.3C. Overlay shows how crystals grow away from the inner surface of the cortex, suggesting a solution cavity fill mechanism. PPL. Scale bar 20 μm .

OVERLAY KEY (for 4.3 C and D)

Area outlined - original aragonite.

Area lined - replacement fabric resembling neomorphic spar.

Area stippled - replacement fabric resembling solution cavity fill calcite.

PLATE 4.3

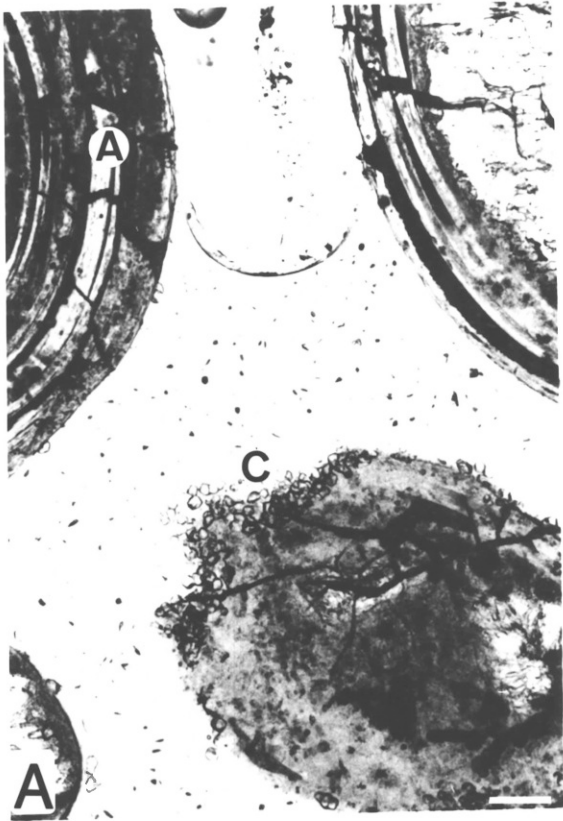
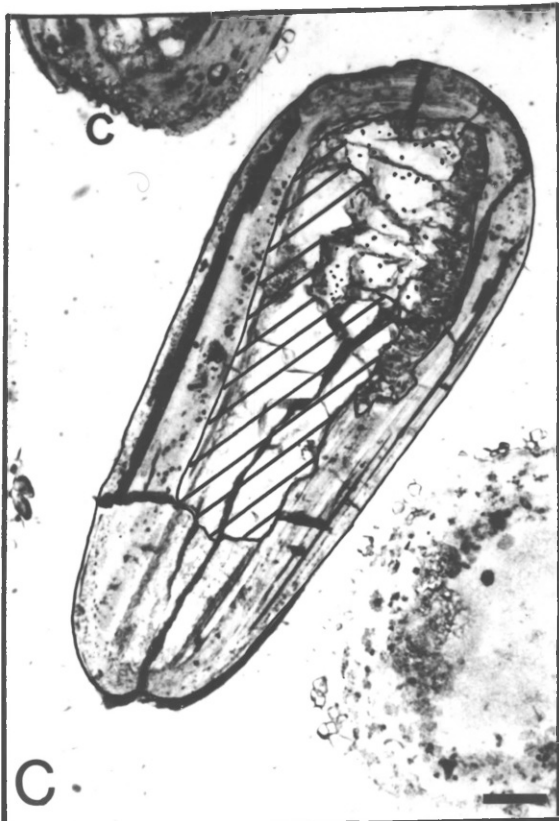
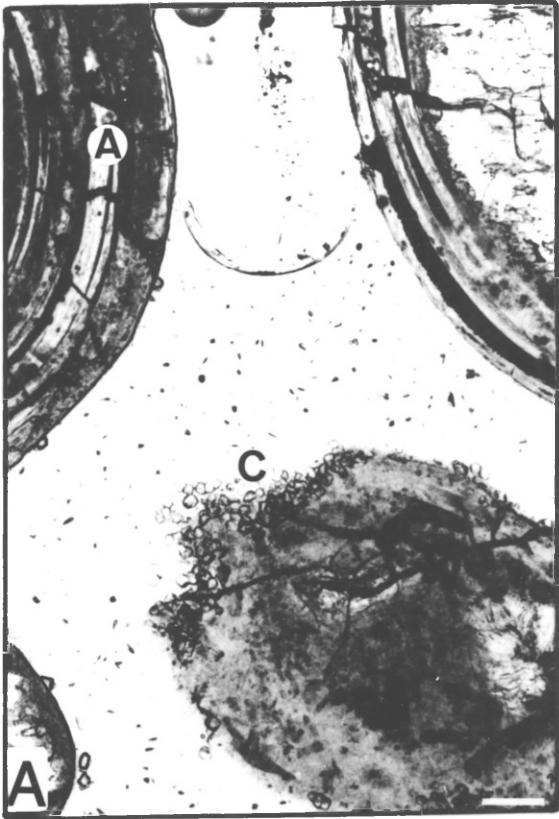


PLATE 4.3



sediment of experiment 2685 than that in experiment 2585 (maximum crystal diameter 7 - 8 μm , see Plate 4.3 A-C). As usual, uncoated grains show the development of more cement Crystals than coated grains (see Plate 4.3 A-C) and the bored surfaces of coated grains (see Plate 4.3 C) show the development of more crystals than unbored edges. The creation of secondary porosity by the dissolution of aragonite has been very limited with XRD showing that less than 5% of the original aragonite was removed. However, Plate 4.3 C and D show that some of the replacement may have been through a solution cavity fill mechanism. Plate 4.3 C shows an irregular mosaic of calcite, similar to that produced by neomorphism with the interface between the replacement calcite and the original aragonite being across a very narrow alteration front (see overlay). Detailed examination of the other end of the grain however (see Plate 4.3 D) shows how the replacement crystal size increases away from the inner edge of the cortex, suggesting the infilling of a void space. This points to the difficulty that is often encountered when trying to distinguish fabrics generated by the two modes of replacement.

These samples show the precursor to the equant cement fabric. Cement crystals are isolated, becoming more abundant with increasing length of experimental time. Each crystal however has a certain amount of space in which it could develop further.

Experiment 18/4 (26 days) - Using sediment ADDO, the results of this experiment show the early stages of development of the granular bladed fabric. A very narrow but isopachous rim (3 μm wide) of crystals surrounds each grain (see Plate 4.4 A and B). On coated grains, this is generally composed of one layer of crystals only (Plate 4.4 A and B) but on peloids, the cement rim can be several layers of crystals thick as shown in Plate 4.4 C. Very little oomoldic porosity has been created (see Plate 4.4 B) with no infilling of this porosity occurring. XRD analysis shows that again less than 5% of the original aragonite has been removed.

(2) Cement Crystals Formed in Aborted Experiments

Any cement crystals that have been formed in these experiments (3586 and 3886, which ran for 4 and 3 days respectively) are so small (maximum size 1-2 μm), that they can only be seen using an electron microscope (see Plate 4.5 A). These crystals are of a rhombic morphology as seen in Plate 4.5 A. Plate 4.5 B shows two grain surfaces, one of a coated grain, the other a micritic peloid. A layer of crystals is observed on the peloid while the coated grain surface is almost devoid of any crystals. Cement crystals are also observed filling algal borings (see Plate 4.4 A and B).

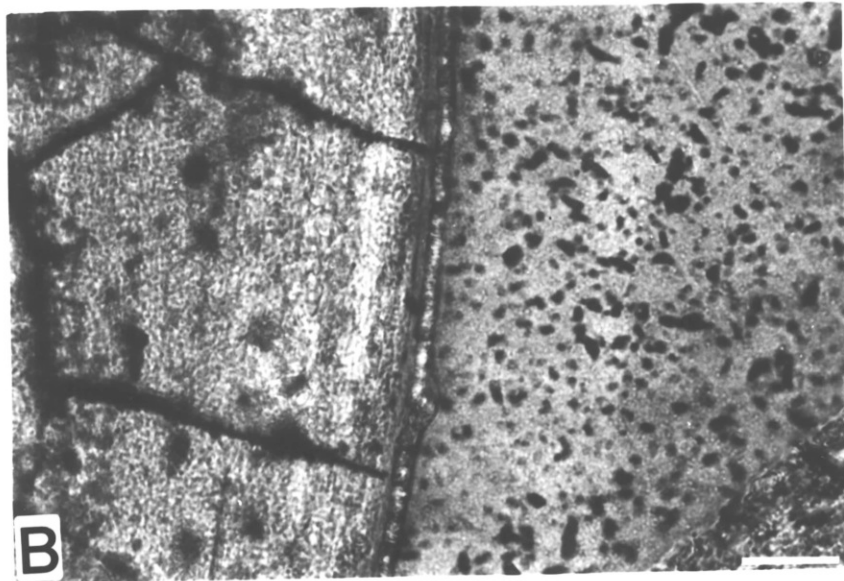
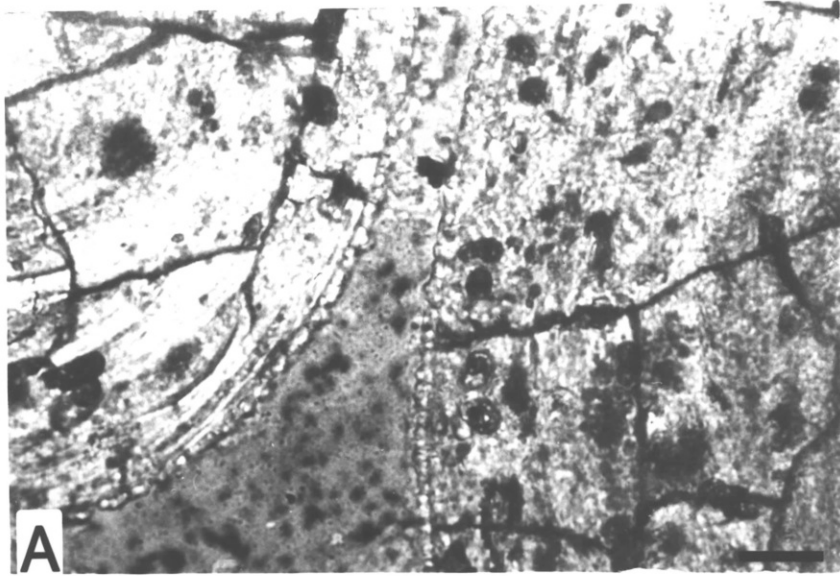
PLATE 4.4 - EXPERIMENT 18/4, EXPERIMENTAL TIME 26 DAYS

(A) Narrow, isopachous fringes of granular-bladed cement crystals are observed surrounding sediment grains. Almost no alteration of the sediment grains is observed. PPL. Scale bar 20 μm .

(B) Narrow isopachous fringe of bladed cement crystals fringing the coated grain. Secondary porosity has been created by the dissolution of aragonite immediately below the cement fringe. PPL. Scale bar 20 μm .

(C) Multiple layers of granular cement crystals on peloid. Micro-porosity has been created by the removal of original micrite and neomorphic spar replacing some of the original micrite. Linear cracks are due to thin sectioning. XP. Scale bar 20 μm .

PLATE 4.4



4.2.2 CEMENT CRYSTAL CHEMISTRY

No pore fluid samples were collected during any of the experiments presently under discussion. Electron microprobe analyses (EMPA) however are available for cement crystals from all experiments. The MgCO_3 and SrCO_3 contents (mole %) are shown in Fig 4.1 and the SO_4^{2-} content (mole %) is shown in Fig. 4.2.

(1) Cement Crystals Precipitated in Aborted Experiments

Back-scatter observation (see Plate 4.5 A and B) show the cement crystals precipitated in experiments 3586 and 3886, to be of a high-Mg composition (the dark grey shade signifies a much higher MgCO_3 content than either low-Mg calcite or aragonite, see section 2.4.1(2)). EMPA have shown the MgCO_3 level in these crystals to range from 29-76 mole % in experiment 3586 and from 47-72 mole% in experiment 3886. The compositions are similar to proto-dolomite, dolomite and Ca-rich magnesite but no mineralogical data are available. This is discussed in Chapter 8. A significant although low level of SrCO_3 is also observed in these crystals (0.1 - 0.34 in experiment 3585 and 0.15 - 0.35 in experiment 3886). The SO_4^{2-} contents of the crystals are shown in Fig. 4.2. In experiment 3586, this ranges from 0.78 - 1.15 mole % while in experiment 3886, the range is

PLATE 4.5 - MG-RICH CEMENT CRYSTALS

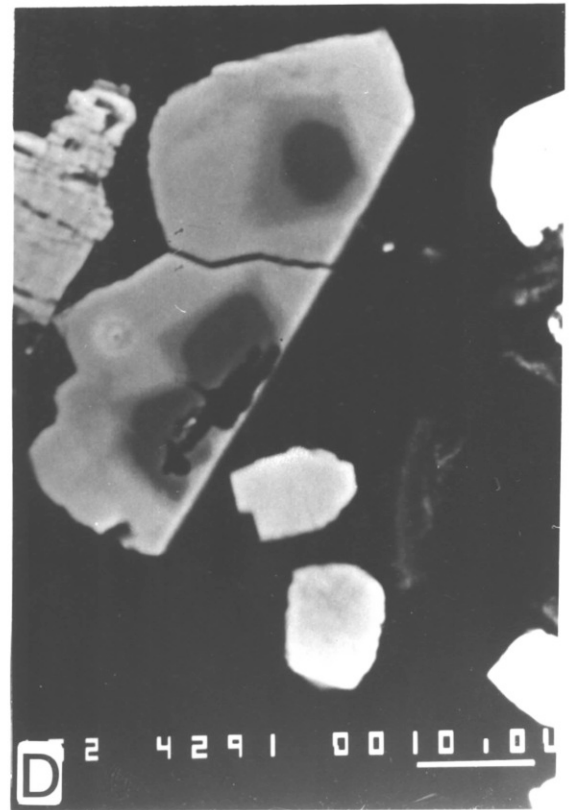
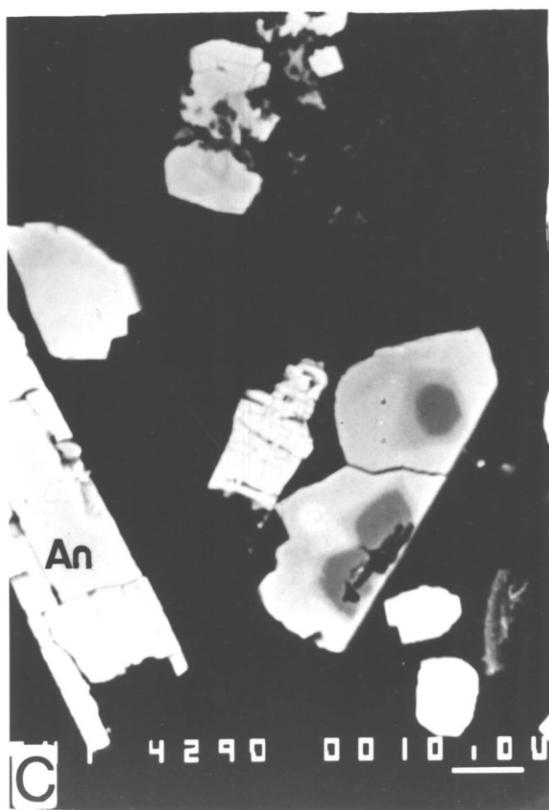
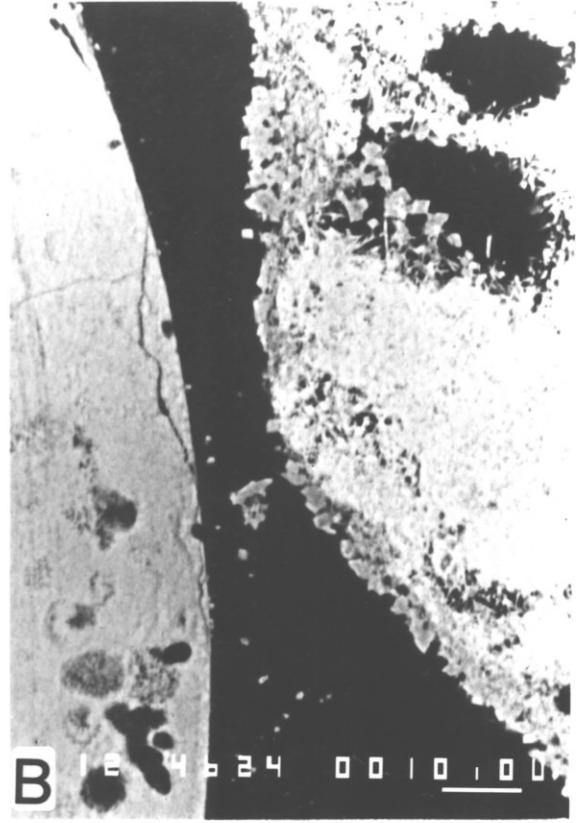
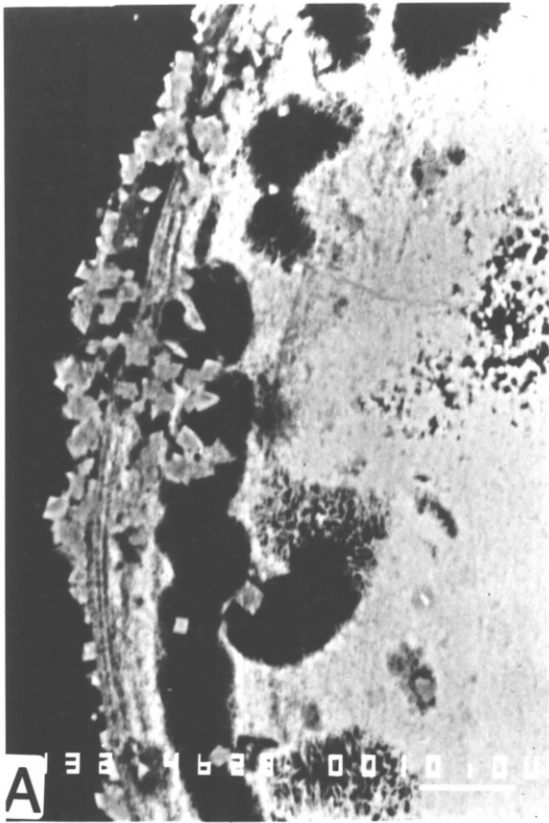
(A) Experiment 3886 - Back-scatter electron microscopy shows that the small cement crystals are of a much higher Mg content (dark grey) than the aragonitic grain on which they have been precipitated (dark grey). Crystals are more abundant where the cortex of the coated grain has been broken by the boring action of endolithic algae. Scale bar 10 μm .

(B) Experiment 3886 - Cement crystals are much more abundant on the surface of the peloid than on the surface of the coated grain. Back-scattered electron image. Scale bar 10 μm .

(C) Experiment 1785 - A cement crystal group with three compositional phases occurs in the sediment pore space. The darker shade of the crystal cores indicates a much higher Mg content than the outer layers. Each compositional phase shows a distinct, nearly straight edged boundary with the later phase. The crystal group shows a straight edge and is in close association with an anhydrite lath (An). Back-scattered electron image. Scale bar 10 μm .

(D) Experiment 1785 - Detail of cement crystals group shown in Plate 4.5 C. The Mg-rich cores are have undergone partial dissolution. Scale bar 10 μm .

PLATE 4.5



approximately 0.9 - 1.16 mole %.

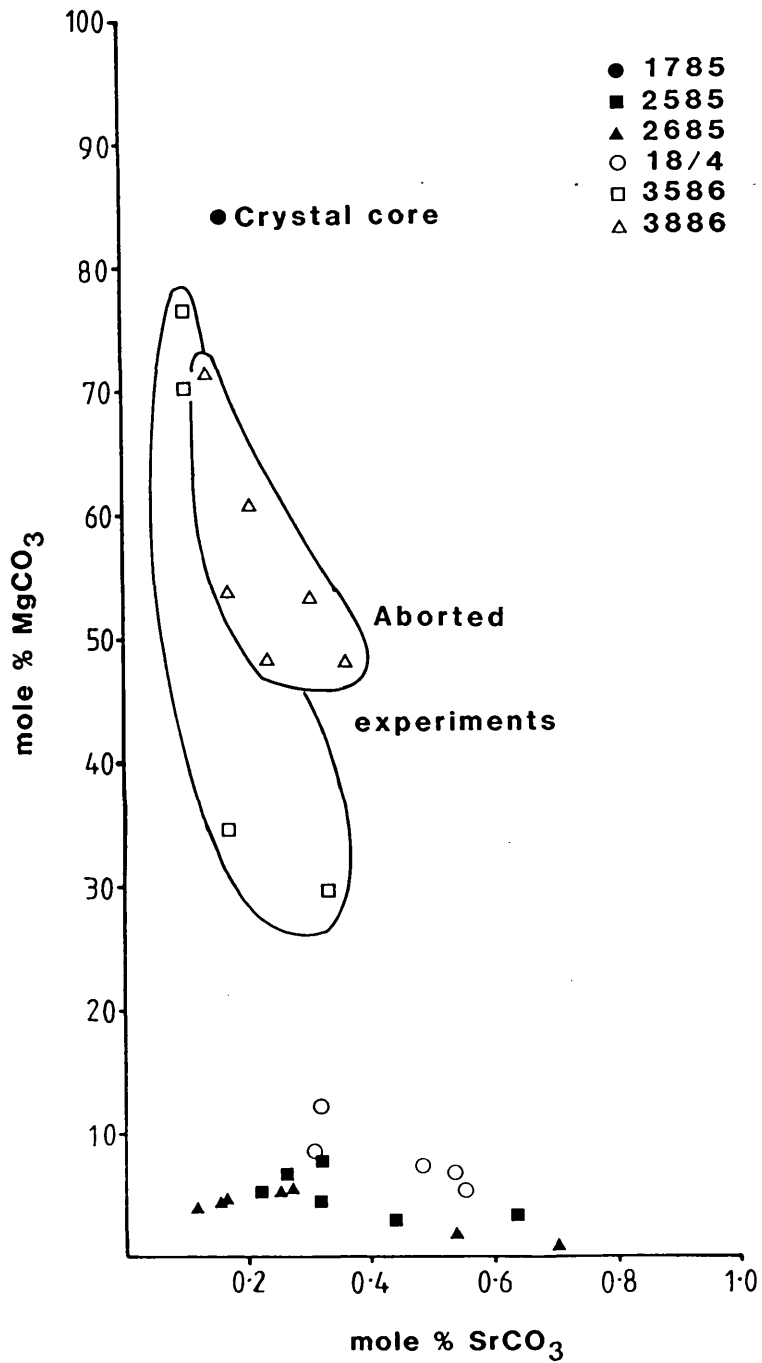


Fig. 4.1 - Mole % MgCO_3 and SrCO_3 contained in cement crystals precipitated during aborted and short term experiments.

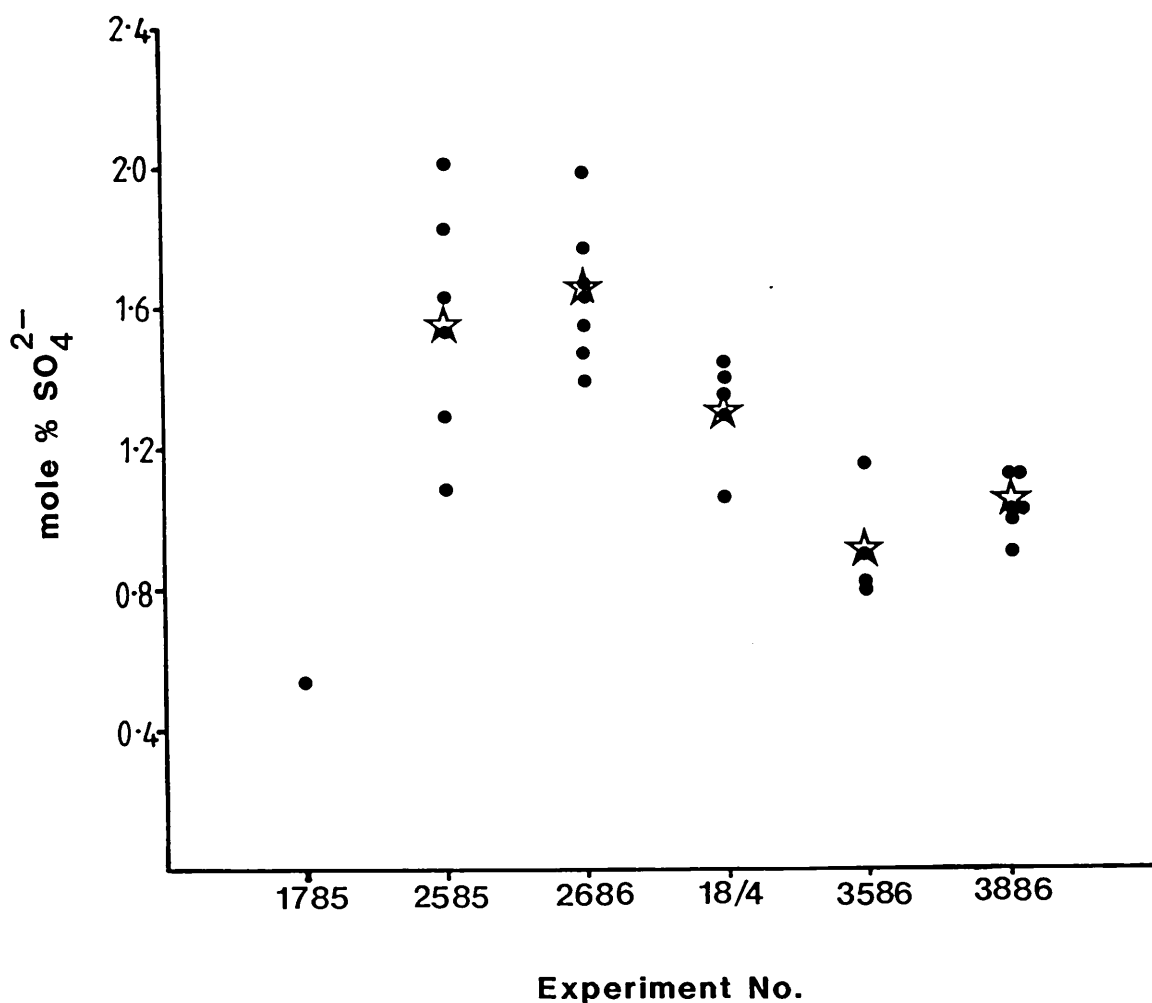


Fig. 4.2 - Mole % SO₄²⁻ contained in cement crystals precipitated in aborted and short term experiments. Mean values (☆) are shown.

(2) Early Mg-rich Crystal Cores in Standard Experiment 1785 (with substitution)

Cores to cement crystals which are sufficiently distinct in chemical character from later cement phases to be observed using back-scatter electron microscopy (see section 2.4.1),

are very rare - only one occurrence has been found (in experiment 1785 using the sediment ADBO). A group of three crystals has been found in close association with an anhydrite lath (see Plate 4.5 C). The straight edge of the cement crystal group suggests that the early crystals were close enough to the lath for the continued growth of later phases to be restricted by it. Back-scatter microscopy shows three compositional layers to the crystals (see Plate 4.5 D):

(i) Dark grey cores - these are 6-10 μm in diameter. The dark shade of grey signifies a very high MgCO_3 content (84 mole %, see Fig. 4.1).

(ii) Grey middle layers - distinct overgrowths on the Mg-rich nuclei are noted. These display distinct crystal edges and vary in thickness from 1-5 μm . No EMPA are available but the shade of grey would signify 40-50 mole % MgCO_3 ,

(iii) Light grey outer layers - these are the largest area of the crystals and are of a similar shade to the other cement crystals. EMPA showed this to contain 2.8 mole % MgCO_3 .

The very Mg-rich cores to this crystal group have been affected by dissolution (see Plate 4.5 D). The mid and light grey layers of the crystal group however are unaffected.

(3) Experiments of 7 to 26 Days Duration (no fluid substitution)

No cement crystals were observed in the sediment from experiment 2485. Experiments 2585 and 2685 were run using the same sediment as in 2485 but for 15 and 21 days respectively. The cement crystals precipitated in experiment 2585 contain a slightly higher level of MgCO_3 than those precipitated in experiment 2685 (see Fig. 4.1). The cement crystals of both experiments contain comparable levels of SrCO_3 , ranging from 0.2 - 0.65 mole % in experiment 2585 and 0.1-0.7 mole % SrCO_3 in experiment 2685. Similar levels of SO_4^{2-} are contained in the cement crystals precipitated in both experiments. In experiment 2585, the level ranges from 1-2 mole % while in experiment 2685, it ranges from 1.3-2 mole %.

Experiment 18/4 (using sediment ADDO) was run for 26 days, longer than either experiments 2585 or 2685. The MgCO_3 (mole %) content of the cement crystals however is higher than in those of experiments 2585 and 2685, ranging from 5-12 mole %. The level of SrCO_3 (mole %) in the cement crystals falls within the range observed in 2585 and 2685 but the variation is lower ranging from 0.3 to 0.6 mole %. The level of SO_4^{2-} (mole %) observed in the cement crystals of experiment 18/4 (see Fig. 4.2) is lower than for those of experiment 2585 or experiment 2685, ranging between 1 and

1.5 mole %.

In a comparison with results from long term experiments using sediment ADBO with fluid substitution, the level of MgCO_3 and SrCO_3 observed was very similar (1-12 mole % MgCO_3 with most analyses showing less than 7 mole % MgCO_3 and 0.1 - 0.8 mole % SrCO_3). SO_4^{2-} contents in the cement crystals in the long term experiments were found to be generally lower than those in the short term experiments (0.5 - 1.35 mole % SO_4^{2-} compared to 1-2 mole % SO_4^{2-}). Using sediment ADDO, the levels of MgCO_3 in the long term experiments were found to be slightly lower (2-8 mole %) with levels of SrCO_3 being slightly higher (0.35 - 0.85 mole %) than in the short term experiments. SO_4^{2-} contents in the long term experiments using sediment ADDO showed more variability but were generally comparable in the range 0.85 - 1.82 mole % SO_4^{2-} (typically 0.85- 1.6 mole % SO_4^{2-}).

4.2.3 SUMMARY

The early development of the diagenetic textures has been studied using sediments ADDO and ADBO in successful short term experiments and using sediment BSO in aborted experiments.

The small cement crystals that were precipitated in the

aborted experiments and in experiment 1785, using both sediment BSO (characterised by a final cement fabric of a granular-bladed morphology) and sediment ADBO (characterised by a final cement fabric of an equant morphology), are of a rhombic nature and are enriched in Mg^{2+} . Dissolution was seen to affect the very rich Mg phase observed in the standard experiment. These phases are very rare.

In experiments run for 1-3 weeks without any pore fluid substitution, the precursors to the equant and granular-bladed cement fabrics are observed.

(1) Early equant fabrics - isolated cement crystals are observed on grain surfaces. The maximum sizes of these crystals are 2 μm (15 days) to 8 μm (21 days). Due to the isolated nature of these crystals, they have room in which they could further develop into the large equant crystals (average size 15 μm) observed in experiments run for 40-50 days. These cement crystals have MgCO_3 contents ranging from 1-8 mole %, with the shorter experiment (15 days) having a slightly higher overall level of MgCO_3 . The SrCO_3 level is variable, showing a similar distribution to that of longer experiments using the same starting sediment (0.1-0.8 mole %). SO_4^{2-} levels in these crystals are relatively high (1-2 mole %).

(2) Early granular-bladed fabrics - narrow, isopachous rims of granular-bladed crystals are observed (3 μm maximum on coated grains compared to 6 - 13 μm in longer experiments).

These crystals have a higher level of $MgCO_3$ (5-13 mole %) than the equant fabrics produced during experiments using sediment ADBO, although the experiment ran for a longer time period (26 days). $SrCO_3$ levels are relatively low (0.3 - 0.55 mole %) and the level of SO_4^{2-} observed (1-1.5 mole %), is lower than that in the equant fabrics.

In both cement types, more cement crystals are observed associated with peloids than with the smooth surfaces of coated grains.

Neomorphism of shell fragments is an early process, beginning before the precipitation of cement. It begins as isolated patches of calcite within the original aragonitic shell structure. With further growth of the neomorphic spar, spar crystals may coalesce to form an irregular mosaic of calcite which has irregular boundaries both with other sparry calcite crystals and with the aragonite that it replaces. Secondary porosity has not been greatly developed in any of these experiments.

4.3 EFFECT OF TEMPERATURE

To make it possible to carry out a sufficient number of experiments during the allotted experimental time, all of the experiments were run at temperatures between 183-200 °C,

which enabled experiments to be carried out in 4-6 weeks. Lower temperatures (e.g. 120 °C would have meant experimental times of up to 6 months (see Ferguson et al., 1984).

The effect of temperature was studied in detail by Ferguson et al. (1984) and it was therefore not considered necessary to duplicate those experiments in this investigation.

Ferguson et al. (1984) showed that there was very little change in the $m\text{Mg}^{2+}/m\text{Ca}^{2+}$ ratio of the pore fluids over the temperature range that the experiments were run (180-200 °C) but that the $m\text{Sr}^{2+}/m\text{Ca}^{2+}$ ratio increased by approximately $2-3 \times 10^{-2}$. If the differences in the pore fluid evolution trends presented in Fig. 3.3 (a) are considered,

(experiments run using sediment BSO and at similar pressures) a difference of $2-3 \times 10^{-2}$ in the $m\text{Sr}^{2+}/m\text{Ca}^{2+}$ ratio is noted between experimental temperatures of 183 and 200 °C.

This is consistent with the data of Ferguson et al. (1984). However, the results presented in section 3.5.2 (1) (ii) indicate that the differences observed in Fig. 3.3 (a) were not attributable to increasing levels of Sr^{2+} in the pore fluids with increasing temperature. In this study, no significant difference has been noted in the aragonite dissolution rate in the temperature range 183-200 °C.

4.4 EXPERIMENTS CONDUCTED AT DIFFERENT LEVELS OF HYDROSTATIC PRESSURE

Ferguson et. al.(1984) noted that, like temperature, the level of hydrostatic pressure applied had an effect on the reactions. However, no detailed investigation or discussion was conducted at that time. A series of three experiments, using sediment BSO, was therefore conducted under similar conditions of temperature ($200 \pm 2^{\circ}\text{C}$) and pore fluid sampling but at different levels of hydrostatic pressure (5, 7 and 9 MPa, experiments 4186, 4086 and 3686 respectively). The length of the experiments were similar during the first two (3686 and 4086, 47 and 50 days respectively), but the third experiment (4186) had to be ended after 34 days due to a lack of experimental time (see experimental details in Appendix III).

4.4.1 TEXTURAL DEVELOPMENT

Cement: An isopachous fringe of granular-bladed crystals is observed surrounding all grains at the end of each experiment. In the partially lithified sediment of experiment 3686, the average width of this fringe on coated grains is $8 \mu\text{m}$ (Plate 4.6 A-C), in that of experiment 4086, $6 \mu\text{m}$ (Plates 4.6 D and 4.7 A and B) and in that of

PLATE 4.6 - INVESTIGATION OF HYDROSTATIC PRESSURE

(A) Experiment 3686 (9MPa) - An isopachous fringe of bladed cement crystals surrounds grains. The grain on the bottom has been replaced by solution cavity fill calcite (R) which takes two forms (see overlay):

(i) elongate crystals, which can be seen underlying the cement fringe and mimicking the original outline of the lamellar structure and

(ii) blocky calcite crystals which have no specific form.

A very small amount of secondary porosity remains (see overlay). PPL. Scale bar 20 μm .

(B) Experiment 3686 - An isopachous fringe of granular-bladed crystals surround the originally coated grain and several layers of granular cement crystals are observed on the peloid. Solution cavity fill calcite (R) has replaced the original cortex of the coated grain and the overlay shows how these crystals grow inwards from the outer edge of the grain. Some unfilled secondary porosity remains (see overlay). PPL. Scale bar 20 μm .

(C) Experiment 3686 - Each grain is surrounded by an isopachous fringe of granular-bladed cement crystals and the uncoated peloid (bottom left hand corner) shows the development of several layers of cement crystals. The original cortex of the right hand grain has been almost totally replaced by solution cavity fill calcite (R) with a small amount of residual secondary porosity (P). The cortex of the left hand grain has been removed by dissolution leaving a large area of secondary porosity (P). Limited infilling of this by solution cavity fill calcite has occurred. PPL. Scale bar 50 μm .

(D) Experiment 4086 (7 MPa) - Isopachous fringes of granular-bladed cement crystals surround grains of the partially lithified sediment. Peloids show the development of several cement crystals. Secondary porosity (P) has been well developed, especially in the cortices of coated grains. Neomorphic alteration of the micrite by neomorphism (N) is observed in many of the grains. PPL. Scale bar 100 μm .

OVERLAY KEY

Area outlined - solution cavity fill calcite.

Area stippled - remnant secondary porosity.

PLATE 4.6

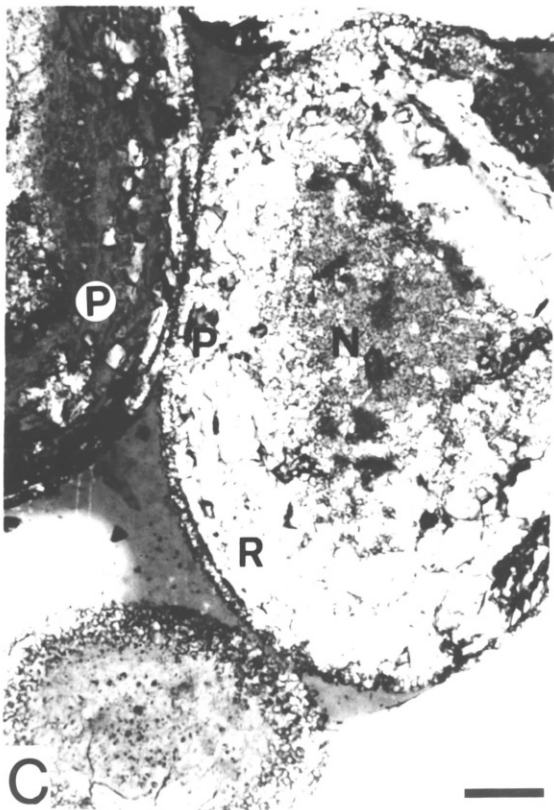
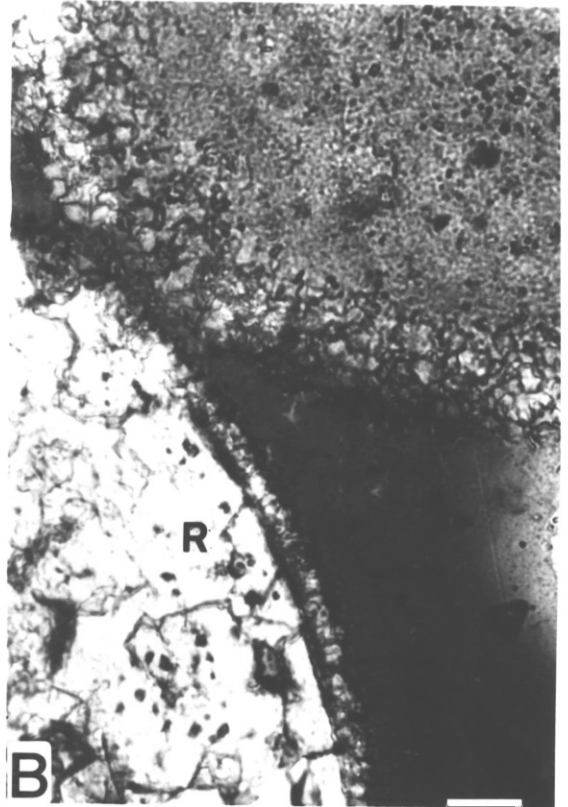


PLATE 4.6

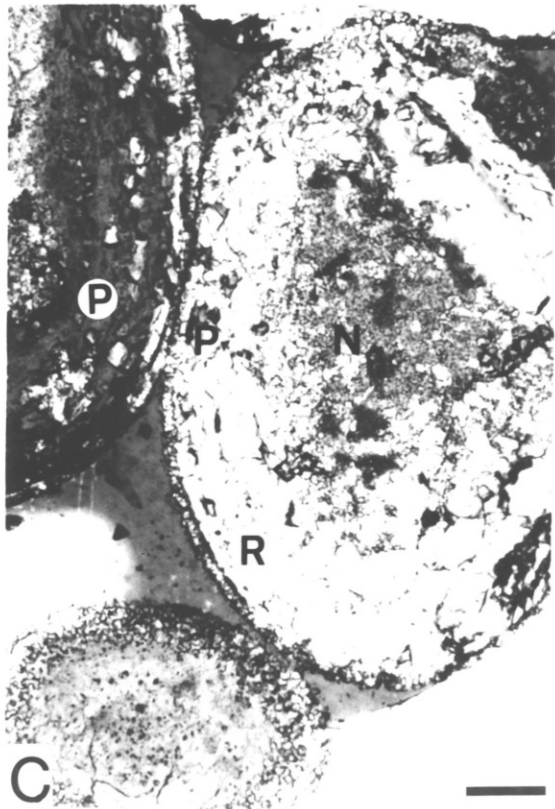
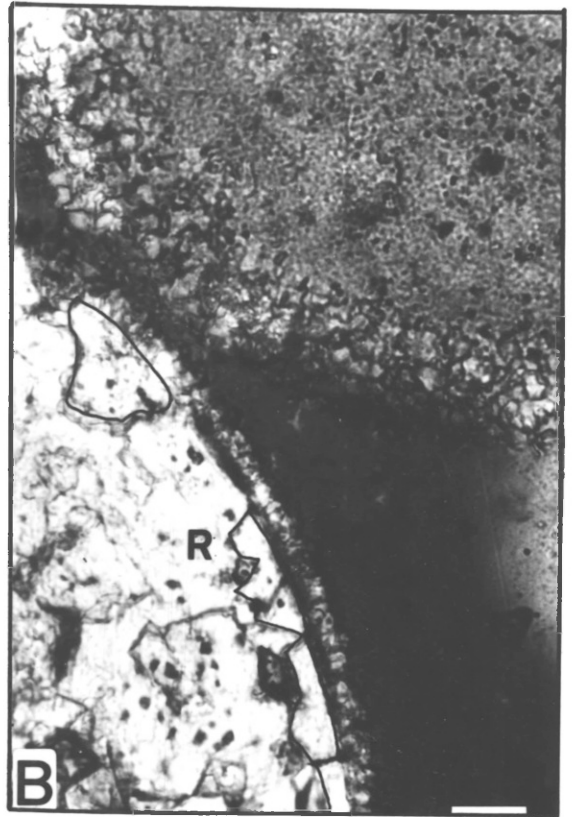
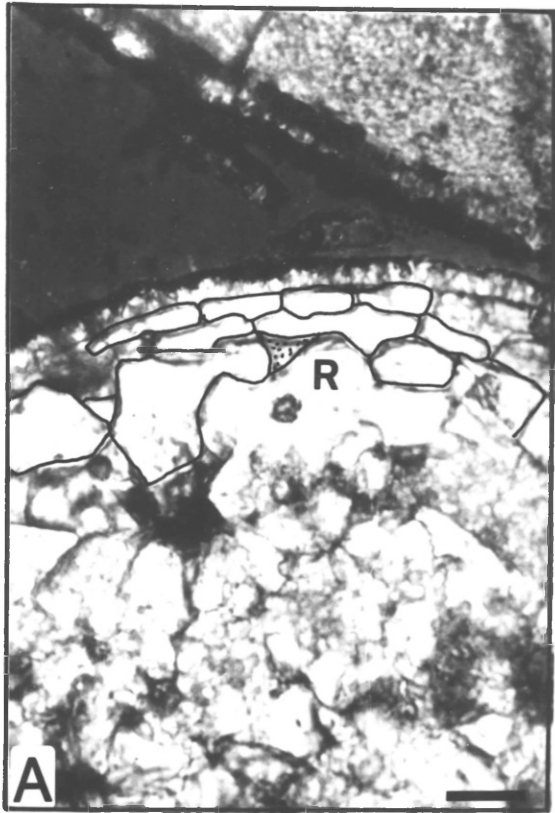


PLATE 4.7 - INVESTIGATION OF HYDROSTATIC PRESSURE

(A) Experiment 4086 (7 MPa) - An isopachous fringe of bladed cement crystals is observed surrounding the coated grain while a fringe composed of several layers of granular crystals surrounds the peloid. PPL. Scale bar 20 μm .

(B) Experiment 4086 - Isopachous fringes of granular-bladed cement crystals surround sediment grains except where a cluster of cement crystals is observed. PPL. Scale bar 20 μm .

(C) Experiment 4186 (5 MPa) - Isopachous fringes of granular-bladed cement crystals surround sediment grains. Secondary porosity has been widely created (P) and is predominantly unfilled. Neomorphism (N) (see overlay) has affected some of the micritic nuclei of the originally coated grains. PPL. Scale bar 50 μm .

(D) Experiment 4186 - Detail of the cement fabric. Again uncoated grains show the development of several layers of cement crystals. The overlay shows where areas of neomorphic spar replacing micrite occur and the occurrence of solution cavity fill calcite which is of a lamellar form mimicking the original structure of the aragonitic cortex. PPL. Scale bar 20 μm .

OVERLAY KEY

Area outlined - solution cavity fill calcite.

Area stippled - neomorphic spar replacing micrite.

PLATE 4.7

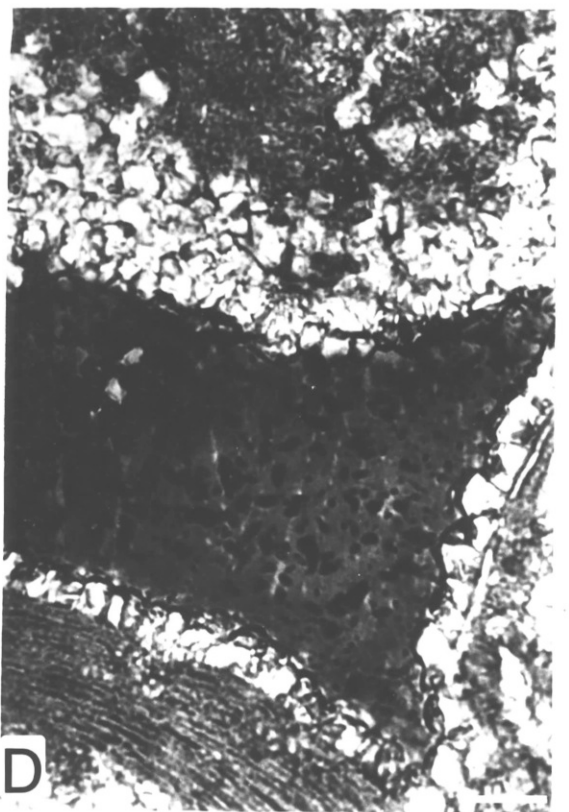
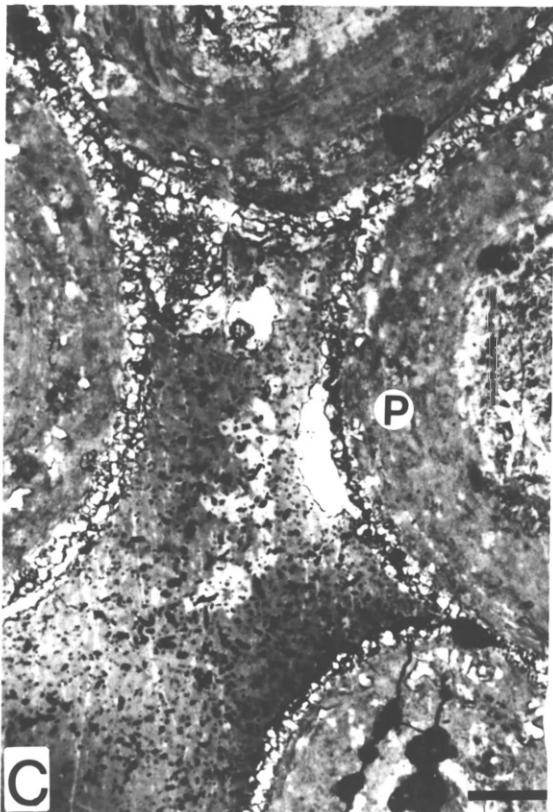
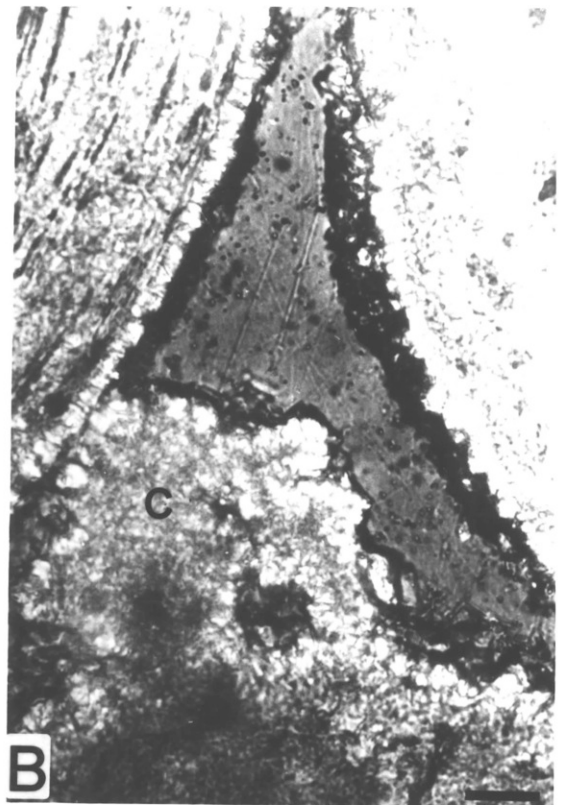
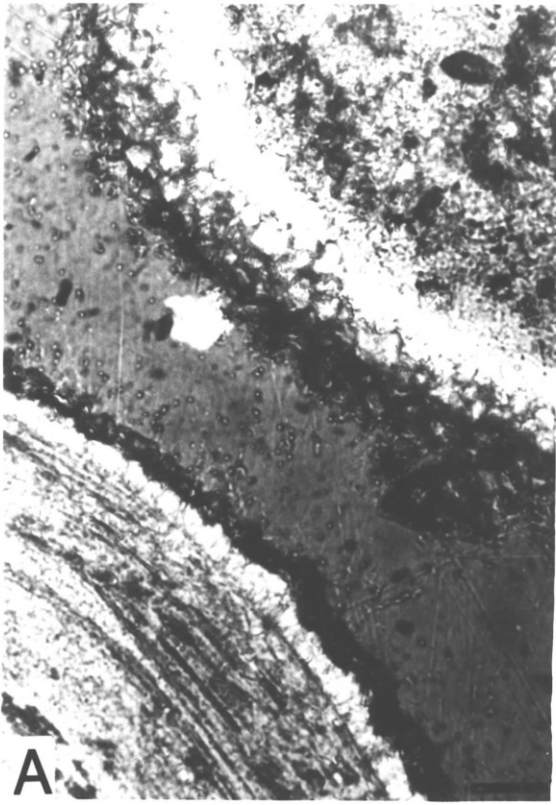
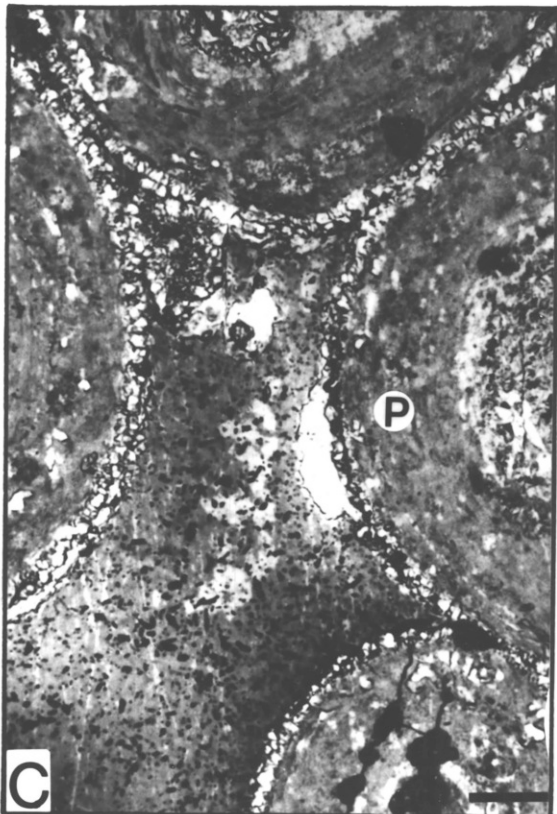
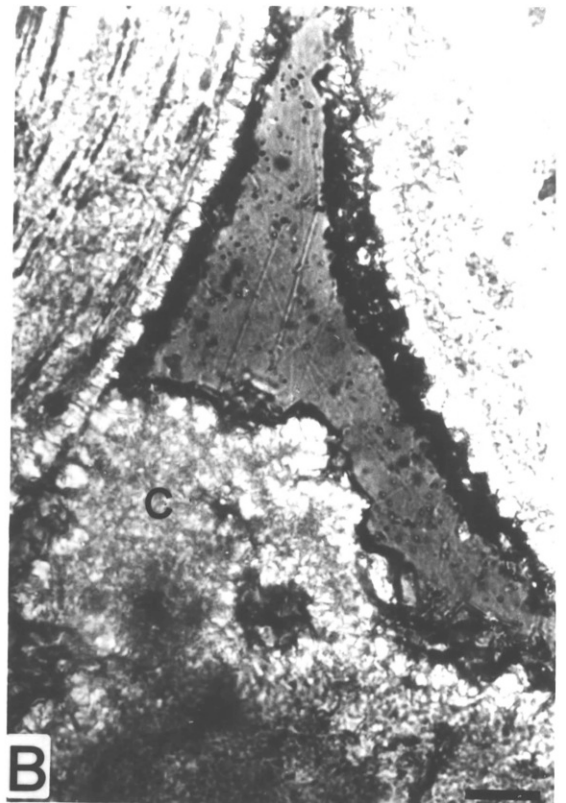
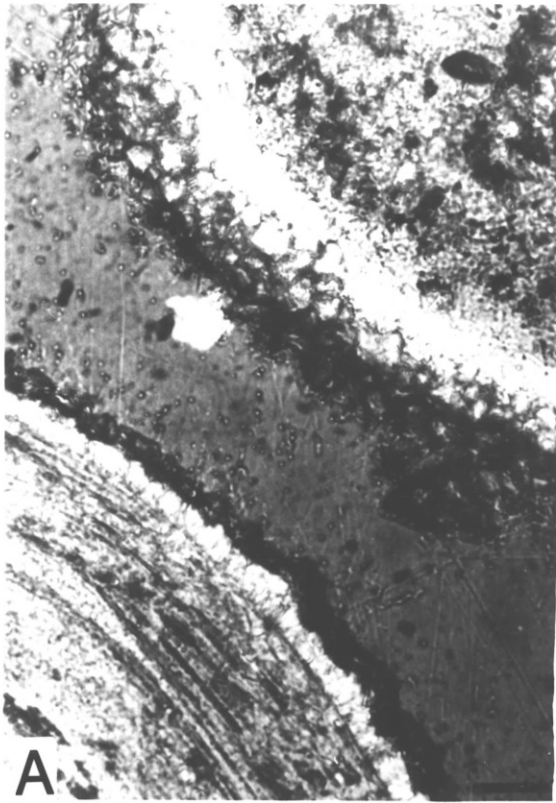


PLATE 4.7



experiment 4186 had to be cut short yet the cement fringes in the partially lithified sediment of 4186 are wider (Plates 4.7C and 4.7D). All of the average cement fringe widths however fall into the typical range of 6-13 μm found in other experiments using sediment BSO (see section 3.5.1 (1)).

Secondary Porosity and Replacement Textures: A considerable amount of solution-cavity fill calcite is observed in the partially lithified sediment of experiment 3686 (see Plate 4.6 A-C). In Plate 4.6 A this takes two forms, one of blocky calcite crystals, the other elongate crystals which partially mimic the original lamellar structure of the coated grain. Some of the secondary porosity which must have been created prior to infilling can be observed in Plate 4.6 A-C (P). Neomorphism of micritic carbonate (N) has also occurred, the original micrite being replaced by crystals less than 10 μm in diameter (see Plate 3.6 C).

A lot of secondary porosity (P) has been created in the lamellar cortices of coated grains in the partially lithified sediment of experiment 4086 (see Plate 4.6 D). This however is very fine and not particularly easily seen

in the photomicrographs. This secondary porosity has mostly remained unfilled. Micrite enlargement has affected some of the grains (see Plate 4.6 D (N)).

A considerable amount of secondary porosity (P) has been created in the partially lithified sediment of experiment 4186 (see Plate 4.7 C). Almost no filling of this porosity by solution cavity fill calcite has occurred (see Plate 4.7 C and D). Micritic carbonate has again been replaced by neomorphic spar (N), the diameters of which are less than 10 μm (see Plate 4.7 C and D).

XRD analysis showed that in experiment 3686, 20-25 wt. % of the original aragonite had been removed, in experiment 4086, 10-15 wt. % and in experiment 4186, 25-30 wt. %.

4.4.2 PORE FLUID AND CEMENT CRYSTAL CHEMISTRY

(1) Pore fluids.

During the early stages of the experiments, successively higher $\text{mMg}^{2+}/\text{mCa}^{2+}$ ratios were observed with successively lower experimental pressures (see Fig. 4.3). If the elemental analyses are considered (see Appendix I), several points are noted.

(i) Smaller amounts of Mg^{2+} and S^{6+} were removed from the pore fluids of experiments conducted at lower hydrostatic

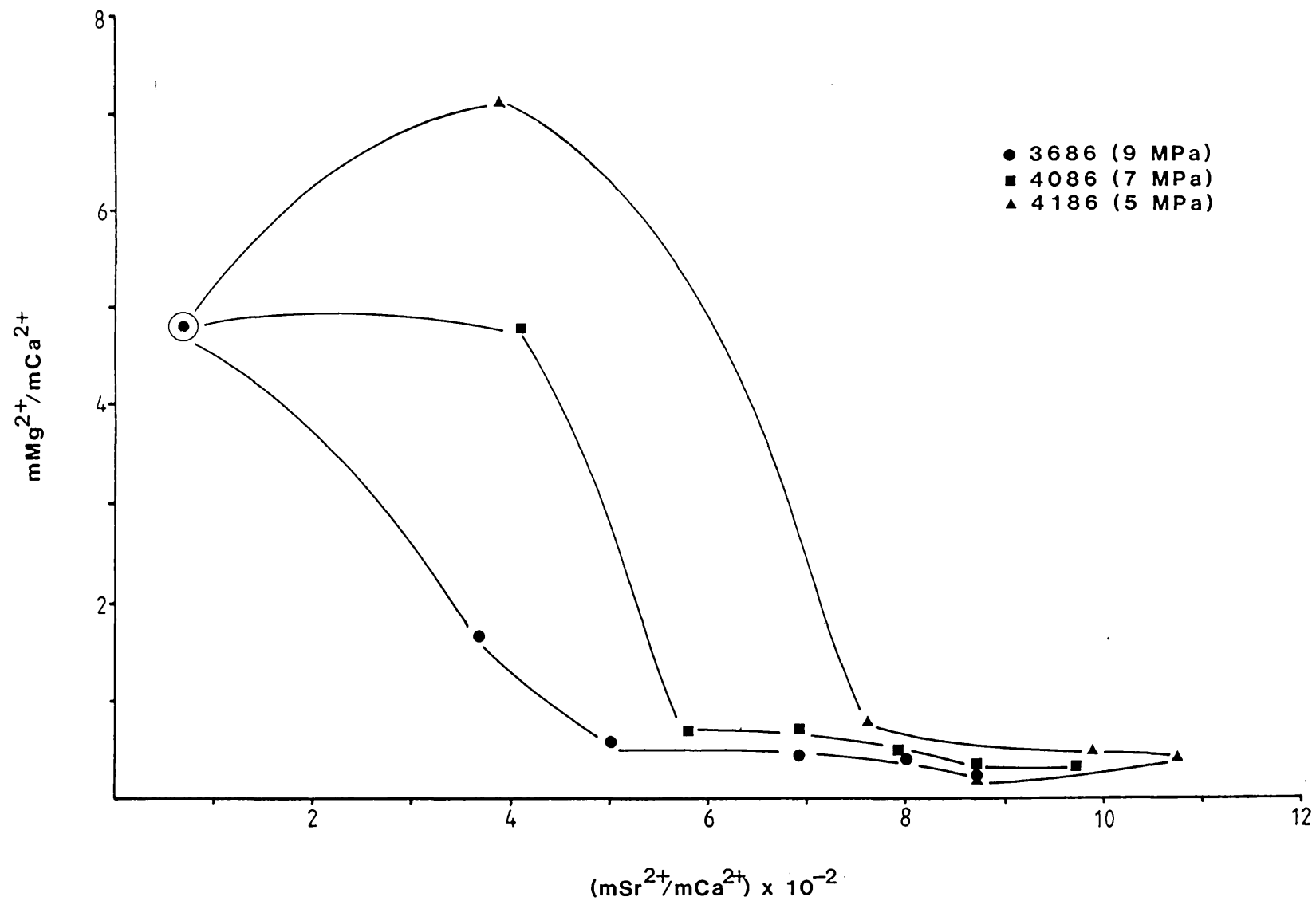


Fig. 4.3 - Evolution of pore fluids from the composition of seawater (⊙) during experiments 3686, 4086 and 4186, investigating the effect of hydrostatic pressure.

pressures.

(ii) At 9 MPa (experiment 3686) an increase in the Ca^{2+} level of the pore fluids from that of seawater was noted.

(iii) Successively greater amounts of Ca^{2+} were removed from the pore fluids of experiments conducted at lower pressures of 7 and 5 MPa.

The results are summarised in Table 4.2. The differences observed in the $\text{mMg}^{2+}/\text{mCa}^{2+}$ ratios at the beginning of the experiments are therefore a function of both the Mg^{2+} and Ca^{2+} level of the pore fluids.

Expt. No.	Mg	Ca	S
3686 (9 MPa)	-716	+ 95	-667
4086 (7 MPa)	-476	-162	-528
4186 (5 MPa)	-330	-218	-463

Table 4.2 - Differences in concentrations (ppm) of Mg^{2+} , Ca^{2+} and S^{6+} in the first pore fluid sample from that of seawater in experiments 3686, 4086 and 4186.

The S^{6+} data would suggest that greater amounts of SO_4^{2-} phases (anhydrite and magnesium oxysulphate) may have been precipitated during the early stages of the experiments with greater amounts being precipitated at lower pressures. The complex nature of the Ca^{2+} data however suggests that the level of hydrostatic pressure also affected other reactions

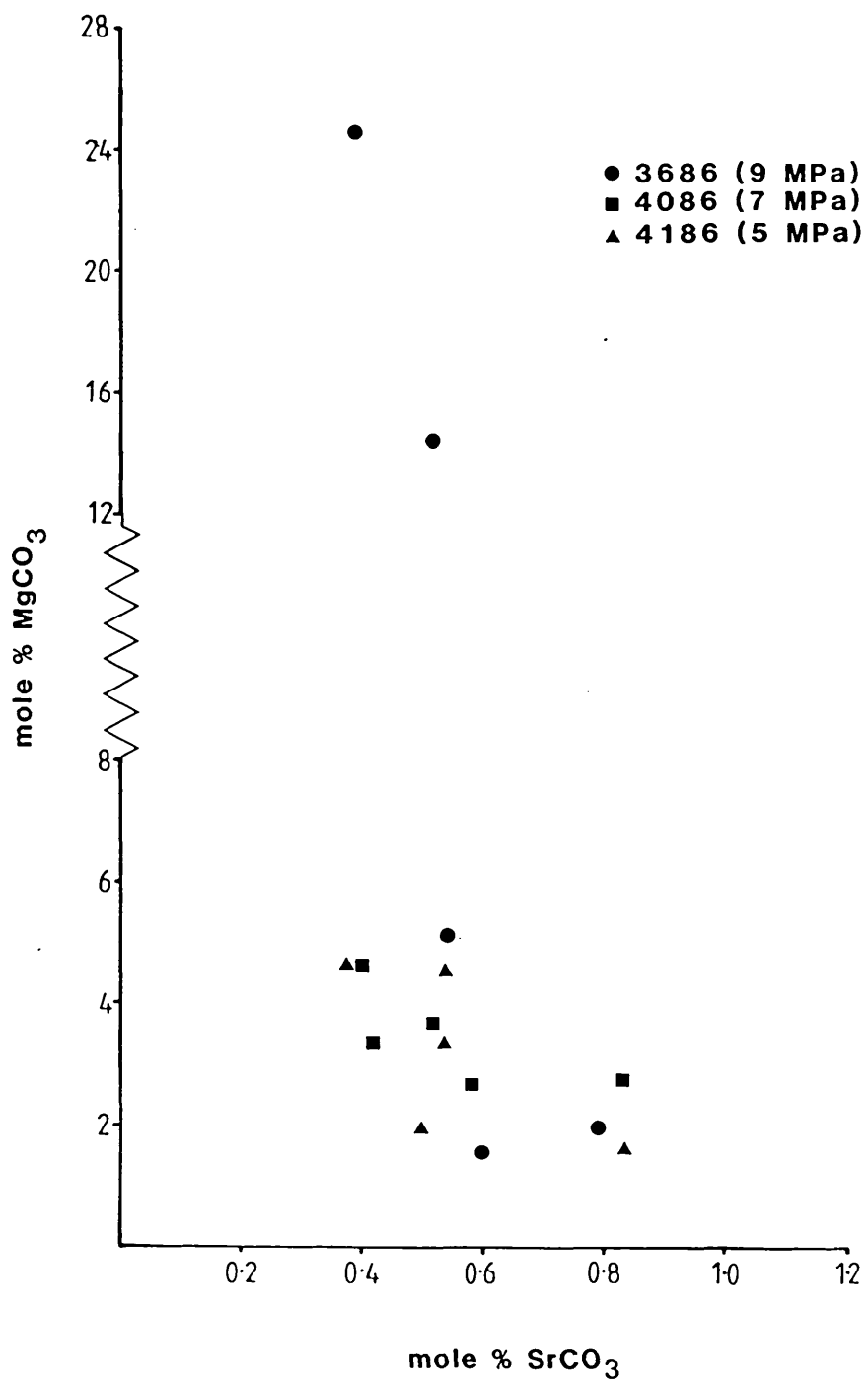


Fig. 4.4 - Mole % MgCO₃ and SrCO₃ contained in cement crystals precipitated during experiments 3686, 4086 and 4186, investigating the effect of hydrostatic pressure.

involving Ca^{2+} i.e. the dissolution of aragonite and the precipitation of calcite.

(2) Cement Crystal Chemistry

With the exception of two analyses of cement crystals generated in experiment 3686, all of the analyses for cement crystals (in terms of MgCO_3 and SrCO_3 mole % content) have a strikingly similar distribution (see Fig. 4.4). The typical range of the MgCO_3 level is 1.5-5 mole % while the SrCO_3 level is moderate ranging from 0.35-0.85 mole %. The range of MgCO_3 and SrCO_3 levels is very comparable to those observed in cement crystals generated using sediment BSO in other experiments (see Fig. 3.4).

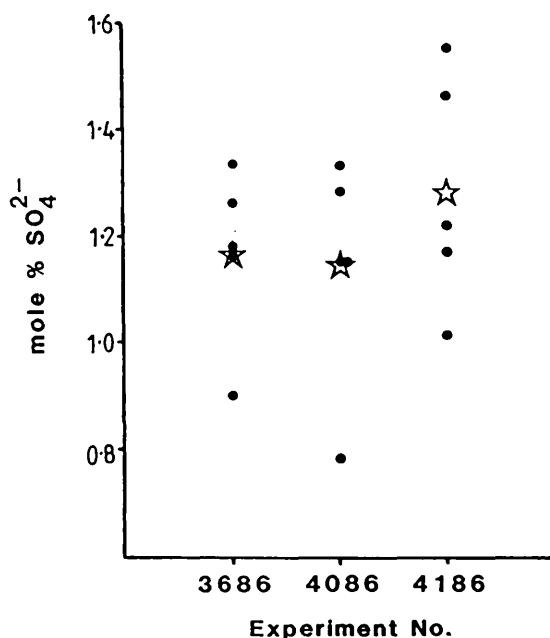


Fig. 4.5 - Mole % SO_4^{2-} contained in the cement crystals precipitated during experiments 3686, 4086 and 4186. Mean values (♠) are shown.

SO_4^{2-} levels in the cement precipitated in experiments 3686, 4086 and 4186 are comparable with each other, with no significant differences in mean compositions (see Fig. 4.5). The range of the SO_4^{2-} levels observed is 0.9-1.35 mole % at 9MPa; 0.78-1.35 mole % at 7MPa and 1.0-1.55 mole % at 5MPa.

4.4.3 SUMMARY

There is some evidence to suggest that an increase in the degree of reaction accompanied a decrease in the hydrostatic pressure applied during the experiments. Petrographic study suggests that more cement was precipitated and aragonite removed in the experiment run at the lowest hydrostatic pressure. No direct correlation in all experiments is noted however as supported by the XRD data (although it must be borne in mind that this is only accurate to +/- 5-10 wt.%). Pore fluid $\text{mSr}^{2+}/\text{mCa}^{2+}$ ratios would also appear to support the conclusion that an increase in the degree of reaction accompanied a decrease in the hydrostatic pressure applied although the data are complicated by the apparent effect of hydrostatic pressure on the precipitation of CaSO_4 and magnesium oxysulphate. Lower pressures favour the precipitation of greater amounts of these phases (see S^{6+} data in Table 4.2 and section 4.4.2 (1)).

Differences in the hydrostatic pressure applied did not affect the composition of the cement which was precipitated.

4.5 EFFECT OF NON-SAMPLING OF THE PORE FLUIDS

The results of two experiments run for the same length of time, using the same starting sediment under similar experimental conditions except for the pore fluid sampling regime have been compared. Experiment 18/1 was run for exactly the same length of time (using sediment ADDO) as experiment 37/1. Experiment 37/1 was run under normal experimental procedures of pore fluid substitution while no pore fluid substitution occurred in experiment 18/1. The results of these experiments are presented in sections 3.5.1 (2) and 3.5.2 (2). No differences in the textural development of the sediment were observed and the degree of alteration in the partially lithified sediments at the end of both experiments was similar. However, slight variations in the composition of the cement precipitated in each experiment were observed (see Fig. 4.6). An overall decrease in the level of $MgCO_3$ (mole %) and increase in the level of $SrCO_3$ (mole %) contained within the structure of the calcite precipitated as a cement was noted when no pore fluid substitution occurred (see Fig. 4.6)

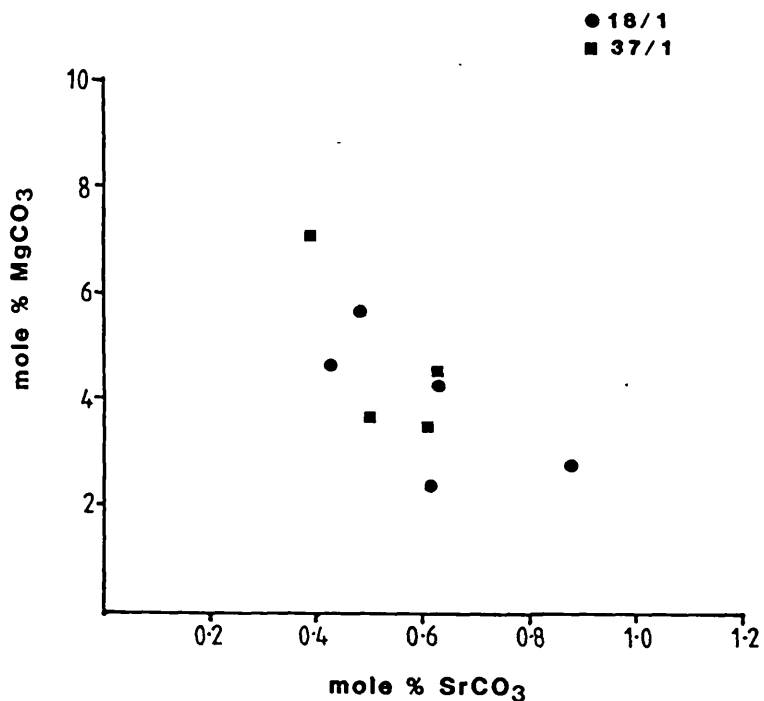


Fig. 4.6 - Mole % MgCO₃ and SrCO₃ contained in the cement crystals precipitated during experiments 18/1 and 37/1.

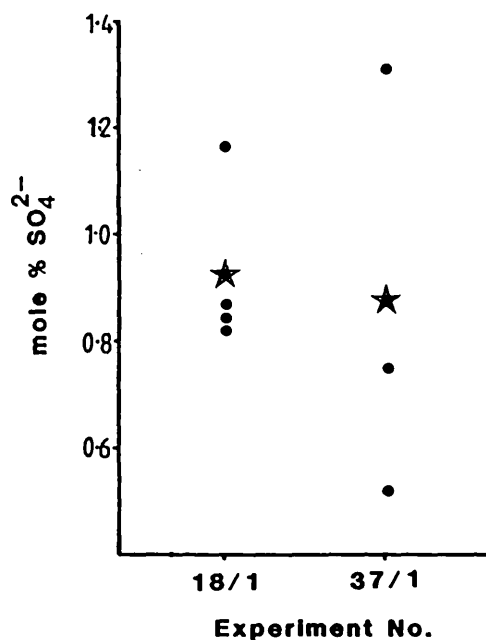


Fig. 4.7 - Mole % SO₄²⁻ contained in the cement crystals precipitated during experiments 18/1 and 37/1. Mean values (☆) are shown.

The SO_4^{2-} contents (mole %) of the cement phase are shown in Fig. 4.7. No significant difference is observed in mean values between the two experiments but a greater variation in the amount of SO_4^{2-} in the cement precipitated in experiment 18/1 is observed.

Sampling of the pore fluids therefore appeared to slightly affect the composition of the cement that is precipitated. This would be expected as the process of pore fluid sampling introduced small volumes of unused seawater. Sampling however, did not significantly affect the texture generated or the degree of reaction.

CHAPTER 5 - EXPERIMENTS USING PORE FLUIDS OTHER THAN SEAWATER

5.1 INTRODUCTION

Two experiments were carried out using pore fluids other than normal seawater, the first using seawater in which the SO_4^{2-} had been reduced, the second using freshwater.

A great deal of interest in the effect that SO_4^{2-} has on carbonate reactions, in particular on dolomite precipitation, has arisen over the past few years (e.g. Baker and Kastner, 1981). It was therefore considered useful to run an experiment using seawater, in which the SO_4^{2-} had been reduced, and natural sediments, to study the effect that the reduction of SO_4^{2-} in the pore fluids had on the diagenetic reactions. The results of this experiment would also be useful when considering the effect of anhydrite and magnesium oxysulphate precipitation (removal of SO_4^{2-}) at the beginning of the experiments using normal seawater although this would not occur in nature.

The other experiment which was conducted used freshwater as the pore fluid. Great differences in the early diagenetic textures generated in the marine and freshwater environments

are observed in nature. Many of the ions which are present in seawater and which are complicating factors in early diagenetic reactions (e.g. Mg^{2+} , PO_4^{2-} , SO_4^{2-}), are not present in such high concentrations in freshwater. One experiment using freshwater was therefore conducted to see if any major differences were observed in the experimental results.

5.2 SULPHATE REDUCED SEAWATER

One experiment was conducted under conditions of $186^{\circ}C \pm 2^{\circ}C$, 6.4 MPa (s.d. 1.2 MPa) for 36 days using sediment AKSO and SO_4^{2-} -reduced seawater (for chemical composition see Appendix I).

5.2.1 Textural Development

Diagenesis proceeded to a much greater extent during this experiment than in any other previously reported. XRD analysis showed that 40% of the original aragonite was removed compared to 25% in experiment 2185 which was run using the same sediment and similar experimental conditions but with seawater (see 3.5.1).

Cement: The morphology of the cement crystals which were precipitated is variable (occasionally bladed, see Plate 5.1 A and B, but typically granular-equant). The extent of the

PLATE 5.1 - EXPERIMENT 2986, SO_4^{2-} -REDUCED SEAWATER

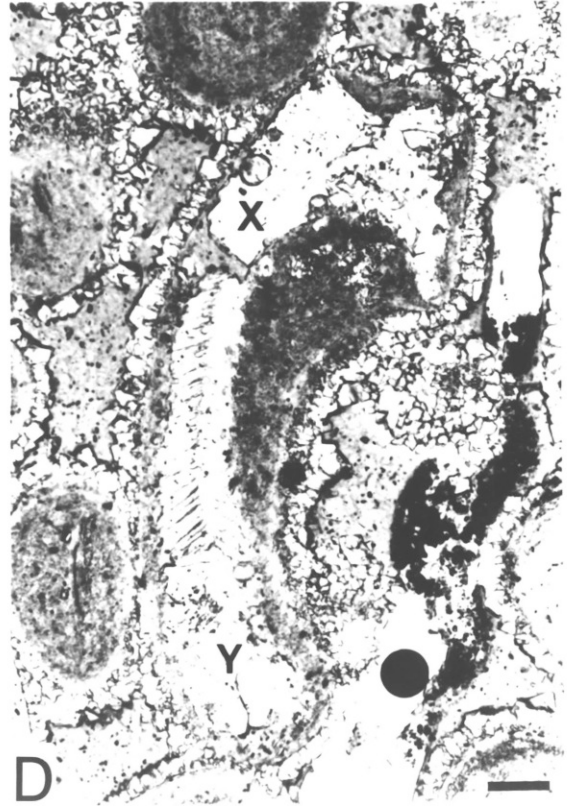
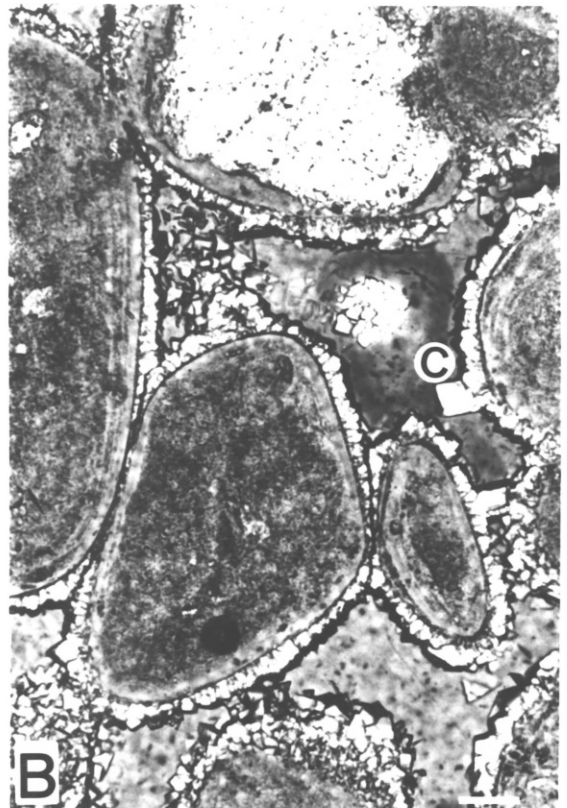
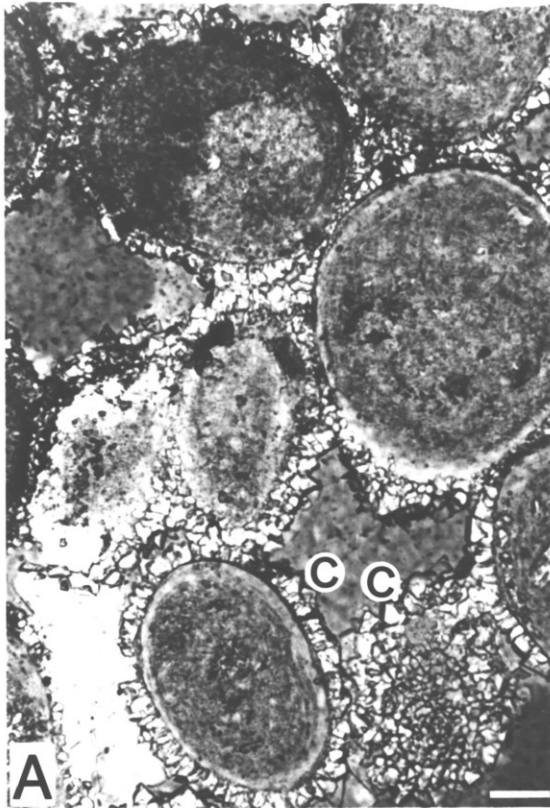
(A) Continuous fringes of granular, bladed and equant cement crystals surround sediment grains. Cement crystals on outer layers of the fringes (C) are more equant than the underlying granular or bladed crystals. Clusters of cement crystals are observed in primary pore spaces. A considerable amount of secondary porosity has been created in all sediment grains but no replacement textures are observed. PPL. Scale bar 50 μm .

(B) Cement crystals of granular, bladed and equant morphology fringe sediment grains. Later, large rhombic crystals are observed in primary pore spaces (C). Clusters of cement crystals are again found in primary pore spaces and a considerable amount of secondary porosity has been created. No replacement textures are observed. PPL. Scale bar 50 μm .

(C) Overgrowth of echinoderm fragment by calcite which is in optical continuity with the fragment. The overgrowth envelopes cement crystals on adjoining grains and an earlier fringe of bladed cement crystals, which are not in optical continuity with the fragment is observed (see detail in Plate 7.1 C). PPL. Scale bar 100 μm .

(D) Coated shell fragment which has undergone two modes of replacement by calcite. Solution cavity fill calcite (X) is separated from the shell fragment by a void cavity greater than 20 μm . Neomorphic spar (Y) is separated from the original aragonitic shell fragment by an alteration front of less than 5 μm , often less than 1 μm . Relics of the original aragonite are observed, incorporated in the neomorphic spar. PPL. Scale bar 50 μm .

PLATE 5.1



cementation is shown in Plate 5.1 A, B and D. Cement fringes vary in width from 10-35 μm with an average width of around 20 μm). Large optically continuous overgrowths of low-Mg calcite are found on echinoderm fragment grains (see Plate 5.1C) which may encompass an earlier phase of cement crystals.

Secondary Porosity: A considerable amount of secondary porosity has been created (see Plate 5.1 A-D). Oomoldic porosity is particularly well developed in coated grains (see Plate 5.1 A, B and D) where many of the aragonitic cortices have been totally removed. Micritic carbonate has also been removed to form micro-porosity (see Plate 5.1 A-D).

Replacement: The infilling of oomoldic porosity or vuggy micro-porosity has not been widely developed. Most porosity remains unfilled (see Plate 5.1 A-D)

Plate 5.1 D and 5.2 A show an aragonitic shell fragment which has been partially replaced. Part of the fragment has been replaced by sparry calcite (X) which is separated from the original fragment by a pore space a minimum of 20 μm in width. The pore space is large enough for the mechanism of replacement to be termed solution cavity fill. The other end of the fragment has also been replaced by sparry calcite (Y). Plate 5.2 A shows a detail of this where areas of

relic aragonite (A) can be seen within the neomorphic spar (N). The replacement has occurred across a very narrow alteration front (AF), maximum width 5 μm (often $<1 \mu\text{m}$). The mechanism of this type of replacement is therefore neomorphism.

5.2.2 Pore Fluid and Cement Crystal Chemistry

(1) Pore Fluid Evolution

The typical pattern of pore fluid evolution for normal seawater during the experiments, using AKSO, of an early decrease in the $\text{mMg}^{2+}/\text{mCa}^{2+}$ ratio and an increase in the $\text{mSr}^{2+}/\text{mCa}^{2+}$ ratio, is observed using SO_4^{2-} -reduced seawater (see Fig. 5.1). The maximum pore fluid $\text{mSr}^{2+}/\text{mCa}^{2+}$ ratio of 10.7×10^{-2} (reached on day 34 of experiment 2985) is greater than that using seawater and sediment AKSO of 9.8×10^{-2} in experiment 2185 (see section 3.5.2). One point to be noted is that while the pore fluids of experiment 2185 approached this maximum $\text{mSr}^{2+}/\text{mCa}^{2+}$ ratio of 9.8×10^{-2} which then dropped, no such reduction has been observed using the SO_4^{2-} -reduced seawater.

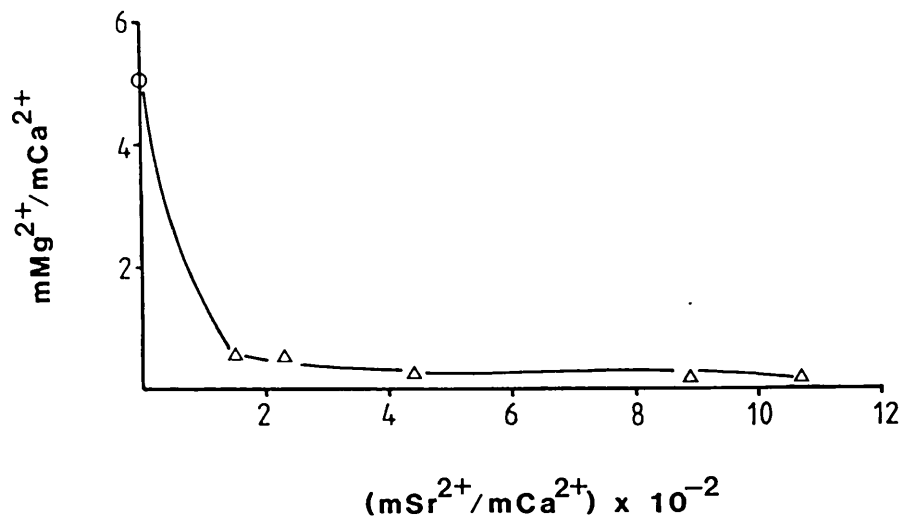


Fig. 5.1 - Evolution of pore fluids in terms of $\text{mMg}^{2+}/\text{mCa}^{2+}$ and $\text{mSr}^{2+}/\text{mCa}^{2+}$ ratios of experiment 2985 from that of the SO_4^{2-} -reduced seawater (O).

(2) Cement Crystal Chemistry

The composition of the cement phase precipitated in experiment 2985 is very similar to that of experiment 2185 which used AKSO and seawater.

The MgCO_3 and SrCO_3 contents (mole%) of the cement phases precipitated in each case are shown in Fig 5.2. The cement precipitated in experiment 2185 shows a slightly higher MgCO_3 content than that of 2985 but in terms of the SrCO_3 content, the cement phases are almost identical.

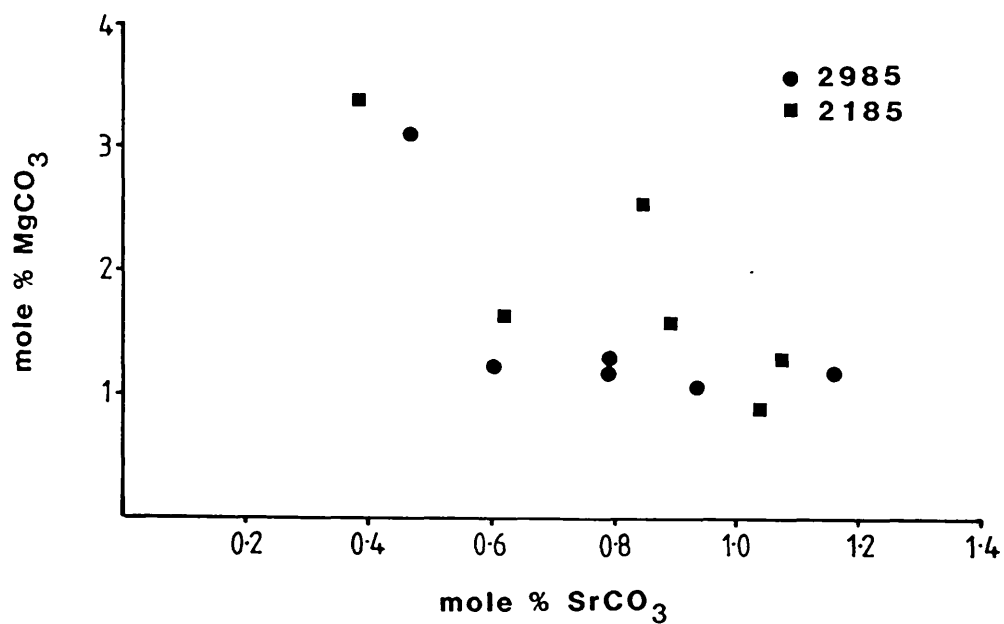


Fig. 5.2 - Mole % MgCO₃ and SrCO₃ in cement crystals precipitated during experiments 2985 and 2185.

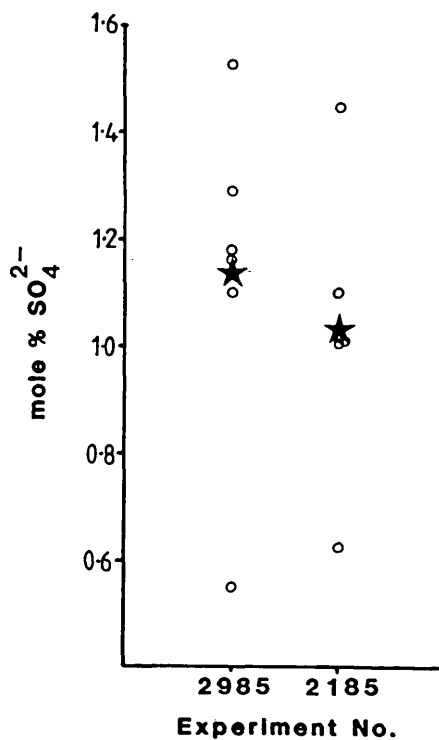


Fig. 5.3 - Mole % SO₄²⁻ contained in cement crystals precipitated during experiments 2985 and 2185. Mean values (★) are shown.

The range of SO_4^{2-} contents (mole%) in the cement phases precipitated in each experiment are also similar (see Fig. 5.3). Average values for the SO_4^{2-} content of the cement phases are 1.14 mole % for experiment 2985 and 1.03 mole % for experiment 2185.

5.2.3 SUMMARY

This one experiment suggests that the reduction in SO_4^{2-} of the seawater may increase the degree to which experimental diagenesis proceeds although the lower pH of 6.5 compared to that of seawater (7.1) would have helped initiate the reactions. It does not however, affect the type of fabrics which are generated.

Although more change has been observed in the sediment from petrographic and XRD evidence, the pore fluid evolution is remarkably similar. One difference is observed. Using seawater, a maximum $\text{mSr}^{2+}/\text{mCa}^{2+}$ ratio for the pore fluids is reached and then it decreases. Using SO_4^{2-} -reduced seawater, no such $\text{mSr}^{2+}/\text{mCa}^{2+}$ reduction occurs, the $\text{mSr}^{2+}/\text{mCa}^{2+}$ ratio of the pore fluids increasing continually throughout the experiment.

The composition of the cement precipitated, using SO_4^{2-} -reduced seawater and AKSO, in terms of its MgCO_3 , SrCO_3

and SO_4^{2-} contents (mole %), is almost identical to the experiment using seawater and AKSO. The source of the SO_4^{2-} is considered in section 8.3.4.

5.3 FRESHWATER

One experiment was conducted under conditions of $190^\circ\text{C} \pm 2^\circ\text{C}$, 6.3 MPa (s.d. 0.8 MPa) for 53 days using sediment AKSO and freshwater, which was collected as rainwater in Aberdeenshire (for chemical analysis see Appendix I).

5.3.1 Textural Development

Textural alteration of the sediment due to experimental diagenesis has been extensive.

Cement: The cement formed is of a rhombic morphology (see Plate 5.2 B-D). Cement crystals occur in the range of 7-30 μm in diameter. These cement crystals are randomly arranged along grain edges. High-Mg calcite shell fragments show overgrowths of calcite cement crystals which are in optical continuity (see Plate 5.2D).

Porosity: A considerable amount of secondary porosity has been created by the dissolution of aragonite as seen in Plate 5.2 B-D. XRD analysis shows that 90-95 % of the original aragonite was removed. Most of this secondary

PLATE 5.2 - SO_4^{2-} -REDUCED SEAWATER AND FRESHWATER

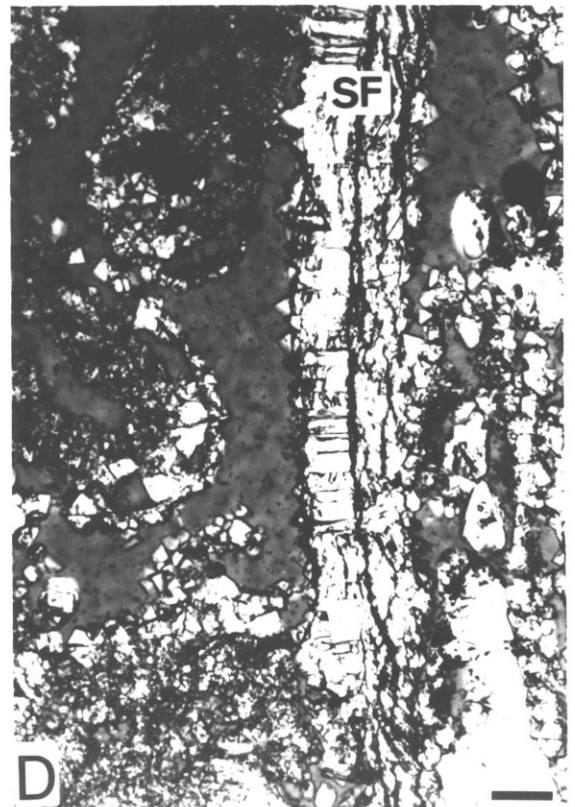
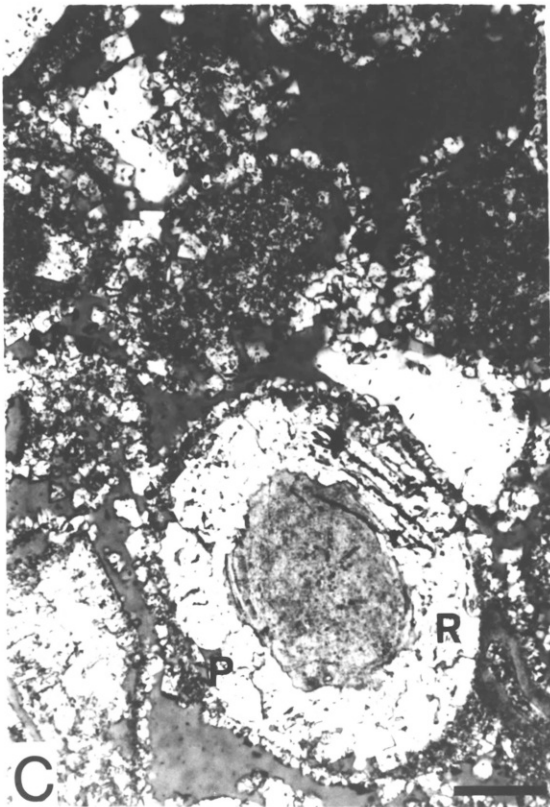
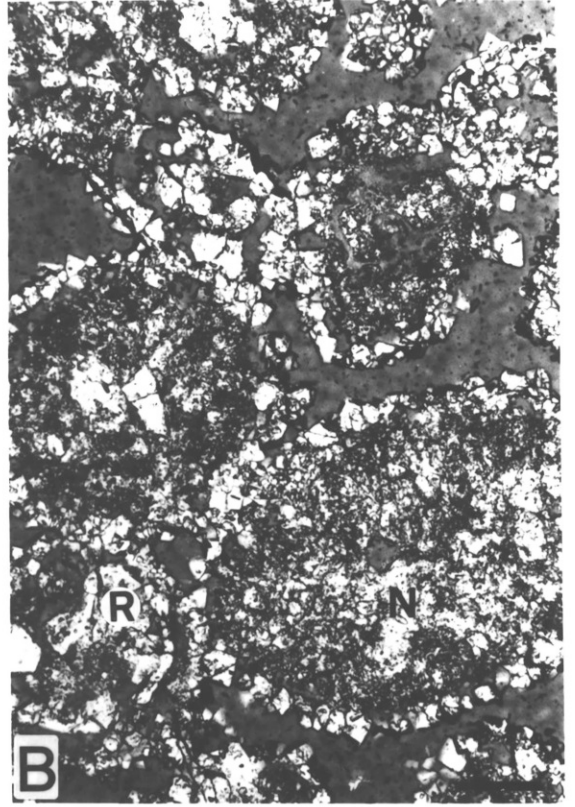
(A) Experiment 2985 (SO_4^{2-} -reduced seawater) - Detail of neomorphic alteration shown in Plate 5.1D. Neomorphic spar (N) replaces the original shell fragment across a micron-sized alteration front (AF). Relics of the original aragonitic structure (A) have been incorporated in the spar. PPL. Scale bar 20 μm .

(B) Experiment 3186 (Freshwater) - Rhombic calcite crystals surround sediment grains. A considerable amount of secondary porosity has been created. This porosity has been partially infilled by irregular mosaics of rhombic calcite (R). However, replacement of the micrite by neomorphic spar has also occurred. PPL. Scale bar 50 μm .

(C) Experiment 3186 - Shows the development of the rhombic cement, irregular replacement fabrics and vuggy secondary porosity. A complete cortex of a coated grain has been replaced by a mosaic of sparry calcite crystals (R) between which areas of secondary porosity (P) remain. PPL. Scale bar 100 μm .

(D) Experiment 3186 - Shell fragment composed of prismatic high-Mg calcite (SF). Cement crystals which grow off these prisms are in optical continuity. PPL. Scale bar 50 μm .

PLATE 5.2



porosity is oomoldic with the complete removal of coated grain cortices having occurred. Much of the micritic aragonite however has also been removed leaving a great deal of vuggy porosity in all grains (see Plate 5.2 B-D).

Replacement: The infilling of the secondary porosity, created via the dissolution of aragonite is common and often extensive (e.g. see the replaced cortex of the coated grain shown in Plate 5.2 C). Most of the oomoldic porosity and vuggy porosity has been irregularly replaced by sparry calcite crystals (some of which range in size up to 30-40 μm in diameter. Replacement of micritic carbonate by sparry calcite crystals (see Plate 5.2 B) has also occurred, many of these appear to be of neomorphic origin but some are closely associated with secondary pore space. Replacement crystals range in size up to 40 μm in diameter.

5.3.2 Pore Fluid and Cement Crystal Chemistry.

(1) Pore Fluids

The original composition of the pore fluids (as shown on Fig. 5.4) is quite different to that of seawater, primarily in terms of the $\text{mMg}^{2+}/\text{mCa}^{2+}$ ratio which is much lower (<1) in freshwater. The $\text{mSr}^{2+}/\text{mCa}^{2+}$ ratio is also slightly lower than that of seawater and all elemental concentrations are much lower (see Appendix I). When the pore fluid evolution curve

is compared to that of seawater evolution curves (e.g. see section 3.5.2), very little change appears to have occurred and any changes appear to be random. The $m\text{Mg}^{2+}/m\text{Ca}^{2+}$ ratio increased slightly during the beginning of the experiment and then dropped to levels of <0.5 . However, very little Mg^{2+} was available in the system, either in the original pore fluids or in the sediment in the form of high-Mg calcite. The $m\text{Sr}^{2+}/m\text{Ca}^{2+}$ ratio increased overall to approximately 4×10^{-2} , much lower than in experiments using AKSO and seawater (e.g. 2185, see section 3.5).

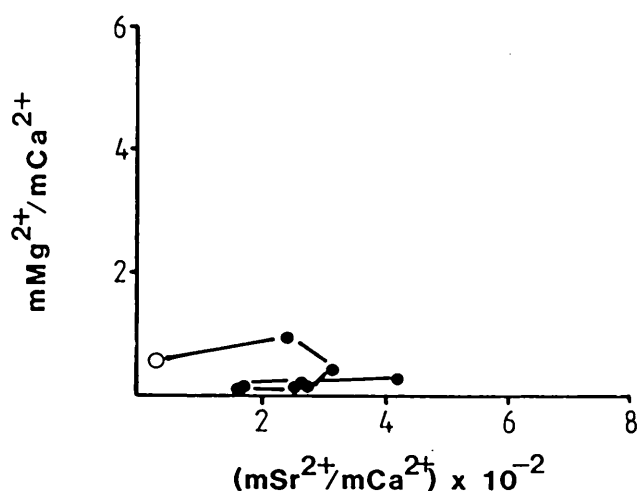


Fig. 5.4 - Evolution of pore fluids in terms of $m\text{Mg}^{2+}/m\text{Ca}^{2+}$ and $m\text{Sr}^{2+}/m\text{Ca}^{2+}$ ratios from the composition of freshwater during experiment 3186.

(b) Cement crystal chemistry

XRD analysis showed that 86 wt. % of the sediment after the experiment was composed of calcite (see Appendix V). Electron microprobe analysis (see Fig. 5.5) shows this calcite to be of a low-Mg composition, containing less than

1 mole % MgCO_3 correlating with the low level of Mg^{2+} in the pore fluids. Considerable amounts of SrCO_3 are contained within the calcite structure, ranging from 0.5-1.6 mole%.

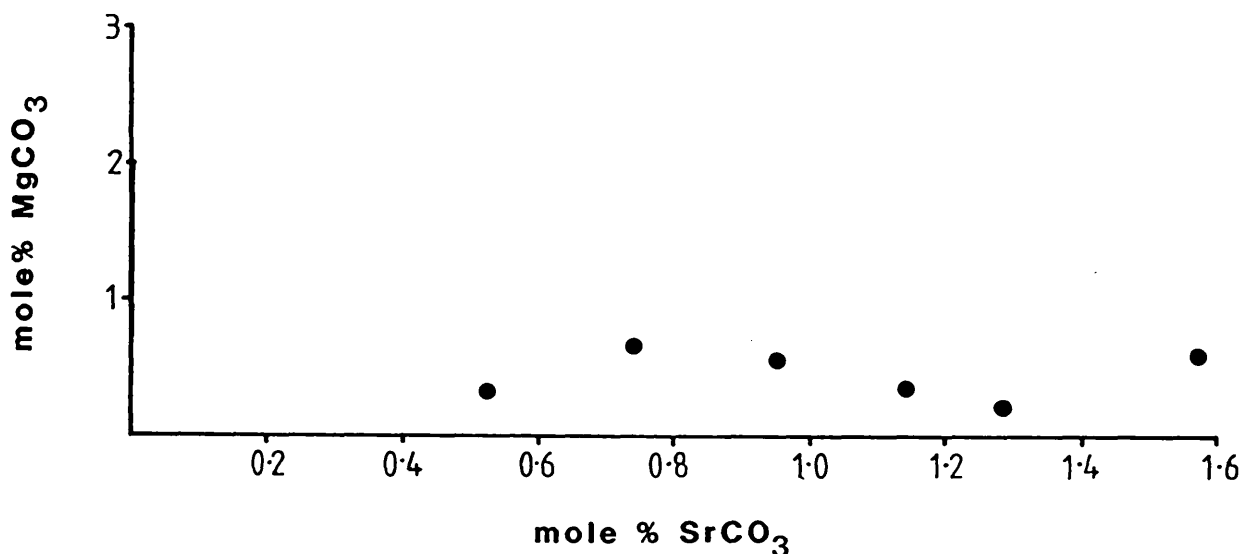


Fig. 5.5 - Mole % MgCO_3 and SrCO_3 contained in the cement crystals precipitated during experiment 3186.

Fig. 5.6 shows the range of SO_4^{2-} levels in the calcite cement phase precipitated. This is low when compared to other experiments (less than 0.1 up to a maximum of 0.75 mole % compared to typical ranges of 0.7-1.5 or 1-2 mole %, see Chapters 3 and 4).

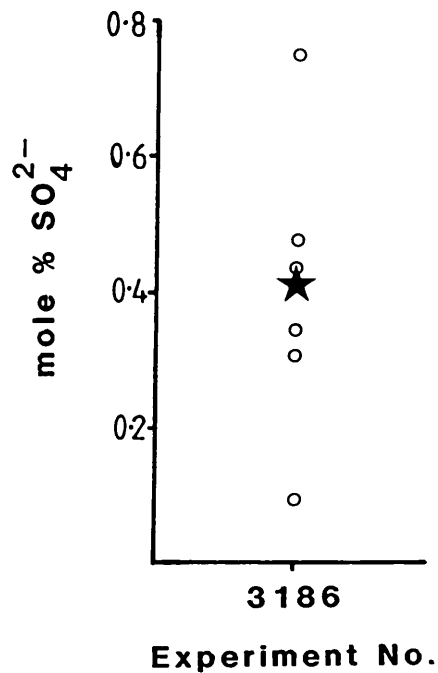


Fig. 5.6 - Mole % SO₄²⁻ contained in the cement crystals precipitated during experiment 3186. Mean value (★) is shown.

5.3.3 SUMMARY

Using freshwater, diagenetic alteration has been extensive (90-95 % of the original aragonite has been removed). Calcite has been precipitated as a rhombic cement and as rhombic crystals partially filling the extensive amount of secondary porosity which has been created. Some neomorphic alteration of micrite and shell fragments has occurred.

The pore fluids have much lower Ca²⁺, Mg²⁺, Sr²⁺ and SO₄²⁻

concentrations than the seawater and show limited change with maximum $m\text{Sr}^{2+}/m\text{Ca}^{2+}$ ratios remaining low ($<4.5 \times 10^{-2}$).

Mineralogically the cement and replacement phases are calcitic (as identified by XRD), containing less than 1 mole % MgCO_3 and less than 0.8 mole % SO_4^{2-} . It does however contain comparatively high levels of SrCO_3 (0.4 - 1.6 mole %), with maximum levels being higher than in any other experiment.

CHAPTER 6 - GEOCHEMISTRY OF THE REPLACEMENT FABRICS

6.1 INTRODUCTION

The petrographic results of the replacement processes which have operated during the experiments have already been presented in Chapters 3, 4 and 5. Electron probe microanalyses (EPMA) for the unaltered and replacement material which were not presented in those chapters because of the restricted nature of the data set, are presented in this chapter (the analyses can be found in Appendix IV).

The EPMA for the unaltered and replacement fabrics were obtained, like those for the cements, using a JEOL 733 superprobe coupled with back-scatter imagery, as described in section 2.4. Replacement textures however proved to be very difficult to identify using back-scatter imagery because of the similarity in composition of the unaltered and replacement phases. Of the replacement fabrics, neomorphic spar, which was in close association with the original aragonite, proved to be particularly difficult in this respect. All grains for analysis had therefore to be clearly marked using optical microscopy prior to examination using the electron microscope and analyses were conducted on grains which had been totally replaced by neomorphic spar.

6.2 SOLUTION CAVITY FILL CALCITE

Calcite which infills porosity created during the experiments has been termed 'solution cavity fill'. This is typically found where the porosity was generated by the dissolution of the aragonitic cortices of coated grains. It can also be sometimes found infilling secondary porosity created by the dissolution or partial dissolution of shell fragments.

Fig. 6.1 shows the distribution of MgCO_3 and SrCO_3 (mole %) in unaltered, non-skeletal aragonite and of solution cavity fill calcite. The analyses of the non-skeletal aragonite are predominantly of cortical aragonite but a few analyses of original aragonitic needles which were found lining chamber walls of foraminifera or gastropods have been included.

A low level of variation in both the MgCO_3 and SrCO_3 content of this unaltered aragonite is observed. The level of MgCO_3 contained within the aragonite ranges up to a maximum of 0.6 mole % but is typically less than 0.5 mole % (concentrations less than 0.4 mole % are not significantly above the detection limit to be statistically valid using the JEOL 733 superprobe). The level of SrCO_3 observed in the aragonite also has a restricted range from 1.0-1.25 mole %. The SO_4^{2-} content of the aragonite (see Fig. 6.2) is low, typically

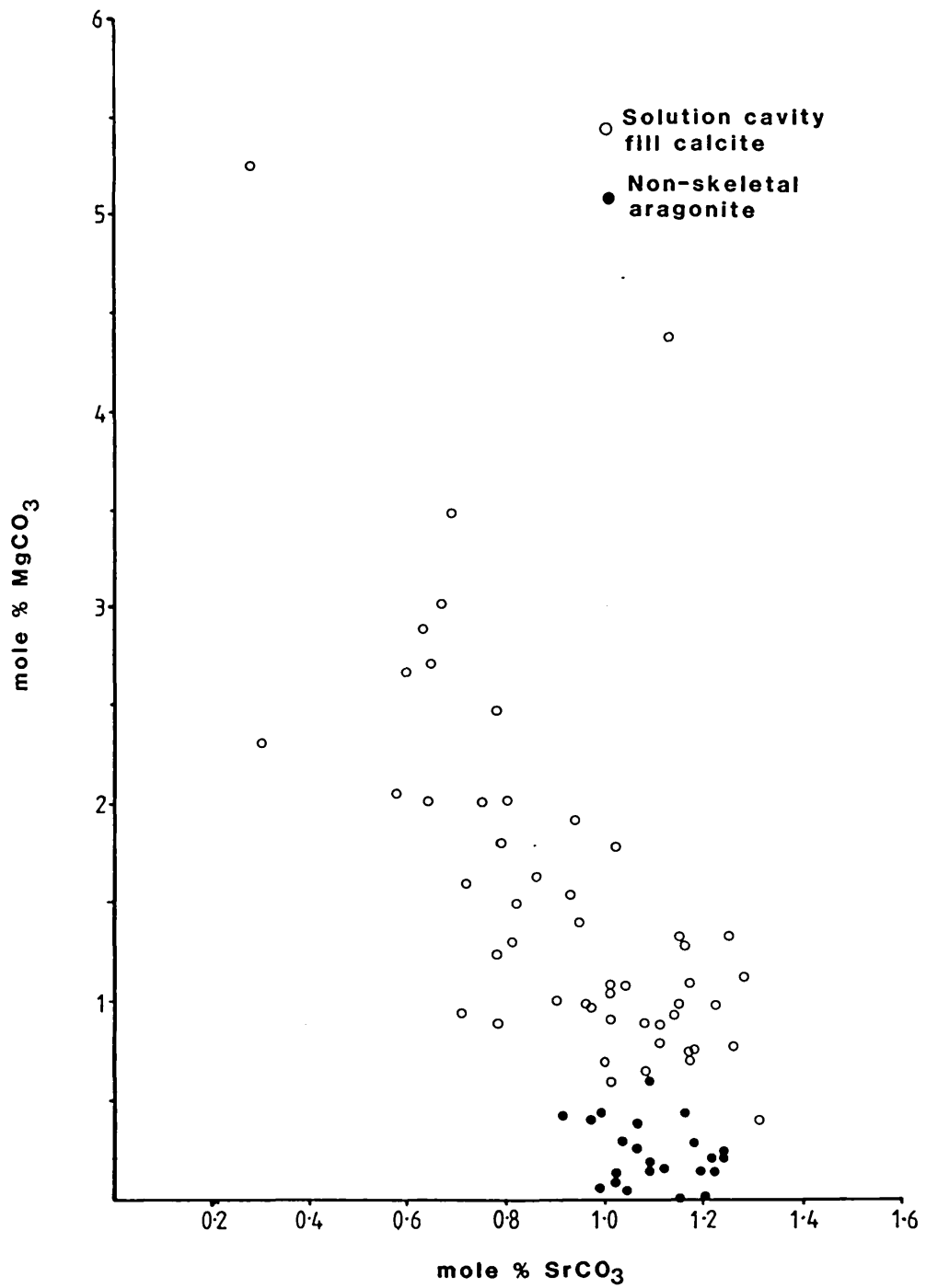


Fig. 6.1 - Mole % MgCO₃ and SrCO₃ contained in unaltered non-skeletal aragonite and solution cavity fill calcite.

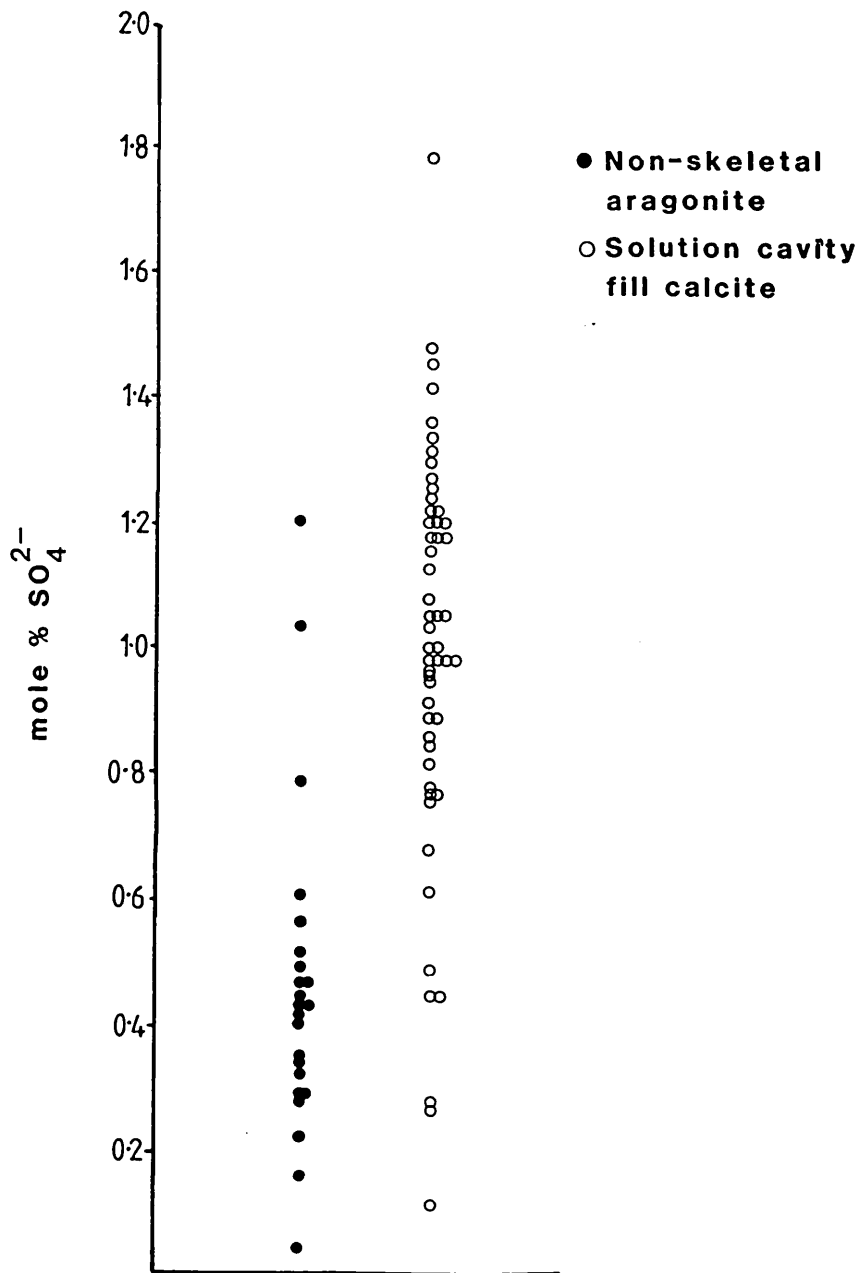


Fig. 6.2 - Mole % SO_4^{2-} contained in unaltered non-skeletal aragonite and solution cavity fill calcite.

less than 0.6 mole% with occasional values of 0.8-1.2 mole% (concentrations less than 0.2 mole % are not significantly above the detection limit).

Fig. 6.1 also shows the distribution of MgCO_3 and SrCO_3 (mole %) in the solution cavity fill calcite. This has a much more variable composition than that of the unaltered aragonite. The composition of the solution cavity fill calcite is distinct from that of the unaltered aragonite in terms of MgCO_3 and SrCO_3 contents (mole %). A general trend of increasing MgCO_3 content (mole %) with a decreasing SrCO_3 content (mole %) is observed. The SO_4^{2-} content of the solution-cavity fill calcite is shown in Fig. 6.2. It shows a wider distribution of SO_4^{2-} than in the original aragonite with most of the analyses being in the range 0.7-1.5 mole% (c.f. 0-0.6 mole % for the unaltered aragonite).

6.3 NEOMORPHIC SPAR

During the experiments, calcite which has replaced aragonitic shell fragments across a micron-sized alteration front with no observable solution cavity, producing a mosaic of spar or, which has replaced micrite by larger crystals, has been termed 'neomorphic spar'. The neomorphic spar which has partially replaced some of the micrite, is extremely difficult to identify using back-scatter techniques although it can be easily observed using optical

microscopy (see Chapters 3, 4, and 5) and unless it was of a large enough size as in the example shown in Plate 6.2 B, no analyses have been presented as the identification of these may be unreliable.

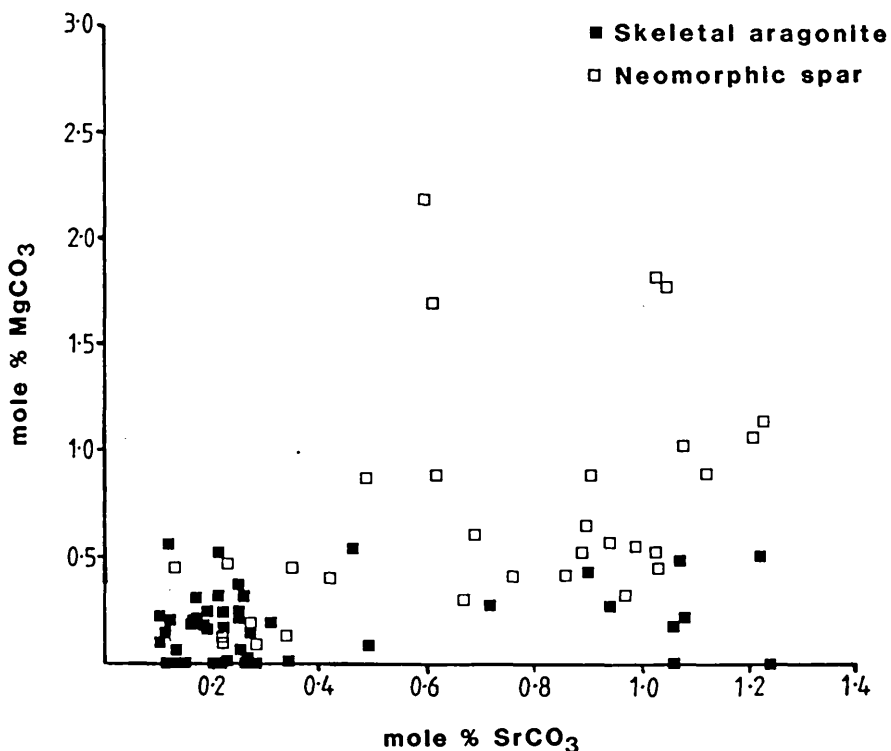


Fig. 6.3 - Mole % MgCO₃ and SrCO₃ contained in the skeletal aragonite and the neomorphic spar.

Fig. 6.3 shows the distribution of MgCO₃ and SrCO₃ (mole %) in unaltered shell fragments. Two distinct compositional groupings are observed. Both contain low levels of MgCO₃ (less than 0.6 mole %, typically less than 0.4 mole% i.e. not significantly above the detection limit of the JEOL 733). The majority of the molluscs analysed were found to

contain low levels of SrCO_3 (0.1-0.5 mole %) consistent with the data presented in Bathurst 1975, Fig. 225. Others were found to contain higher levels of SrCO_3 (0.9-1.3 mole%). The SO_4^{2-} content of the shell fragments is variable (as shown in Fig. 6.4) ranging from 0 - 1.5 mole %. Most analyses are in the range 0-0.5 mole %.

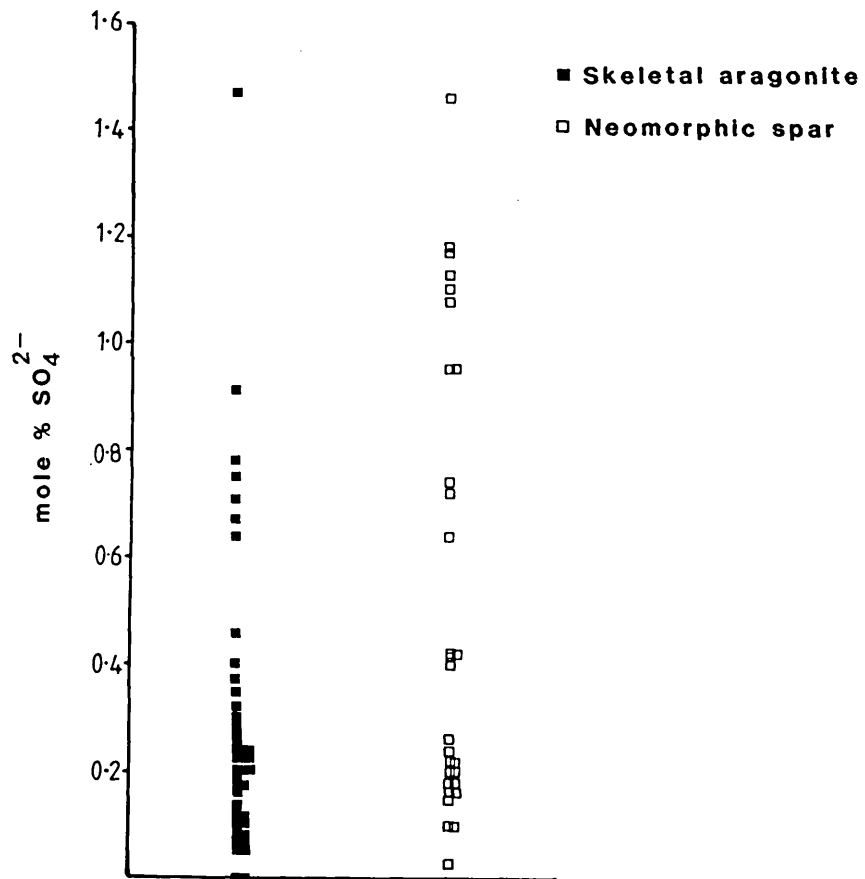


Fig. 6.4 - Mole % SO_4^{2-} contained in the skeletal aragonite and the neomorphic spar.

The MgCO_3 and SrCO_3 (mole %) content of the neomorphic spar is also shown in Fig. 6.3. This is variable but generally

the composition of the neomorphic spar varies very little from that of the biogenic aragonite, often overlying the composition of the unaltered shell fragments. The similarity in composition of the two phases is further emphasised by the SO_4^{2-} data (see Fig. 6.4) which shows a similar compositional range.

A few specific examples of the composition of neomorphic spar are given below.

(1) **Experiment 2185:** Plate 6.1 A shows a gastropod shell, the structure of which has been totally replaced by neomorphic spar. The EPMA for this neomorphic spar are given in Table 6.1. The average composition of the cement precipitated during this experiment is also given.

	Neomorphic Spar				Cement
	1	2	3	4	
MgCO_3	0.40	(0.09)	0.44	0.48	1.88
SrCO_3	0.42	0.28	0.35	0.23	0.81
SO_4^{2-}	(0.10)	(0.15)	(0.03)	(0.16)	1.05

Table 6.1 - EPMA (mole %) for relic gastropod shown in Plate 6.1A. Figures in brackets are not significantly above the detection limit to be statistically valid.

The composition of the neomorphic spar which has replaced the original shell structure of the relic gastropod shows

PLATE 6.1 - REPLACEMENT FABRICS

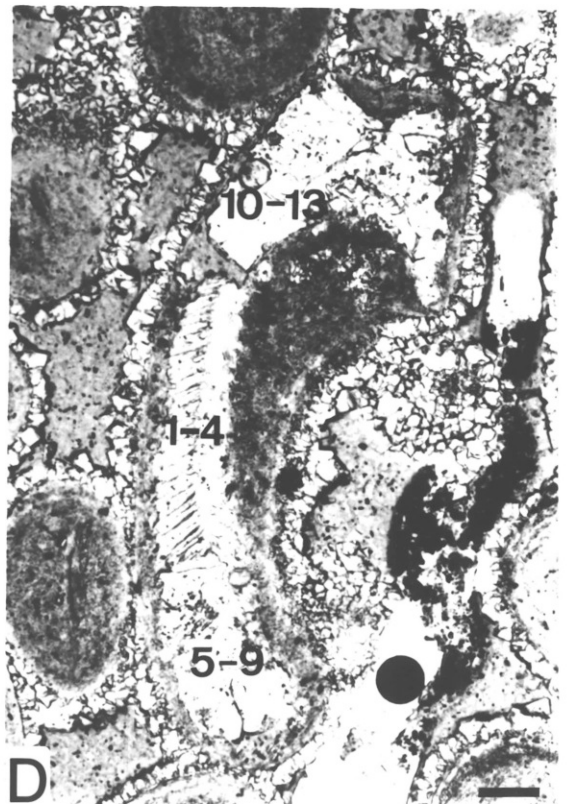
(A) Experiment 2185 - Gastropod shell (originally aragonite) totally replaced by neomorphic spar. Numbers show analyses points. PPL. Scale bar 100 μm .

(B) Experiment 2485 - Micritised grain (2-4) partially replaced by neomorphic spar (1-3). Numbers show analyses points. PPL. Scale bar 100 μm .

(C) Experiment 2585 - Grain partially replaced by neomorphic spar. Numbers show analyses points. XP. Scale bar 50 μm .

(D) Experiment 2985 - Shell fragment (1-4) partially replaced by neomorphic spar (5-9) and solution cavity fill calcite (10-13). Numbers show areas of analysis. PPL. Scale bar 50 μm .

PLATE 6.1



little variation in the mole% MgCO_3 content (with the exception of one analysis) or the SO_4^{2-} content but the SrCO_3 content does vary between the different areas (see Table 6.1) although this variation might be less when the analytical error of +/- 8% is considered. When compared to the average composition of the cement precipitated during this experiment, the composition of the neomorphic spar is quite different (even taking the analytical error into account), containing less MgCO_3 , SrCO_3 and SO_4^{2-} than the cement.

(2) **Experiment 2485:** Plate 6.1B shows a micritic peloid, presumably originally a shell fragment because of its size, which has been partially replaced by neomorphic spar. The EPMA for the original micrite and the neomorphic spar which replaces it is shown in Table 6.2. The level of both MgCO_3 and SrCO_3 (mole %) in the relic micrite and replacement neomorphic spar is similar. The neomorphic spar however contains a lower level of SO_4^{2-} than the original micrite. No cement were precipitated in this experiments to be used as a comparison.

	Micrite		Neomorphic Spar	
	2	4	1	3
MgCO ₃	0.43	0.42	0.42	0.64
SrCO ₃	0.91	0.97	0.86	0.90
SO ₄ ²⁻	0.79	0.46	0.20	0.42

Table 6.2 - EPMA (mole %) for the peloid shown in Plate 6.1B.

(3) **Experiment 2585:** Plate 6.1C shows a grain which has been partially replaced by neomorphic spar. Small areas of the original micrite can be seen as shown on the overlay. Table 6.3 shows the EPMA available for the neomorphic spar and the average composition of the cement precipitated during the experiment. The MgCO₃ and SO₄²⁻ levels observed in the spar are not significantly above the detection limit in any of the analyses. The SrCO₃ content however is variable, up to a maximum of 0.34 mole % although again this may not be significant when the analytical error is taken into account. When compared to the average composition of the cement, the MgCO₃ and SO₄²⁻ contents (mole %) of the neomorphic spar are less than that of the cement. The level of SrCO₃ is similar to that in the cement.

	Neomorphic Spar				Cement
	1	2	3	4	
MgCO ₃	(0.18)	(0.13)	(0.12)	(0.10)	5.12
SrCO ₃	0.17	0.34	0.22	0.27	0.36
SO ₄ ²⁻	(0.06)	(0.22)	(0.18)	0	1.55

Table 6.3 - EPMA (mole %) for the grain shown in Plate 6.1C. Figures in brackets are not significantly above the detection limit to be statistically valid.

(4) **Experiment 2185:** Plate 6.2A shows a relic shell fragment which has undergone complete neomorphism. The EPMA for the neomorphic spar and the average composition of the cement are given in Table 6.4.

	Neomorphic Spar		Cement
	1	2	
MgCO ₃	0.52	0.60	1.88
SrCO ₃	0.94	0.69	0.81
SO ₄ ²⁻	0.24	0.22	1.05

Table 6.4 - EPMA (mole %) for relic gastropod shown in Plate 6.2A.

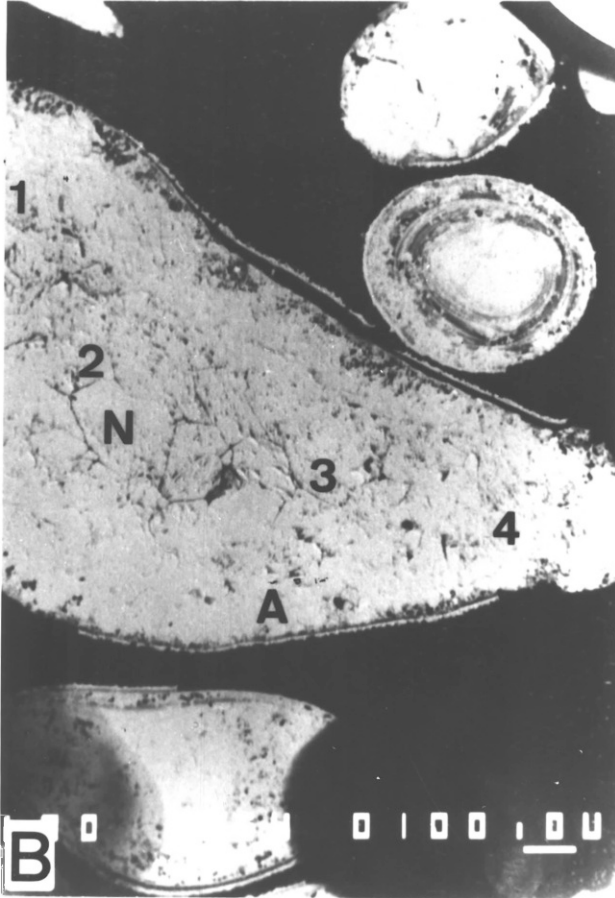
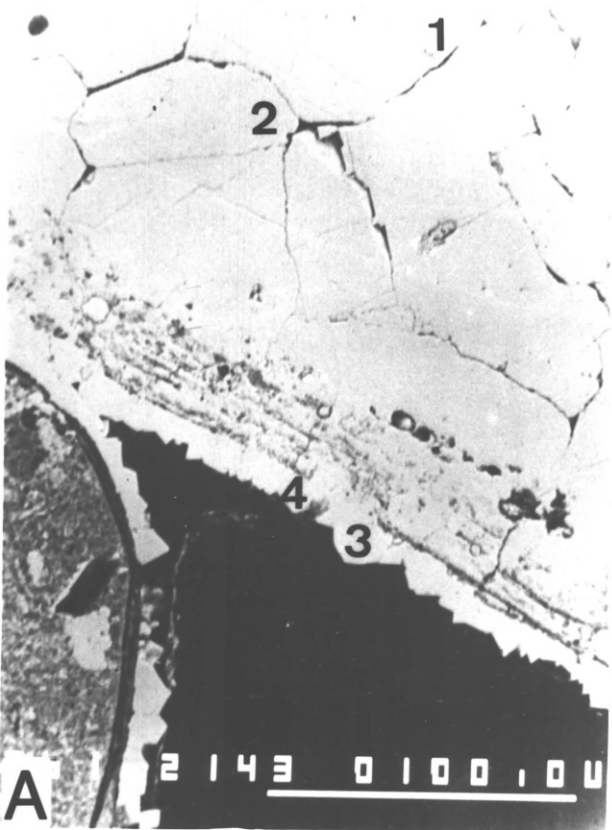
The composition of the neomorphic spar which replaces the original structure of the shell fragment in Plate 6.2A contains a lower amount of MgCO₃ and SO₄²⁻ than the cement but a similar level of SrCO₃.

PLATE 6.2 - REPLACEMENT FABRICS

(A) Experiment 2185 - Shell fragment totally replaced by neomorphic spar (1-2). Numbers show points of analysis. Back-scattered secondary electron image. Scale bar 100 μm .

(B) Experiment 30/3 - Shell fragment (A) partially replaced by neomorphic spar (N). Numbers in show points of analysis. Back-scattered secondary electron image. Scale bar 100 μm .

PLATE 6.2



(5) **Experiment 30/3:** Plate 6.2B shows another shell fragment which has been almost totally replaced by neomorphic spar. This spar contains variable levels of MgCO_3 and SO_4^{2-} (see Table 6.5) and relatively high levels of SrCO_3 (0.9-1 mole %). When this is compared to the average cement composition, it can be seen that the neomorphic spar contains less MgCO_3 and SO_4^{2-} but more SrCO_3 .

	Neomorphic Spar				Cement
	1	2	3	4	
MgCO_3	0.46	0.52	0.88	(0.32)	2.18
SrCO_3	1.03	0.90	1.01	0.97	0.64
SO_4^{2-}	0.26	(N/D)	(0.20)	0.41	1.20

Table 6.5 - EPMA (mole %) for the grain shown in Plate 6.2B. Figures in brackets are not significantly above the detection limit to be statistically valid.

6.4 EXAMPLE OF SHELL FRAGMENT REPLACED BY BOTH NEOMORPHIC SPAR AND SOLUTION CAVITY FILL CALCITE.

In section 5.2, an example of a shell fragments which was undergoing both neomorphic alteration and dissolution to be replaced by solution cavity fill calcite was reported (see Plate 6.1D). EPMA are presented for these phases in Table 6.6. It should be noted that this was in the experiment which was run using SO_4^{2-} -reduced seawater.

	Aragonite				Cement	
	1	2	3	4		
MgCO ₃	(0.37)	(0.04)	(0.35)	0.0	1.82	
SrCO ₃	(0.13)	(0.19)	(0.07)	(0.17)	0.72	
SO ₄ ²⁻	(0.05)	(0.18)	(0.07)	(0.10)	1.05	
	Neomorphic Spar					
	5	6	7	8	9	Average
MgCO ₃	2.33	1.26	1.38	1.28	2.76	1.80
SrCO ₃	0.97	0.99	0.94	0.95	0.61	0.89
SO ₄ ²⁻	1.32	0.93	1.42	1.03	1.12	1.16
	Solution Cavity Fill Calcite					
	10	11	12	13		Average
MgCO ₃	2.63	1.02	3.19	2.49		2.08
SrCO ₃	0.60	1.07	0.79	0.68		0.78
SO ₄ ²⁻	0.89	0.98	0.98	0.98		0.96

Table 6.6 - EPMA (mole %) for the grain shown in Plate 6.1D. Figures in brackets are not significantly above the detection limit to be statistically valid.

No significant difference is observed between the neomorphic

spar and the solution cavity fill calcite although there is a significant increase in the MgCO_3 , SrCO_3 and SO_4^{2-} contents (mole %) in both phases from the original aragonite.

Comparing the data for the replacement phases and the average cement composition given in Table 6.6, the average composition of both phases is very similar to that of the cement that was precipitated.

6.5 SUMMARY

Two types of replacement fabric have been developed (1) solution cavity fill calcite and (2) neomorphic spar.

(1) Solution Cavity Fill Calcite

This is found to have infilled secondary porosity, predominantly created by the removal of cortical aragonite in coated grains. Geochemically, the solution cavity fill calcite which infills oomoldic porosity, shows an increase in the MgCO_3 content and a decrease in the SrCO_3 content when compared to the original aragonite. It shows a composition which is similar to many cement crystals. The SO_4^{2-} content of the solution cavity fill calcite is higher than that of the original aragonite and again the SO_4^{2-} content is very similar to many cement crystals.

(2) Neomorphic Spar

This has been found to replace shell fragments and micritic aragonite across a micron-sub-micron sized alteration front. The composition of the neomorphic spar appears to reflect that of shell fragments or micritised grains which it replaces in experiments conducted using seawater. This is shown by the MgCO_3 , SrCO_3 and SO_4^{2-} (mole %) contents.

(3) Replacement of Single Grains by Solution Cavity Fill and Neomorphic Processes

In the example of the shell fragment which has been partially replaced by solution cavity fill calcite and neomorphic spar, both replacement phases were very comparable in composition to the cement that was precipitated during the experiment. Unlike the others, this experiment was conducted using SO_4^{2-} -reduced seawater.

PART III

DISCUSSIONS AND CONCLUSIONS

CHAPTER 7 - FACTORS AFFECTING CEMENT CRYSTAL NUCLEATION AND MORPHOLOGY

7.1 INTRODUCTION

Two types of cement fabric have been generated during the experiments. The first is composed predominantly of small, granular-bladed calcite crystals which form an isopachous fringe (maximum width 20 μm , typically 6-13 μm) around the grains of the partially lithified sediment. The second is composed of calcite crystals of a predominantly equant morphology, individual crystals ranging from 10-30 μm across and forming continuous or discontinuous fringes around the grains of the partially lithified sediment. Variations in the predominant fabric which are observed have however been noted from grain to grain (see results presented in Part II) and optically continuous overgrowths on echinoderm fragments have been observed.

The first type of cement fabric has developed during experiments using sediments BSO, ADDO and AKDO. The second type of cement fabric has developed during experiments using sediments ADBO and SBO (including SBSO and SBDO). In experiments using sediment AKSO, the cement fabric generated was a mixture of crystals of both morphologies.

These cement crystals are typically composed of calcite which contains less than 10 mole% MgCO_3 although crystals containing up to 84 mole % MgCO_3 have been observed. Significant amounts of SrCO_3 (0.1-1.3 mole%) and SO_4^{2-} (0.3-2.1 mole%) are also contained within this calcite. The composition of the cement crystals is discussed in detail in Chapter 8.

7.2 CONTROLS ON THE MORPHOLOGY OF THE CALCITE CEMENT CRYSTALS

One of the major questions concerning carbonate diagenesis is what controls the morphology and mineralogy of cements in different natural, diagenetic environments.

7.2.1 Effect of Mg^{2+} Concentration of the Precipitating Fluids on Crystal Morphology

Folk (1974) suggested that one of the main controlling factors on the morphology of calcite crystals was the $\text{mMg}^{2+}/\text{mCa}^{2+}$ ratio of the precipitating fluids. He suggested that a fluid with a low $\text{mMg}^{2+}/\text{mCa}^{2+}$ ratio (ranging from 0.1-2.0) favours the formation of equant calcite while a fluid with a high $\text{mMg}^{2+}/\text{mCa}^{2+}$ ratio (>2) favours the formation of bladed high-Mg calcite. The mechanism by which he envisaged this occurring was by the incorporation of the

smaller Mg^{2+} ion (33% smaller than Ca^{2+}) into the calcite structure. This would cause distortion, inhibiting growth of the calcite lattice in any direction other than that of the c-axis, resulting in an acicular or bladed crystal.

In nature, the relationship between the composition of the pore fluids and calcite morphology appears to hold in most cases. The marine environment (typical mMg^{2+}/mCa^{2+} ratios of seawater are around 5) is characterised by acicular aragonite and bladed high-Mg calcite cement crystals. The freshwater environment (typical mMg^{2+}/mCa^{2+} ratios of freshwater are less than 1) is characterised by equant calcite cement crystals (e.g. see Longman, 1980).

Given and Wilkinson (1985) however, have pointed out that there are significant deviations from this pattern in nature. Examples of this are the equant high-Mg calcite cement crystals which are found in the marine environment (e.g. Schroeder, 1972, Fig. 5A p.715) and whisker calcite cement crystals which are found in the freshwater environment (see Longman 1980, Fig. 11 p.472). The experimental results presented in this thesis likewise do not support the magnesium inhibition mechanism suggested by Folk (1974) which implies that the mMg^{2+}/mCa^{2+} ratio of the fluid is the dominant control on the calcite crystal morphology.

If the evolution of the pore fluids of experiment 1584 is considered (see Fig. 3.3 (e)), at no point during the experiment did the $m\text{Mg}^{2+}/m\text{Ca}^{2+}$ ratio drop to below 2, the level above which Folk (1974) suggested that Mg^{2+} will act as an inhibitor to growth of calcite in any direction other than that of the c-axis. If the petrographic results of this experiment are considered (see section 3.5.1 (6)), then it can be seen that the morphology of the precipitated calcite crystals is equant (see Plates 3.5 C and D and 3.9 A and B). These equant calcite crystals have been precipitated from pore fluids with a $m\text{Mg}^{2+}/m\text{Ca}^{2+}$ ratio ranging from 2.1-5.5, so it would appear that, at least in this case, the high $m\text{Mg}^{2+}/m\text{Ca}^{2+}$ ratio of the pore fluid did not selectively inhibit growth of the crystals in directions other than that of the c-axis.

In other experiments, the $m\text{Mg}^{2+}/m\text{Ca}^{2+}$ ratio of the pore fluids dropped from that of the seawater used here (4.8) to less than 1 (see section 3.5.2). Both equant and granular-bladed cement crystal morphologies were generated hence in these experiments, the $m\text{Mg}^{2+}/m\text{Ca}^{2+}$ ratio cannot be the main controlling factor on morphology and some mechanism of morphological control, other than the $m\text{Mg}^{2+}/m\text{Ca}^{2+}$ ratio of the pore fluids, must have operated during the experiments.

7.2.2 Effect of CO_3^{2-} Concentration of the Precipitating Fluids on Crystal Morphology

Given and Wilkinson (1985) suggested that as Ca^{2+} ions are more strongly hydrated than CO_3^{2-} ions in aqueous solution (the energy of hydration decreases as the radius of the unhydrated ion increases, Cotton and Wilkinson, 1962), growth of calcite crystals should be controlled by the dehydration of Ca^{2+} in the aqueous solution i.e. the actual availability of Ca^{2+} for reaction. However, they point out that although this applies to growth in directions other than that of the c-axis, it is not the case for growth along the c-axis. Planes perpendicular to the c-axis (i.e. those on which reaction takes place to promote growth in that direction), consist of alternating layers of Ca^{2+} and CO_3^{2-} ions. In seawater, because of the great excess of Ca^{2+} over CO_3^{2-} , a face perpendicular to the c-axis would usually be composed of Ca^{2+} ions (Lahann, 1978; Given and Wilkinson, 1985). This positively charged face would immediately attract CO_3^{2-} ions, if and when they were available. In the natural environment, the growth of the calcite lattice in the direction of the c-axis would be controlled by the availability of CO_3^{2-} ions (Lahann, 1978; Given and Wilkinson, 1985).

In support of this, Given and Wilkinson (1985) observed that

the range of calcite morphologies seen in nature can be easily explained by the rate of supply of CO_3^{2-} in each particular environment. They give the examples of the temperate and deep marine environments, where Ca^{2+} ion concentrations are maintained at levels much higher than CO_3^{2-} ion concentrations. In both cases, they suggest that growth sites on precipitating crystals are "starved" of carbonate ions, c-axis growth is not enhanced and precipitation results in equant crystals (growth in directions other than that of the c-axis occurs more easily because faces which are not perpendicular to the c-axis are composed of both Ca^{2+} and CO_3^{2-} ions). The other extreme of elongate high-Mg calcite is only found in the shallow marine environment where precipitation is driven by rapid outgassing of CO_2 and the subsequent generation of CO_3^{2-} ions from the dissociation of HCO^- . The system is therefore rich in CO_3^{2-} and growth parallel to the c-axis is enhanced.

Direct testing of this model for the control on crystal morphology, based on CO_3^{2-} concentration, is not possible in the case of the experimental results given here, for the following reasons.

(i) The CO_3^{2-} concentration of the pore fluids during the experiments is unknown. All pore fluid samples were analysed using ICP techniques, with which it is not possible to measure the CO_3^{2-} concentration. It could have been possible to use other methods to calculate the CO_3^{2-}

concentration of the liquids after their removal from the experimental cell but this would bear no relationship to the composition of the pore fluids in the cell as they separate into a gaseous and liquid phase on collection. The gaseous phase is composed mainly of CO_2 (Ferguson et.al., 1984) and the release of CO_2 would alter the CO_3^{2-} content of the liquids from that of the pore fluids inside the cell.

(ii) Under the present experimental system, measurement of pH (which would be essential in order to calculate the CO_3^{2-} content given all the other necessary data) would be very difficult within the cell. High temperature/pressure pH electrodes do exist and enquiries were made to obtain one. They are however expensive and unreliable, tending to break easily. It is unlikely that they could have been used satisfactorily during experiments which lasted for up to 6-8 weeks. The pH of the fluids could therefore only be measured at the end of the experiments and it was realised that this would not bear any relationship to that inside the cell during the experiments.

For these reasons, direct comparison of the CO_3^{2-} level in the pore fluids with the fabrics generated cannot be made but as shown in section 7.5, the CO_3^{2-} concentration of the pore fluids may have been a secondary factor in controlling the cement crystal morphology during the experiments.

The papers of Lahann (1978) and Given and Wilkinson (1985)

discussed above relate to the extreme variation in morphology between acicular and equant calcite crystals and to the control of enhanced growth parallel to the c-axis. In the cement crystals generated in this study however, the variations in crystal morphology with which we are concerned are not so extreme, varying from equant to granular-bladed calcite crystals. The bladed crystals have a length-breadth ratio of 2 or 3 to 1. Also, the cement fabric has been found to vary from place to place within a single sample, in addition to considering their growth only, it is essential to investigate their nucleation history.

If the early fabrics that were reported in section 4.2 are considered, then it can be seen that the differences observed in better developed cement fabrics are also observed in early fabrics. In experiment 18/4 (using sediment ADDO, see section 4.2.1), an isopachous layer (3 μm wide) of tightly packed calcite cement crystals was precipitated on coated grain surfaces. This was the precursor of the granular-bladed cement fabric. During experiments 2585 and 2685 (using sediment ADBO, see section 4.2.1), small, isolated calcite cement crystals formed along grain edges and these were the precursors to the equant fabric. These isolated crystals were larger (5-7 μm wide) but fewer than the crystals precipitated in experiment 18/4, perhaps suggesting that the rate of crystal nucleation controlled the type of fabric which was developed. Equant

fabrics were developed using two sediments (ADBO and SBO) and factors which may have restricted the rate of cement crystal nucleation will therefore be considered.

7.3 CHEMICAL CONTROLS ON THE NUCLEATION RATE OF CRYSTALS DURING EXPERIMENTS

7.3.1 Effect of Mg^{2+} in Controlling the Nucleation Rate

The nucleation of the cement crystals occurs in the early stages of the experiments. In experiments using sediment BSO which were aborted during the first 5 days, nucleation of cement crystals had already occurred. If the evolution of the pore fluids of experiments run using Shark Bay Ooids (SBO) are considered (see Fig. 3.3 (e)), then it can be seen that a rise in the mMg^{2+}/mCa^{2+} ratio of the pore fluids, above that of the seawater used, is observed. Sediment SBO contained between 10 and 15 wt. % high-Mg calcite. The higher mMg^{2+}/mCa^{2+} ratios were due to increased levels of Mg^{2+} (ppm) in the solution and it is believed that incongruent dissolution of some of the high-Mg calcite (e.g. Land, 1967) provided the excess Mg^{2+} . In two of the experiments (1384 and 1584), the mMg^{2+}/mCa^{2+} ratio remained high, never falling below 1, as was the case for all other experiments. The lowest mMg^{2+}/mCa^{2+} ratios that were observed during experiments 1384 and 1584 were 1.2 and 2.1 respectively.

The effect of Mg^{2+} on the nucleation of calcite must therefore be considered.

As long ago as 1910, Leitmeier suggested that Mg^{2+} was an inhibitor to the precipitation of calcite (Bathurst, 1975, p.244) and several studies of the effect of Mg^{2+} on calcite nucleation have been conducted. Fyfe and Bishoff (1965), Bishoff and Fyfe (1968), Bishoff (1968) and Chave and Suess (1970) suggested that calcite nuclei could precipitate continually from solution, but that they would not grow beyond a subcritical size as the Mg^{2+} , adsorbed onto their surfaces, would increase their solubility. Berner (1975) also studied the effect of Mg^{2+} on the nucleation and growth of both aragonite and calcite. He likewise concluded that Mg^{2+} is adsorbed readily onto the surface of calcite and that most of the Mg^{2+} inhibition was due to the non-equilibrium incorporation of Mg^{2+} into growing calcite crystals, which greatly increased their solubility. Lippman (1960) and more recent studies by Lahann (1978), Mucci and Morse (1983) and Morse (1983) suggest that the inhibiting effect of Mg^{2+} is due to difficulties in rapidly dehydrating it once it has been adsorbed onto active growth sites.

In the case of the experiments run using Shark Bay Ooids, the results suggest that although the Mg^{2+} concentration of the pore fluids probably did not control the morphology of the crystals by the mechanism suggested by Folk (1974), it

is likely that the high concentration of Mg^{2+} ions in the pore fluids during the early stages of the experiments (length of time varying from 7-28 days) inhibited the precipitation of many cement crystal nuclei. In contrast, during experiments using other sediments, the mMg^{2+}/mCa^{2+} ratio of the pore fluids dropped below that of seawater within the first week. Further growth of these equant crystals precipitated using Shark Bay Ooids may well have been controlled by the CO_3^{2-} mechanism suggested by Lahann (1978) and Given and Wilkinson (1985) but the nuclei, unlike those in the granular-bladed fabric, had room in which they could grow sideways provided that sufficient ions, both Ca^{2+} and CO_3^{2-} , were present in the pore fluids.

7.3.2 Effect of the Supply of Ions Through Aragonite Dissolution on the Nucleation Rate

As with experiments using Shark Bay Ooids, equant cement fabrics were generated during experiments using sediment ADBO. However, no increase in the mMg^{2+}/mCa^{2+} ratio of the pore fluids at the beginning of the experiments was observed (see Fig. 3.3 (b)).

At the outset of all experiments relatively low concentrations of Ca^{2+} and CO_3^{2-} were available in the seawater for the nucleation of $CaCO_3$. Further, much of the Ca^{2+} which was available, was removed by the early precipitation of

anhydrite (see section 3.2). During the first 7 days of the experiments involving seawater only, 280 ppm Ca^{2+} was removed from the seawater (original content approximately 432 ppm, see Fig. 3.1), being precipitated as CaSO_4 . The development of an isopachous fringe of calcite cement crystals such as that observed associated with the partially lithified sediment of experiment 18/4 (see Plate 4.4), would therefore require a source of ions in addition to that which existed in the initial pore fluids. The only source of CaCO_3 which was available in the system was from the dissolution of aragonite which would also release Sr^{2+} into the pore fluids. Assuming a constant distribution coefficient for Sr^{2+} in the calcite precipitated during experiments run at the same temperatures (see discussion of distribution coefficients in section 8.3.2), the level of the $\text{mSr}^{2+}/\text{mCa}^{2+}$ ratio in the pore fluids coupled with XRD data would therefore give an indication of the amount of aragonite which had gone into solution during experiments run under similar experimental conditions.

Comparing the $\text{mSr}^{2+}/\text{mCa}^{2+}$ ratios of experiments run at 183 °C using sediment ADBO (equant cement fabrics) and sediment BSO (granular-bladed fabrics), the ratios in the experiments using sediment ADBO were always lower. In the early stages of the experiments $\text{mSr}^{2+}/\text{mCa}^{2+}$ ratios of 1.4×10^{-2} and 2.1×10^{-2} were observed in ADBO and BSO experiment respectively. Maximum values of 6×10^{-2} compared to $7-8 \times 10^{-2}$ were

observed (see Fig. 3.3 (a) and (b)). If the XRD data is considered, in sediment ADBO, less than 5% of the original aragonite was removed by dissolution while 10-20% of the original aragonite was removed from sediment BSO. The conclusion from both these lines of evidence is, that at all times during experiments using sediment ADBO, fewer ions were available through the dissolution of aragonite for the nucleation and growth of calcite cement crystals than during experiments using sediment BSO. Relative saturation states prior to nucleation and growth would have been lower during experiments using sediment ADBO, fewer nuclei would have been formed initially and it is suggested that once a limited amount of nucleation occurred, continued growth of those nuclei would have been preferential to further nucleation events because of the relatively high energy and saturation states required for nucleation. Experiments using sediment AKSO which showed intermediate cement fabrics also showed intermediate levels of aragonite dissolution (see Table 3.9).

7.3.3 Summary

During the experiments a major control on the cement crystal morphology appears to have been the relative rate of nucleation. Early nucleation may have occurred from the limited amount of Ca^{2+} and CO_3^{2-} in the pore fluids during the very early stages of the experiments but, once the

dissolution of aragonite proceeded, the saturation state of the pore fluids with respect to Ca^{2+} and CO_3^{2-} would increase. If no constraints on the nucleation rate by either increased levels of Mg^{2+} , low rates of aragonite dissolution or substrate control (see section 7.4) operated, then rapid nucleation events could have taken place, resulting in a granular-bladed fabric (composed of many small crystals). Where the nucleation rates were relatively lowered by either Mg^{2+} inhibition or a lower rate of aragonite dissolution, growth on existing nuclei would have been favoured, resulting in relatively large crystals of equant morphology.

Support for this hypothesis comes from experiment 28/1 where the larger grain size of the sediment compared to that in experiments 28/2-4, reduced the rate of aragonite dissolution (see section 9.3.2). Equant cement crystals were observed (see Plate 3.13 A and B) while granular-bladed crystals were observed in the other experiments (see Plates 3.13 C and D, 3.14 A-D). Cement crystals of a more equant morphology were also observed in the experiment run using sediment AKSO treated with H_2O_2 where a lower nucleation rate was observed while in the non-treated sediment sample, granular-bladed cement crystals were observed (see Plate 3.15 A-D and discussion in section 7.4.2 (3)).

7.4 PHYSICAL CONTROLS ON THE NUCLEATION RATE DURING THE EXPERIMENTS

Each sediment type is typically characterised by a predominant fabric. However, variations in the cement fabric from grain to grain do occur. Local control must therefore have been either chemical or physical.

7.4.1 Effect of Grain Substrate

The effect of grain substrate in cement nucleation has been considered by many authors e.g. Folk (1965) and Bathurst (1975). Echinoderm fragments in particular act as substrates for syntaxial growth of cement.

(1) Echinoderm Fragments

The overgrowth of echinoderm fragments during early diagenesis by calcite in optical continuity with the fragment, has been well documented. Evamy and Shearman (1965) in describing the development of echinoderm overgrowths in Bajocian limestones from the southern French Jura, found that the initial morphology of the overgrowth depended on the crystallographic orientation of the calcite fragment (single crystal of calcite). Fragments composed of a basal section were initially overgrown by calcite which followed the outline of the fragment, while elongate

fragments, parallel to the c-axis, were initially overgrown by calcite spires (scalenoedra), perpendicular to the c-axis of the fragment. This early pattern of development in the overgrowths of the Jura, was further supported by material from cores of sub-Recent - Pleistocene age from the Arabian Gulf (Evamy and Shearman, 1969).

Later, a more detailed investigation of echinoderm overgrowths by Walkden and Berry (1984 a,b) suggested that the morphology of echinoderm overgrowths may be controlled not only by the crystallographic orientation of the fragment but by the environment in which they grow. They suggested that overgrowths of the Evamy-Shearman type are characteristic of marine basinal setting. Other types of overgrowth described by Walkden and Berry (1984 a,b) are listed below.

(i) Needle overgrowth - typically formed where there has been an early input of mud into the sediment, stopping the continued development of the overgrowth.

(ii) Contouring overgrowth - typical of shallow marine environments which have a meteoric influence. The overgrowths are periodically subjected to exposure in the meteoric environment and the development of spires is therefore inhibited by partial-solution.

(iii) Idiomorphic overgrowth - these represent several cycles of cementation during a typical cycle of deposition followed by burial, uplift and erosion prior to being

redeposited and buried.

All echinoderm fragment overgrowths observed in this experimental study are of the Evamy-Shearman type (1965, 69) and in Walkden and Berry's (1984 (a), (b)) classification, typical of marine basinal settings (see Plate 7.1 A-C). Basal echinoderm fragments show overgrowths which contour the fragment. Often however, the overgrowths do not completely surround the grains. Areas of the grain edges are fringed by small, granular calcite crystals which are not in optical continuity i.e. normal cement (see Plate 7.1A). These however may later be incorporated in the overgrowth (see Plate 7.1C). These fringes have developed where more canals are present on the echinoderm fragment surface or where the surface of the fragment has been extensively bored (see Plate 7.1 A and C). Clean, unbored surfaces of the echinoderm fragment, which show fewer canals at the surface, are overgrown by a continuous rim of calcite (see Plate 7.1A). All of these features were described by Evamy and Shearman (1965) from the natural material of the French Jura. Elongate echinoderm fragments are characterised by a spired overgrowth (see Plate 7.1 B), again similar to that described by Evamy and Shearman (1965, 69) and Walkden and Berry (1984 a,b). The calcite spires (scalenoedra) are also in optical continuity with the fragment.

PLATE 7.1 - OPTICALLY CONTINUOUS OVERGROWTHS

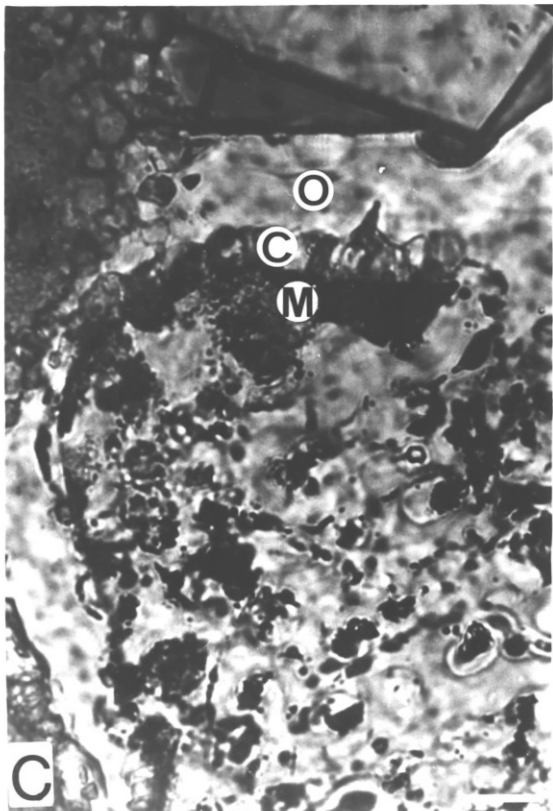
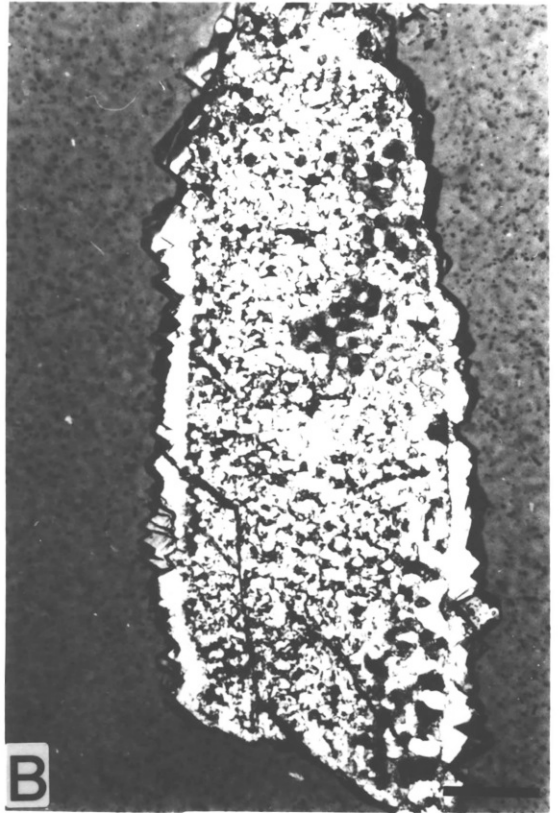
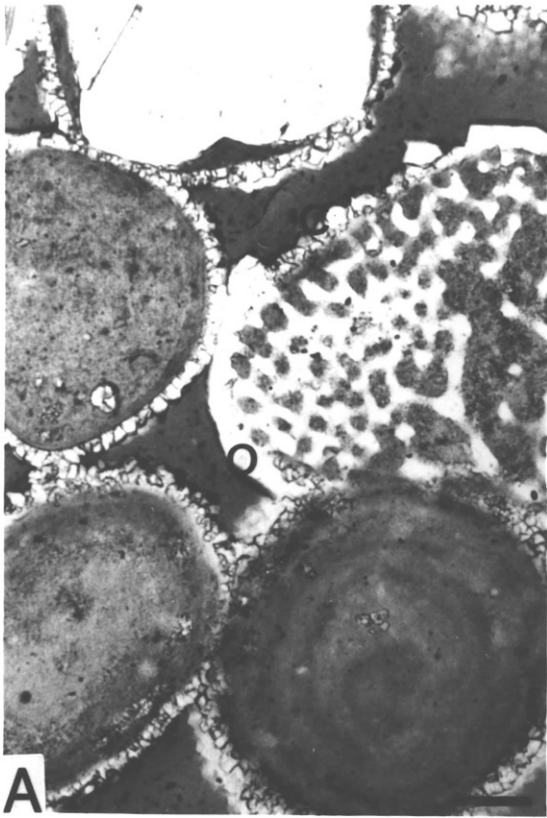
(A) Experiment 37/3. An echinoderm fragment, cut perpendicular to the c-axis (i.e. basal section) is partially overgrown by a calcite overgrowth (O) which is in optical continuity and which parallels the outline of the fragment. A cement fringe of granular crystals (C) is developed on part of the grain surface which has a higher proportion of canals, most of which are filled with micrite. This cement fringe is not in optical continuity. PPL. Scale bar 50 μm .

(B) Experiment 30/3. An echinoderm fragment, cut parallel to the c-axis (i.e. vertical section) is overgrown by calcite spires (scalenohedra) which are in optical continuity with the fragment. PPL. Scale bar 100 μm .

(C) Experiment 2985. A basal section of an echinoderm fragment. A micritised area (M) is overgrown by bladed-granular cement crystals (C). The calcite overgrowth (O) which is developed on the other areas of the fragment, envelops this early cement fringe. PPL. Scale bar 20 μm .

(D) Experiment 3186. A shell fragment composed of prisms of high-Mg calcite (P) on which calcite cement crystals (C) have grown in optical continuity. PPL. Scale bar 50 μm .

PLATE 7.1



Echinoderm fragments are one very obvious example of substrate control on the nucleation and growth of calcite during the experiments.

(2) Shell Fragments

Calcitic bivalve fragments have been found to display overgrowths of calcite scalenohedra which are in optical continuity with the shell fragments, similar to those of vertical echinoderm fragments. One particular example is shown in Plate 7.1 D where calcite cement crystals have grown parallel to the c-axes of the calcite prisms which form the shell structure. However, very few calcite bivalve fragments are present in any of the sediments used.

(3) Coated Grains Compared to Peloids

One major influence of substrate control is seen when examining the cement fringes of coated grains and peloids. In almost all of the partially lithified sediments retrieved at the end of the experiments, peloids have been found to display several layers of cement crystals (in both the granular-bladed cement fabric and the equant cement fabric) while nearby coated grains display one layer of cement crystals only (see Plates 3.2 A, 3.3 A,B, 3.10 C, 3.11 C, 3.13 D). However, where the smooth surfaces of coated grains have been bored, crystal clusters are observed (e.g.

Plate 3.13 B) and this is especially noticeable during the early development of the cement fabrics. Plate 4.5 A and B (experiment 3886) shows some of the small crystals which were precipitated in one of the aborted experiments (see section 4.2). These cement crystals are found to have precipitated on the surface of the peloid and in the bored surface pit of the coated grain but not on the smooth surface of the coated grain.

Peloids and the bored surfaces of coated grains may act as preferential nucleation sites for two reasons.

(i) The very fine size of the CaCO_3 particles of peloids and associated with the bored surface pits of coated grains, may provide a considerably greater number of nucleation sites (e.g. see Evans and Ginsburg, 1987).

(ii) The organic matter which is associated with peloids and with the bored surface pits of coated grains, may provide a considerably greater number of nucleation sites (see section 7.4.2).

Morse (1983) pointed out that higher energy crystal sites such as edges and defects were preferential for growth and dissolution. Micritic carbonate would have more of these sites than aragonitic needles. However, most of the grains from which the peloids have been generated in the depositional environment, were aragonitic. It is therefore unlikely that calcite cement crystals would preferentially

nucleate on sites provided by micritic aragonite.

The micritic aragonite of the peloids should also be favoured for dissolution because of the increased solubility of small particles (see Pantin, 1965, Bathurst, 1975 p.254). This would increase the saturation state of the pore fluids around peloids, encouraging nucleation in that microenvironment. However, it is difficult to see why the saturation state of the microenvironment surrounding a neighbouring grain (such as that shown in Plate 4.5 B) should not be similarly increased. Also the experimental evidence suggests that cortical aragonite is less stable than micritic aragonite (see section 9.3.1) which would imply that the saturation state of the microenvironment around the coated grains should be increased.

7.4.2 Effect of Organic Matter

The association between micritisation and endolithic algae has been well documented. Shearman et al. (1970), Loreau and Purser (1973), Harris et al. (1979) and Gaffey (1983), attributed the formation of surface pits (some of which were connected to internal borings) to the action of endolithic algae. Shearman et al. (1970) also noted that some of the pits were actually occupied by colonies of blue-green (endolithic) algae.

The infilling of such borings by aragonite and high-Mg calcite cements, resulting in micritisation, has also been well documented (e.g. Bathurst, 1966; Shearman et al., 1970; Loreau and Purser, 1973; Harris et al., 1979 and Gaffey, 1983). A close association between the activity of algae (which secrete different forms of organic matter) and the bored surfaces and micritisation of grains in the depositional environment, has therefore been established (Bathurst, 1966).

Seawater contains dissolved organic matter (DOM) which is adsorbed onto carbonate grain surfaces. Experimental evidence for this comes from the studies of Chave (1965), Chave and Suess (1967) and Suess (1970, 73). Most of the adsorptive properties of DOM appear to be related to the negatively charged carboxyl group ($-\text{RCOO}^-$) which occurs in natural organic matter (Mitterer and Cunningham, 1985).

Mitterer (1968, 1972) and Suess (1973) suggested that organic matter on the surface of grains may play an important role in the nucleation of calcium carbonate. This hypothesis is supported by the results of experimental studies by Suess and Futterer (1972) and Davies et al. (1978) who formed ooids in the presence of humic substances. These ooids contained organic membranes, interlayered with aragonite. Further evidence which may support this hypothesis is the close association which exists between the

skeletal structure of invertebrates and the proteinaceous membranes which are found in their structure (e.g. Mitterer, 1972; Mitterer and Cunningham, 1985) and the widespread occurrence of CaCO_3 in animals and plants (e.g. Pautard and Williams, 1982). The question therefore arises as to whether organic matter can act as a nucleation point for CaCO_3 .

The role of organic matter (particularly adsorbed organic matter) has been widely presumed to be that of an inhibitory nature against carbonate precipitation. The experimental studies of Berner et.al. (1978) showed that some humic substances strongly inhibited aragonite precipitation. Pautard and Williams (1982) however point out that some proteins and polysaccharides act as inhibitors to growth of calcium salts while others act as accelerators to crystal growth. Mitterer and Cunningham (1985) also raise the point that, if the organic matter coating on grains acts purely as an unreactive sheath, then why do cements in the marine environment nucleate at all.

Mitterer and Cunningham (1985) argue that because many of the negatively charged carboxyl groups on each adsorbed molecule of organic matter will not be interacting with the CaCO_3 surface onto which they are adsorbed and thereby neutralised, an increasingly negative electrical potential will accumulate at the CaCO_3 /organic matter interface as

more molecules are adsorbed. At some point, the electrical potential becomes large enough to act as an effective barrier against further adsorption of organic matter. Cunningham and Mitterer (1980) had previously shown that non-skeletal intra-grain (such as that in coated grains) and adsorbed organic matter binds Ca^{2+} to a significant degree. Mitterer and Cunningham (1985) therefore suggest that organic matter can act as a nucleation point for CaCO_3 . The large negative charge which develops on the surfaces of carbonate grains during the adsorption of organic matter, could attract Ca^{2+} ions to satisfy this negative charge. The structure of the carboxyl group further supports this theory in that it is very similar to the carbonate group (see Fig 7.1). It can be easily incorporated into the calcite lattice and certainly accounts for the adsorption of molecules which contain it.

The similarity of the groups and the evidence of Cunningham and Mitterer (1980), have lead Mitterer and Cunningham (1985) to suggest that the adsorbed carboxyl group could act as a nucleation point for CaCO_3 as shown in Fig. 7.2 but because of a lack of evidence, they concluded that it is uncertain.

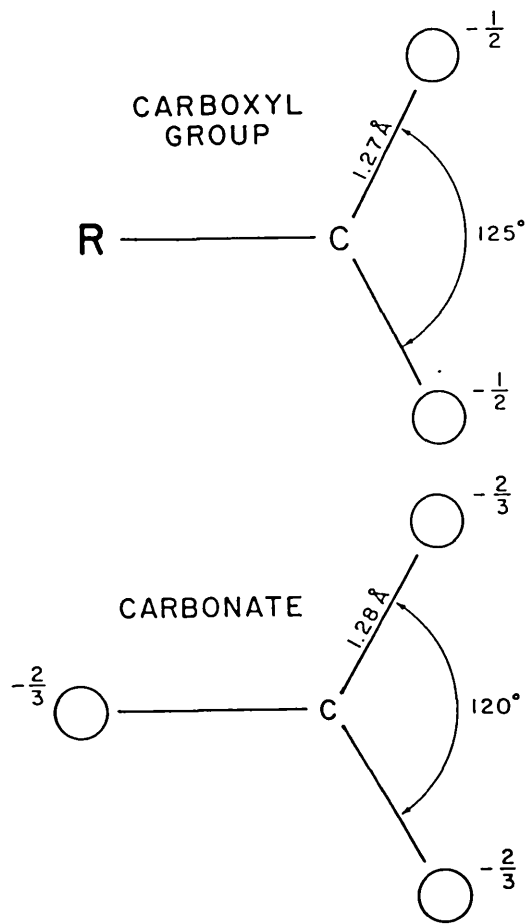


Fig. 7.1 - Geometric comparison of carboxyl group and carbonate anion. R represents the remainder of the molecule to which the carboxyl group is attached (from Mitterer and Cunningham, 1985).

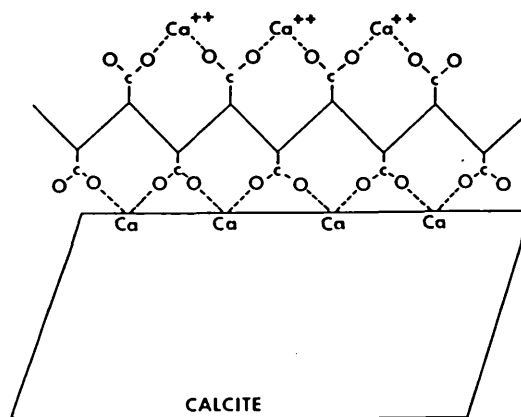


Fig. 7.2 - Highly idealized illustration of the interaction of carboxyl groups with calcite surface (taken from Mitterer and Cunningham, 1985).

Three areas of evidence are presented in this thesis which may support the suggestion made by Mitterer (1968, 1972), Suess (1973), Cunningham and Mitterer (1980) and Mitterer and Cunningham (1985) that organic matter may act as a nucleation site for CaCO_3 . These are:

- (i) the differences in cement fabric observed between peloids or the bored surfaces of coated grains and the smooth surfaces of coated grains,
- (ii) crystal nucleation on algal filaments and organic matter within the pore spaces of the sediment and
- (iii) the series of experiments which were designed to study the effect of surface organic matter in sediments composed of both coated grains and peloids and of sediments composed predominantly of skeletal fragments.

(1) Differences in Cement Fabric Between Peloids and Coated Grains

Because of their origin, bored surfaces and most peloids have a close association with organic matter (mucilaginous sheaths and filaments produced by the boring activity of endolithic, blue-green algae). Also, because of the higher surface area exposed to seawater in their depositional environment, a higher level of adsorbed DOM will be associated with these grains than with the smooth surfaces of coated grains. It is therefore possible that the larger

number of nucleation sites which are associated with peloids and the bored surfaces of coated grains are due to a higher amount of associated organic matter whether it be of a blue-green algal origin or of an adsorbed DOM origin.

(2) Algal Filaments and Areas of Organic Matter Within Sediment Pore Spaces

One line of evidence which suggests that organic matter of algal origin, and not just adsorbed DOM as suggested by Mitterer and Cunningham (1985) acts as a nucleation site for CaCO_3 comes from the presence of 'strings' of cement crystals in the partially lithified sediments (see Plate 3.2 B) which appear to have grown on the surface of algal filaments. Some algal filaments have been observed protruding from grains and show layers of cement crystals on either side, mimicking its form (see Plates 3.2 C and 3.3 C). Clusters of cement crystals which occur associated with organic matter have been found 'floating' in the pore spaces of the sediments (see Plate 3.4 A). The reason for the association of multiple layers of crystals with areas of organic matter and filaments is unclear. If organic matter has acted as a nucleation area then it appears that a 'microenvironment' in which enhanced nucleation rates around the organic matter has also been created.

(3) Experimental Investigation of the Effect of Surface Organic Matter

Further investigation of the role of organic matter was considered necessary and a series of experiments was designed to study the effect of surface organic matter on the cement fabrics. Organic matter was removed from samples of sediments AKSO and AKS4 by soaking in hydrogen peroxide. Efferevescence of CO_2 had stopped in the sample of shell fragments (AKS4) but a small amount of CO_2 was still being released from the sample of sediment AKSO. This is likely to be due to the much higher level of organic matter contained within coated grains and peloids. Experiments were conducted using these sediments and their untreated counterparts (the results are reported in section 3.6.3).

Using sediment AKSO, the degree of cementation which was observed was less in the sediment sample which was treated with H_2O_2 than in the sediment samples which was not (compare Plate 3.15 C and D with 3.15 A and B). Little cementation has been found in association with shell fragments, as shown in section 3.6.1 and the sample of shell fragments used in this set of experiments, which was untreated with H_2O_2 , only showed the development of a limited number of cement crystals (see Plate 3.16 A and B). The small cement crystals which were developed in the sample of shell fragments soaked in H_2O_2 however were very rare

(see Plate 3.16 C and D) and the observation of any present required the use of an electron microscope. A distinct decrease in the degree of cementation was therefore observed in both sediments which were treated with H_2O_2 when compared with their untreated counterparts.

The removal of organic matter from the sediments could have affected the reactions in two ways.

(i) By decreasing the level of CO_2 in the system which is generated through the breakdown of organic matter at the experimental temperatures ($180-200^\circ C$, Ferguson et al., 1984).

(ii) By decreasing the number of nucleation sites on grains if the surface organic matter does indeed act as a nucleation site for $CaCO_3$.

Some of the organic matter which is contained within the sediment is believed to breakdown during the experiments releasing CO_2 (Ferguson et al., 1984). Removal of organic matter should therefore decrease the pCO_2 and reduce the degree of aragonite dissolution. This was observed in the shell fragment sample soaked in H_2O_2 where a decrease in the degree of aragonite dissolution was observed. Lower mSr^{2+}/mCa^{2+} ratios (see Fig. 3.24 (c) and (d)) and Sr^{2+} (ppm) levels (see Table 7.1) were observed in the pore fluids. Fewer ions would therefore have been available for calcite nucleation.

AKSO		AKS4	
32/1	32/2	32/3	32/4
10	11	10	7
29	28	41	20
37	38	45	24
41	43	51	26
56	60	60	28
108	101	65	30
151	147	71	34

Table 7.1 - Increase in Sr^{2+} (ppm) from the level of seawater during experiments 32/1-4. The sediments used in experiments 32/2 and 32/4 were soaked in H_2O_2 prior to the experiment being conducted.

In contrast, no difference in the evolution of the pore fluid chemistry was observed during experiments run using sediment AKSO (see section 3.6.3). Any difference in the pCO_2 caused by a reduction in the level of organic matter caused by the H_2O_2 treatment did not apparently affect the dissolution of aragonite (see Sr^{2+} (ppm) data presented in Table 7.1). This however may be because the level of organic matter contained within the coated grains and peloids is considerably greater when compared to the level of surface organic matter and although the bulk of effervescence had stopped in the sample of sediment AKSO treated with H_2O_2 , CO_2 was still being released unlike the sample of shell fragments (AKS4), in which all reaction had

stopped.

In the case of the sample of sediment AKSO treated with H_2O_2 , fewer cement crystals were observed in the partially lithified sediment (see Plate 3.15 C and D). The pore fluids did not show any significant difference in the degree of aragonite dissolution (see Fig. 3.24 a and b) and hence this may support the hypothesis that organic matter does act as a nucleation site for $CaCO_3$. The occurrence of $CaCO_3$ in association with organic matter certainly suggests this. The cement crystals which were precipitated in the experiment run with the sample of sediment AKSO treated with H_2O_2 , were much more equant in morphology (see Plate 3.15 C and D) than in the untreated sample where the nucleation rate was apparently higher (see Plate 3.15 A and B).

7.5 GEOLOGICAL SIGNIFICANCE

The results of the experimental study are very complex and many factors have been found to interact at the same time. However, the natural carbonate system is equally if not more complex in many aspects. Although the conditions in the experimental cells were far from those of the natural environment, a striking similarity between the diagenetic fabrics that have been experimentally produced and those generated in nature is observed.

In the case of the experimentally generated cement fabrics, it is believed that the nucleation rate is one of the factors which controls the overall cement fabric which is developed. Granular-bladed cement fabrics were developed where the nucleation rates were relatively high and equant cement fabrics where the nucleation rate was relatively low. The chemical factors which have been shown to affect this are the Mg^{2+} concentration of the pore fluids and the supply of ions for nucleation and continued growth supplied by aragonite dissolution.

The effect of Mg^{2+} in inhibiting calcite precipitation in the marine environment has been well documented and in this experimental study, higher Mg^{2+} concentrations have been found to decrease the rate of calcite nucleation. The mMg^{2+}/mCa^{2+} ratio however does not control the morphology of calcite crystals in the manner suggested by Folk (1974).

In the freshwater environment, the precipitation of calcite cement also depends on the dissolution of aragonite. It may therefore be more relevant to compare the results of the experimental diagenesis to this regime. The fabrics which were produced were certainly very reminiscent of those found in the freshwater diagenetic environment.

Halley and Harris (1979) made a study of a 1000 year old

oolite on Joulters Cays, Bahamas which was undergoing cementation in a freshwater lens which was divided by a water table into vadose and phreatic environments. Most aragonite dissolution and cementation by calcite (3-6 mole % MgCO_3) occurred above the water table. The rate of calcite precipitation was directly related to the rate of aragonite dissolution and cementation decreased with depth accompanying a decrease in the degree of aragonite dissolution. The meniscus cement developed where the pore fluids were held between sediment grains by capillary action (Dunham, 1971) which Halley and Harris (1979) observed in the vadose zone, cannot be simulated in the fully saturated conditions of the cell. The fabrics which were generated in the phreatic environment however are almost identical to those produced in the experimental cells where the nucleation rate was low. The cement crystals described by Halley and Harris (1979) formed discontinuous fringes around grain edges, similar to those observed in the equant experimental fabrics. The cement morphology was therefore related to the supply of ions through aragonite dissolution, similar to one of the processes which operated during the experiments.

Halley and Harris (1979) also found that certain grain types in the sediment of the phreatic zone "were better suited for calcite nucleation and precipitation than ooids". Peloids (see Fig. 8B p.976) were found to display isopachous cement

fringes of "more bladed" calcite crystals while neighbouring ooids showed discontinuous fringes of "rhombohedral"(equant) calcite crystals. This has also been found in the experimentally generated fabrics and it has been suggested here that the difference in nucleation rate may, in part, be related to the role of organic matter.

Given and Wilkinson (1985) however have suggested that the overall controlling factor on calcite morphology is the CO_3^{2-} concentration of the pore fluids. In the microenvironment displayed in Fig. 8B of Halley and Harris (1979) where equant and bladed fabrics are separated by a pore space of microns, it is difficult to envisage a CO_3^{2-} concentration gradient control on crystal morphology. The importance of CO_3^{2-} concentration control has been well argued by Lahann (1978) and Given and Wilkinson (1985) and certainly most examples of calcite cement crystal morphologies fit the scheme that Given and Wilkinson (1985) presented in their paper. However, the paper still fails to explain all of the differences in calcite cement morphology observed in nature such as those shown in Fig. 8B of Halley and Harris (1979). It is therefore suggested that no one controlling factor will dominate in all circumstances due to the complexities of the carbonate system. In this experimental study, it would appear that a lower nucleation rate has resulted in isolated crystals, the nuclei of which, unlike those of the granular-bladed fabric, would have had room in which to grow

(e.g. see Plate 3.14 A and D). It may therefore be that the nucleation and not only the growth history of calcite cement crystals will be of importance in determining their resultant morphology. Largely unconsidered factors such as the role of organic matter in nucleation may be of significant importance.

CHAPTER 8 - CONTROLS ON THE COMPOSITION OF THE CEMENTING PHASE

8.1 INTRODUCTION

Most of the cement which has been precipitated is calcitic with varying MgCO_3 content. In most cases, this calcite contains less than 10 mole % MgCO_3 . Phases containing higher levels of MgCO_3 , up to a maximum of 84 mole %, have been observed. The question therefore arises as to whether these are highly disordered calcites or members of a solid-solution series between dolomite and magnesite. Significant amounts of SrCO_3 and SO_4^{2-} are also contained within all cement phases. It must be noted however that because of the high temperature and pressures used in the experiments and the rapid rate of growth of the crystals, the composition of all cementing phases is highly unnatural.

8.2 PHASES CONTAINING SIGNIFICANT AMOUNTS OF MgCO_3

A major question arises as to whether the cement phases precipitated form part of a mineralogical solid-solution of calcite - proto-dolomite - dolomite - Ca-rich magnesite or whether the cement is composed of a highly disordered calcite which can contain varying levels of MgCO_3 . Table

8.1 summarises the compositional range in terms of MgCO_3 that has been observed in each group of experiments based on sediment type. It can be seen from those data that a range of MgCO_3 (mole %) values from 1-84 with no significant breaks occurs.

Sediment Type	Reference Figure	Mole % MgCO_3
BSO	3.4	< 10 ; 18-32
ADDO	3.6	< 8
ADBO	3.8	< 12; one crystal group with maximum 84 (Fig. 4.1)
AKSO	3.10	< 10
AKDO	3.12	< 8
SBO	3.14	< 7
ADDO	4.1	< 12
ADBO	4.1	< 8
BSO (Aborted Expts.)	4.1	18-77
BSO	4.4	14-25

Table 8.1 - Range of MgCO_3 (mole %) contents of cement precipitated during experiments using each sediment type.

8.2.1 Cement Containing More Than 50 mole % MgCO_3

Cement containing more than 50 mole % MgCO_3 has only been found in the partially lithified sediment of three experiments 1785, 3586 and 3886. The highest level of MgCO_3

(approximately 84 mole %) was found as the cores of three cement crystals in the partially lithified sediment of experiment 1785 (see Plate 4.5 C and D). Other Mg-rich crystals were found in the partially lithified sediments of experiments 3586 (70 and 77 mole % MgCO_3) and 3886 (53 - 72 mole % MgCO_3) both of which had to be aborted during the first 5 days. All of these occurrences as very small crystals suggest that this enriched phase precipitated during the early stages of the experiments.

8.2.2 Cement Containing 30-50 mole % MgCO_3 .

Cement containing 30-50 mole % MgCO_3 is slightly more common than that containing more than 50 mole % but is still unusual. The occurrences of such crystals are summarised in Table 8.2.

Expt.No.	MgCO_3 (mole %)	Sediment	No. of Analyses	Fig.No
*32/4	35	AKS4	1	3.25
*34/3	30.5	BSO	1	3.4
*3586	30-35	BSO	2	4.1
3886	47-48	BSO	2	4.1

Table 8.2 - Details of the occurrences of intermediate Mg-rich phases. * indicates the presence of cement phases containing less than 30 mole% MgCO_3 .

Crystals containing 30-50 mole % MgCO_3 have usually only been found as very small crystals (maximum 3 μm in diameter, see Plate 4.5 A and B). In the group of cement crystals with the Mg-rich cores described from the partially lithified sediment of experiment 1785 (see Plate 4.5 D) an intermediate phase lies between the Mg-rich core and the outer low-Mg phase. The precipitation of such intermediate phases must therefore occur during the early stages of the experiments but after the precipitation of the very Mg-rich phase (over 50 mole % MgCO_3).

8.2.3 Cement Containing Less Than 30 mole % MgCO_3 .

This is by far the most common phase to be found as a cement. Table 8.1 shows that most cement contains less than 10-12 mole % MgCO_3 but a small amount which occurs as small crystals in less well developed cement fringes contains 12-30 mole % MgCO_3 . For example, a significant proportion of the cement crystals in the partially lithified sediment of experiment 34/3 using sediment BSO, contained between 18 and 30 mole % MgCO_3 while the cement of other experiments using sediment BSO contained less than 7 mole % MgCO_3 (see Fig. 3.14).

8.2.4 Mineralogy of the Cementing Phase

XRD analysis of the sediments before and after the

experiments has shown that the bulk of the cement is composed of low and high-Mg calcite (see Appendix V). Problems arise however when considering the mineralogy of the Mg-rich phases (over 30 mole % MgCO_3).

Ideal dolomite is a 1/1 cation ordered carbonate where the Mg^{2+} and Ca^{2+} ions are arranged in separate layers (Bathurst 1975, p.238). Graf and Goldsmith (1956, p.184) reported that at high temperatures (above 200-300 °C) ordered dolomites were precipitated. In experiments conducted at lower temperatures the precipitated material was Ca-rich and did not show order-reflections but did have a high degree of structural arrangement. This they defined as proto-dolomite. Gaines (1977, p.543) defined proto-dolomite as a "metastable single-phase rhombohedral carbonate.....which is imperfectly ordered but which possesses a high degree of cation-order as evidenced by the unambiguous presence of order reflections in diffraction patterns."

Carbonates with the composition $\text{Ca}_{50}\text{Mg}_{50}$ are known which are not dolomites, despite their chemical composition (Glover and Sippel, 1967). Gaines (1977, p.543-544) also suggested that "in view of the ease of formation of metastable solid-solution in the rhombohedral carbonate system (Goldsmith 1967) and of the known kinetic difficulties involved in the formation of dolomite, it seems likely that

other materials of dolomitic composition are also cation-disordered solid-solutions".

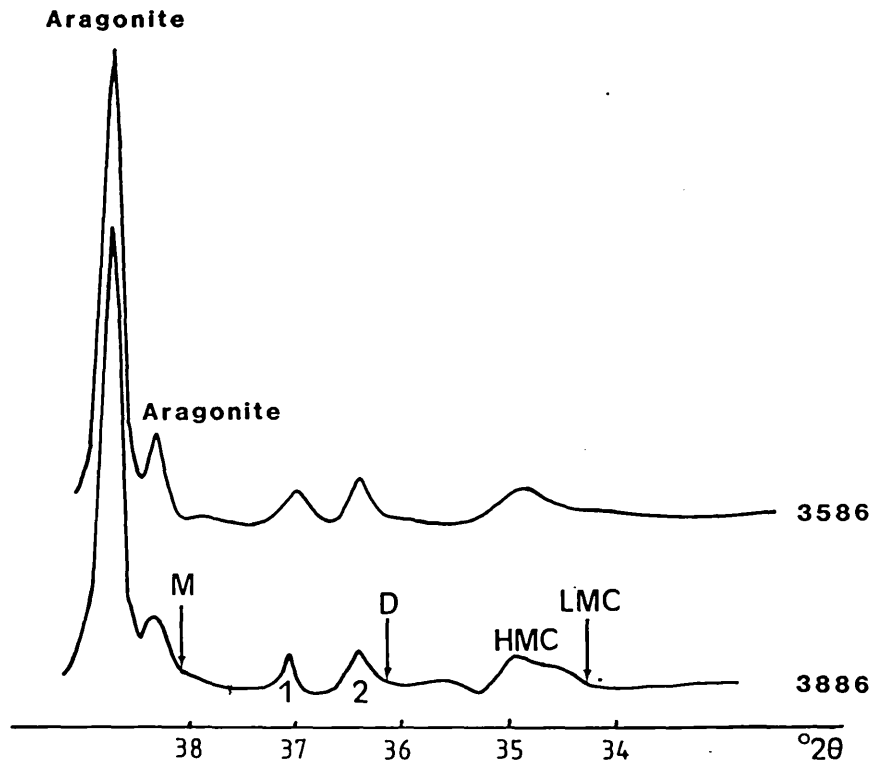


Fig. 8.1 - X-ray diffraction (XRD) traces for the sediments collected at the end of experiments 3586 and 3886. The positions of the main low-Mg calcite (LMC), dolomite (D) and magnesite (M) peaks have been superimposed. HMC - high-Mg calcite.

One problem encountered when identifying the mineralogical composition of the Mg-rich cement phases, is that very little is present when compared to the bulk sediment. XRD traces of the partially lithified sediments of experiments 3586 and 3886 are shown in Fig. 8.1. The positions of the main reflection peaks for low-Mg calcite (LMC), dolomite (D) and magnesite (M) have been marked on those traces. A broad

peak is observed to the left of the position of the LMC peak. This can be identified as high-Mg calcite (Goldsmith et. al., 1955). Two small peaks also occur between the position of the magnesite and dolomite peaks (1 and 2) which may represent Mg-rich dolomite and Ca-rich magnesite compositional phases respectively. This would correlate with some of the compositions observed in the microprobe analyses (see Fig 4.1) but the apparent absence of order-reflections for dolomite may suggest that they are highly disordered calcite phases, containing significant amounts of MgCO_3 as suggested by Gaines (1977, p.543-544). Without larger amounts of the phase so that detailed XRD analyses could be performed, it is difficult to make any valid conclusions about the mineralogical structure of such phases.

When these Mg-rich phases (i.e. around 30 mole % MgCO_3 upwards) were analysed using the microprobe, a considerable amount of difficulty was encountered in obtaining consistent oxide totals. Most analyses in the region of 50 mole % MgCO_3 (see experiment 3886), showed totals around 52.28 %, the 'ideal' oxide total calculated by Schofield and Adams (1986), while analyses in the region 70-85 mole % MgCO_3 showed totals of around 51-49 %. This would be expected bearing in mind the increased level of Mg^{2+} . However, on a few occasions, very low oxide totals were obtained for no apparent reason e.g. in the crystals precipitated during

experiment 3586, one analysis showed 29.93 mole % MgCO_3 but had an oxide total of 43.97 %. This may suggest that, in some cases, a brucite ($\text{Mg}(\text{OH})_2$) phase may have been present in the lattice, H_2O being driven off along with CO_2 , further reducing the oxide total or that simply fluid inclusions were present in the rapidly formed crystals.

All cement crystals contain significant amounts of SrCO_3 and SO_4^{2-} (see sections 8.3.2 and 8.3.4). These will cause further distortions of the lattices. It may therefore seem likely that cement phases may be composed of a highly disordered calcite.

8.3 CONTROLS ON THE MgCO_3 , SrCO_3 and SO_4^{2-} CONTENTS OF THE CEMENT PHASE.

8.3.1 Factors Affecting the MgCO_3 Content

Mucci and Morse (1983) in precipitating calcite overgrowths on calcite seeds at 25°C from synthetic and natural seawater (ibid. p.85) with $\text{mMg}^{2+}/\text{mCa}^{2+}$ ratios less than or equal to 5.1, found that the precipitated calcite contained between 5 and 9 mole % MgCO_3 . This is comparable to the bulk of the calcite precipitated as cement in this study. They also studied precipitation from fluids with $\text{mMg}^{2+}/\text{mCa}^{2+}$ ratios greater than 5.1 and found that below a ratio of 7.5, there

was a positive relationship between the MgCO_3 content of the cement and the $\text{mMg}^{2+}/\text{mCa}^{2+}$ ratio of the fluid. They found however, that it was the composition of the surface adsorbed layers which were controlled by the solution composition and that it was these which controlled the composition of the overgrowth. This however may not be applicable to this study as most of the cement precipitation occurs on aragonitic grains rather than on calcite seeds.

In contrast, Lahann and Siebert (1982) suggested that the $\text{mMg}^{2+}/\text{mCa}^{2+}$ ratio of the pore fluids did not affect the MgCO_3 content of the calcite which was precipitated. They suggested that the main factors which influenced the distribution coefficient of Mg^{2+} in calcite were:

(i) the temperature and

(ii) the ratio of the solubility product constant for calcite to the activity product for magnesite and calcite (ibid., p.2229).

Thorstenson and Plummer (1977) suggested that the magnesium content of high-Mg calcite precipitated from natural waters should be governed primarily by the activity product of Ca^{2+} and CO_3^{2-} only.

Mackenzie et al. (1983) have suggested that the MgCO_3 content in the solid is related to the CO_3^{2-} concentration of the pore fluids. This relationship they suggest, is favoured both thermodynamically and kinetically. Given and

Wilkinson (1985) have also found that a high CO_3^{2-} favours the precipitation of high-Mg calcite of a higher MgCO_3 content.

If the data for the pore fluids and cement phases are considered, then it can be seen that a trend of decreasing mole % MgCO_3 in the cement accompanies a decrease in the $\text{mMg}^{2+}/\text{mCa}^{2+}$ ratio of the pore fluids during the experiments (e.g. see Tables 3.7 and 3.8 and Plate 4.5 C and D).

However, bearing in mind the analytical error, a plot of the mean daily $\text{mMg}^{2+}/\text{mCa}^{2+}$ ratio of the pore fluids against the average MgCO_3 content (mole %) of the precipitated cement phases suggests that no direct correlation exists between the bulk composition of the cement at the end of the experiment and the average composition of the pore fluids during the experiment (see Fig. 8.2). If any general trend does exist, then it appears that there is an exponential trend of increasing MgCO_3 content with decreasing average $\text{mMg}^{2+}/\text{mCa}^{2+}$ pore fluid ratios. Data from the standard experiments using all the sediment types (i.e. those reported in section 3.5.2) have been used.

If the occurrences of the very Mg-rich phases are considered then they are found to have precipitated during the early stages of the experiments while the pore fluid $\text{mMg}^{2+}/\text{mCa}^{2+}$ ratios were high. Fyfe and Bishoff (1965, p.11) found that Mg^{2+} was removed from solution by the precipitation of MgCO_3 enriched nuclei during the early, slow stages of

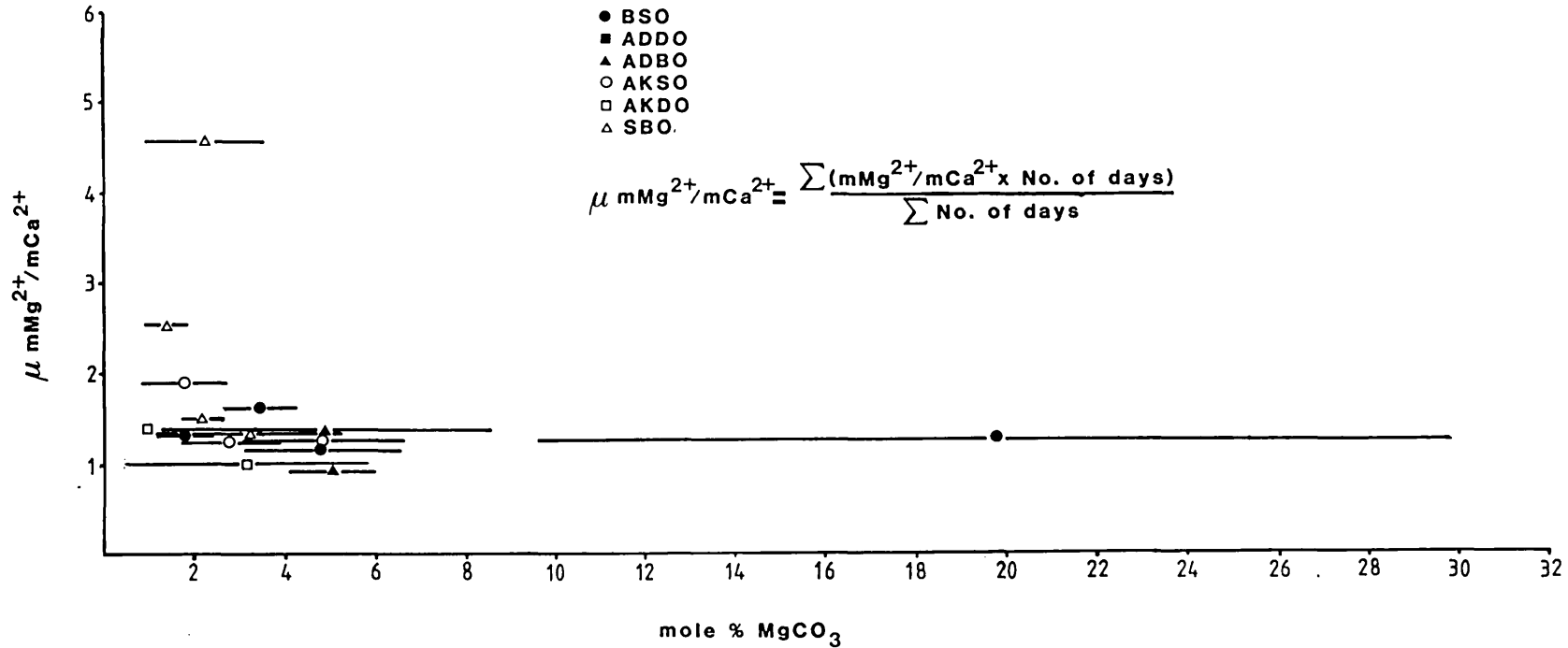


Fig. 8.2 - Plot of average MgCO_3 content of cement crystals precipitated during experiments using each sediment type against daily mean $\text{mMg}^{2+}/\text{mCa}^{2+}$ pore fluid ratio. Standard deviation on mean MgCO_3 content shown by bars.

aragonite-calcite transformations, until the Mg^{2+} concentration in the pore fluid was reduced to a level where inhibition of calcite formation by Mg^{2+} stopped. The reactions could then proceed at a faster rate. Bruni and Wenk (1985, p.1168) suggested that this early incorporation of Mg^{2+} into calcite nuclei would produce a very disordered crystal with calcium and magnesium randomly distributed in cation sites.

This mechanism of removal of Mg^{2+} into highly disordered calcite nuclei can explain the occurrences of the Mg-rich crystals that are observed and the early depletion of most of the Mg^{2+} in the pore fluids would support this (Mg^{2+} drops from 1260 ppm to less than 200 ppm in the first two to three weeks of the experiment, depending on the experiment (see Appendix I)). Further, Baker and Kastner (1981) observed experimentally that at 200 °C using seawater, the calcite-dolomite (ordered and proto-dolomite) phase boundary occurred at a $\text{mMg}^{2+}/\text{mCa}^{2+}$ ratio of between 0.57 and 1.06 and the dolomite - magnesite boundary between 2.11 and 3.41. If these boundaries are superimposed onto the pore fluid evolution curves presented in section 3.5.2 (see Fig. 8.3 (a)-(e)) then it can be seen that the pore fluids of each experiment passed through the stability fields of magnesite and dolomite before reaching the stability field of calcite. Precipitation of Mg-rich phases might therefore occur when the pore fluids are in these stability fields. If this

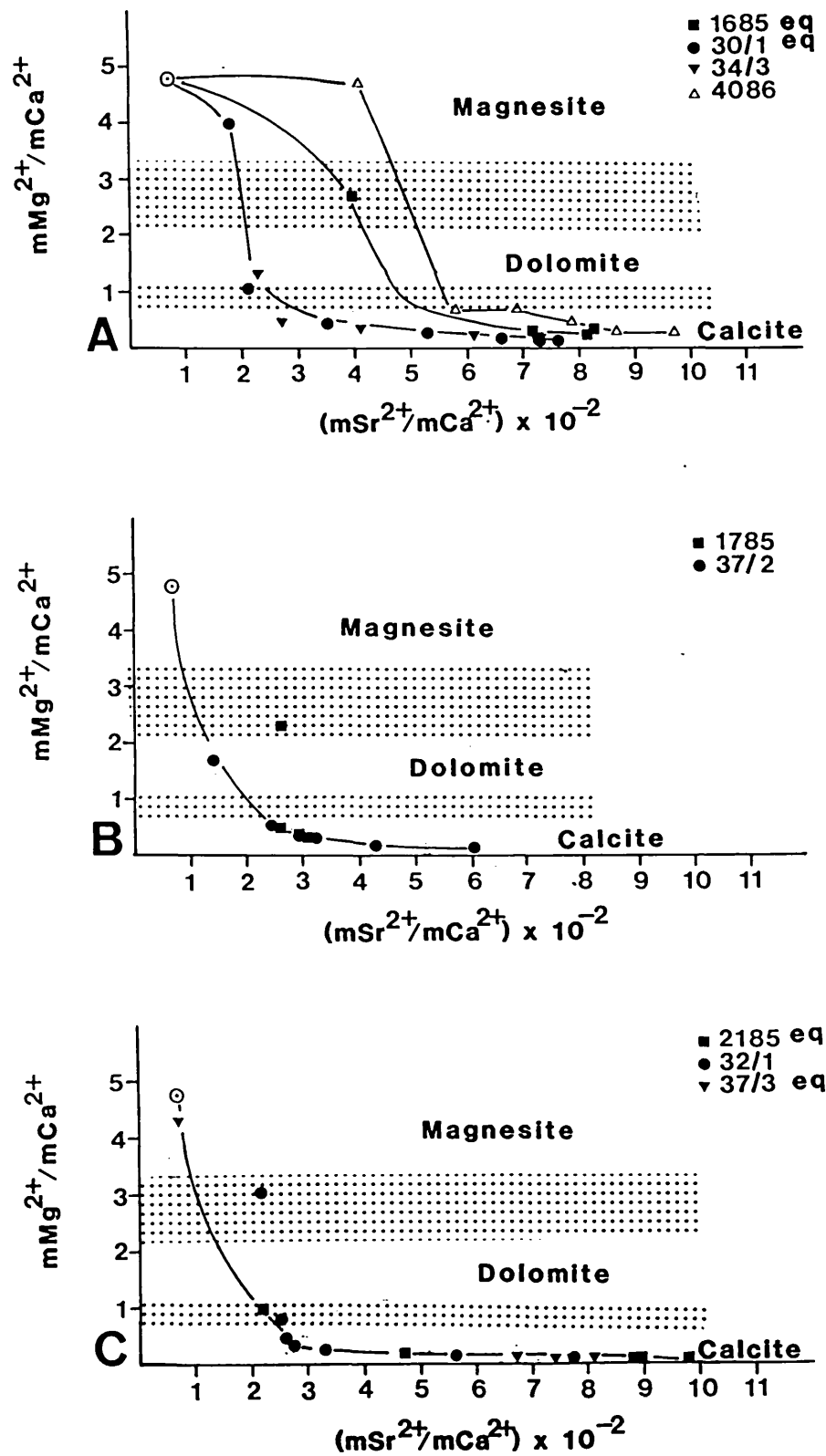


Fig. 8.3 - Evolution of the pore fluids from the composition of seawater (⊙) during experiments using (A) sediment BSO, (B) ADBO and (C) AKSO. Baker and Kastner's (1981) stability fields for Magnesite, Dolomite and Calcite have been superimposed.

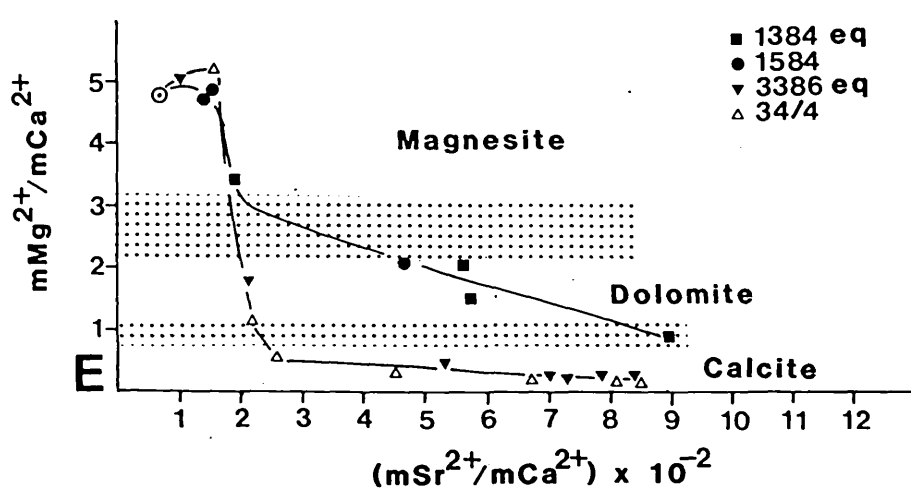
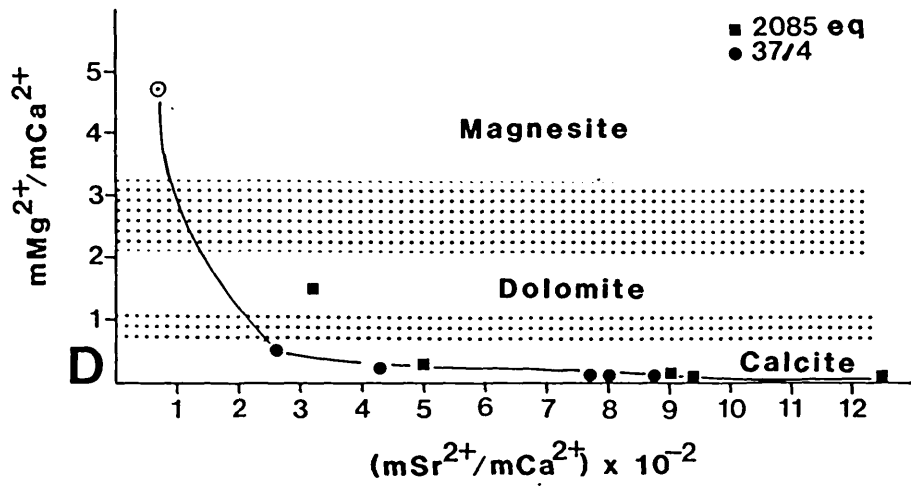


Fig. 8.3 - Evolution of pore fluids from the composition of seawater (⊙) during experiments using (D) sediment AKDO and (E) Shark Bay Ooids. Baker and Kastner's (1981) stability fields for Magnesite, Dolomite and Calcite have been superimposed.

hypothesis is accepted, the main problem is why, if it is possible to precipitate Mg-rich phases at the beginning of the experiments, have they been found in so few. Also, why has no trace of any Mg-rich phase been observed in the partially lithified sediments of experiments 1384 and 1584, when the pore fluids were never outside the stability fields of dolomite and magnesite (ibid.). The maximum level of MgCO_3 in the precipitated calcites of experiments 1384 and 1584 was 6.8 mole %.

One possible explanation is that Mg-rich phases were precipitated at the beginning of the experiments but underwent dissolution once the $\text{mMg}^{2+}/\text{mCa}^{2+}$ ratio began to drop. Some support for this can be found in Plate 4.5 C and D where the Mg-rich phase of the crystal group observed in the partially lithified sediment of experiment 1785 was found to be undergoing dissolution. Mackenzie et al. (1983) have reported that in calcite containing up to 30 mole % MgCO_3 , increasing instability accompanies increasing MgCO_3 contents. If the cement phase is a disordered calcite then incorporation of more than 30 mole% MgCO_3 could only decrease the stability further.

In the case of dolomite, Stossell et al. (1987) synthesised dedolomitisation reactions in laboratory experiments using chloride-rich brines containing 2m Na^+ and 0.5m Ca^{2+} . These were conducted over a period of seven weeks at 100, 150 and

200 °C. Between 100 and 200 °C, the mode of calcite replacement of the dissolving dolomite changed from crystal growth into void space to pseudomorphic replacement at 200 °C. They found that in all types of replacement, significant amounts of the dolomite remained. Although dolomite will be much more stable than a highly disordered calcite, the full scale removal of all crystals precipitated during these experiments by dissolution or neomorphic replacement with no trace of the original phase seems unlikely. Also, the $m\text{Mg}^{2+}/m\text{Ca}^{2+}$ ratio would increase through the dissolution of the Mg-rich phases although the effect of this would be masked through increased levels of Ca^{2+} in the pore fluids due to the dissolution of aragonite.

Another possible explanation is that enriched nuclei were precipitated during the early stages of all experiments but that diffusion of Mg^{2+} occurred within the structure of the growing crystal. This could be easily accomplished if the crystals were highly disordered calcites and is also much more likely at 200 °C than 25 °C. Loomis (1983, p.5), in a discussion of compositional zoning of crystals during metamorphism, suggested that diffusion would eliminate growth zoning which had occurred as a consequence of fractionation processes. Thus, many common minerals such as the micas, chlorite, amphiboles and alkali feldspars are usually unzoned because of homogenisation due to diffusion during crystal growth or afterwards rather than because

fractionation could not occur. Support for diffusion comes from the analyses of the equant crystals precipitated during experiments 2585 and 2685 (see Fig. 4.1). These experiments, using sediment ADBO, ran for 15 and 21 days respectively. More cement was precipitated in the longer experiment (2685) and an overall drop in the level of MgCO_3 (mole %) was observed in that cement (see section 4.2). If all of the Mg^{2+} that was available in the pore fluids was incorporated into the initial nuclei as suggested by Fyfe and Bishoff (1965), a factor which is supported by the early decrease in Mg^{2+} in pore fluids, then diffusion could redistribute Mg through later overgrowths of calcite on the early crystals. The overall composition of the bulk cement crystals in terms of the MgCO_3 content would be relatively lowered. This mechanism for redistributing Mg^{2+} from the core of the crystal outwards may also account for the higher MgCO_3 level observed in the narrow cement fringe precipitated during experiment 34/3 using sediment BSO when compared to the levels in wider cement fringes generated using sediment BSO. Where analyses have been made through cement crystals from core to margin (see Table 3.7 and 3.8) a maximum decrease of 3 mole % MgCO_3 is observed. This may be a remnant signature of a previously much greater variation.

8.3.2 Effect of SO_4^{2-} on Dolomite Precipitation

Baker and Kastner (1981) found that SO_4^{2-} inhibited the precipitation of dolomite from seawater. The Mg-rich crystal cores found in association with the anhydrite lath in the partially lithified sediment of experiment 1785 (see Plate 4.5 C and D) may suggest that these crystals precipitated in response to the removal of SO_4^{2-} via the precipitation of the CaSO_4 . The problem is complicated by the fact that precipitation of CaSO_4 would also increase the $\text{mMg}^{2+}/\text{mCa}^{2+}$ ratio in that particular microenvironment by the removal of Ca^{2+} . The Mg-rich phases could therefore have been precipitated in direct response to this relative enrichment in Mg^{2+} in the pore fluids by the mechanism suggested by Fyfe and Bishoff (1965) i.e. by the precipitation of Mg-rich crystals. Further investigation of the effect of SO_4^{2-} was considered necessary and an experiment was run using SO_4^{2-} -reduced seawater (see section 5.2 for results).

Although the initial $\text{mMg}^{2+}/\text{mCa}^{2+}$ ratio of the pore fluids was 4.8, it dropped to below 1 within the first 5 days of the experiment due to the increased rate of aragonite dissolution. The pore fluids were quickly modified by aragonite dissolution and calcite precipitation so that their composition was no longer in Baker and Kastner's (1981) stability field for dolomite. It is therefore not surprising that no dolomite was found in the partially lithified sediment of that experiment.

8.3.3 Summary

The identification of the controls on the level of MgCO_3 found in the cement phase is fraught with difficulties. The most likely explanation of the variations in composition that are observed in the partially lithified sediments is that a Mg-rich carbonate phase was precipitated during the early stages, removing most of the available Mg^{2+} from the pore fluids. The mineralogy of these crystals is not definitely known but it is suspected that they may be a highly disordered calcite. Later, as the dissolution of aragonite proceeded, growth of much lower Mg-calcite occurred on these crystals cores. This may support the hypothesis that early crystals were of a calcitic structure rather than dolomite or magnesite, as Fyfe and Bishoff (1965, p.12) suggested that ordered dolomite in the aragonite-calcite transformation would be effectively "removed from the battle". At 183-200°C, in order to attain some sort of equilibrium with the rapidly changing pore fluids, diffusion of Mg^{2+} outwards through the crystal from the Mg-rich cores could destroy any original zoning in the crystal. This would leave at most, a remnant signature of enrichment in Mg at the centre of crystals when compared to the outer edges. The relative enrichment in MgCO_3 of narrow cement fringes as opposed to wider fringes (e.g. that of 34/3 compared to other cement fringes generated using sediment BSO, see Fig.

3.4) could be explained in this way.

8.3.4 Factors Affecting the SrCO₃ Content

Significant concentrations of Sr²⁺ and SO₄²⁻ (see section 8.3.5) are present in the lattices of the cementing phases. To check whether the Sr²⁺ and SO₄²⁻ were present as SrSO₄, foils of the cement crystals that were generated during experiment 2985 (average contents of SrCO₃ and SO₄²⁻ were 0.79 and 1.14 mole % respectively) were made and studied using a transmission electron microscope (TEM). No evidence for a separate SrSO₄ phase was found although the crystal lattices were found to be highly strained. Intense strain in synthetically precipitated calcite has also been reported by Angus et al. (1979). No relationship is observed between the mole % of SrCO₃ and SO₄²⁻ that are contained within the cement. For example, experiments run using sediment SBO contain high levels of SO₄²⁻ and SrCO₃ while experiments run using sediment ADBO also contain high levels of SO₄²⁻ but much lower levels of SrCO₃ (see Table 3.9). Reeder (1983) reports that extensive solid solution of SrCO₃ in calcite occurs at elevated temperature and significant levels of SO₄²⁻ have been found in experimentally precipitated calcites by Busenberg and Plummer (1985). There is therefore a considerable amount of evidence which suggests that SrCO₃ and SO₄²⁻ are not present as a separate SrSO₄ phase in the

structure of the cementing crystals.

If the data for the pore fluids and cement phases are considered in the same way as for the Mg^{2+} data (see section 8.3.1), again bearing in mind the analytical error, then it can be seen that no clear relationship exists between the daily mean mSr^{2+}/mCa^{2+} ratio and the average $SrCO_3$ (mole %) content of the cement crystals (using the data in section 3.5.2 - see Fig. 8.4). However, apart from two of the experiments using sediment SBO, there is a general trend of increasing $SrCO_3$ with an increasing mean daily mSr^{2+}/mCa^{2+} pore fluid ratio.

Also bearing in mind the analytical error, in each set of experiments using sediments ADBO, AKSO and SKDO (see Table 8.3), there is some evidence to suggest that there is a positive correlation between the mean level of $SrCO_3$ (mole %) in the cement and the temperature at which the experiment was conducted. No significant correlation is observed in experiments using sediments BSO and SBO. All experiments however were conducted over the restricted temperature range of 183-200 °C. This temperature difference may not be sufficient for any significant differences in the average $SrCO_3$ levels to be observed in the data.

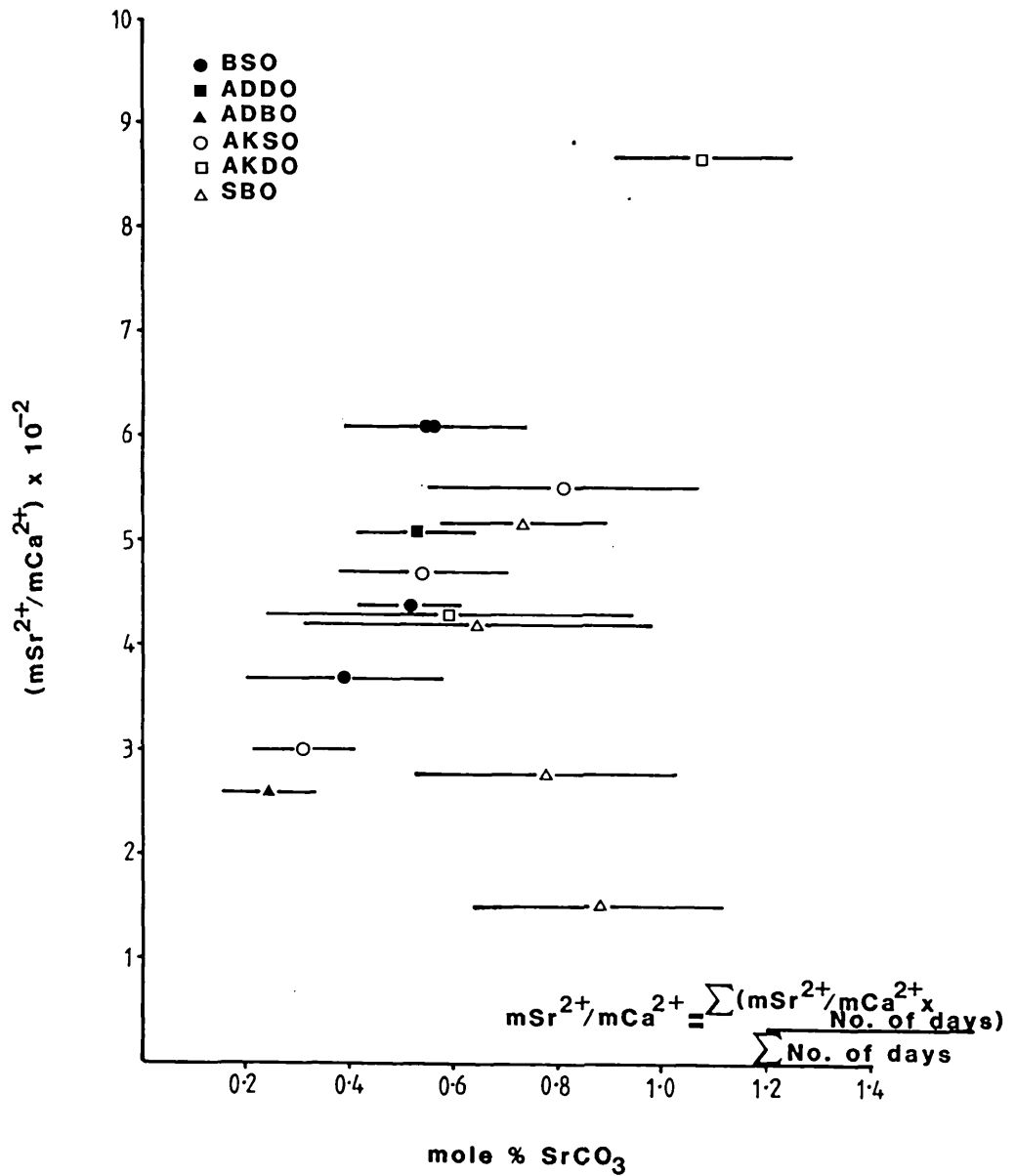


Fig. 8.4 - Plot of average $SrCO_3$ content of cement crystals precipitated during experiments using each sediment type against daily mean mSr^{2+}/mCa^{2+} pore fluid ratio. Standard deviation on mean $SrCO_3$ content shown by bars.

Temp. (°C)	BSO	ADBO	AKSO	AKDO	SBO
183	0.51 (30/1) 0.39 (34/3)	0.23 (37/2)	0.31 (32/1) 0.54 (37/2)	0.59 (37/4)	0.64 (34/4)
186	0.55 (1685)	0.44 (1785)	0.81 (2185)	1.08 (2085)	0.78 (1384) 0.88 (1584) 0.73 (3385)
200	0.55 (4086)	N/D	N/D	N/D	N/D

Table 8.3 - SrCO₃ content (mole %) of cement crystals precipitated at different temperatures using the same starting sediments.

Two ways of calculating the distribution coefficient (K) of an ion in a crystal exist.

(i) By assuming equilibrium crystallisation using both the pore fluid data and the crystal chemistry data. This is not of any use here because crystallisation does not occur at equilibrium, the system changing continuously.

(ii) By assuming non-equilibrium and using the pore fluid data only. Calculation of K_{Sr}^C by this method however is meaningless in this system as K_{Sr}^C would only reflect the final mSr^{2+}/mCa^{2+} ratio of the pore fluids, which is dependent on factors which affect the rate of aragonite dissolution (see section 9.3) and not just the relative uptake of Sr^{2+} and Ca^{2+} into the calcite from the pore fluids. It is therefore more relevant to study the levels of SrCO₃ observed in the calcite.

Studies of the distribution coefficient of Sr^{2+} in calcite (K_{Sr}^{C}) by Holland et. al. (1964), Kinsman (1969) and Kinsman and Holland (1969) suggest that K_{Sr}^{C} decreases with an increase in temperature which is the opposite of what is suggested by the data presented in Table 8.4. All of these earlier studies however studied K_{Sr}^{C} in calcite precipitated directly from saturated solutions at temperatures below 100°C . A more recent study by Stossell et. al. (1987) has found that at temperatures between $100\text{-}200^{\circ}\text{C}$, K_{Sr}^{C} increases with an increase in temperature.

Lorens (1981) found that K_{Sr}^{C} was also dependent on the crystal growth rate. In experiment 3186 (see section 5.2) using freshwater, diagenesis proceeded at a much faster rate than in any other experiment which would imply a greater growth rate for the calcite crystals. The cement crystals precipitated during this experiment contained the highest level of Sr^{2+} observed, up to a maximum of 1.6 mole %. Mucci and Morse (1983) however found that the incorporation of both MgCO_3 and SrCO_3 was independent of the precipitation rate. Again, there appears to be some confusion in the literature concerning the factors which control distribution coefficients.

8.3.5 Correlation Between MgCO_3 and SrCO_3

A negative correlation exists between the MgCO_3 and SrCO_3 content of the cementing phases paralleling the trend of decreasing $m\text{Mg}^{2+}/m\text{Ca}^{2+}$ and increasing $m\text{Sr}^{2+}/m\text{Ca}^{2+}$ pore fluid ratios observed with time. Mucci and Morse (1983) also found that there was a correlation between the level of MgCO_3 and SrCO_3 in their calcites but that it was positive rather than negative.

If the ionic radii of Mg^{2+} and Sr^{2+} are compared to that of Ca^{2+} , then it can be seen that Mg^{2+} has an ionic radius which is 33% smaller than Ca^{2+} while Sr^{2+} has an ionic radius which is 11.6 % larger than Ca^{2+} and 59% larger than Mg^{2+} .

Goldsmith et. al. (1961) found that incorporation of the smaller Mg^{2+} ion into the calcite lattice caused shortening of the c-axis dimension. This caused the CO_3^{2-} layers near the Mg^{2+} to be pulled closer together. The deformation would create a site above it where a cation larger than Ca^{2+} such as Sr^{2+} , could be easily accommodated which explains the apparent correlation observed by Mucci and Morse (1983). However, the calcite precipitated by Mucci and Morse (1983) contained much lower levels of SrCO_3 (<0.25 mole%) than those observed here. Incorporation of up to 1.6 mole % SrCO_3 in experiments using seawater, would cause significant distortion in the calcite lattice (coupled with the incorporation of SO_4^{2-}). Also, the experiments under

discussion here were conducted in a partially-closed system, where most of the available Mg^{2+} was removed during the early stages of the experiments and the mSr^{2+}/mCa^{2+} ratio increased continuously. The experiments of Mucci and Morse (1983) were conducted in an open system where Ca^{2+} , Mg^{2+} , Sr^{2+} and CO_3^{2-} were maintained at constant levels. Also their experiments (*ibid.*) were conducted at $25^{\circ}C$ rather than $183-200^{\circ}C$ and are therefore more applicable to the natural environment. Variation in the experimental conditions are likely to be responsible for the apparent differences in the behaviour of $MgCO_3$ and $SrCO_3$ observed.

8.3.6 SO_4^{2-} Content of Cement

(1) Level of SO_4^{2-}

Significant levels of sulphur were identified in the calcite using the JEOL 733 superprobe. Busenberg and Plummer (1985) have found significant amounts of SO_4^{2-} to be present in their experimentally precipitated calcite and it is believed that the sulphur is present as SO_4^{2-} in the cement phases under discussion here. Maximum levels of 2 mole % SO_4^{2-} were incorporated in cement crystals.

Busenberg and Plummer (1985) found that the amount of SO_4^{2-} which was incorporated into their precipitated calcite, was directly proportional to the rate of crystal growth i.e. the

faster the growth rate, the greater the incorporation of SO_4^{2-} . The rapid growth rates of these crystals would account for the incorporation of such high levels of SO_4^{2-} in the carbonate structure.

(2) Source of SO_4^{2-}

As noted in section 3.2, most of the SO_4^{2-} in the seawater is removed early in each experiment by the precipitation of anhydrite and magnesium oxysulphate. In Chapter 5, the results of experiments run using SO_4^{2-} -reduced seawater and freshwater were reported. Both fluids initially contained negligible amounts of SO_4^{2-} yet the cement precipitated in both cases contained appreciable amounts of SO_4^{2-} ranging from 0.55-1.55 and 0.1-0.75 mole % respectively. The source of the SO_4^{2-} must therefore be considered.

In modern carbonate grains, the highest concentration of SO_4^{2-} can be found in biogenic high-Mg calcite (mainly echinoderms, algae and certain corals) and in ooids (4160 ppm SO_4^{2-} , approximately 0.5 mole %). Other non-biogenic calcites and aragonites contain very low levels of SO_4^{2-} (less than 100 ppm) while biogenic aragonite typically contains less than 2000 ppm SO_4^{2-} (approximately 0.2 mole %). A full list of the data can be found in Busenberg and Plummer (1985).

During this study the cortices of coated grains have been found to contain less than 0.6 mole % SO_4^{2-} which is in close agreement with Busenberg and Plummer's data (ibid.). The bulk of the SO_4^{2-} which is found in the cement is likely to be sourced within the coated grains and many of the micritic peloids (up to 0.7 mole %). The level of SO_4^{2-} contained in the sediments is therefore significant and release of this SO_4^{2-} during the dissolution of the grains could account for the SO_4^{2-} which is found in the cement crystals.

8.5 GEOLOGICAL SIGNIFICANCE

It has to be recognised that the composition of the calcite cement which is precipitated is greatly affected by the high temperature and rapid rates of reaction during the experiments. As such, it is highly unnatural in terms of its SrCO_3 and SO_4^{2-} contents and, in some cases, its MgCO_3 content. It is therefore necessary to exercise great care before any attempt is made to draw parallels with the natural processes of mineral formation. The results of the experiments however emphasise the complexity of the processes controlling the composition of the calcite cements. This, together with the obvious differences in opinion in the literature concerning distribution coefficients, support the conclusion of Lahann and Siebert (1982) that distribution coefficients determined experimentally may only be relevant for the particular set

of experiments under which they are determined.

Another problem when considering the processes affecting the composition of calcite cement has been encountered recently by Reeder and Grams (1987). They have also shown that compositional sector zoning in natural calcite cements can account for differences of up to 95 % in Mg^{2+} and 50 % in Sr^{2+} between different faces which have grown at the same time. This requires that the distribution coefficients differed from face to face during the growth of single crystals and perhaps questions the use of bulk distribution coefficients when concerning calcite cements.

CHAPTER 9 - CREATION OF SECONDARY POROSITY AND FACTORS AFFECTING ARAGONITE DISSOLUTION

9.1 INTRODUCTION

The reactions that occur in the experimental cells proceed through a dissolution-reprecipitation process. At the experimental temperatures and pressures employed, the stable polymorph of CaCO_3 is calcite (see Fig. 9.1). The removal of aragonite has been in such a way as to create secondary porosity which is typical of the types observed in natural material. Oomoldic porosity has been created, the cortices of many coated grains being totally removed. Peloids have also been affected by dissolution usually resulting in microporosity but occasionally larger, vuggy pore spaces have been created. Shell fragments have not usually undergone dissolution to produce secondary porosity but where change has taken place, they have been replaced by neomorphic calcite (see section 10.3.1). In the few cases where they have undergone dissolution, the shell structure has been exploited (see Plate 3.7 B).

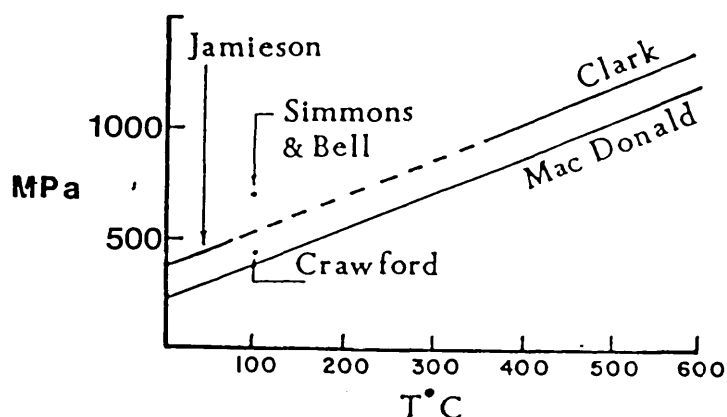


Fig. 9.1 - Data showing the aragonite-calcite equilibrium curve as a function of temperature and pressure. Aragonite is stable above the curve, calcite below (from Fyfe and Bishoff, 1965).

This chapter discusses both the factors which have affected the dissolution of aragonite and compares the fabrics that have been generated with those found in natural material.

9.2 OCCURRENCES OF SECONDARY POROSITY

9.2.1 Coated Grains - Oomoldic Porosity

Modern coated grains (including ooids) are composed of a nucleus with an outer cortex of varying size (see Scholle, 1978, p.vii). This cortex has been shown to be composed of two types of concentric laminae, one of aragonite set in an organic groundmass, the other purely organic (Shearman et al., 1970, p.564). Experimental generation of ooids by Suess and Futterer (1973) and Davies et al. (1978) showed that the organic matter lamellae were necessary for the formation of ooids. In their depositional environment,

coated grains are susceptible to micritisation due to the boring action of algae. The aragonite layers may therefore also alternate with layers or zones of micrite (Bathurst, 1975, p.298), similar to the micrite envelopes described by Bathurst (1966).

During the experiments, most of the secondary porosity was created in the cortices of coated grains (see Plates 3.8, 3.15 and 5.1). The form and size of the pore spaces that were created displayed a close relationship with the structure of the original cortex. Where a cortex was composed almost totally of tangentially arranged aragonite needles (see cortex marked (C) in Plate 9.1A), then a large pore space was developed (e.g. see Plates 3.4A, 3.7A, 3.8D and 3.15B). Where a lamellar structure of aragonite and micritic carbonate or organic matter was well developed (see the coated grain in Plate 9.1 B), then much finer scale lamellar porosity was created (e.g. see Plates 3.14A, 3.7A and 3.8B), again by aragonite dissolution.

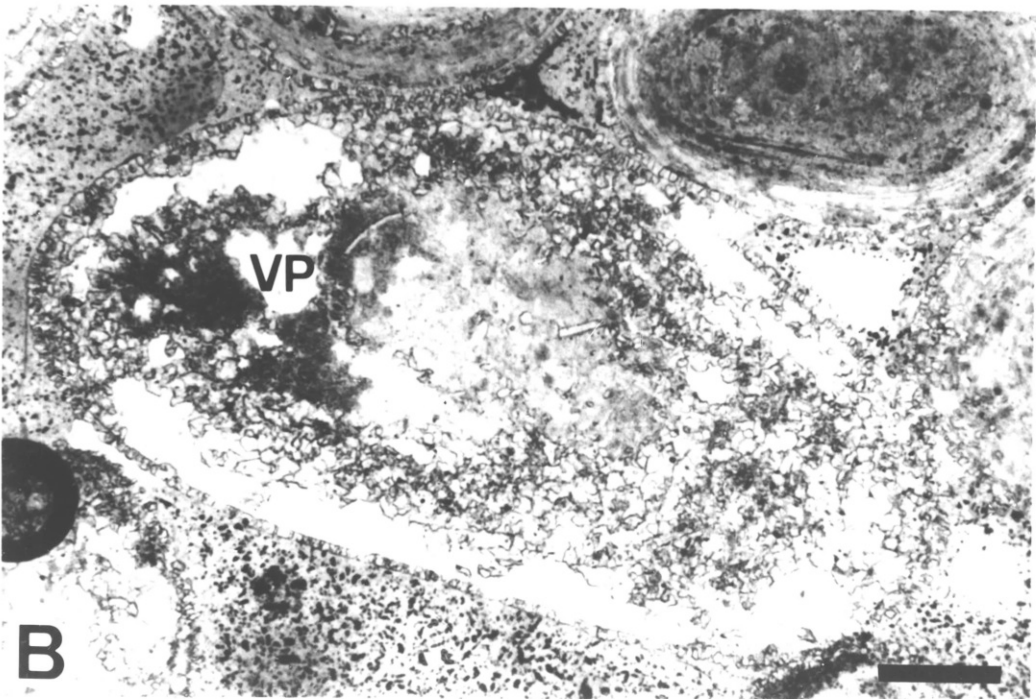
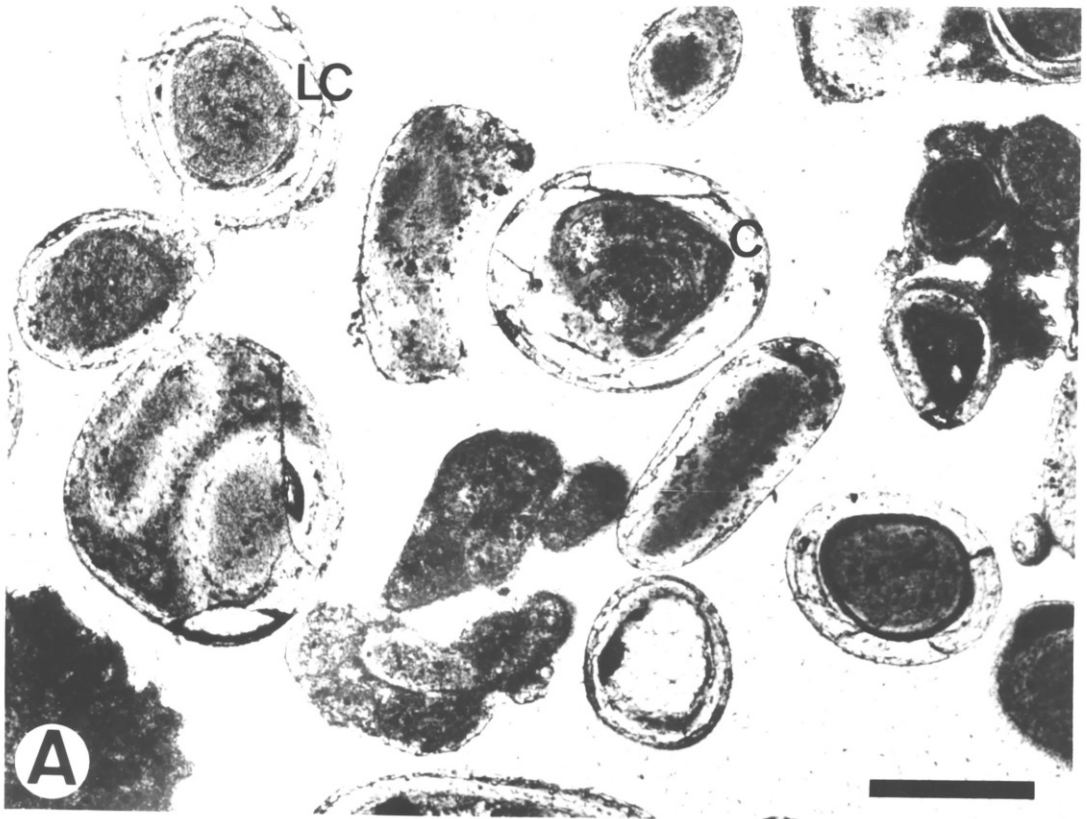
In another experimental study by Donath et al. (1980), in which oomoldic porosity was created by passing CO₂-charged fluids through a low-Mg calcite Mississippian oolitic limestone, similar fabrics to those generated during this study were observed (ibid. Fig. 5 C and E, p.1254 and Fig. 6 B-E, p.1256). Donath et al. (1980) compared this with the Great Oolite (Bathonian) and showed that, in nature, the

PLATE 9.1 - ORIGINAL AND SECONDARY POROSITY FABRICS

(A) Sediment ADDO - Many of the cortices of the unaltered coated grains show few signs of organic matter or micritic lamellae (C). The cortex is predominantly composed of aragonite. During dissolution, large pore spaces would be created. The cortex marked LC, shows more evidence of a lamellar structure but even this is limited. PPL. Scale bar 200 μm .

(B) Experiment 18/2 - Vuggy porosity has been created in micritic carbonate. The form of the secondary porosity at the edge of the grain may suggest that it had originally been a coated grain. The grain at the top right hand corner shows a relic lamellar structure in the cortex. Very dark lamellae are micritic and are separated by layers of lamellar secondary porosity. Areas also occur however, where several lamellae have been partially removed. PPL. Scale bar 100 μm .

PLATE 9.1



cortical layers are also preferred for the creation of oomoldic porosity while micritic nuclei have not been affected (ibid. Fig. 7A and D, p.1257). It should be noted that the processes described by Donath et. al. (1980) are occurring in calcitic limestones, the fabric selective porosity however is identical to that formed during the early diagenesis of aragonitic sediments.

Examples of naturally formed oomoldic porosity, similar to that created during the experiments reported here can be seen in the following papers:

- (i) Halley and Harris, 1979, Fig. 10A, p.978. Holocene.
- (ii) Picha, 1978, Fig. 10B, p.439. Pleistocene.
- (iii) Evans and Ginsburg, 1987 Fig. 11 A-C, p.316 where the sequence of porosity creation and infilling can be seen. Pleistocene.
- (iv) Cussey and Friedman, 1977, Fig. 10A, p.515. Jurassic.
- (v) Mazzulle, 1981, Fig. 13 E and F, p.862. Permian.

The last two examples are from petroleum reservoirs where the porosity was created prior to the emplacement of the hydrocarbons.

In these examples, the lamellae composed of aragonite appear to have been the first to be affected by dissolution. Layers of micritic carbonate appear to be unaffected.

9.2.2 Micritic Carbonate and Peloids

Micritic carbonate forms a large proportion of each type of sediment used in these experiments, in the form of uncoated and coated peloids, micritic layers in cortices and micritised areas in shell fragments. Where porosity has been created in this micritic carbonate, it takes the form of microporosity near grain edges (see Plates 3.7A, 3.8C, 3.10A and 3.9A and B) and a small amount of vuggy porosity (Plates 3.11D and 3.12B and 9.1B). Natural examples of microporosity can be found in Asquith (1986, Fig. 3 C and D, p.9, Mississippian Ste Genevieve Limestone) and Keith and Pittman (1983, Fig. 10 and 11, p.1397 and the discussion on p.1395, Lower Cretaceous Rodessa Limestone).

Much of the micritic carbonate in the experimental material, has either remained unaltered or has undergone neomorphism (see section 10.3.2). Chave and Suess (1967) concluded from their experiments that particles of calcite less than 0.1 μm in diameter were unstable in water and that an increase in solubility was to be expected between particle sizes of 0.1 μm and 0.01 μm . The Small Particle Solubility Effect (SPSE) which can be defined as the increase in solubility, due to the higher surface energy, that occurs with a decrease in particle size or a decrease in the radius of curvature of a particle has also been

discussed by Pantin (1965, p.453). Bathurst (1975, p.258) however suggests that the effect of particle size on solubility may be offset by the action of organic films on the particles. Reactions between suspended micritic carbonate and seawater were studied by Chave (1965) who remarked on the lack of reactivity despite attempts to hasten reaction in the laboratory by varying temperature and pH. Chave and Suess (1967) found that samples treated with H_2O_2 to remove organic matter, acquired a greatly enhanced reactivity. This observation led Bathurst (1975, p.258) to conclude that the micritic carbonate grains were enveloped in a coat of organic material which protected them from dissolution.

The development of microporosity in peloids or micritised grains during the experiments, is most commonly found near the edges of peloids where reaction between solid and pore fluid may occur with greatest ease. The preservation of peloids or micritic lamellae can be likened to the preservation of micrite envelopes (Bathurst 1966, p.15). In the diagenetic environment, neomorphic recrystallisation of the micrite envelope is favoured to the formation of a solution cavity.

9.2.3 Shell Fragments

During the course of the experiments, most of the shell

fragments in the sediments have not undergone any alteration (e.g. sections 3.6.1 and 3.6.3). Those skeletal fragments that have reacted have done so early in the experiments and have generally been found to undergo alteration by neomorphic processes (see section 4.2). In contrast to nature where most aragonite shell fragments are found to have undergone dissolution to form moldic porosity (see Longman, 1980 and Bathurst, 1966, Plate 2), only a few examples of shell fragment dissolution have been observed. Where they are found (e.g. see Plate 3.7 A and B) the structure of the shell fragment has been exploited. Extensive studies by Walter (1985) and Walter and Morse (1985) show that the microstructure of aragonite and high-Mg calcite skeletal grains is very important in determining the relative dissolution rates. This may account for the exploitation of the shell structure during the formation of secondary porosity.

9.2.4 Summary

Analogues of all of the forms of secondary porosity that have been created during the experiments can be found in natural material. The form of the secondary porosity appears to be dependent on the internal microstructure of the grain being dissolved and the relationship of the microstructure to any organic matter which may be present. The degree to which aragonite dissolution has occurred has

been found to vary. Factors which have affected this will be discussed in the following section.

9.3 FACTORS AFFECTING THE DISSOLUTION RATE OF ARAGONITE

During the experiments, different factors have been found to affect the dissolution rate of aragonite. These range from differences in the sediments like grain type and grain size, to differences in the experimental conditions like pore fluid composition and pressure.

9.3.1 Grain Type

The effect of grain type in controlling the rate of aragonite dissolution has already been discussed in section 9.2.3. Experiments were therefore conducted under the same experimental conditions using sediment samples composed of different proportions of coated grains, peloids and shell fragments. The results of these experiments are reported in section 3.6.1. Shell fragments were found to be less likely to suffer dissolution than coated grains or peloids hence the degree of reaction during the experiments was found to depend inversely on the proportion of shell fragments contained within the sediment sample. This is important when considering the relative rates of aragonite dissolution for the precipitation of cement crystals (see section

7.3.2). Sediments ADBO and SBO contained a higher proportion of shell fragments than the other sediments (see Appendix II). The dissolution rate would therefore have been lowered, affecting the rate of supply of ions for nucleation and growth of the cement crystals. Both were characterised by equant cement crystals. Picha (1978, p.440) also found that in naturally cemented oolitic ridges at Al-Khiran, Kuwait (area of collection of some of the sediments used in the experiments) that the skeletal grains were more resistant to leaching by meteoric waters than ooids i.e. the same sequence of stability as found in the experiments. As Walter noted (1985, p.3), the relative grain stability in sediments is also of importance when considering diagenesis in environments where the precipitation of calcite is dependent on the dissolution of aragonite e.g. in the freshwater environment.

9.3.2 Effect of Grain Size

A series of experiments was conducted, under similar experimental conditions, to study the effect that grain size had on the rate of reaction. One sediment type was taken (AKDO) and split into 4 size classes (> 0.42 mm; $0.35-0.42$ mm; $0.25-0.35$ mm; < 0.25 mm). A decrease in the grain size accompanied an increase in the external surface area. The results of these experiments are presented in section 3.6.2.

An increase in the rate of aragonite dissolution and calcite precipitation was found to accompany a decrease in the grain size. Kier (1980) and Walter and Morse (1984) have also found this to be the case. Kier (1980) found that the rate constant of dissolution for both calcite and aragonite shell fragments varied from sediment type to sediment type and that in many cases the rate constant of dissolution was inversely correlated to the grain size of the sediment sample. Walter and Morse (1984) found that the dissolution rate of different biogenic carbonate grain fractions showed that their dissolution rates followed a simple inverse radius ($1/R$) dependence.

The grain size effect (hence external surface area) may be of particular importance in controlling early dissolution rates of coated grains in the natural environment, since Halley and Harris (1979) and Donath et. al. (1980) have shown that dissolution begins in the surface layers. Halley and Harris (1979) also showed that during the early diagenesis of an oolitic grainstone in a freshwater lens, the precipitation of cement depended on the dissolution of the cortical aragonite. In similar cases, grain size could be of importance in determining the degree of cementation which is observed.

9.3.3 Effect of Pore Fluid Composition

All except two of the experiments were conducted using seawater. In the two exceptions, SO_4^{2-} -reduced seawater and freshwater were used (see Chapter 5 for results). The results of these experiments were interesting when considering the effect of the pore fluid composition on the rate of aragonite dissolution.

The inhibitory effect of Mg^{2+} on the precipitation of calcite has already been discussed in section 7.2.1. Other ions in seawater which have been studied for their inhibiting effect on CaCO_3 reactions are SO_4^{2-} and PO_4^{2-} . Morse (1983) in a review paper, pointed out that both SO_4^{2-} and PO_4^{2-} were reaction inhibitors in seawater.

(1) Effect of SO_4^{2-}

The only major seawater component (as opposed to minor and trace) apart from Mg^{2+} which has been identified as an inhibitor to CaCO_3 reaction is SO_4^{2-} (Morse, 1983). Sjoberg (1978) found its influence in the inhibition of calcite dissolution to be significant and a good deal of attention has been paid to the role of SO_4^{2-} in inhibiting the precipitation of dolomite (e.g. Baker and Kastner, 1981; Gunitalaka et. al., 1984). Baker and Kastner (1981)

conducted several experiments studying the transformation of aragonite and calcite to dolomite and they found that the presence of dissolved SO_4^{2-} significantly inhibited the transformation. It was therefore decided to conduct an experiment during this study using seawater in which most of the SO_4^{2-} had been removed. This was achieved by adding a calculated amount of barium chloride to a set volume of seawater, the SO_4^{2-} being precipitated as BaSO_4 . The resultant water therefore had an enhanced chloride ion concentration. It also had a slightly lower pH (6.5) which may have had some initial effect on the reactions. The results of the experiment (2985) can be found in section 5.2.

During experiment 2985, diagenetic changes proceeded to a much greater extent than in experiments conducted using the same sediment under similar experimental conditions but with untreated seawater (e.g. 2185). Much more cement and secondary porosity was created in the partially lithified sediment of experiment 2985 (see Plate 5.1 A-D and 5.2 A) than in experiment 2185 (see Plate 3.7A). XRD analysis indicated that there was an approximate reduction in aragonite of 40% compared to 25% in experiment 2185. The pore fluids also showed the relative increase in the degree of reaction with maximum $\text{mSr}^{2+}/\text{mCa}^{2+}$ ratios reaching 10.7×10^{-2} compared with 9.8×10^{-2} during experiment 2185. These figures may appear to be relatively similar but, as noted in

section 5.2.2, the pore fluids of experiment 2185 reached this maximum value and then dropped, while no such drop was observed in experiment 2985. This drop in the mSr^{2+}/mCa^{2+} ratio of 2185 is attributed to a decrease in the rate of aragonite dissolution (see Sr^{2+} data in Table 9.1). Also, the output of Ca^{2+} into solution was greater during experiment 2985 and more of this Ca^{2+} was used in the precipitation of calcite as shown by the decrease in the Ca^{2+} level at the end of the experiment (see Table 9.1).

Day No.	Sr^{2+}		Ca^{2+}		Sample No.
	2185	2985	2185	2985	
5		29		870	1
6	21	44	450	590	
12	46	74	200	1460	2
14	67	98	650	310	
19	70	172	60	1770	3
22	137	178	710	30	
26	20	350	20	1800	4
28	157	60	730	-50	
34	21	410	180	1750	5
35	178		910		

Table 9.1 - Levels of Sr^{2+} and Ca^{2+} (ppm) in the pore fluids of experiments 2185 and 2985. The day on which each sample was collected is shown and the figures to the right of the brackets show the difference in ppm between the two samples.

All of the evidence, both petrographic, mineralogical and chemical, suggests that both the rate of aragonite dissolution and of calcite precipitation was greatly

enhanced by the removal of SO_4^{2-} from the seawater.

Sjoberg (1978) found that SO_4^{2-} significantly inhibited calcite dissolution and it would appear from the data presented here that it also inhibits aragonite dissolution. This inhibition of aragonite and calcite dissolution by SO_4^{2-} is likely to be caused by the adsorption of SO_4^{2-} onto higher energy crystal sites which are also favoured for dissolution (Morse, 1983).

Unlike natural diagenesis, much of the SO_4^{2-} contained within the normal seawater is removed by the precipitation of CaSO_4 and magnesium oxysulphate when the temperature and pressure of the pore fluids are raised at the beginning of the experiments (see section 3.2). Considering the effect of SO_4^{2-} on the reactions, the precipitation of SO_4^{2-} phases will help initiate aragonite dissolution. In experiments where pore fluid sampling was conducted, a small volume of unused seawater (5 volume % maximum, see section 2.2.2) was substituted for the pore fluids. This would have temporarily added more SO_4^{2-} to the pore fluids although it is likely that this too would have eventually been precipitated as CaSO_4 or taken up into the structure of the calcite cement (see section 8.3.5). As noted in section 8.3.5, SO_4^{2-} would also have been continually added to the pore fluids of all experiments from the sediments although again this appears to have been taken up into the structure of the

calcite cement. However, the regular addition of SO_4^{2-} to the pore fluids appears to have reduced the amount of aragonite dissolution in experiment 2185 by 35-40 % compared to that in experiment 2985. This figure is calculated from the values for aragonite dissolution in both experiments (see Appendix V) and shows the low level at which SO_4^{2-} can act as an inhibitor to aragonite dissolution.

(2) Effect of PO_4^{3-}

Phosphate and phosphorous compounds have also received a good deal of attention because of their potential as reaction inhibitors for CaCO_3 at very low concentrations. Morse (1974) and Berner and Morse (1974) investigated the influence of phosphate on calcite dissolution kinetics. They found that it changed the critical undersaturation required for the onset of rapid dissolution. deKanel and Morse (1978), after conducting an extensive study of the interaction of PO_4^{3-} with aragonite, calcite and high-Mg calcite, concluded that the adsorption of PO_4^{2-} onto the surface effectively blocks dissolution even at low PO_4^{2-} concentrations.

(3) Experiments using freshwater

The results of the experiment run using freshwater (see section 5.3) also show the inhibiting effect of ions found

in seawater such as Mg^{2+} , SO_4^{2-} and PO_4^{3-} . A higher degree of reaction was observed during this experiment than any of the previous experiments. Petrographic evidence showed that a considerable amount of textural alteration had occurred while XRD analysis showed that over 90% of the original aragonite had been removed. Further experimentation using freshwater could be valuable. This was not followed up during this study because of a lack of time and the wish to thoroughly investigate the reactions using seawater.

9.3.4 Effect of Temperature

Earlier studies by Ferguson et. al. (1984) showed that an increase in the experimental temperature from 120 to 200 °C significantly affected the rate of diagenesis i.e. the rate of aragonite dissolution. In the restricted temperature range of 183-200 °C, no significant increase in the rate of Sr^{2+} release into solution has been noted (see section 4.3). Similarly, no significant difference in textural fabrics have been observed (e.g. compare petrographic results using sediments BSO conducted at different temperatures, Plate 3.2).

9.3.5 Effect of Pressure

There is some evidence to suggest that an increase in the

degree of aragonite dissolution accompanied a decrease in the hydrostatic pressure applied during the experiments (see results in section 4.4). This appeared to be most significant in the experiment run at 5 MPa (4186). The difference in the degree of aragonite dissolution in the experiments run at 7 (experiment 4086) and 9 (experiment 3686) MPa was less pronounced. The levels of Sr^{2+} in the pore fluids would support this observation (see Appendix I).

9.4 GEOLOGICAL SIGNIFICANCE

All the secondary porosity fabrics which have been created during the experiments are comparable to those which can be found in the natural environment. During the experiments, the microstructure of the carbonate grain appeared to be crucial in determining the type of porosity which was created and Evans and Ginsburg (1987) have shown that this is also the case in the freshwater environment where the aragonitic layers of ooids and coated grain cortices appear to be particularly susceptible to dissolution to form oomoldic porosity. Micritic carbonate, either as lamellae in coated grain cortices, as envelopes to shell fragments or as peloids, is much more likely to undergo neomorphism.

The reasons for the relative stability of micritic carbonate appears to be its close association with organic coatings as

discussed by Bathurst (1975, p.258). Microporosity may be created near the surfaces of grains by removal of some of the micritic carbonate, apparently leaving the organic meshwork or vuggy porosity where both the micritic carbonate and the organic meshwork is removed e.g. see Plate 9.1B. This example was from an experiment conducted using sediment ADDO (dune ooids) where some of the organic matter may have been removed in the subaerial environment.

During this experimental study, shell fragments have been found to be relatively stable when compared to coated grains. Where they have reacted, they have tended to undergo neomorphism rather than dissolution forming moldic porosity (see section 10.3.1). Earlier studies by Friedman (1964) showed that in the freshwater diagenetic environment, aragonitic grains had a metastability sequence which in order of increasing stability was skeletal grains < ooids < pellets and cryptocrystalline grains. Picha (1978), found that during freshwater diagenesis, skeletal grains were relatively stable when compared to ooids. Hence there appears to be some conflict in observations of effects in the natural environment.

Walter (1985) has conducted extensive studies on the relative dissolution rates of biogenic grains (both aragonite and high-Mg calcite) and has found that it depends on the saturation state of the pore fluid and the

microstructure of the grains. In these experiments where dissolution has been found to affect shell fragments, the microstructure has been exploited. Perhaps further experiments of the type conducted by Walter (1985) on mixed carbonate sediments could provide yet more useful information.

Grain size has also been found to affect the relative dissolution rate of all grain types except where organic coatings prevent large scale dissolution as in micritic carbonate. With this exception, the smaller the grain size, the greater the rate of dissolution. The effect of both grain type and size on aragonite dissolution rates will be of importance in the freshwater and burial environments where the precipitation of calcite partly depends on the rate of aragonite dissolution.

The composition of the pore fluid has also been found to affect the rate of aragonite dissolution. SO_4^{2-} has been identified as a reaction inhibitor to the aragonite-calcite transformation. This will be of importance in the burial environment where the fluids are often brines, depleted in SO_4^{2-} (Friedman, 1975), allowing the reaction to proceed more quickly.

CHAPTER 10 - CONTROLS ON THE DEVELOPMENT OF REPLACEMENT FABRICS - TEXTURE AND COMPOSITION.

10.1 INTRODUCTION

Two types of replacement fabric have been generated during the course of the experiments. The first, which has been termed solution cavity fill calcite, infills the secondary porosity created during the experiments by the dissolution of aragonitic grains. The second, neomorphic spar (also calcite), has been found to have replaced skeletal aragonite and micritic grains across an alteration front of micron-submicron size. Both are the result of solution-reprecipitation processes, the difference lying in the width of the alteration front that separates the phases and the time lapse between solution and reprecipitation.

Using both petrographic and geochemical data, the development of the fabrics will be discussed and the relevance of these observations to those seen in nature, considered.

10.2 SOLUTION-CAVITY FILL CALCITE.

10.2.1 Coated Grains

Most of the solution cavity fill calcite infills secondary porosity which has been created by the dissolution of the cortical aragonite of coated grains. This takes two forms: (i) narrow bands of calcite which infill secondary pore spaces created by the removal of individual aragonite lamellae (see Plate 3.2D) and section 9.2.1 and (ii) irregular mosaics of sparry calcite which infill larger secondary pore spaces created by the removal of several lamellae (see Plate 3.3C) and section 9.2.1.

The first type of replacement can be seen in Plates 3.2 A and D and 10.1 A and B. Natural examples, similar to these, can be found in Friedman (1964, Fig.24, p.791, Pleistocene). and Evans and Ginsburg (1987, Fig. 11C, p.316, Pleistocene), being attributed to the infilling of lamellar molds by calcite. The retention of cortical lamellar fabrics after replacement by calcite can also be seen in Mazzullo (1981, Figs. 10 B, F, 11 and 12 A, Permian) although no mechanism for the generation of these fabrics was discussed. Fabricus and Klingele (1970) also observed similar textures in Pleistocene ooids from Greece (Figs. 14-17). However, they interpreted the replacement of the original aragonite lamellae by layers of single calcite crystals as neomorphic

without a pre-existing dissolution cavity (p.596), "marks of the former aragonite particles....proving a replacement of the shell (i.e.lamellae) and not a cavity filling by calcite cement" (p.610). However, Sandberg (1975, p.520) argued that the features observed by Fabricus and Klingele (1970) were not like the relic aragonite crystals which occur in the calcite of replaced ooids but that the replacement textures which were produced were due to single calcite crystals filling a very thin shell-like secondary void like those observed by Multer (1971, p.139 and Fig.74). The fabrics observed by Fabricus and Klingele (1970) are very similar to those generated during the experiments.

The process of porosity development and infilling in the natural environment can be seen in Evans and Ginsburg (1987). Study of the Miami Oolite (Pleistocene) has shown that ooids undergo selective leaching of the aragonitic cortical lamellae which are subsequently infilled by calcite spar with the retention of the primary ooid structure (p.316-318). This natural process compares directly with that which is seen experimentally.

During the experiments, large pore spaces have been filled by irregular mosaics of sparry calcite. Examples of this type of replacement fabric generated during the experiments can be found in Plates 3.3 C, 4.6 A-C and 10.1 A. The infilling of moldic porosity by irregular mosaics of sparry

calcite is well documented. Natural examples of this type of replacement can be found in the following:

(i) Bathurst (1975). Figs. 297-299, 301 (of various ages).

(ii) Friedman (1964). Fig. 23, p.791. Pleistocene.

(iii) Singh (1987). Fig. 3A, p.119. Pre-Cambrian.

Some authors (e.g. Bathurst, 1975, p.417-419) use the term 'cement' to describe this type of replacement calcite. In this study however, the use of the term cement has been restricted to describe crystals which have been precipitated on the outer surfaces of sediment grains, helping to bind the grains together.

Early studies by Folk (1965, p.45) and Land (1967, p.921) have pointed to the difficulty of identification of textures developed by solution cavity fill processes as opposed to those generated by neomorphic processes if the grains have been totally replaced (also see Scholle, 1978, p.201). It is possible to identify irregular mosaics of sparry calcite as being of neomorphic origin if they contain relics of the original aragonite (e.g. Sandberg 1975, Sandberg and Hudson, 1983) but if no such textures are preserved then distinguishing between the replacement mechanisms can be difficult.

Bathurst (1975, p.417-419) cites many criteria for the

identification of cement. Criteria which can be applied to the 'cement' which infills secondary porosity are:

(i) the size of the crystals increase away from the initial substrate of the sparry mosaic and

(ii) that the spar lines a cavity which it fills incompletely.

The first criteria can be seen in some of the examples of solution cavity fill (see Plates 4.6 B and 10.1 A) but it is not always clear as shown in Plate 3.3 C and 4.6 A). In all cases observed however, criteria (ii) can be applied. Some of the secondary porosity remains, albeit a small proportion in some examples (see Plate 3.3 C, 4.6 A and B and 10.1 A).

The morphology of the solution cavity fill calcite which replaces coated grains is therefore apparently controlled by the size and shape of the secondary pore space which is being infilled. In some cases, combinations of the two types of cortical replacement fabrics (i.e. lamellar and irregular mosaics of sparry calcite) can be found in the same cortex (e.g. see Plate 4.6 A), as well as in the same sediment type (see Plate 10.1 A). This suggests that a close relationship exists between the original structure of the cortex, the creation of secondary porosity as discussed in section 9.2 and the infilling of that porosity. The development of two types of replacement fabric does not necessarily require that the ooid was originally bimineralic

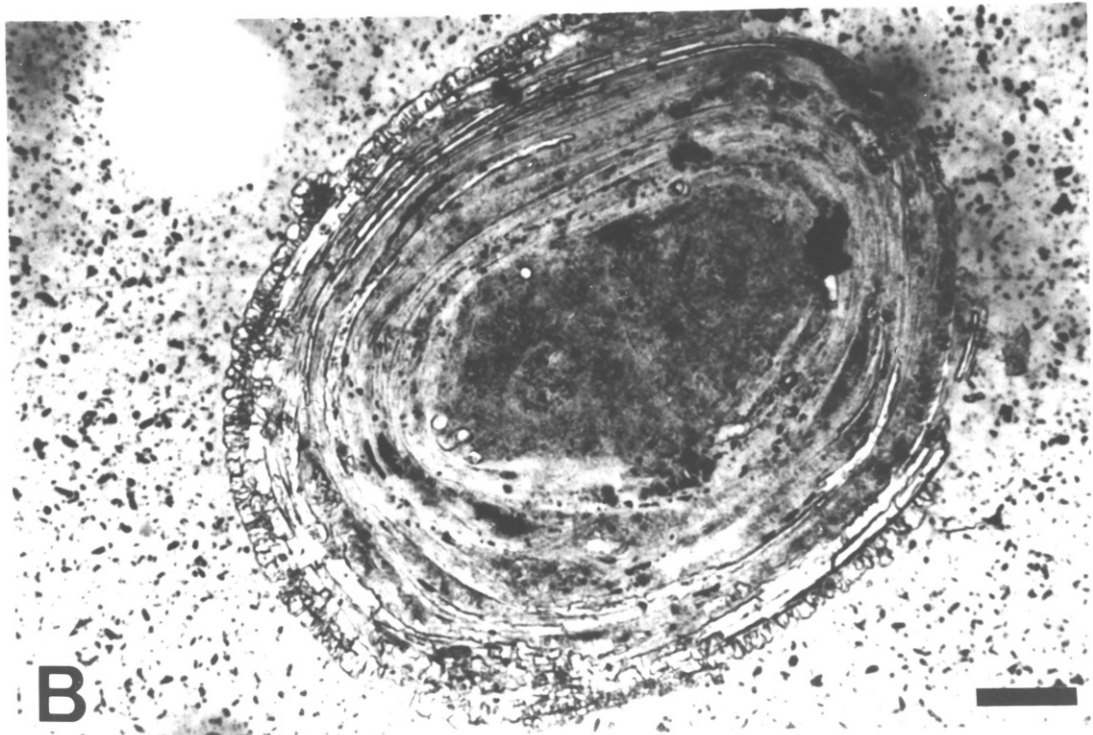
PLATE 10.1 - REPLACEMENT FABRICS

(A) Experiment 18/2 - Contrasting forms of solution cavity fill replacement in neighbouring grains. Oomoldic porosity has been created in the left hand grain and is partially infilled by sparry calcite which grows in the opposite direction from cement crystals.

Much of the original structure of the right hand grain has been retained. Lamellar porosity has been created and is partially infilled by solution cavity fill calcite, retaining the original outline of the grain. PPL. Scale bar 50 μm .

(B) Experiment 18/2 - Lamellar replacement by solution cavity fill. The original structure of the coated grain is retained by the infilling of lamellar porosity. The original micrite/organic matter lamellae are unaffected by the solution-reprecipitation process. PPL. Scale bar 50 μm .

PLATE 10.1



as suggested by Sandberg (1983, p.20) although bimineralic ooids do exist (e.g Land et al., 1979).

10.2.2 Shell Fragments

Few shell fragments have undergone dissolution during the experiments to form secondary porosity (see section 9.2.3). Solution cavity fill calcite in association with shell fragments is therefore very limited (e.g. see Plate 3.7 A). The relative stability of skeletal fragments during the experiments is further considered in section 10.3.1.

10.2.3 Composition of the Solution Cavity Fill Calcite

The concentrations of MgCO_3 , SrCO_3 and SO_4^{2-} in the solution cavity fill calcite are shown in Figs. 6.1 and 6.2. These figures also show the composition of the inorganic aragonite (cortical aragonite and occasional relic aragonite needles which line the chamber walls of gastropods and foraminifera) which was unaffected during the experimental reactions. Both Figs. 6.1 and 6.2 show that the composition of the solution cavity fill calcite is chemically distinct from that of the unaltered aragonite. Comparison of this with the geochemical data for the neomorphic fabrics (see section 10.3.3), where the composition of the unaltered and replacement phases showed strong similarities, would support the case that the lamellar replacement fabrics were not

generated as the result of neomorphic processes.

The relatively 'open' nature of the solution cavity fill process compared to that of neomorphic replacement, can be demonstrated by comparing the average composition of the solution cavity fill calcite with the composition of the cement precipitated during each experiment conducted using the different sediments (see data in section 3.5.2). If the average MgCO_3 and SrCO_3 contents are considered (see Fig. 10.1), then it can be seen that the MgCO_3 and SrCO_3 contents of the solution cavity fill calcite are very similar to many of the cement phases which contain low levels of MgCO_3 and high levels of SrCO_3 . Also, if the average SO_4^{2-} contents of the solution cavity fill calcite (1.01, s.d. 0.34 mole %) are compared with those of the cement crystals (1.11, s.d. 0.33) then again it can be seen that they are very similar, suggesting that the solution cavity fill calcite was precipitated directly from a solution which had an easy contact with the bulk pore fluids.

10.2.4 Age of the Solution Cavity Fill Calcite

Petrographic observations e.g. the growth of sparry solution cavity fill calcite crystals in the opposite direction from the cement crystals (see Plate 10.1A), suggest that the solution cavity fill calcite was precipitated during the late stages of the experiments. Most of the porosity was

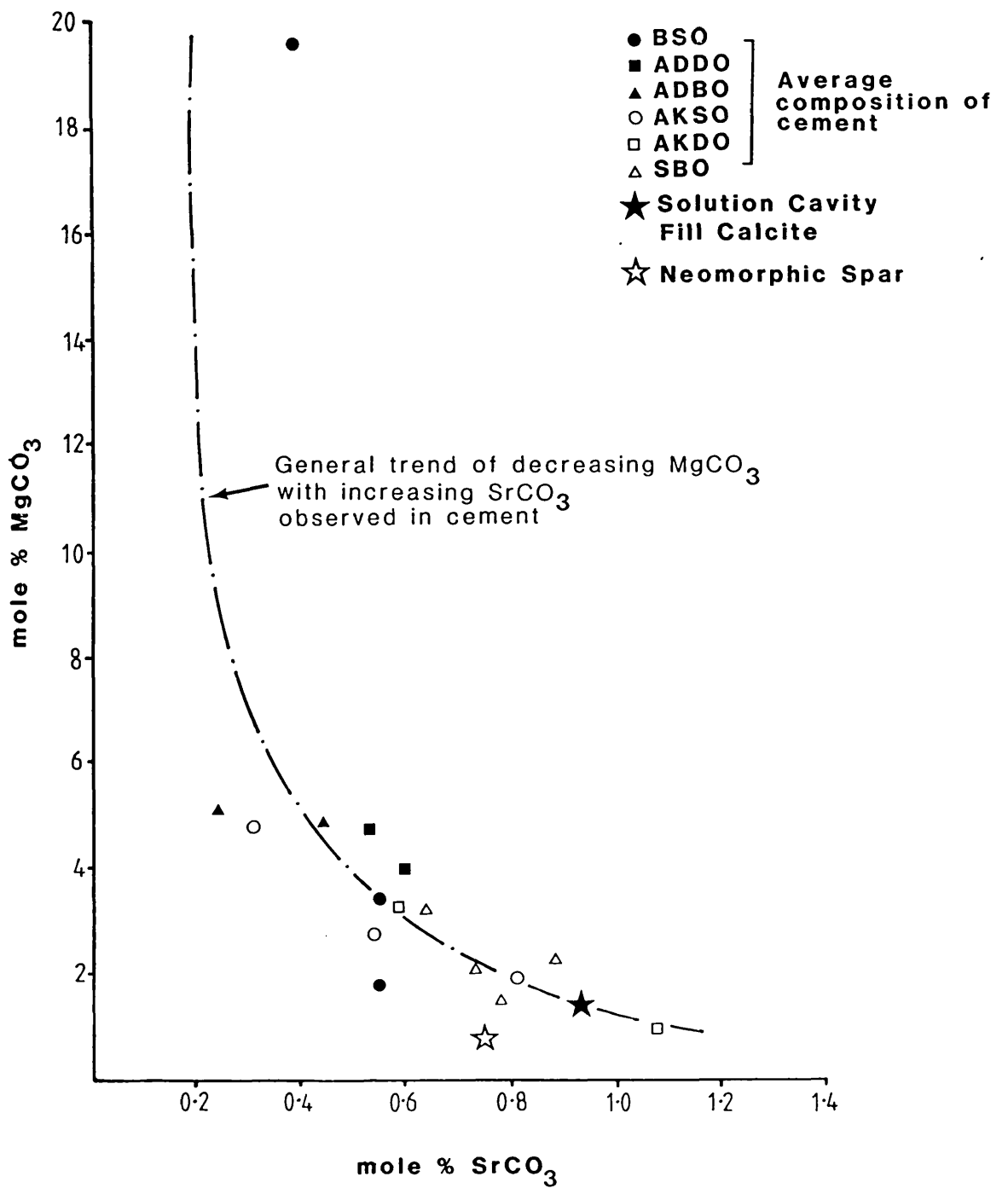


Fig. 10.1 - Average mole % $MgCO_3$ and $SrCO_3$ contained in the cement precipitated during experiments using each sediment type, solution cavity fill calcite and neomorphic spar.

created after the initiation of cementation (see section 4.2) and the infilling of that porosity must therefore have been of an even later date. Support for this conclusion also comes from the geochemical data. If the evidence which is discussed in section 8.3.2 suggesting that the $m\text{Sr}^{2+}/m\text{Ca}^{2+}$ pore fluid ratio may have controlled the SrCO_3 content of the precipitated calcite is considered, then the relatively high SrCO_3 content of the solution cavity fill calcite would similarly suggest that it was of a late origin when the pore fluids were relatively enriched in Sr^{2+} .

10.3 NEOMORPHIC SPAR.

Neomorphic spar has been found to have replaced shell fragments and micritic carbonate.

10.3.1 Shell Fragments

Shell fragments on the whole have been found to be relatively stable (see results in sections 3.6.1 and 3.6.3). Where they have reacted however, they have been found to react rapidly, prior to the precipitation of cement crystals (see section 4.2). In this mechanism of replacement, small, irregular patches of calcite form due to the recrystallisation of the skeletal aragonite (see Plates 4.1 and 4.2 B and C) across a sub-micron sized alteration front. These calcitic patches grow and may coalesce to form an

irregular mosaic of sparry calcite crystals of varying size. The degree of replacement can vary from isolated areas of calcite to the complete replacement of a shell fragment with no relics of the original aragonitic structure (e.g. see Plate 3.6 C). Only occasionally have relic aragonite structures been found in the replacement neomorphic calcite (e.g. see Plate 5.1 D and 5.2 A).

The few shell fragments which have reacted, have done so before any other reaction in the sediment (see section 4.2). Land (1967) conducted a similar experimental study investigating the relative rates of reactivity of aragonitic skeletal fragments. The experiments were conducted using various aragonitic skeletal materials (corals, molluscs and algae) and seawater at 285 °C. The aragonite was found to convert to calcite and proto-dolomite by inversion in less than 40 hours. Land (1967) however found that ooids inverted to calcite much more slowly than skeletal aragonite (p.917). During the early stages of the experiments presently under discussion, this relative sequence of inversion has also been found to apply. The results presented in section 4.2 show that the first reaction in the sediment is the inversion of some of the skeletal aragonite to calcite. After this however, dissolution of inorganic aragonite and precipitation of calcite become the dominant reactions.

Land (1967) found that there was no significant difference of inversion rates between a variety of skeletal fragments (including different types of mollusc). Walter (1985) and Walter and Morse (1985) have conducted extensive studies into the dissolution of shell fragments and have found that differences in the dissolution rate did occur between skeletal groups (i.e. Halimeda, pelecypods, gastropods, red algae, forams, corals, barnacles and echinoids) and that it depended not only on the mineralogy of the fragment but also on the saturation state of the pore fluids and the grain microstructure. It was found that in experiments with pore fluids where aragonite dissolved in preference to high-Mg calcite, microstructural control was the most important factor in determining the reaction rate (Walter 1985, p.9). Grains with the most complex microstructures dissolved first (Walter 1985, p.13). Bruni and Wenk (1985) have also suggested that recrystallisation of shell fragments occurs primarily along crystal defects, which also suggests that the kinetics of replacement are controlled mainly by the microstructure of the aragonite.

Only certain aragonitic shell fragments have reacted during these experiments. Low and high-Mg calcite was found to be stable (although some evidence suggested that high-Mg calcite underwent incongruent dissolution e.g. experiments using sediment SBO). Aragonite dissolution was therefore preferential, hence microstructure would have been important

in controlling the rate of reaction of the skeletal fragments during the experiments (Walter, 1985; Walter and Morse 1985). Walter (1985) and Walter and Morse (1985) in their studies did not examine the relative rates of dissolution of different types of bivalve or gastropod. The molluscs which have reacted during these experiments, either by dissolution or by inversion, have been composed of cross-lamellar (see Plates 3.4 B, 3.7 A and B and 5.1 D) and homogeneous (see Plates 4.1 B-D and 6.1 B) structures. Others of the same structure however have not reacted (see Plate 10.2) which would suggest that it is not purely the type of shell structure which controls the reaction rate.

Sandberg and Hudson (1983, p.879) suggest that neomorphic recrystallisation is a "rapid, one-step process" which is in agreement with the process documented both here and in Land (1967). Sandberg and Hudson (1983) suggested that the survival of aragonite relics appears to be closely related to the presence of organic envelopes or coatings on the aragonite crystals. Only on a few occasions however have aragonite relics been found in the neomorphic spar created during these experiments (e.g. Plate 5.1 D and 5.2 A). One would have expected that in such a rapid inversion process more evidence of relic aragonite would have been preserved. The absence of such relics may suggest that where neomorphism occurred it may have done so in areas more susceptible to alteration e.g. areas of increased

PLATE 10.2 - UNALTERED SHELL FRAGMENTS

None of the shell fragments display any evidence of alteration although the remainder of the sediment in (A), (B) and (D) is highly altered. Some of the shell fragments in the sediment of experiment 30/4 (Plate 10.2C) did show alteration to neomorphic spar but the two fragments shown in the centre of the photomicrograph show no evidence of this.

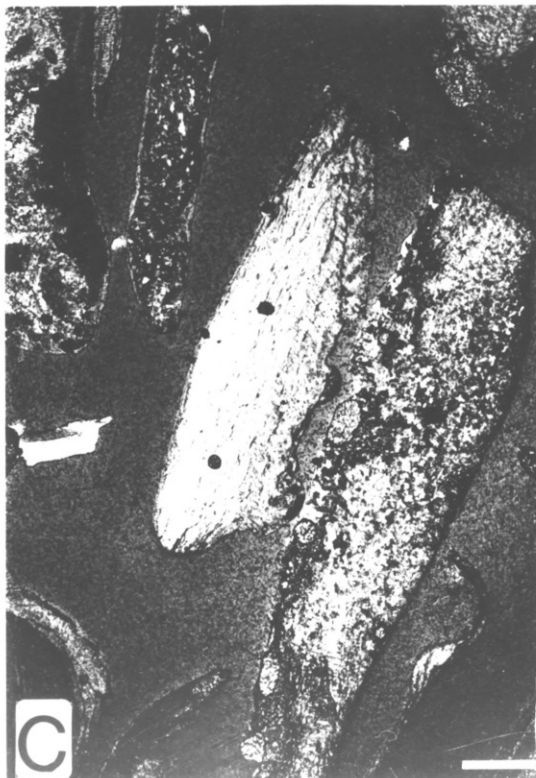
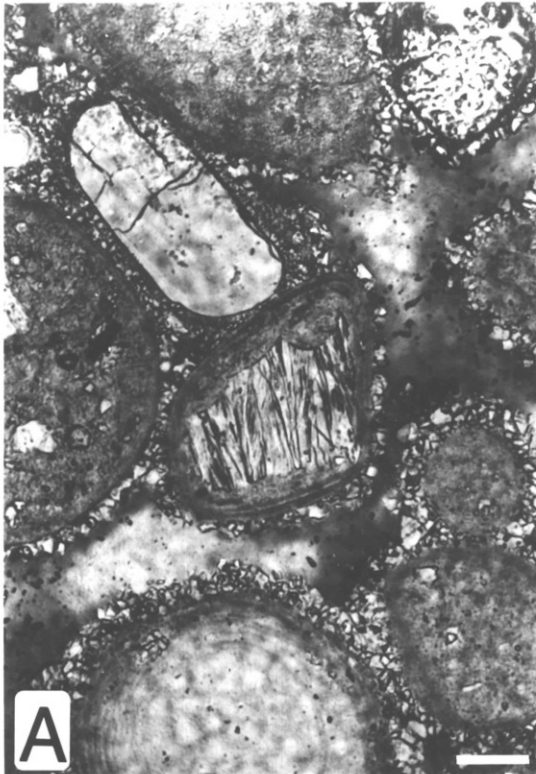
(A) Experiment 28/3. PPL. Scale bar 50 μm .

(B) Experiment 2085. XP. Scale bar 50 μm .

(C) Experiment 30/4. PPL. Scale bar 300 μm .

(D) Experiment 2185. XP. Scale bar 50 μm .

PLATE 10.2



microstructural complexity due to crystal defects as suggested by Bruni and Wenk (1985) or in areas less protected by organic matter. As the bulk of the shell fragments have been found not to react, information is limited and any conclusions concerning causes for preferential inversion must be tentative. It is an area however where further experimentation would be valuable.

10.3.2 Micritic Carbonate.

Grains composed of micritic carbonate such as peloids, coated grain nuclei and the micritised areas of shell fragments, have, in some cases, been replaced by irregular patches of coarser calcite crystals (see Plates 3.3D, 3.8C, 3.9D, 3.10D, 4.1A, 4.2D and 4.3B). This is a process which starts very early in the experiments (see Plates 4.1A, 4.2D and 4.3B).

Most of the neomorphic crystals which have replaced the micritic carbonate are in the size range 5-10 μm (see Plates 3.3A, 3.10D and 4.3B) but crystals up to 30 μm in diameter can also be found (see Plates 3.14D, 4.1A and 4.2D). Where small crystals occur, they are either isolated in a 'sea' of unaltered micrite (see Plates 3.3A and 3.10D) or occur as clusters of varying size (see Plates 3.3D, 3.8C and 4.3B). The larger sparry calcite crystals are very unusual (20-30 μm in diameter) and occur as irregular mosaics (see Plates

3.14D, 4.1A and 4.2D). The size and shape of the grains (see Plates 4.1A and 4.2D) may suggest that they were of an originally biogenic origin.

Examples of the recrystallisation of micritic grains can also be found in the natural environment, e.g. Evans and Ginsburg (1987), Fig 12 B, p.316, Pleistocene where micritic peloids have undergone recrystallisation to neomorphic spar while coated grain cortices were susceptible to dissolution. Evans and Ginsburg (1987, p.317) suggested that the micrite of trace fossil tubes and matrix in the sediments would have had a low permeability and high porosity and therefore a good capacity to hold water in the vadose regime encouraging recrystallisation of aragonite to calcite. They believed that the small size and large number of secondary calcite crystals suggested an abundance of nucleation sites, consistent with the fine grain size of the original sediment. They suggested that the large number of nucleation sites and the presence of water would allow recrystallisation to take place without the production of pore space. Peloids would be recrystallised in the same manner.

Although the conditions in the experimental cells in no way replicate those in the natural vadose environment, the process involved could be similar. Aragonite instability would cause dissolution of the micritic aragonite to occur.

The low permeability of the micritic carbonate could restrict the movement of ions out of the grain into the bulk pore fluids. The fine size of the micrite and the presence of organic matter (see section 7.4.2) could allow rapid nucleation of the replacement crystals. The relatively rapid rate of reaction in the experimental cells would also aid this. The irregular distribution of the neomorphic crystals suggests that recrystallisation is an apparently random process which would be entirely dependent on the internal structure of the grain, in keeping with the explanation given by Evans and Ginsburg (1987).

The size of the neomorphic spar crystals which have been generated are similar to the 'microspar' described by Folk (1965, p.32). However, unlike Folk's microspar, many of the fabrics which have been generated do not always show crystals of a uniform size. This is particularly true of the few fabrics composed of crystals greater than 10 μm . Direct comparison of the processes involved is therefore not possible because of the apparent difference in crystal size uniformity and because two entirely different sediment types are being considered i.e. carbonate mud and grainstones.

10.3.3 Composition of the Neomorphic Spar

The concentrations of MgCO_3 , SrCO_3 and SO_4^{2-} in the neomorphic spar crystals which have replaced shell fragments are shown

in Figs. 6.3 and 6.4. These figures also show the composition of aragonitic shell fragments which were unaffected by neomorphism during the reactions.

If the composition of the original shell fragments in terms of SrCO_3 is considered then it can be seen that two compositional groups exist, one with low SrCO_3 in which most of the shell fragments occur, the other with high SrCO_3 contents. Bathurst (1975, Fig. 225) shows that most recent molluscs contain low levels of Sr^{2+} in agreement with the data presented here.

If the composition of the neomorphic spar in terms of MgCO_3 and SrCO_3 is considered then it appears that there is a much greater overlap in the composition of the replacement and unaltered phases than was observed in the solution cavity fill calcite. The average MgCO_3 and SrCO_3 contents of the neomorphic spar crystals are 0.75 mole % (s.d. 0.56 mole %) and 0.75 mole % (s.d. 0.33 mole %) respectively. If these data are superimposed on Fig. 10.1, then it can be seen that the composition of the neomorphic spar has been influenced by the composition of the biogenic aragonite which it replaces, falling below the curve which fits average cement compositions and solution cavity fill calcite. This is even more apparent if the composition of the spar (which is generated during the early stages of the experiments) is compared with the composition of early cement crystals which

contain high levels of MgCO_3 and low levels of SrCO_3 (see Fig. 4.1). The SO_4^{2-} content of the neomorphic spar (see Fig. 6.4) also supports the hypothesis that there is a direct control of the shell fragment composition on the neomorphic spar. The average SO_4^{2-} content is 0.55 mole % (s.d. 0.43 mole %) which is much lower than the cement or solution cavity fill phases (see section 10.2.4).

The retention of chemical signatures during neomorphism has been noted by many authors e.g. Sandberg and Hudson (1983) and Davies (1977). The retention of such chemical signatures will however depend on the porosity and permeability of the shell fragments which are replaced as suggested by Martin et.al. (1986). In a study of the neomorphism of Monastrea and Strombus shells, Martin et. al. (1986) found that replaced Strombus shells retained much higher levels of Sr^{2+} than replaced Monastrea shells. This they attributed to the difference in porosity between the two taxa. Monastrea, with its higher initial porosity showed much more exchange with the formation fluids than the denser Strombus. The composition of the replacement spar is therefore also dependent on the structure of the shell fragment which is being replaced.

In the experiment conducted using SO_4^{2-} -reduced seawater, the composition of the neomorphic spar was found to be much more like the other phases which were precipitated (see section

6.4). The difference in chemical signature may be related to the fact that removal of SO_4^{2-} increased the rate of diagenesis and perhaps aided diffusion of ions to and from the dissolution front to the bulk pore fluids. Any conclusion regarding this however must be speculative due to the lack of information.

10.4 GEOLOGICAL SIGNIFICANCE

The way in which the cortices of coated grains have been replaced is similar to many of the early replacement processes which operate in the natural environment i.e. the infilling of lamellar porosity by single calcite crystals which mimic the original outline of the cortex or by the infilling of larger pore spaces by mosaics of sparry calcite crystals. This contradicts the conclusion of Mackenzie and Pigott (1981, p.193) that " if the microtextures of the ooid is preserved then the ooid originally had a calcite mineralogy; if the ooid exhibits textural disruption, its original mineralogy was aragonite".

The type of solution cavity fill replacement fabrics that have been observed are similar to the Type II and VI fabrics of Singh (1987) where Type II represents the irregular mosaic of sparry calcite and Type VI represents the lamellar type of replacement. Singh (1987) suggests that both his Type II and Type VI fabrics were developed from original

aragonitic ooids but that while Type II formed in response to a solution cavity fill mechanism, Type VI formed through a calcitisation mechanism (i.e. neomorphic). The criteria used by Singh (1987) to identify the neomorphic origin of the fabrics was an elevated Sr^{2+} content in the calcite. The generation of very similar fabrics through different mechanisms of replacement points to the need for good geochemical data in association with petrographic observations when considering diagenetic mechanisms. The type of replacement fabrics that are observed in coated grains may therefore depend on the original structure of the cortex e.g. whether much of the organic matter has been removed or not during exposure, prior to lithification in the subaerial environment.

No evidence for the alteration of tangential fabrics in the cortices of coated grains to radial diagenetic fabrics as suggested by Shearman et. al. (1970), has been observed in any of the experimentally altered material. All cortices of coated grains have been replaced by lamellar calcite which mimics the outline of the original cortex or by blocky calcite.

With regard to the question of the stability of skeletal fragments, factors such as the grain microstructure (including the internal micro-porosity) will be of importance when considering neomorphism. The presence or

absence of organic matter in the structure of shell fragments may also be of importance in determining the rate of reaction. This will depend not only on the growth history of the shell (i.e. type of shell) but also on processes which affect the shell after the death of the organism e.g. extensive micritisation or destruction of organic matter during subaerial exposure.

The neomorphism of the shell fragments began at isolated points in the skeletal structure with the development of single calcite crystals. With growth of these crystals and the generation of new crystals, irregular mosaics of calcite were produced. No pattern of increasing crystal size away from inner grain edges was therefore observed and coupled with the retention of the chemical signature, these served as means for identification of a neomorphic origin when grains had been totally replaced with no remaining aragonite relics. The irregular nature of the mosaics may be of use in determining neomorphic as opposed to solution cavity fill calcite fabrics in natural material.

Micritic carbonate was partially replaced by irregularly spaced, neomorphic crystals (usually less than 10 μm in diameter). On the few occasions where micritised grains were partially replaced by much larger neomorphic crystals (less than 30 μm), the size and shape of such grains suggested that they may have originally been shell

fragments. The recrystallised areas may represent areas of shell fragments which had not been micritised although this is not conclusive. No comparison has been drawn between the recrystallisation of micritic grains and that of muds because of the major difference in sediment types.

CHAPTER 11 - SUMMARY AND CONCLUSIONS

11.1 INTRODUCTION

Experiments have been conducted to try to simulate the early diagenesis of carbonates in a period of a few weeks. These experiments were conducted using Recent oolitic and skeletal sands from the Bahamas, the Arabian Gulf and Western Australia. The sediments were placed in a hydrothermal cell capable of being maintained at elevated temperatures and pressures (180-200 °C, 5-11 MPa). Most of the experiments were conducted using seawater but two, using SO_4^{2-} -reduced seawater and freshwater were also run. Diagenetic processes were found to proceed to such an extent that textural, mineralogical and chemical changes could be studied. The reactions that occurred involved the dissolution of aragonitic sediments and reprecipitation of the CaCO_3 as calcite.

Clearly natural early diagenetic reactions occur at much lower temperatures and pressures and this has to be borne in mind throughout. The results of the study which can be most easily compared with those of the natural environment are the diagenetic textures. Most of the thesis has therefore been concerned with the products of the diagenetic

reactions in terms of textures and the processes that produced them. The chemistry of the reactions has also been studied but this has been done primarily to gain a better understanding of the diagenetic reactions rather than to study the chemical reactions in a purely quantitative or theoretical way. However, the two cannot be separated without the loss of vital information and this is particularly true of carbonates.

11.2 FACTORS AFFECTING THE DISSOLUTION OF ARAGONITE

As noted above, the diagenetic reactions proceeded through an aragonite dissolution - calcite precipitation mechanism. Factors found to affect the aragonite dissolution rate will be briefly summarised.

11.2.1 Grain Type

During the experiments the cortices of coated grains have been found to be much more susceptible to dissolution forming secondary porosity than micritic carbonate or shell fragments (see section 9.3.1). The original structure of the coated grain appears to have been important in determining the form of the secondary porosity which is developed (see section 9.2.1). Where the cortex contained many organic or micritic lamellae, then a lamellar type of porosity was created by the layers of aragonite needles

being removed. Wider pore spaces were created in the cortices of coated grains where few organic or micritic lamellae were present. Microporosity was created at the edges of peloids. More commonly however, micritic carbonate was found to undergo neomorphism. Shell fragments (aragonitic bivalves and gastropods) were generally found to be the most stable of all aragonitic grains. Very few secondary pore spaces were formed by the dissolution of shell fragments.

The composition of the sediment therefore had a profound effect on the relative rate of aragonite dissolution and the supply of CaCO_3 for calcite precipitation.

11.2.2 Effect of Grain Size

An increase in the degree of reaction was found to accompany a decrease in the sediment grain size (see section 9.3.2). This agrees with the data of Kier (1980) and Walter and Morse (1984).

11.2.3 Effect of Dissolved SO_4^{2-} in the Pore Fluids

The composition of the pore fluid was also found to be important in controlling the rate of aragonite dissolution. Dissolved SO_4^{2-} (see section 9.3.3) was found to greatly inhibit the diagenetic reactions. Dissolution and

reprecipitation proceeded to a greater extent when the SO_4^{2-} was removed from the initial pore fluids.

11.3 PRECIPITATION OF CEMENT

The CaCO_3 which was precipitated as calcite cement was derived from the original aragonite grains which underwent dissolution.

11.3.1 Effect of Organic Matter on Nucleation

The experiments carried out provide some evidence which suggests that organic matter may have acted as a nucleation site for some of the calcite cement crystals (see section 7.4.2). Increased cementation was observed around algal filaments and other organic matter in pore spaces. Also, more cement crystals were associated with the surfaces of peloids than with the smooth surfaces of coated grains. Many peloids are formed by the micritisation of carbonate grains as the byproduct of the boring activities of endolithic algae. This results in more mucilaginous organic matter being associated with the peloids. In addition, the larger external surface area of the micritic carbonate peloids compared to that of coated grains, would allow the adsorption of more dissolved organic matter on the external surface of the grain from seawater in the depositional environment. Further evidence which supports the hypothesis

that organic matter may act as a nucleation site for CaCO_3 is provided by the observation that a decrease in the number of cement crystals occurs in samples of coated grains, which had been treated with H_2O_2 to remove most of the surface organic matter compared to untreated samples. As no difference in the pore fluid geochemistry was observed, this may have been the result of fewer nucleation sites.

11.3 2 Controls on Cement Morphology

Two types of cement fabrics were generated during the experiments. These were found to have specific distributions with regard to the sediments in which they were found (see section 3.5.1). Isopachous fringes of granular-bladed cement crystals occurred in the partially lithified sediments of experiments using sediment samples composed predominantly of coated grains and peloids. Continuous or discontinuous rims of equant cement crystals were found in the partially lithified sediments of experiments using sediment samples containing higher proportions of shell fragments and non-carbonate grains (3-10 volume %). Equant crystals were larger in size than granular-bladed crystals although fewer were found. Sediment samples composed entirely of shell fragments were found not to have cemented (see section 3.6.1).

(1) Effect of the Nucleation Rate on Cement Crystal Morphology

As noted above, two cement crystal morphologies were observed (i) granular-bladed and (ii) equant. Equant fabrics are believed to have been developed where nucleation rates were lowered either by increased levels of Mg^{2+} in the pore fluids (see section 11.3.2 (2)) or where the rate of supply of Ca^{2+} and CO_3^{2-} was lowered due to lower rates of aragonite dissolution (see section 7.3.2). Granular-bladed fabrics are believed to have developed where nucleation rates were relatively higher.

(2) Effect of Mg^{2+} in Controlling Cement Crystal Morphology

Equant fabrics are believed to have developed where the nucleation rates of calcite were lowered (see section 1.3.2 (1)). While the mMg^{2+}/mCa^{2+} ratio of the pore fluids did not control the morphology of the cement crystals in the way described by Folk (1974) and as discussed in section 7.2.1, Mg^{2+} in solution does inhibit the nucleation of calcite greatly. This is supported by the fact that in some experiments, where there was a higher proportion of high-Mg calcite shell fragments, the mMg^{2+}/mCa^{2+} ratio of the pore fluids increased above that of seawater during the early stages of the experiments and this seems to have reduced the nucleation rate of cement crystals (see section 7.3.1).

Equant cement fabrics were generated during these experiments.

(3) Effect of CO_3^{2-} Concentration on Cement Crystal Morphology

Suggestions have been made by Lahann (1978) and Given and Wilkinson (1985) that the CO_3^{2-} concentration of the pore fluids controls the morphology of calcite cement crystals. Unfortunately no CO_3^{2-} data is available from this study as discussed in section 7.2.2. However, it has been shown that the morphology of cement crystals in both experimental and natural fabrics (see section 7.5) can vary between grains across the width of one pore space. It is difficult to envisage that a sufficiently large gradient in CO_3^{2-} ion concentration over such small distances and involving such small pore fluid volumes could significantly affect cement morphology in those cases. It is therefore suggested that, due to the complexities of the carbonate system, one factor alone will not control cement morphology in every situation.

11.3.3 Cement Crystal Chemistry

(1) MgCO_3 Content of Cement Crystals

Most of the cement precipitated during the experiments is composed of calcite containing less than 10 mole % MgCO_3 .

However, in some short term experiments (up to 5 days), crystals containing up to 76 mole % MgCO_3 were observed. Only on one occasion were such Mg-rich phases (84 mole % MgCO_3) found in experiments conducted for longer periods of time (up to 6 weeks). It is believed that Mg-rich nuclei were precipitated at the beginning of experiments which would agree with the work of Fyfe and Bischoff (1965). This would have reduced the level of Mg^{2+} in the pore fluids, helping to facilitate the aragonite-calcite transformation. The evidence presented in section 8.2.4 suggests that these phases, chemically of dolomitic-magnesitic composition, may in fact have been highly disordered calcites although no positive identification has been obtained. Diffusion of Mg is thought to have occurred outwards from crystals cores through later low-Mg calcite phases precipitated on earlier Mg-rich crystals. This process left, at most, a remnant signature of decreasing MgCO_3 content from the centre to the edge of crystals. This decrease in the MgCO_3 content of the cement crystals parallels that in the pore fluids but no direct correlation between the bulk composition of the solid and fluid phases is observed.

(2) SrCO_3 Content of Cement Crystals

All the cement crystals generated during the experiments using seawater, contain significant amounts of SrCO_3

(maximum 1.3 mole %, see Table 3.9). There is some evidence to suggest that an increase in the amount of SrCO_3 contained in the cement accompanied an increase in the $\text{mSr}^{2+}/\text{mCa}^{2+}$ ratio of the pore fluids (see section 8.3.2). Higher levels of SrCO_3 (1.6 mole %) were observed in the cement precipitated during the experiment conducted using freshwater (see section 5.2). This may have been due to the more rapid rate of reaction noted and the higher growth rate of the crystals (see section 8.3.2).

(3) SO_4^{2-} Content of Cement Crystals

The cement crystals also contain significant amounts of SO_4^{2-} (maximum 2 mole % SO_4^{2-} , see Table 3.9). One of the sources of the SO_4^{2-} is believed to be that contained in the sediments used (see section 8.3.5).

11.4 REPLACEMENT OF GRAINS

11.4.1 Solution Cavity Fill Calcite

Most of the secondary, moldic porosity was created in the cortices of coated grains (see section 11.5.1). The lamellar pore spaces were partially infilled by single calcite crystals (see section 10.2.1) the original outline of the cortex being retained. Retention of lamellar

cortical structure therefore does not necessarily imply that the process of replacement was neomorphic unless other evidence such as elevated Sr^{2+} signatures points towards that. Where wider pore spaces were generated (see section 10.2.1), these were partially infilled by irregular mosaics of sparry calcite. Both types of replacement fabrics have been found in neighbouring grains and in single cortices within one grain.

The chemical composition of both types of replacement calcite was similar to many of the cement crystals precipitated during the experiments. This confirms the observation that replacement proceeded through a solution cavity fill process rather than through a neomorphic process.

11.4.2 Neomorphism

Where they reacted, micritic carbonate and shell fragments underwent neomorphic replacement, rather than undergoing dissolution to form secondary, moldic porosity. The process of neomorphism in micritic carbonate results in small crystals (<10 μm in diameter, typically 3-5 μm) forming at irregularly spaced centres and developing small patches of crystals.

Shell fragments (aragonitic bivalves and gastropods) were

generally found to be the most stable of all aragonitic grains. However, where they did react, they did so rapidly in the first few days of the experiments. Reaction resulted in replacement by neomorphic processes which, like those affecting the micritic carbonate, began at irregularly spaced centers (see section 10.3.1). Further growth of these crystals caused them to coalesce, forming irregular mosaics of sparry calcite. The crystal size of the calcite spar replacing the skeletal material was generally coarser than that replacing the micritic carbonate with a maximum size of around 30 μm .

Earlier studies by Walter and Morse (1985) and Walter (1985) have suggested that grain microstructure is of importance in controlling reaction rates in skeletal grains. In these experiments, the molluscan shell fragments which were found to react were composed of cross-lamellar and homogeneous structures. However, grains of similar structure in the same experiment were found to be unaffected so the reason why certain fragments only should undergo neomorphism is unclear.

11.5 CONCLUSIONS AND SUGGESTIONS FOR FURTHER WORK

In conclusion, the study has been particularly successful in reproducing the textures produced during early diagenesis. By using natural materials, many of the complexities which

may affect the reactions in the natural environment such as the role of organic matter in CaCO_3 nucleation have not been excluded. However, it must be remembered that the experimental study has used elevated temperature and pressure conditions. Textures which may take at least a thousand years (e.g. Halley and Harris, 1979) to form in the natural environment have been generated in a matter of weeks. These factors will add uncertainties, especially to the chemical results. As with any experimental study, it has therefore been necessary to continually compare the experimental results with those of natural diagenesis before any conclusions were reached as to the processes involved.

If the study was to be continued, then a useful extension of the work would be to investigate early diagenetic reactions through the use of material from the Ocean Drilling Program. It is believed that if core and pore fluid samples were available from marine basinal settings, that a considerable amount of new information and insight into carbonate diagenesis in the marine and shallow subsurface could be obtained.

Further experimental work could investigate diagenetic reactions involving skeletal fragments, fresh and SO_4^{2-} -reduced seawater and the effect of the CO_3^{2-} concentration of the pore fluids on cement morphology. If further experimental were to be carried out then I would suggest

that modification to the hydrostatic pressure control system was made to ensure that the hydrostatic pressure could be set and maintained at some predetermined level throughout the experiments.

The combined use of information from the natural environment linked to the possibility of simulating diagenesis experimentally could be a powerful tool.

REFERENCE LIST

- AL-AASM, I.S. and VEIZER, J., 1986 - Diagenetic stabilisation of aragonite and low-Mg calcite: I- Trace elements in rudists. Jour. Sed. Pet., v.56, p.138-152.
- ANGUS, J.G., RAYNOR, J.B., ROBSON, M., 1979 - Reliability of experimental partition coefficients in carbonate systems: evidence for inhomogeneous distribution of impurity cations. Chem. Geol., v.27, p.181-205.
- ASQUITH, G.B., 1986 - Microporosity in the O'Hara oolite zone of the Mississippian Ste. Genevieve Limestone, Hopkins County, Kentucky and its implications for formation evaluation. Carbonates and Evaporites, v.1, p.7-12.
- BADIOZAMANI, K., 1973 - The dorag dolomitisation model - application to the Middle Ordovician of Wisconsin. Jour. Sed. Pet., v. 43, p.965-984.
- BADIOZAMANI, K., MACKENZIE, F.T. and THORSTENSON, D.C., 1977 - Experimental carbonate cementation: Salinity and vadose-phreatic effects. Jour. Sed. Pet., v.47, p.529-542.
- BAKER, P.A., GIESKES, J.M. and ELDERFIELD, H., 1982 - Diagenesis of carbonates in deep-sea sediments - Evidence from Sr/Ca ratios and interstitial dissolved Sr²⁺ data.

Jour. Sed. Pet., v.52, p.71-82.

BAKER, P.A. and KASTNER, M., 1981 - Constraint on the formation of sedimentary dolomite. Science, v.213, p.214-216.

BATHURST, R.G.C., 1966 - Boring algae, micrite envelopes and lithification of molluscan biosparites. Geol. Jour., v.5, p.15-32.

BATHURST, R.G.C., 1975 - Carbonate sediments and their diagenesis. Developments in sedimentology. No. 12. Elsevier, Amsterdam 658 pp.

BATHURST, R.G.C., 1980 - Lithification of carbonate sediments. Sci. Prog. Oxford, v.66, p.451-471.

BERNER, R.A., 1975 - The role of magnesium in the crystal growth of calcite and aragonite from seawater. Geochim. Cosmochim. Acta, v.39, p.489-504.

BERNER, R.A. and MORSE, J.W., 1974 - Dissolution kinetics of calcium carbonate in seawater. IV: Theory of calcite dissolution. Am. Jour. Sci., v.274, p.108-134.

BERNER, R.A., WESTRICH, J.T., GRABER, R., SMITH, J. and MARTENS, C.S., 1978 - Inhibition of aragonite precipitation

from supersaturated seawater. A laboratory and field study.
Am. Jour. Sci., v.278, p.816-837.

BHATTACHARYYA, A and FRIEDMAN, G.M., 1979 - Experimental compaction of ooids and lime mud and its implication for lithification during burial. Jour. Sed. Pet., v.49, p.1279-1286.

BHATTACHARYYA, A and FRIEDMAN, G.M., 1984 - Experimental compaction of ooids. Jour. Sed. Pet., v.54, p.362-372.

BISHOFF, J.L., 1968 - Kinetics of calcite nucleation: magnesium ion inhibition and ionic strength catalysts. J. Geophys. Res., v.73, p.3315-3322.

BISHOFF, J.L. and FYFE, W.S., 1968 - The aragonite-calcite transformation. Am. Jour. Sci., v.266, p.65-79

BISHOFF, J.L. and SEYFRIED, W.E., 1978 - Hydrothermal chemistry of seawater from 25 to 350 °C. Am. Jour. Sci., v.278, p.838-860.

BISHOFF, W.D., MACKENZIE, F.T. and BISHOP, F.C., 1987 - Stabilities of synthetic magnesian calcites in aqueous solution: Comparison with biogenic materials. Geochim. Cosmochim. Acta., v.51, p.1413-1424.

BRUNI, S.F. and WENK, H.R., 1985 - Replacement of aragonite and calcite in sediments from the San Cassiano Formation (Italy). Jour. Sed. Pet., v.55, p.159-170.

BURTON, E.A. and WALTER, L.M., 1987 - Relative precipitation rates of aragonite and Mg calcite from seawater: Temperature or carbonate ion control? Geology, v.15, p.111-114.

BUSENBERG, E. and PLUMMER, L.N., 1985 - Kinetic and thermodynamic factors controlling the distribution of SO_4^{2-} and Na^+ in calcites and selected aragonites. Geochim. Cosmochim. Acta, v.49, p.713-725.

BYRES, S.C., MILLS, E. and SREWART, P., 1978 - A comparison of methods of determining organic carbon in marine sediments with suggestion for a standard method. Hydrobiologica, v.58, p.43-47.

CHAVE, K.E., 1965 - Calcium carbonate: Association with organic matter in surface seawater. Science, v.148, p.1723-1724.

CHAVE, K.E. and SUESS, E., 1967 - Suspended minerals in seawater. Trans. New York Acad. Sci., v.29, p.991-1000.

CHAVE, K.E. and SUESS, E., 1970 - Calcium carbonate in seawater: Effects of dissolved organic matter. Limnol.

Oceanog., v.15, p.633-637.

COTTON, F.A. and WILKINSON, G. , 1962 - Advanced Inorganic Chemistry. John Wiley and Sons, New York. 959p.

CUFF, C., 1972 - The crystallography and geochemistry of authigenic calcium sulphate and carbonate minerals of the Recent sediments of the Trucial Coast. Unpublished Ph.D. Thesis. University of London.

CUNNINGHAM, R. and MITTERER, R.M., 1980 - Metal binding study of fulvic acids from carbonate sediments using manganese as a magnetic resonance probe. In Hare, Hoering and King (eds) Biogeochemistry of Amino Acids. New York, Wiley. p.129-143.

CUSSEY, R. and FRIEDMAN, G.M., 1977 - Patterns of porosity and cement in ooid reservoirs in Dogger (Middle Jurassic) of France. Bull. Am. Assoc. Pet. Geol., v.61, p.511-518.

DAVIES, G.R., 1977 - Former magnesian calcite and aragonite submarine cements in Upper Palaeozoic reefs of the Canadian Arctic: a summary. Geology, v.5, p.11-15.

DAVIES, P.J., BUBELA, B., and FERGUSON, J., 1978 - The formation of ooids. Sedimentology, v.25, p.703-730.

de KANEL, J and MORSE, J.W., 1978 - The chemistry of orthophosphate uptake from seawater onto calcite and aragonite. Geochim. Cosmochim. Acta., v.42, p.1335-1340.

DONATH, F.A., CAROZZI, A.V., FRUTH, L.S., and RICH, D.W., 1980 - Oomoldic porosity experimentally developed in Mississippian oolitic limestone. Jour. Sed. Pet., v.50, p.1249-1260.

DREVER, J.I., 1982 - The Geochemistry of Natural Waters. Prentice-Hall, New Jersey. 388p.

DUNHAM, R.J., 1971 - Meniscus cement. In O.P. BRICKER (ed) Carbonate Cements. John Hopkins Press. Baltimore, Md., p.297-300.

ECHELIN, P., 1978 - Coating techniques for scanning electron microscopy and x-ray microanalysis. In A.M.F. O'Hare (ed) Scanning Electron Microscopy, Vol. I, SEM Inc. Il. 60666 USA, p.109-131.

EVAMY, B.D. and SHEARMAN, D.J., 1965 - The development of overgrowths from echinoderm fragments. Sedimentology, v.5, p.211-233.

EVAMY, B.D. and SHEARMAN, D.J., 1969 - Early stages in development of overgrowths on echinoderm fragments in

limestones. Sedimentology, v.12, p.317-322.

EVANS, C.C. and GINSBURG, R.N., 1987 - Fabric selective diagenesis in the Late Pleistocene Miami Limestone. Jour. Sed. Pet., v.57, p.311-318.

FABRICUS, V.F. and KLINGELE, H., 1970 - Ultrastrukturen von ooiden und oolithen: Zur genese und diagenese quartarer Flachwasserkarbonate des Mittelmeeres. Ver. Geol. Bundesanstalt, p.594-617.

FERGUSON, J., BUSH, P.R. and CLARK, B.A., 1981 - A note on the simulation of the early diagenesis of Recent carbonate ooids. Jour. Pet. Geol., v.4, p.191-193.

FERGUSON, J., BUSH, P.R. and CLARK, B.A., 1984 - The role of organic matter in the early diagenesis of carbonate ooids - an experimental study. Jour. Pet. Geology, v.7. p.245-266.

FERGUSON, J. and IBE, A.C., 1981 - Origin of light hydrocarbons in carbonate oolites. Jour. Pet. Geol., v.4, p.103-107.

FERGUSON, J. and IBE, A.C., 1982 - Some aspects of the occurrence of proto-kerogen in Recent ooids. Jour. Pet. Geol., v.5, p.267-285.

FOLK, R.L., 1965 - Some aspects of recrystallisation in ancient limestones. In L.C. PRAY and R.C. MURRAY (eds) Dolomitisation and Limestone Diagenesis a symposium - Soc. Econ. Palaeon. Mineralog. Spec. Publ. No. 13, p.14-48.

FOLK, R.L., 1973 - Carbonate petrography in the post-Sorbian age. In R.N. Ginsburg (ed) Evolving concepts in Sedimentology. Johns Hopkins Press, Baltimore, Md., p.118-158.

FOLK, R.L., 1974 - The natural history of crystalline calcium carbonate: effect of magnesium content and salinity. Jour. Sed. Pet., v.44, p.40-53.

FRIEDMAN, G.M., 1964 - Early diagenesis and lithification in carbonate sediments. Jour. Sed. Pet., v.34, p.777-813.

FRIEDMAN, G.M., 1968 - The fabric of carbonate cement and matrix and its dependence on the salinity of water. In G. Muller and G.M. Friedman (eds), Recent developments in carbonate sedimentology in central Europe. New York, Springer-Verlag. p. 11-20.

FRIEDMAN, G.M., 1975 - The making and unmaking of limestones or the downs and ups of porosity. Jour. Sed. Pet., v.45, p.379-398.

- FRUTH, L.S., ORME, G.R., and DONATH, F.A., 1966 -
Experimental compaction effects in carbonate sediments.
Jour. Sed. Pet., v.36, p.747-754.
- FYFE, W.S. and BISHOFF, J.L., 1965 - The calcite-aragonite
problem. In L.C. Pray and R.C. Murray (eds) Dolomitisation
and Limestone diagenesis: a Symposium - SEPM Spec. Pub.
No.13, p.3-13.
- GAFFEY, S.J., 1983 - Formation and infilling of pits in
marine ooid surfaces. Jour. Sed. Pet., v.53, p.193-208.
- GAINS, A.M., 1977 - Protodolomite redefined. Jour. Sed. Pet., v.47,
p.543-546.
- GAVISH, E. and FRIEDMAN, G.M., 1969 - Progressive diagenesis
in Quaternary to late Tertiary carbonate sediments: sequence
and time scale. Jour. Sed. Pet., v. 39, p.980-1006.
- GIVEN, R.K. and WILKINSON, B.H., 1985 - Kinetic control of
morphology, composition and mineralogy of abiogenic
sedimentary carbonates. Jour. Sed. Pet., v.55, p.109-119.
- GLOVER, E.D. and SIPPEL, R.F., 1967 - Synthesis of magnesian calcites.
Geochim. Cosmochim. Acta., v.31, p.603-613.
- GOLDSMITH, J.R., 1967 - Metastability and hangovers in crystals.
Geochim. Cosmochim. Acta., v.31, p.913-919.

GOLDSMITH, J.R., GRAF, D.L. and JOENSUV, O.I., 1955 - The occurrence of magnesian calcites in nature. Geochim. Cosmochim. Acta., v.7, p.212-230.

GOLDSMITH, J.R., GRAF, D.L. and HEARD, H.C., 1961 - Lattice constants of the calcium magnesium carbonates. Amer. Mineral., v.46, p.453-457.

GOODMAN, S., 1986 - The relationships between light hydrocarbons, carbonate diagenesis and base metal ore deposits. Unpublished Ph.D. Thesis. University of London. 253 pp.

GRAF, D.L. and GOLDSMITH, J.R., 1956 - Some hydrothermal synthesis of dolomite and proto-dolomite. Jour. Geol., v.64, p.173-186.

GUNATILAKA, A., SALEH, A., AL-TEMEEMI, A. and NASSAR, N., 1984 - Occurrence of subtidal dolomite in a hypersaline lagoon, Kuwait. Nature, v.311, p.450-452.

HALL, M.G. and LLOYD, G.E., 1981 - The SEM examination of geological samples with a semiconductor back-scattered electron detector. Amer. Miner., v.66, p.362-368.

HALLEY, R.B. and HARRIS, P.M., 1979 - Fresh-water cementation of a 1,000 year old oolite. Jour. Sed. Pet., v.49, p.969-988.

HARDIE, L.A., 1987 - Dolomitisation: a critical view of some current views. Jour. Sed. Pet., v. 57, p.166-183.

HARRIS, P.M., 1978 - Holocene marine-cemented sands, Joulters ooid shoal, Bahamas. Gulf Coast Assoc. Geol. Soc. Trans., v.28, p.175-184.

HARRIS, P.M., HALLEY, R.B. and LUKAS, K.J., 1979 - Endolith microborings and their preservation in Holocene-Pleistocene (Bahama - Florida) ooids. Geology, v.7, p.216-220.

HARRISON, R.S., 1975 - Porosity in Pleistocene grapestones from Barbados: some preliminary observations. Canadian Pet. Geol. Bull., v.23, p.383-392.

HOLLAND, H.D., HOLLAND, J.J. and MUNOZ, J.L., 1964 - The co-precipitation of cations with CaCO_3 II: The co-precipitation of Sr^{2+} with calcite between 90-100 °C. Geochim. Cosmochim. Acta, v.28, p.1287-1301.

JAMES, N.P. and GINSBURG, R.N., 1979 - The seaward margin of Belize barrier and atoll reefs. Int. Assoc. Sedimentol. Spec. Publ. No.3, 191p.

KATZ, A., SASS, E., STARINSKY, A. and HOLLAND, H.D., 1971 - Strontium behaviour in the aragontie-calcite transformation: An experimental study at 40-98 °C. Geochim. Cosmochim. Acta., v.36, p.481-496.

KEIR, R.S., 1980 - The dissolution kinetics of biogenic calcium carbonates in seawater. Geochim. Cosmochim. Acta., v.44, p.241-252.

KEITH, B.D. and PITTMAN, E.D., 1983 - Bimodal porosity in oolitic reservoir - Effect on productivity and Log response, Rodessa Limestone (Lower Cretaceous). East Texas Basin. Bull. Am. Assoc. Pet. Geol., v.67, p.1391-1399.

KINSMAN, D.J., 1969 - Interpretation of Sr^{2+} concentration in carbonate minerals and rocks. Jour. Sed. Pet., v.39, p.486-508.

KINSMAN, D.J. and HOLLAND, H.D., 1969 - The co-precipitation of cations with $CaCO_3$ - IV. The co-precipitation of Sr^{2+} with aragonite between 16 and 96 °C. Geochim. Cosmochim. Acta, v.33, p.1-17.

LAHANN, R.W., 1978 - A chemical model for calcite crystal growth and morphological control. Jour. Sed. Pet., v.48, p.337-344.

LAHANN, R.W. and SIEBERT, R.M., 1982 - A kinetic model for distribution coefficients and application to Mg calcites. Geochim. Cosmochim. Acta, v.46, p.2229-2237.

LAND, L.S., 1967 - Diagenesis of skeletal carbonates. Jour. Sed. Pet., v.37, p.914-930.

LAND, L.S., 1970 - Phreatic versus vadose meteoric diagenesis of limestones: evidence from fossil water table. Sedimentology, v.14, p.175-185.

LAND, L.S., 1971 - Submarine lithification of Jamacian reefs. In O.P. Bricker (ed), Carbonate Cements. Johns Hopkins Press, Baltimore, Md., p. 59-62.

LAND, L.S., 1973a - Contemporaneous dolomitisation of middle Pleistocene reefs by meteoric water, north Jamaica. Bull. Marine Sci., v.23, p.64-92.

LAND, L.S., 1973b - Holocene meteoric dolomitisation of Pleistocene limestones, north Jamaica. Sedimentology, v.20, p.411-422.

LAND, L.S., BEHRENS, E.W. and FRISHMAN, S.A., 1979 - The ooids of Baffin Bay, Texas. Jour. Sed. Pet., v.49, p.1269-1278.

LIPPMAN, F., 1960 - Versuche zur Aufklarung der Bildungsbedingungen van Kalzit und Aragonit. Fortschr. Mineral., v.38, p.156-161.

LOGAN, B.W., 1974 - Inventory of diagenesis in Holocene-Recent carbonate sediments, Shark Bay, Western Australia. Am. Assoc. Pet. Geol. Memoir No. 22, p.195-249.

LOGAN, B.W., READ, J.F. and DAVIES, G.R., 1970 - History of carbonate sedimentation, Western Australia. Am. Assoc. Pet. Geol. Memoir No. 13, p.38-84.

LONGMAN, M.W., 1980 - Carbonate diagenetic textures from near surface environments. Bull. Am. Ass. Pet. Geol., v.64, p.461-481.

LOOMIS, T.P., 1983 - Compositional zoning of crystals: A record of growth and reaction history. In S.K. Saxena (ed), Kinetics and equilibrium in mineral reactions: Advances in physical geochemistry. New York, Springer-Verlag, p.1-60.

LOREAU, J.P. AND PURSER, B.H., 1973 - in Purser, B.H. (ed.) The Persian Gulf. Springer-Verlag, p.279-328.

LORENS, R.B., 1981 - Sr, Cd, Mn and Co distribution coefficients in calcite as a function of calcite precipitation rate. Geochim. Cosmochim. Acta, v.45, p.553-561.

MACKENZIE, F.T. and PIGOTT, J.D., 1981 - Tectonic controls of Phanerozoic sedimentary rock cycling. Jour. Geol. Soc. Lond., v.138, p.183-196.

MACKENZIE, F.T., BISHOFF, W.D. BISHOP, F.C., LOIJENS, M., SCHOONMAKER, J. and WOLLAST, R., 1983 - Magnesian calcite: Low-temperature occurrence, solubility and solid-solution behaviour. Reviews in Mineralogy., v.11, p.97-144.

MARTIN, G.D., WILKINSON, B.H. and LOHMANN, K.C., 1986 - The role of skeletal porosity in aragonite neomorphism - Strombus and Monastrea from the Pleistocene Key Largo Limestone, Florida. Jour. Sed. Pet., v.56, p.194-203.

MATTHEWS, R.K., 1967 - Diagenetic fabrics in biosparites from the Pleistocene of Barbados, West Indies. Jour. Sed. Pet., v.37, p.1147-1153.

MATTHEWS, R.K., 1968 - Carbonate diagenesis: equilibrium of sedimentary mineralogy to the subaerial environment; coral cap of Barbados, West Indies. Jour. Sed. Pet., v.38, p.1110-1119.

MATTHEWS, R.K., 1974 - A process approach to diagenesis of reefs and reef associated limestones. In L.F. Laporte (ed), Reefs in Time and Space. SEPM Spec. Pub. No. 18, p.234-256.

MAZZULLO, S.J., 1981 - Facies and burial diagenesis of a carbonate reservoir: Chapman Deep (Aktoka) Field, Delaware Basin, Texas. Bull. Am. Assoc. Pet. Geol., v.65, p.850-865.

MEYERS, J.H., 1987 - Marine vadose beachrock cementation by cryptocrystalline magnesian calcite - Maui, Hawaii. Jour. Sed. Pet., v.57, p.558-570.

MITTERER, R.M., 1968 - Amino acid composition of organic matrix in calcareous oolites. Science, v.162, p.1498-1499.

MITTERER, R.M., 1972 - Biogeochemistry of aragonite mud and oolites. Geochim. Cosmochim. Acta, v.36, p.1407-1422.

MITTERER, R.M. and CUNNINGHAM, R., 1985 - The interaction of natural organic matter with grain surfaces: implication for calcium carbonate precipitation. In N. Schneiderman and P.M. Harris (eds), Carbonate Cements, SEPM Spec. Publ. No. 36, p.17-32.

MORSE, J.W., 1974 - Dissolution kinetics of calcium carbonate in seawater. V. Effects of natural inhibitors and the position of the chemical lysocline. Am. Jour. Sci., v.274, p.638-647.

MORSE, J.W., 1983 - The kinetics of calcium carbonate distribution and precipitation. in R.J. Reeder (ed.) Reviews in Mineralogy. v.11, p.227-264.

MUCCI, A. and MORSE, J.W., 1983 - The incorporation of Mg²⁺ and Sr²⁺ into calcite overgrowths: influences of growth rate and solution composition. Geochim. Cosmochim. Acta, v.47, p.217-233.

MULTER, H.G., 1971 - Cementation and recrystallisation in Miami Limestone Ooids. In O.P. Bricker (ed.) Carbonate Cements, Johns Hopkins Press, Baltimore, Md., p.139-140.

PANTIN, H.M., 1965 - The effect of adsorption on the attainment of physical and chemical equilibrium in sediments. N.Z. J. Geol. Geophys., v.8, p.453-464.

PAUTARD, F.G.E. and WILLIAMS, R.J.P., 1982 - Biological Minerals. Chemistry in Britain, v.18, p.191-193.

PICHA, F., 1978 - Depositional and diagenetic history of Pleistocene and Holocene oolitic sediments and sabkas in Kuwait, Persian Gulf. Sedimentology, v.25, p.427-450.

REEDER, R.J., 1983 - Crystal chemistry of the rhombohedral carbonates. In R.J. Reeder (ed) Reviews in Mineralogy, v.11, p.1-48

REEDER, R.J. and GRAMS, J.C., 1987 - Sector zoning in calcite cement crystals. Implications for trace element distributions in carbonates. Geochim. Cosmochim. Acta, v.51, p.187-194.

- ROBERSTON, E.C., SYKES, L.R. and NEWELL, M., 1962 -
Experimental consolidation of calcium carbonate sediment.
U.S. Geol. Survey Prof. Paper No. 350, p.82-131.
- SANDBERG, P.A., 1975 - New interpretations of Great Salt
Lake ooids and of ancient non-skeletal carbonate mineralogy.
Sedimentology, v.22, p.497-537.
- SANDBERG, P.A., 1983 - An oscillating trend in Phanerozoic
non-skeletal carbonate mineralogy. Nature, v.305, p.19-22.
- SANDBERG, P.A. and HUDSON, J.D., 1983 - Aragonite relic
preservation in Jurassic calcite-replaced bivalves.
Sedimentology, v.30, p.879-892.
- SCHOLLE, P.A., 1978 - Carbonate rock constituents, textures,
cements and porosities. Am. Assoc, Pet. Geol. Memoir 27,
241p.
- SCHNEIDERMAN, N and HARRIS, P.M. (eds), 1985 - Carbonate
Cements. SEPM Spec. Publ. No. 36, 379p.
- SCHOFIELD, K. and ADAMS, A.E., 1986 - Burial dolomitisation
of the Woo Dale Limestone Formation (Lower Carboniferous)
Derbyshire, England. Sedimentology, v.33, p.207-219.

SCHROEDER, J.H., 1972 - Fabrics and sequence of submarine carbonate cements in Holocene Bermuda cup reefs. *Geol. Rundsch.*, v.61 p.708-730.

SHEARMAN, D.J., TWYMAN, J. and KARIMI, M.Z., 1970 - The genesis and diagenesis of oolites. *Proc. Geol. Ass.*, v.81, p.561-575.

SHINN, E.A. and ROBBIN, D.M., 1983 - Compaction, pressure solution and lithification in fine-grained shallow-water limestones. *Jour. Sed. Pet.*, v.53, p.595-618.

SINGH, U., 1987 - Ooids and cements from the late Precambrian of the Flinders Ranges, South Australia. *Jour. Sed. Pet.*, v.57, p.117-127.

SJOBERG, E.L., 1978 - Kinetics and mechanism of calcite dissolution in aqueous solutions at low temperatures. *Acta. Univ. Stockholm, Contrib. Geol.*, v. 32, p.1-92.

STEINEN, R.P., 1974 - Phreatic and vadose diagenetic modification of Pleistocene limestone: petrographic observations from subsurface of Barbados, West Indies. *Bull. Am. Assoc. Pet. Geol.*, v.58, p.1008-1024.

STOSSELL, R.K., KLIMENTIDIS, R.E. and PREZBINDOWSKI, D.R.,

1987 - Dedolomitisation in Na-Ca-Cl brines from 100 to 200 °C at 300 bars. Geochim. Cosmochim. Acta, v.51, p.847-855.

SUESS, E., 1970 - Interaction of organic compounds with calcium carbonate - I. Association phenomena and geochemical implication. Geochim. Cosmochim. Acta, v.34, p.157-168.

SUESS, E., 1973 - Interaction of organic compounds with calcium carbonate - II. Organic-carbonate association in recent sediments. Geochim. Cosmochim. Acta, v.37, p.2435-2448.

SUESS, E. and FUTTERER, D., 1972 - Aragonitic ooids - experimental precipitation from seawater in the presence of humic acids. Sedimentology, v.19, p.129-139.

THOMPSON, M. and WALSH, J.N., 1983 - A handbook of Inductively Coupled Plasma Spectrometry. Blackie, 273p.

THORSTENSON, D.C., MACKENZIE, F.T., and RISTVET, B.L., 1972 - Experimental vadose and phreatic cementation of skeletal carbonate sand. Jour. Sed. Pet., v.42, p.162-167.

THORSTENSON, D.C. and PLUMMER, L.N., 1977 - Equilibrium criteria for two-component solids reacting with fixed composition in an aqueous phase - Example: The Magnesian Calcites Am. Jour. Sci., v.277, p.1203-1223.

TUCKER, M.E., 1984 - Calcitic, aragonitic and mixed calcitic-aragonitic ooids from the mid-Proterozoic Belt Supergroup, Montana. Sedimentology, v.31, p.627-644.

TURNER, J.V., ANDERSON, T.F., SANDBERG, P.A. and GOLDSTEIN, S.J., 1986 - Isotopic, chemical and textural relations during the experimental alteration of biogenic high-magnesian calcite. Geochim. Cosmochim. Acta, v.50, p.495-506.

VAN IPEREN, J. and HELDER, W., 1985 - A method for the determination of organic carbon in calcareous marine sediments. Marine Geology, v.64, p.179-187.

WALKDEN, G.M. and BERRY, J.R., 1984a - Syntaxial overgrowths in muddy crinoidal limestones: cathodoluminescence sheds new light on an old problem. Sedimentology, v.31, p.251-267.

WALKDEN, G.M. and BERRY, J.R., 1984b - Natural calcite in cathodoluminescence: crystal growth during diagenesis. Nature v.308, p.525-527.

WALTER, L.M., 1985 - Relative reactivity of skeletal carbonates during dissolution: implications for diagenesis. In N. Schneiderman and P.M. Harris (eds), Carbonate Cements, SEPM Spec. Publ. No. 36, p.3-16.

WALTER, L.M. and MORSE, J.W., 1984 - Reactive surface area of skeletal carbonates during dissolution: Effect of grain size. Jour. Sed. Pet., v.54, p.1081-1090.

WALTER, L.M. and MORSE, J.W., 1985 - The dissolution kinetics of shallow marine carbonates in seawater. A laboratory study. Geochim. Cosmochim. Acta, v.49, p.1503-1513.

WARD, W.C. and HALLEY, R.B., 1985 - Dolomitisation in a mixing zone of near-seawater composition, Late Pleistocene, Northeastern Yucatan Peninsula. Jour. Sed. Pet., v.55, p.407-420.

WARME, J.E. and SCHNEIDERMAN, N., 1983 - Patch-reef cementation: Holocene of Eniwetok Atoll and Jurassic of Morocco (abst.). Bull. Am. Assoc. Pet. Geol., v.67, p.566.

WILKINSON, B.H., JANECKE, S.U. and BRETT, C.B., 1982 - Low-magnesian calcite marine cement in Middle Ordovician hardgrounds from Kirkfield Ontario. Jour. Sed. Pet., v.52, p.47-57.

WILKINSON, B.H., BUCZYNSKI, C. and OWEN, R.M., 1984 - Chemical control of carbonate phases: Implications from Upper Pennsylvanian calcite-aragonite ooids of Southeastern Kansas. Jour. Sed. Pet., v.54, p.932-947.

APPENDIX I - PORE FLUID DATA

All elemental analyses in ppm.

SEAWATER (ppm)

DATE	Na	K	Mg	Ca	Sr	P	S
28.01.85	9700	360	1230	430	7.6	0.4	840
25.02.85	10200	370	1260	420	7.2	0.08	890
16.10.85	10490	374	1251	440	7.0	0.4	925
16.10.86	10480	375	1254	432	7.0	0.4	878
16.10.86	10560	382	1264	432	7.0	0.4	915
04.11.86	10570	380	1266	434	7.11	0.4	899

Average mMg²⁺/mCa²⁺ 4.86
 Average mSr²⁺/mCa²⁺ 0.008

pH = 7.1

SO₄²⁻-REDUCED SEAWATER (ppm)

DATE	Na	K	Mg	Ca	Sr	P	S
07.11.85	10400	370	1280	420	0.5	0.4	84
12.11.85	10200	360	1290	430	0.2	0.4	87

Average mMg²⁺/mCa²⁺ 4.98
 Average mSr²⁺/mCa²⁺ 0.0004

pH = 6.5

FRESHWATER (ppm)

DATE	Na	K	Mg	Ca	Sr	P	S
28.01.86	7.3	2.1	1.0	2.4	0.03	0.4	1.62
08.03.86	7.2	1.59	1.62	4.4	0.063	0.4	2.7

Average mMg²⁺/mCa²⁺ 0.59
 Average mSr²⁺/mCa²⁺ 0.006

pH = 6.2

ICP CALIBRATOR STANDARD

Na 1000 ppm
 K 200 ppm
 Mg 500 ppm
 Ca 1000 ppm
 Sr 100 ppm
 P 20 ppm
 S 20 ppm

EXPERIMENT 1384

Day of collection	Mg	Ca	Sr
6	1020	490	20
13*	360	630	124
21	720	560	68
28	560	610	76
End	340	1630	118
	340	1620	118

EXPERIMENT 1584

Day of collection	Mg	Ca	Sr
9	1546	534	17
19	1785	601	20
29	1066	826	84
End	312	1852	182
	315	1794	178
	315	1935	177

EXPERIMENT 1685

Day of collection	Mg	Ca	Sr
5	690	410	36
15	168	700	127
18	109	700	125
29	86	760	122
36	118	690	109
End	220	1460	116
	220	1440	115

EXPERIMENT 1785

Day of collection	Mg	Ca	Sr
8	750	530	30
16	280	1110	63
23	220	1130	70
47	220	1180	79
End	330	1830	119
	320	1790	119

EXPERIMENT 2085

Day of collection	Mg	Ca	Sr
8	600	660	46
15	650	820	120
22	99	960	183
29	73	950	210
36	64	1020	210
End	210	1640	173
	210	1680	174
	220	1700	174

EXPERIMENT 2185

Day of collection	Mg	Ca	Sr
6	280	450	21
14	87	650	67
22	47	710	137
28	46	730	157
35	46	910	178
End	199	1650	150
	188	1700	155

*Abnormal values when compared to all other trends - data not used

in Fig. 3.3 (e).

372

EXPERIMENT 28/1

Day of collection	Mg	Ca	Sr
8	580	540	29
15	210	900	57
22	142	960	81
29	105	990	105
36	78	1030	135
43	63	990	165
End	290	1690	150
	290	1700	151

EXPERIMENT 28/3

Day of collection	Mg	Ca	Sr
8	330	700	71
15	88	860	160
22	58	820	166
29	41	810	157
36	38	800	150
43	36	810	147
End	240	1290	107
	240	1290	106

EXPERIMENT 2985

Day of collection	Mg	Ca	Sr
5	900	870	29
12	470	1460	74
19	270	1770	172
26	153	1800	350
34	158	1750	410
End	390	1620	340
	380	1600	340
	380	1610	340
	380	1630	340

EXPERIMENT 28/2

Day of collection	Mg	Ca	Sr
8	500	540	38
15	116	860	138
22	58	850	188
29	44	850	154
36	40	840	152
43	41	830	145
End	210	1490	114
	210	1500	114

EXPERIMENT 28/4

Day of collection	Mg	Ca	Sr
8	230	850	63
15	81	950	159
22	49	890	191
29	57	810	154
36	56	820	155
43	53	850	160
End	240	1570	130
	240	1570	129

EXPERIMENT 30/1

Day of collection	Mg	Ca	Sr
5	760	310	12
8	350	510	24
15	176	640	48
22	122	700	81
29	75	730	121
36	63	760	122
43	64	750	109
End	210	1109	100
	213	1136	103

EXPERIMENT 30/2

Day of collection	Mg	Ca	Sr
5	790	360	21
8	310	590	41
15	94	730	89
22	89	740	110
29	61	750	128
36	55	780	130
43	47	760	121
End	206	1438	113
	200	1494	112

EXPERIMENT 30/4

Day of collection	Mg	Ca	Sr
5	630	410	23
8	260	600	36
15	160	680	66
22	141	700	40
29	125	720	41
36	120	750	44
43	115	750	47
End	320	1382	52
	314	1532	56

EXPERIMENT 3186

Day of collection	Mg	Ca	Sr
7	32	55	3
14	12	54	4
21	4	46	3
28	4	47	3
35	3	51	3
37	3	62	2
42	2	34	1
49	1	6	1
End	60	98	4
	56	100	3
	53	101	3

EXPERIMENT 30/3

Day of collection	Mg	Ca	Sr
5	380	620	29
8	178	720	37
15	150	690	38
22	56	710	141
29	51	750	120
36	41	730	116
43	39	730	112
End	488	1130	67
	412	1387	86

374

EXPERIMENT 32/1

Day of collection	Mg	Ca	Sr
5	770	403	20
10	357	695	38
15	217	833	46
19	186	865	51
26	160	910	65
33	109	963	118
40	82	958	161
End	470	1310	101
	440	1470	110

EXPERIMENT 32/3

Day of collection	Mg	Ca	Sr
5	613	413	28
10	197	597	51
15	121	659	55
19	108	649	60
26	99	703	70
33	86	705	74
40	70	729	80
End	530	1220	52
	500	1400	61

EXPERIMENT 3386

Day of collection	Mg	Ca	Sr
6	1141	376	8
11	562	526	24
15	233	776	90
22	150	973	153
29	157	877	161
36	140	897	153
43	123	1030	165
End	290	1350	115
	290	1370	115
	300	1420	119

EXPERIMENT 32/2

Day of collection	Mg	Ca	Sr
5	730	436	20
10	338	686	37
15	215	831	47
19	182	873	53
26	150	914	70
33	105	944	111
40	76	935	157
End	240	1640	154
	230	1710	156

EXPERIMENT 32/4

Day of collection	Mg	Ca	Sr
5	707	357	16
10	224	539	29
15	133	604	34
19	116	634	36
26	109	649	37
33	97	662	39
40	88	683	44
End	370	1540	55
	350	1580	56

EXPERIMENT 34/1

Day of collection	Mg	Ca	Sr	S
3	1044	179	6	522
7	1113	142	5	523
13	1129	137	5	532
20	1159	136	5	533
27	1167	137	5	531
34	1472	159	6	693
37	1718	183	7	813
End	1289	442	8	855
	1273	640	11	1006

EXPERIMENT 34/2

Day of collection	Mg	Ca	Sr
3	883	288	5
7	583	607	6
13	487	713	6
20	478	729	5
27	443	787	6
34	436	1048	7
37	542	1529	12
End	525	1345	8
	528	1602	10

EXPERIMENT 34/4

Day of collection	Mg	Ca	Sr
3	1021	335	12
7	474	771	37
13	309	943	53
20	203	1092	108
27	135	1171	171
34	137	1225	217
37	137	1256	232
End	467	1710	185
	476	1882	194

EXPERIMENT 3686

Day of collection	Mg	Ca	Sr	S
8	538	526	42	224
13	298	854	93	84
19	335	1292	194	102
27	231	870	152	72
37	Sample lost during analysis			
47	128	960	182	58
End	301	1257	135	492
	308	1281	137	510
	304	1331	136	539

EXPERIMENT 34/3

Day of collection	Mg	Ca	Sr
3	Sample lost during analysis		
7	469	555	27
13	258	825	50
20	218	886	80
27	163	965	129
34	137	1087	171
37	142	1128	180
End	684	1085	88
	669	1236	99

EXPERIMENT 3586

Day of collection	Mg	Ca	Sr
4	737	139	5
Aborted	331	1285	55
	336	1358	60
	357	1462	60

EXPERIMENT 37/1

Day of collection	Mg	Ca	Sr
4	1256	396	16
12	Sample lost during analysis		
22	82	914	165
32	80	902	162
41	72	863	146
47	89	853	139
End	626	1073	83
	566	1466	110

375

376

EXPERIMENT 37/2

Day of collection	Mg	Ca	Sr
4	659	652	20
12	357	1040	55
22	220	1207	77
32	170	1047	73
41	112	1041	99
47	85	1073	140
End	591	1449	111

EXPERIMENT 37/4

Day of collection	Mg	Ca	Sr
4	Sample lost during analysis		
12	276	938	54
22	160	1165	111
32	91	1154	193
41	56	1034	196
47	58	994	174
End	234	1478	153

EXPERIMENT 4086

Day of collection	Mg	Ca	Sr	S
9	778	269	24	363
14	290	701	88	100
19	295	678	103	85
26	232	779	135	64
37	173	833	159	61
50	155	796	169	59
End	202	1489	172	568
	207	1539	176	584
	208	1552	173	605

EXPERIMENT 37/3

Day of collection	Mg	Ca	Sr
4	1307	494	8
12	224	957	57
22	149	1392	204
32	82	1119	199
41	57	958	161
47	59	972	157
End	535	1088	92
	511	1337	103

EXPERIMENT 3886

Day of collection	Mg	Ca	Sr
1	1149	298	14
3	769	417	15
Aborted	458	1494	48
	453	1534	48
	443	1548	47

EXPERIMENT 4186

Day of collection	Mg	Ca	Sr	S
8	924	213	18	428
14	295	629	105	92
18	214	756	164	58
28	184	751	177	62
35	123	979	186	56
End	225	1188	169	464
	226	1201	169	472
	227	1290	171	538

EXPERIMENT 1384

Day of collection	mMg ²⁺ /mCa ²⁺	mSr ²⁺ /mCa ²⁺
6	3.43	0.019
13*	0.94	0.09
21	2.119	0.056
28	1.513	0.057
End	0.34	0.033
	0.35	0.033

EXPERIMENT 1685

Day of collection	mMg ²⁺ /mCa ²⁺	mSr ²⁺ /mCa ²⁺
5	2.774	0.04
15	0.39	0.083
18	0.26	0.082
29	0.19	0.073
36	0.28	0.072
End	0.25	0.036
	0.25	0.037

EXPERIMENT 2085

Day of collection	mMg ²⁺ /mCa ²⁺	mSr ²⁺ /mCa ²⁺
8	1.50	0.032
15	0.34	0.05
22	0.17	0.09
29	0.13	0.125
36	0.10	0.094
End	0.21	0.048
	0.21	0.047
	0.21	0.047

EXPERIMENT 1584

Day of collection	mMg ²⁺ /mCa ²⁺	mSr ²⁺ /mCa ²⁺
9	4.77	0.014
19	4.89	0.015
29	2.13	0.047
End	0.28	0.045
	0.29	0.045
	0.27	0.042

EXPERIMENT 1785

Day of collection	mMg ²⁺ /mCa ²⁺	mSr ²⁺ /mCa ²⁺
8	2.33	0.026
16	0.42	0.026
23	0.32	0.028
47	0.31	0.031
End	0.30	0.030
	0.30	0.030

EXPERIMENT 2185

Day of collection	mMg ²⁺ /mCa ²⁺	mSr ²⁺ /mCa ²⁺
6	1.02	0.022
14	0.22	0.047
22	0.11	0.088
28	0.10	0.098
35	0.08	0.089
End	0.20	0.042
	0.18	0.042

*Abnormal values when compared to all other trends - data not used

in Fig. 3.3 (e).

EXPERIMENT 28/1

Day of collection	mMg ²⁺ /mCa ²⁺	mSr ²⁺ /mCa ²⁺
8	0.56	0.025
15	0.38	0.029
22	0.24	0.038
29	0.18	0.050
36	0.12	0.060
43	0.10	0.080
End	0.28	0.040
	0.28	0.040

EXPERIMENT 28/3

Day of collection	mMg ²⁺ /mCa ²⁺	mSr ²⁺ /mCa ²⁺
8	0.78	0.047
15	0.17	0.09
22	0.12	0.09
29	0.08	0.09
36	0.08	0.09
43	0.07	0.08
End	0.31	0.038
	0.31	0.038

EXPERIMENT 2985 (SO₄²⁻-REDUCED SEAWATER)

Day of collection	mMg ²⁺ /mCa ²⁺	mSr ²⁺ /mCa ²⁺
5	0.59	0.015
12	0.53	0.023
19	0.25	0.044
26	0.14	0.089
34	0.15	0.107
End	0.40	0.096
	0.39	0.097
	0.39	0.097
	0.38	0.095

EXPERIMENT 28/2

Day of collection	mMg ²⁺ /mCa ²⁺	mSr ²⁺ /mCa ²⁺
8	1.53	0.032
15	0.22	0.073
22	0.11	0.101
29	0.08	0.083
36	0.08	0.083
43	0.08	0.080
End	0.23	0.035
	0.23	0.035

EXPERIMENT 28/4

Day of collection	mMg ²⁺ /mCa ²⁺	mSr ²⁺ /mCa ²⁺
8	2.24	0.034
15	0.14	0.077
22	0.09	0.098
29	0.12	0.087
36	0.11	0.086
43	0.10	0.086
End	0.25	0.038
	0.25	0.038

EXPERIMENT 30/1

Day of collection	mMg ²⁺ /mCa ²⁺	mSr ²⁺ /mCa ²⁺
5	4.04	0.018
8	1.13	0.021
15	0.45	0.035
22	0.29	0.053
29	0.17	0.076
36	0.14	0.073
43	0.14	0.066
End	0.31	0.041
	0.31	0.041

EXPERIMENT 30/2

Day of collection	mMg ²⁺ /mCa ²⁺	mSr ²⁺ /mCa ²⁺
5	3.62	0.027
8	0.87	0.032
15	0.21	0.056
22	0.20	0.068
29	0.13	0.078
36	0.12	0.076
43	0.10	0.073
End	0.24	0.036
	0.22	0.034

EXPERIMENT 30/4

Day of collection	mMg ²⁺ /mCa ²⁺	mSr ²⁺ /mCa ²⁺
5	2.53	0.026
8	0.71	0.027
15	0.39	0.044
22	0.33	0.026
29	0.29	0.026
36	0.26	0.027
43	0.25	0.029
End	0.38	0.017
	0.34	0.017

EXPERIMENT 32/1

Day of collection	mMg ²⁺ /mCa ²⁺	mSr ²⁺ /mCa ²⁺
5	3.15	0.022
10	0.85	0.025
15	0.43	0.026
19	0.35	0.027
26	0.29	0.033
33	0.19	0.056
40	0.14	0.077
End	0.59	0.035
	0.49	0.034

EXPERIMENT 30/3

Day of collection	mMg ²⁺ /mCa ²⁺	mSr ²⁺ /mCa ²⁺
5	1.01	0.022
8	0.41	0.024
15	0.36	0.025
22	0.13	0.091
29	0.11	0.073
36	0.09	0.073
43	0.09	0.07
End	0.71	0.027
	0.49	0.028

EXPERIMENT 3186 (FRESHWATER)

Day of collection	mMg ²⁺ /mCa ²⁺	mSr ²⁺ /mCa ²⁺
7	0.96	0.024
14	0.38	0.032
21	0.16	0.026
28	0.13	0.027
35	0.09	0.025
37	0.08	0.016
42	0.11	0.017
49	0.25	0.042
End	1.01	0.016
	0.92	0.016

EXPERIMENT 32/2

Day of collection	mMg ²⁺ /mCa ²⁺	mSr ²⁺ /mCa ²⁺
5	2.76	0.021
10	0.81	0.025
15	0.43	0.026
19	0.34	0.028
26	0.27	0.035
33	0.18	0.054
40	0.13	0.077
End	0.24	0.043
	0.22	0.042

EXPERIMENT 32/3

Day of collection	mMg ²⁺ /mCa ²⁺	mSr ²⁺ /mCa ²⁺
5	2.45	0.031
10	0.54	0.039
15	0.30	0.038
19	0.27	0.042
26	0.23	0.045
33	0.20	0.048
40	0.16	0.050
End	0.72	0.020
	0.59	0.020

EXPERIMENT 32/4

Day of collection	mMg ²⁺ /mCa ²⁺	mSr ²⁺ /mCa ²⁺
5	3.26	0.021
10	0.68	0.025
15	0.36	0.026
19	0.30	0.026
26	0.28	0.026
33	0.24	0.027
40	0.21	0.029
End	0.40	0.016
	0.38	0.016

EXPERIMENT 33/6

Day of collection	mMg ²⁺ /mCa ²⁺	mSr ²⁺ /mCa ²⁺
6	5.01	0.010
11	1.76	0.021
15	0.50	0.053
22	0.26	0.072
29	0.30	0.084
36	0.26	0.078
44	0.20	0.073
End	0.35	0.034
	0.35	0.038
	0.35	0.038

EXPERIMENT 34/1

Day of collection	mMg ²⁺ /mCa ²⁺	mSr ²⁺ /mCa ²⁺
3	9.61	0.014
7	12.93	0.015
13	13.60	0.017
20	13.992	0.017
27	14.06	0.018
34	15.26	0.017
37	15.48	0.015
End	4.81	0.008
	3.28	0.008

EXPERIMENT 34/2

Day of collection	mMg ²⁺ /mCa ²⁺	mSr ²⁺ /mCa ²⁺
3	5.05	0.008
7	1.58	0.004
13	1.13	0.004
20	1.08	0.003
27	0.93	0.003
34	0.69	0.003
37	0.58	0.004
End	0.64	0.003
	0.54	0.003

EXPERIMENT 34/3

Day of collection	mMg ²⁺ /mCa ²⁺	mSr ²⁺ /mCa ²⁺
3	Sample lost during analysis.	
7	1.39	0.023
13	0.51	0.027
20	0.41	0.041
27	0.28	0.061
34	0.21	0.072
37	0.21	0.073
End	1.04	0.037
	0.89	0.036

EXPERIMENT 34/4

Day of collection	mMg ²⁺ /mCa ²⁺	mSr ²⁺ /mCa ²⁺
3	5.07	0.016
7	1.01	0.023
13	0.55	0.028
20	0.31	0.046
27	0.19	0.068
34	0.18	0.082
37	0.18	0.086
End	0.45	0.050
	0.44	0.049

EXPERIMENT 3586

Day of collection	mMg ²⁺ /mCa ²⁺	mSr ²⁺ /mCa ²⁺
4	8.74	0.016
Aborted	0.42	0.019
	0.41	0.018
	0.41	0.017

EXPERIMENT 3686

Day of collection	mMg ²⁺ /mCa ²⁺	mSr ²⁺ /mCa ²⁺
8	1.69	0.037
13	0.58	0.050
19	0.43	0.070
27	0.44	0.080
37	Sample lost during analysis.	
47	0.22	0.087
End	0.40	0.049
	0.40	0.049
	0.38	0.047

EXPERIMENT 37/1

Day of collection	mMg ²⁺ /mCa ²⁺	mSr ²⁺ /mCa ²⁺
4	5.23	0.018
12	Sample lost during analysis	
22	0.15	0.082
32	0.15	0.082
41	0.14	0.077
47	0.17	0.074
End	0.96	0.035
	0.64	0.034

EXPERIMENT 37/2

Day of collection	mMg ²⁺ /mCa ²⁺	mSr ²⁺ /mCa ²⁺
4	1.67	0.014
12	0.57	0.024
22	0.30	0.029
32	0.27	0.032
41	0.18	0.043
47	0.13	0.060
End	0.67	0.035

EXPERIMENT 37/3

Day of collection	mMg ²⁺ /mCa ²⁺	mSr ²⁺ /mCa ²⁺
4	4.36	0.007
12	0.39	0.027
22	0.18	0.067
32	0.12	0.081
41	0.10	0.077
47	0.10	0.074
End	0.81	0.039
	0.63	0.035

EXPERIMENT 37/4

Day of collection	mMg ²⁺ /mCa ²⁺	mSr ²⁺ /mCa ²⁺
4	Sample lost during analysis	
12	0.48	0.026
22	0.23	0.043
32	0.13	0.077
41	0.09	0.087
47	0.09	0.080
End	0.26	0.047

EXPERIMENT 4086

Day of collection	mMg ²⁺ /mCa ²⁺	mSr ²⁺ /mCa ²⁺
9	4.77	0.041
14	0.68	0.058
19	0.72	0.069
26	0.49	0.079
37	0.34	0.087
50	0.32	0.097
End	0.22	0.053
	0.22	0.052
	0.22	0.051

EXPERIMENT 3886

Day of collection	mMg ²⁺ /mCa ²⁺	mSr ²⁺ /mCa ²⁺
1	6.35	0.02
3	3.04	0.016
Aborted	0.51	0.015
	0.49	0.014
	0.47	0.014

EXPERIMENT 4186

Day of collection	mMg ²⁺ /mCa ²⁺	mSr ²⁺ /mCa ²⁺
8	7.15	0.039
14	0.77	0.076
18	0.46	0.099
28	0.40	0.108
35	0.21	0.087
End	0.31	0.065
	0.31	0.064
	0.29	0.061

APPENDIX II - STARTING SEDIMENT DESCRIPTIONS

APPENDIX II - DESCRIPTION OF STARTING SEDIMENTS

Table 2.2 summarises the semi-quantitative point-counted data for all the sediments used sediments.

RECENT OOLITIC SAND, JOULTERS CAY, BAHAMAS

BSO: A shelf sand composed of coated grains (64.5%), peloids (35.3%) and trace amounts of shell fragments. Average grain size 0.426mm. See Plate AP1.A.

Coated grains - coated peloids and ooids are present.

Shell fragments - mainly foraminifera (Peneroplis, Marginopora, Quinquiloculina). Ostracodes are also found in trace amounts but very few molluscs.

RECENT OOLITIC SANDS, ABU DHABI, ARABIAN GULF

ADDO: A dune sand composed of coated grains (69.2%), peloids (30.8%) and trace amounts of shell fragments. Average grain size 0.311mm. See Plate 9.1 A

Coated grains - coated peloids and ooids are present.

Shell fragments - occasional foraminifera (Peneroplis) and very worn molluscan fragments.

ADBO: A mixed beach sand composed of coated grains (79.8%), peloids (16.8%), shell fragments (3.1%) and trace amounts of feldspar grains. Average grain size 0.201mm. See Plate AP1.B.

Coated grains - coated peloids, shell fragments and trace amounts of quartz and feldspar grains are present.

Shell fragments - molluscs form the largest part of the skeletal assemblage. Bivalves are restricted to the Superfamilies Cardiaceae and Myaceae while there is a very diverse assemblage of gastropod shells. Smaller contributions come from ostracods, corals and foraminifera (all in trace amounts).

RECENT OOLITIC SANDS, AL-KHIRAN, KUWAIT, ARABIAN GULF

AKSO: Shelf sand consisting of coated grains (60.9%), peloids (28.8%), shell fragments (8.2%) and trace amounts of quartz and feldspar grains. Average grain size 0.154mm. See Plate AP1.C.

Coated grains - coated peloids, shell fragments, quartz and feldspar grains are present.

Shell fragments - predominantly molluscan. Bivalves are mainly of the Superfamilies Cardiaceae and Myaceacea. Very diverse range of gastropod shell fragments. Other contributions come from foraminifera (Peneroplis), echinoderms and ostracods.

AKDO: Dune sand consisting of coated grains (60%), peloids (36.8%), shell fragments (2.4%) and trace amounts of quartz and feldspar grains. Average grain size 0.336mm. Range 0.11-0.27mm. See Plate AP2.A.

Coated grains - coated peloids, shell fragments and trace amounts of quartz and feldspar grains are are present.

Shell fragments - the same assemblage that is found in AKSO is also found in AKDO.

AKS4: Sediment consisting of shell fragments of the types found in sediment AKSO.

RECENT OOLITIC SANDS, CARBLA POINT, SHARK BAY, WESTERN

AUSTRALIA

SBSO: Shelf sand consisting of coated grains (57.6%), peloids (31.2%), shell fragments (9.2%) and quartz grains (2.7%). Average grain size 0.154mm. See Plate AP2.B.

Coated grains - coated peloids, shell fragments and quartz grains are present.

Shell fragments - derived from bivalves, foraminifera and gastropods. Full descriptions of these can be found in Logan et.al., 1970. They recognised two major faunal assemblages in the area:

- (1) Costacallista-Anomalocardia and
- (2) Fragum-Hemicardium.

SBDO: Dune sand consisting of coated grains (79.1%), peloids (20.7%), shell fragments (6%), quartz grains (2.3%) and trace amounts of dolomite. Average grain size 0.250mm. See Plate AP2.C.

Coated grains - coated peloids, shell fragments, quartz grains and dolomite rhombs are present.

Shell fragments - the same assemblage that is found in SBS3 is also found in SBS5.

Dolomite - Rhombs, derived from older formations in the area, are found in trace amounts.

SBO: This was a sediment sample composed of 50% sediments SBSO and SBDO as insufficient material of either sediment was available. Only used in experiment 34/4.

PLATE AP1 - STARTING SEDIMENTS

(A) Bahaman Subtidal Ooids (BSO). PPL. Scale bar 200
um.

(B) Abu Dhabi Beach Ooids (ADBO). PPL. Scale bar 200
um.

(C) Kuwait Subtidal Ooids (AKSO). PPL. Scale bar 100
um.

PLATE AP1

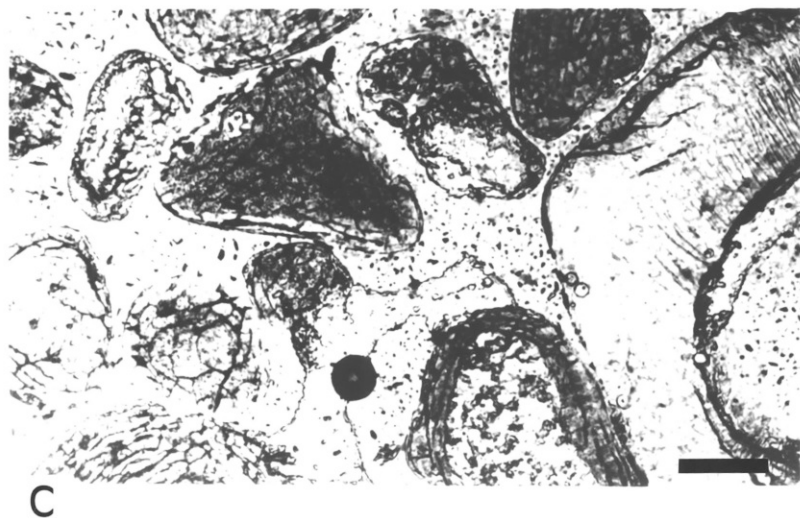
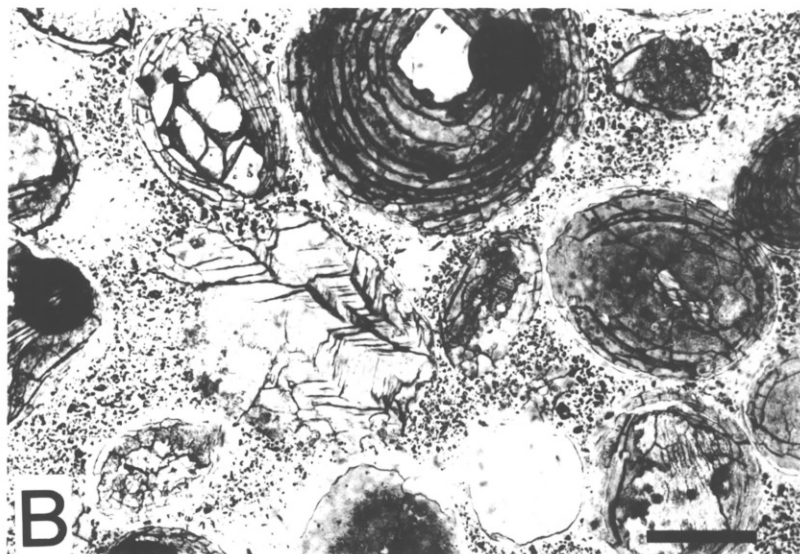
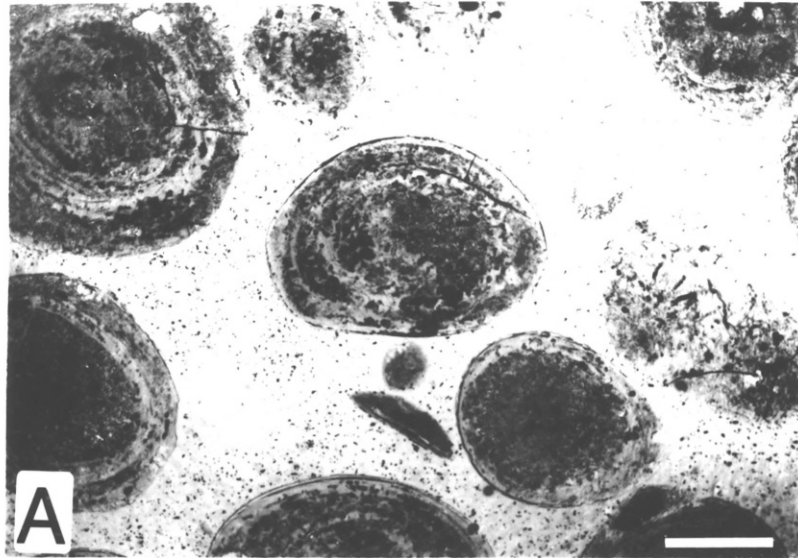


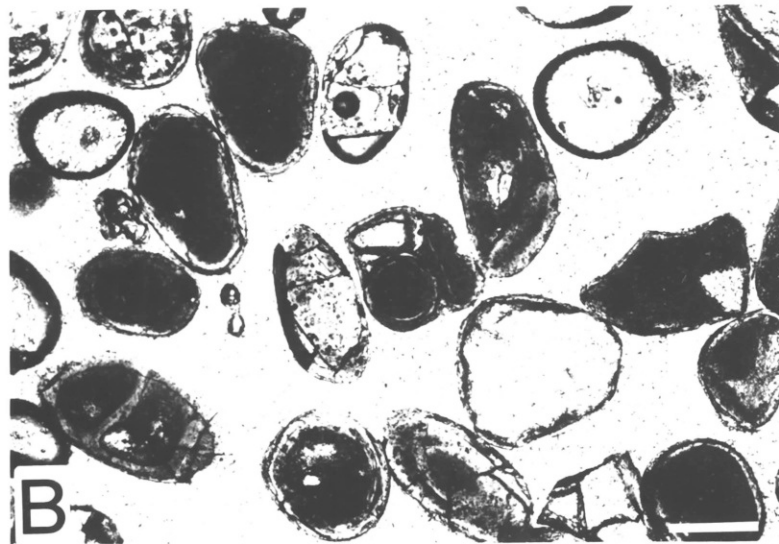
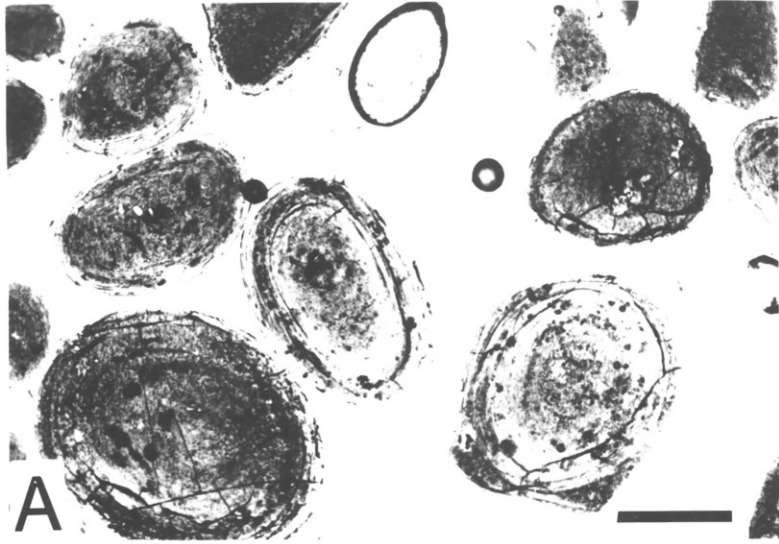
PLATE AP2 - STARTING SEDIMENTS

(A) Kuwait Dune Ooids (AKDO). PPL. Scale bar 200 um.

(B) Shark Bay Subtidal Ooids (SBSO). PPL. Scale bar 100 um.

(C) Shark Bay Dune Ooids (SBDO). PPL. Scale bar 50 um.

PLATE AP2



APPENDIX III - LIST OF EXPERIMENTS AND EXPERIMENTAL CONDITIONS

Expt. No.	Time (days)	Temp. (°C)	Press. (MPa)		Sediment	Liquid	Weight (gms)	Sampled (S) Non-sampled (NS)
			μ	δ				
1384	30	186	9.8	1.4	SBSO	SW	53	S
1584	31	186	6.6	1.2	SBDO	SW	50	S
1685	45	186	6.2	1.0	BSO	SW	57	S
1785	47	186	6.0	0.7	ADBO	SW	45	S
18/1	47	183	6.9	N/D	ADDO	SW	N/D	NS
18/2	61	183	6.9	N/D	ADDO	SW	N/D	NS
18/3	54	183	6.9	N/D	ADDO	SW	N/D	NS
18/4	26	183	6.9	N/D	ADDO	SW	N/D	NS
2085	42	186	7.6	1.4	AKDO	SW	52	S
2185	38	186	11.0	2.3	AKSO	SW	53	S
2485	7	183	7.8	0.6	ADBO	SW	50	NS
2585	15	183	6.9	0.2	ADBO	SW	50	NS
2685	21	183	8.2	0.4	ADBO	SW	49	NS
2785	37	183	5.8	0.4	ADBO	SW	50	NS
28/1	40	183	8.4	0.8	AKDO*	SW	24	S
28/2	40	183	8.4	0.8	AKDO*	SW	46	S
28/3	40	183	8.4	0.8	AKDO*	SW	48	S
28/4	40	183	8.4	0.8	AKDO*	SW	40	S
2985	36	186	6.4	1.2	AKSO	SO ₄ ²⁻ reduced SW	45	S
30/1	43	183	7.8	1.1	BSO	SW	47	S
30/2	43	183	7.8	1.1	77%BSO 23%AKS4	SW	49	S
30/3	43	183	7.8	1.1	67%BSO 33%AKS4	SW	55	S
30/4	43	183	7.8	1.1	AKS4	SW	40	S

* Grain size difference:

28/1 0.42mm

28/2 0.42 - 0.35 mm

28/3 0.35 - 0.25 mm

28/4 0.25mm

Expt. No.	Time (days)	Temp. (°C)	Press. μ	(MPa) σ	Sediment	Liquid	Weight (gms)	Sampled (S) Non-sampled (NS)
3185	53	190	6.3	0.8	AKSO	FW	52	S
32/1	40	183	7.4	1.2	AKSO	SW	32	S
32/2	40	183	7.4	1.2	AKSO (H ₂ O ₂)	SW	37	S
32/3	40	183	7.4	1.2	AKS4	SW	37	S
32/4	40	183	7.4	1.2	AKS4 (H ₂ O ₂)	SW	37	S
3386	44	186	8.9	1.0	SBSO	SW	40	S
34/1	37	183	7.7	0.7		SW		S
34/2	37	183	7.7	0.7	Anala'R'	SW	18	S
34/3	37	183	7.7	0.7	BSO	SW	30	S
34/4	37	183	7.7	0.7	SBO	SW	30	S
3586	4	200	6.9		BSO	SW	50	S
	Aborted							
3686	47	200	8.8	1.1	BSO	SW	50	S
37/1	47	183	7.9	1.3	ADDO	SW	50	S
37/2	47	183	7.9	1.3	ADBO	SW	50	S
37/3	47	183	7.9	1.3	AKSO	SW	50	S
37/4	47	183	7.9	1.3	AKDO	SW	50	S
3886	3	200	6.9		BSO	SW	50	S
	Aborted							
4086	50	200	6.9	0.7	BSO	SW	50	S
4186	34	200	5.0	0.8	BSO	SW	50	S

UNITS OF PRESSURE

$$1 \text{ lb/in}^2 = 6.895 \text{ kN/m}^2$$

$$1 \text{ bar} = 100 \text{ kN/m}^2$$

$$1 \text{ kPa} = 1 \text{ kN/m}^2$$

$$1 \text{ MPa} = 1000 \text{ kPa}$$

APPENDIX IV - MICROPROBE DATA

EXPERIMENT 1384

Oxide Total	MgCO ₃	SrCO ₃	SO ₄ ²⁻
57.21	0.99	1.27	1.75
55.19	1.41	0.62	1.25
58.08	1.03	0.78	1.57
57.46	1.27	0.78	1.81
56.26	1.34	0.88	1.39
57.65	1.42	0.69	1.36
57.40	2.51	0.47	1.73

EXPERIMENT 1584

Oxide Total	MgCO ₃	SrCO ₃	SO ₄ ²⁻
57.12	4.12	0.57	0.66
57.05	1.24	1.00	1.21
57.31	1.38	1.11	0.50
57.91	3.05	0.68	0.99
59.33	1.36	1.06	1.90

EXPERIMENT 1685

Oxide Total	MgCO ₃	SrCO ₃	SO ₄ ²⁻
57.42	1.78	0.49	1.05
59.64	2.13	0.50	0.41
57.61	0.91	0.78	0.93
53.47	2.42	0.41	0.80
54.86	1.41	0.56	1.04

EXPERIMENT 1785

Oxide Total	MgCO ₃	SrCO ₃	SO ₄ ²⁻
57.33	11.78	0.22	1.08
57.21	4.19	0.26	1.52
57.30	3.23	0.43	1.57
56.95	6.96	0.25	1.09
58.53	8.44	0.26	1.15
58.11	2.82	0.42	0.85
57.11	9.74	0.26	0.85
56.64	1.01	0.76	1.10
56.51	1.37	0.70	0.96
57.56	2.36	0.56	1.03
58.09	1.37	0.80	1.82
57.85	5.84	0.32	1.42
49.27	84.05	0.16	0.53

EXPERIMENT 18/1

Oxide Total	MgCO ₃	SrCO ₃	SO ₄ ²⁻
57.58	5.64	0.48	0.82
57.53	4.62	0.43	1.16
57.51	4.25	0.63	0.92
55.83	2.78	0.86	0.87
56.96	2.37	0.61	0.84

EXPERIMENT 18/4

Oxide Total	MgCO ₃	SrCO ₃	SO ₄ ²⁻
54.31	5.44	0.55	1.28
57.04	8.55	0.31	1.34
55.72	6.87	0.54	1.05
57.86	12.08	0.32	1.39
58.48	7.14	0.48	1.42

EXPERIMENT 2085

Oxide Total	MgCO ₃	SrCO ₃	SO ₄ ²⁻
56.81	0.92	0.87	1.08
57.58	1.07	1.06	1.17
57.22	0.80	1.12	1.46
56.70	0.84	1.28	1.44

EXPERIMENT 2585

Oxide Total	MgCO ₃	SrCO ₃	SO ₄ ²⁻
56.91	4.63	0.31	1.61
56.34	3.57	0.64	1.82
56.70	7.83	0.31	1.07
57.44	2.72	0.44	1.98
58.87	5.07	0.22	1.52
58.70	6.87	0.26	1.28

EXPERIMENT 28/1

Oxide Total	MgCO ₃	SrCO ₃	SO ₄ ²⁻
54.82	6.24	0.22	1.01
57.10	4.01	0.24	1.22
57.76	2.85	0.45	0.97
55.56	4.85	0.27	0.81
56.47	5.07	0.29	1.40
55.75	6.10	0.22	1.00
54.90	3.90	0.36	1.25

EXPERIMENT 2185

Oxide Total	MgCO ₃	SrCO ₃	SO ₄ ²⁻
55.42	3.37	0.38	0.62
56.83	0.87	1.04	1.45
57.49	2.54	0.85	1.10
56.42	1.28	1.07	1.01
55.11	1.58	0.89	1.02
56.81	1.62	0.62	1.09

EXPERIMENT 2685

Oxide Total	MgCO ₃	SrCO ₃	SO ₄ ²⁻
58.33	4.68	0.16	1.54
56.90	1.93	0.54	1.97
56.45	4.33	0.11	1.66
54.90	5.11	0.25	1.46
54.64	1.09	0.71	1.76
55.19	4.80	0.16	1.38
56.62	5.36	0.27	1.62

EXPERIMENT 28/2

Oxide Total	MgCO ₃	SrCO ₃	SO ₄ ²⁻
58.22	0.98	0.89	1.70
56.93	1.25	0.85	1.07
57.86	1.10	1.22	1.08
57.13	2.50	0.70	0.91
57.12	2.11	0.52	0.44

EXPERIMENT 28/3

Oxide Total	MgCO ₃	SrCO ₃	SO ₄ ²⁻
57.61	0.49	1.23	1.41
57.68	0.89	0.85	0.93
53.07	1.19	0.90	1.07
58.57	0.64	0.84	1.08
58.67	1.43	0.92	1.53

EXPERIMENT 2985

Oxide Total	MgCO ₃	SrCO ₃	SO ₄ ²⁻
59.30	1.22	0.60	1.53
52.68	1.30	0.79	1.18
52.76	1.17	0.79	0.55
58.23	1.19	1.16	1.29
59.47	3.12	0.46	1.16
58.64	1.06	0.93	1.10

EXPERIMENT 30/1

Oxide Total	MgCO ₃	SrCO ₃	SO ₄ ²⁻
56.36	3.11	0.62	0.81
54.92	5.97	0.39	1.19
56.03	6.39	0.47	1.24
56.57	3.43	0.55	0.99

EXPERIMENT 30/2

EXPERIMENT 28/4

Oxide Total	MgCO ₃	SrCO ₃	SO ₄ ²⁻
57.89	2.40	0.56	1.64
57.95	1.14	0.84	0.70
58.16	2.00	0.90	0.85
58.52	1.23	0.84	1.19
56.20	3.96	0.59	1.20

Oxide Total	MgCO ₃	SrCO ₃	SO ₄ ²⁻
58.22	2.67	0.44	0.73
57.57	2.51	0.41	0.70
56.24	5.54	0.34	1.20
55.09	6.71	0.55	1.03
55.47	4.72	0.48	1.03
57.19	1.22	1.01	1.45
58.74	1.99	0.88	1.20
55.65	2.47	0.65	1.26
54.32	3.87	0.55	1.36
58.47	1.18	1.20	1.17
57.83	1.52	0.89	1.16

EXPERIMENT 30/3

Oxide Total	MgCO ₃	SrCO ₃	SO ₄ ²⁻
56.44	1.11	0.58	1.23
56.41	2.78	0.67	1.14
57.53	2.04	0.95	1.67
54.81	2.64	0.52	1.26
57.66	1.99	0.68	0.97
56.44	1.68	0.59	1.18
56.90	3.00	0.47	0.96

EXPERIMENT 3186

Oxide Total	MgCO ₃	SrCO ₃	SO ₄ ²⁻
58.96	0.66	0.74	(0.10)
57.41	(0.34)	0.52	0.48
55.52	0.57	0.95	0.75
58.87	0.60	1.57	0.44
56.94	(0.24)	1.29	0.35
57.82	(0.37)	1.14	0.31

EXPERIMENT 32/1

Oxide Total	MgCO ₃	SrCO ₃	SO ₄ ²⁻
53.27	4.32	0.34	0.80
57.09	3.99	0.40	0.66
58.10	4.61	0.30	0.84
58.07	4.90	0.32	0.89
58.52	2.94	(0.09)	0.22
57.76	4.78	0.33	1.00
58.30	4.06	0.42	0.91
58.49	4.12	0.37	0.93
53.48	9.21	0.26	1.10

EXPERIMENT 32/2

Oxide Total	MgCO ₃	SrCO ₃	SO ₄ ²⁻
58.81	2.40	0.65	1.26
57.98	4.27	0.47	0.84
57.91	5.18	0.19	1.08
58.01	3.93	0.38	1.01
57.00	4.04	0.38	1.22
53.56	3.66	0.60	0.71
58.48	3.28	0.53	0.88
57.76	4.70	0.18	0.98
56.35	3.64	0.34	1.14

EXPERIMENT 32/3

Oxide Total	MgCO ₃	SrCO ₃	SO ₄ ²⁻
55.42	4.46	0.37	0.98
55.92	6.18	0.24	0.66
58.28	6.26	(0.09)	0.80
56.18	3.87	0.36	1.20
53.06	3.75	0.46	1.20

EXPERIMENT 32/4

Oxide Total	MgCO ₃	SrCO ₃	SO ₄ ²⁻
58.80	10.40	0.17	1.10
55.07	34.38	0.22	1.13

EXPERIMENT 3386

Oxide Total	MgCO ₃	SrCO ₃	SO ₄ ²⁻
55.70	1.82	0.73	1.38
55.54	1.40	1.03	1.25
57.54	1.97	0.71	1.19
58.91	2.70	0.58	1.17
56.67	2.29	0.73	0.97
56.58	2.32	0.61	1.00

EXPERIMENT 34/3

Oxide Total	MgCO ₃	SrCO ₃	SO ₄ ²⁻
57.81	20.98	0.34	1.28
58.45	29.59	0.25	1.19
55.99	28.14	0.29	0.95
55.72	22.84	0.22	0.91
58.04	4.04	0.82	1.10
57.90	30.64	0.31	0.96
58.87	9.43	0.42	0.94
58.19	5.17	0.63	1.08
58.10	26.80	0.31	0.87
58.01	18.46	0.30	1.04

EXPERIMENT 34/4

Oxide Total	MgCO ₃	SrCO ₃	SO ₄ ²⁻
58.44	4.14	0.42	1.23
58.66	1.09	0.97	1.82
57.18	1.38	0.71	1.62
58.35	3.79	0.52	1.28
58.81	3.48	0.62	1.04
58.55	6.81	0.23	1.41
58.69	3.17	0.61	1.55
57.44	5.34	0.37	1.34
55.59	0.21	1.32	0.50

EXPERIMENT 3586

Oxide Total	MgCO ₃	SrCO ₃	SO ₄ ²⁻
49.90	76.53	0.10	0.78
51.88	70.43	0.10	0.80
43.97	29.93	0.33	0.89
52.22	34.76	0.17	1.14

EXPERIMENT 3686

Oxide Total	MgCO ₃	SrCO ₃	SO ₄ ²⁻
57.46	5.04	0.54	0.90
56.38	24.48	0.38	1.18
57.45	14.44	0.51	1.16
59.20	1.52	0.60	1.33
59.26	1.98	0.79	1.26

EXPERIMENT 37/1

Oxide Total	MgCO ₃	SrCO ₃	SO ₄ ²⁻
57.41	3.53	0.61	0.88
58.00	7.15	0.38	1.32
59.28	4.60	0.62	0.52
58.07	3.72	0.50	0.75

EXPERIMENT 37/2

Oxide Total	MgCO ₃	SrCO ₃	SO ₄ ²⁻
57.20	4.58	0.36	1.65
58.19	4.56	0.18	1.27
58.93	4.78	0.31	1.11
56.77	6.46	0.20	1.22
58.48	6.15	0.11	1.22
57.50	4.00	0.26	1.42

EXPERIMENT 37/3

Oxide Total	MgCO ₃	SrCO ₃	SO ₄ ²⁻
56.40	2.17	0.54	1.17
57.95	3.74	0.36	0.86
54.94	2.55	0.65	1.28
54.71	2.03	0.76	1.23
58.53	3.56	0.34	0.92
58.58	2.63	0.51	0.80
57.84	2.16	0.77	1.16
57.72	1.87	0.58	0.97
58.88	3.93	0.30	1.16
58.99	0.96	0.69	1.05
57.09	4.51	0.43	0.96

EXPERIMENT 37/4

Oxide Total	MgCO ₃	SrCO ₃	SO ₄ ²⁻
55.96	7.75	0.16	1.21
56.87	4.99	0.18	1.04
57.17	1.80	0.61	1.08
52.29	1.69	0.34	0.55
52.74	7.92	0.71	0.76
57.06	2.33	0.31	0.36
56.79	2.47	0.53	2.14
56.41	1.25	1.18	1.39
58.44	1.12	0.96	1.40
57.87	1.23	0.91	1.54

EXPERIMENT 3886

Oxide Total	MgCO ₃	SrCO ₃	SO ₄ ²⁻
54.33	48.18	0.36	1.12
53.47	48.42	0.24	0.98
56.40	60.92	0.21	1.05
54.72	52.92	0.31	1.05
49.19	53.86	0.17	0.89
51.36	71.65	0.14	1.11

EXPERIMENT 4086

Oxide Total	MgCO ₃	SrCO ₃	SO ₄ ²⁻
58.76	3.68	0.51	1.33
56.74	3.39	0.41	1.15
58.81	2.76	0.83	1.15
59.00	2.68	0.58	1.28
59.14	4.63	0.40	0.78

EXPERIMENT 4186

Oxide Total	MgCO ₃	SrCO ₃	SO ₄ ²⁻
58.62	1.63	0.84	1.17
57.47	3.36	0.53	1.01
58.80	4.55	0.53	1.55
59.00	1.93	0.50	1.46
59.18	4.66	0.37	1.22

INORGANIC ARAGONITE

Expt. No.	Oxide Total	MgCO ₃	SrCO ₃	SO ₄ ²⁻
1384	55.35	(0.15)	1.19	0.32
	54.04	(0.22)	1.24	0.57
1785	57.60	(0.31)	1.03	0.47
18/1	57.13	(0.38)	1.06	0.43
	56.72	(0.29)	1.18	1.03
	57.11	(0.26)	1.06	0.61
	57.32	(0.06)	0.99	0.43
18/2	56.62	(0.43)	1.16	(0.16)
	56.56	(0.15)	1.09	(0.23)
2485	58.37	(0.03)	1.04	0.36
	55.60	(0.22)	1.21	1.20
	55.96	(0.43)	0.91	0.79
	58.56	(0.42)	0.97	0.45
	57.35	(0.44)	0.99	0.47
28/2	55.48	(0.15)	1.22	0.49
30/1	56.85	(0.01)	1.15	0.29
30/2	57.50	(0.01)	1.20	0.28
30/3	55.38	(0.18)	1.09	0.34
	54.40	(0.16)	1.12	(0.04)
34/3	57.60	(0.26)	1.02	0.35
34/4	56.28	(0.24)	1.24	0.40
3586	55.85	0.60	1.09	0.52
37/4	55.69	(0.08)	1.02	0.42

MICRITIC CARBONATE

Expt. No.	Oxide Total	MgCO ₃	SrCO ₃	SO ₄ ²⁻
1384	56.92	2.30	1.20	0.70
1785	56.03	0.00	1.06	0.70
	56.61	0.00	0.26	(0.05)
	56.47	0.52	0.21	0.26
	57.68	(0.02)	0.34	(0.05)
2485	55.96	0.43	0.91	0.79
	58.56	0.42	0.97	0.45
	57.35	0.44	0.99	0.47
2985	58.81	0.48	0.96	N/D
30/1	56.50	(0.38)	1.19	0.63
3586	56.76	(0.28)	1.14	0.57
37/3	57.31	1.73	0.15	0.24

BIOGENIC ARAGONITE

Expt. No.	Oxide Total	MgCO ₃	SrCO ₃	SO ₄ ²⁻
1384	54.90	0.00	(0.13)	(0.14)
	55.52	(0.22)	0.17	(0.17)
	55.22	0.00	0.22	(0.06)
1785	57.49	(0.17)	0.22	0.35
	56.67	(0.16)	(0.11)	0.91
	54.87	(0.21)	0.25	(0.09)
	56.03	0.00	1.06	0.71
	56.61	0.00	0.26	(0.05)
	56.47	0.52	0.21	(0.26)
	57.68	(0.02)	0.34	(0.05)
	56.47	(0.25)	0.22	(0.19)
2085	57.29	(0.18)	0.18	(0.10)
	56.16	(0.31)	0.21	0.24
2185	56.11	(0.07)	0.25	0.25
	57.69	0.49	1.07	0.78
2485	57.21	0.00	0.38	0.64
	56.59	(0.07)	0.13	(0.20)
	56.54	(0.17)	1.06	0.46
28/1	57.04	(0.25)	0.25	0.20
	56.90	0.00	(0.15)	0.22
	57.85	(0.16)	0.19	(0.11)
2985	58.27	(0.31)	0.17	(0.07)
	58.60	0.00	0.21	(0.13)
	58.71	0.00	0.20	(0.11)
	54.48	(0.21)	0.17	(0.12)

BIOGENIC ARAGONITE (CONT.)

Expt. No.	Oxide Total	MgCO ₃	SrCO ₃	SO ₄ ²⁻
2985	54.83	0.00	0.24	(0.20)
	*60.94	(0.37)	(0.13)	(0.05)
	*60.13	(0.04)	(0.19)	(0.18)
	*59.62	(0.35)	(0.07)	(0.07)
	*59.58	0.00	(0.18)	(0.10)
30/2	54.79	(0.20)	0.17	0.32
	56.82	0.57	(0.12)	0.24
	57.95	0.00	1.24	(0.07)
	57.48	(0.28)	0.94	1.47
	56.77	(0.22)	1.08	0.67
	56.39	(0.43)	0.90	0.75
30/3	56.19	(0.25)	0.19	0.40
	57.39	(0.21)	0.12	0.27
	54.36	(0.15)	0.27	0.00
	56.94	(0.38)	0.25	(0.16)
	56.47	0.54	0.46	0.29
	55.84	(0.20)	0.31	0.00
3186	56.65	(0.20)	0.16	(0.10)
	56.83	(0.10)	(0.10)	(0.08)
	58.11	(0.28)	0.72	0.37
	58.16	(0.22)	(0.10)	0.24
32/2	58.42	0.50	1.22	(0.17)
32/3	57.57	0.00	(0.11)	(0.08)
3386	57.23	(0.34)	0.26	0.30
37/3	54.36	0.00	0.27	0.22
	57.32	(0.10)	0.49	0.22

*Oxide totals are too high for general use. Data has only been used in Section 6.4 where no other data was available.

SOLUTION CAVITY FILL CALCITE

Expt. No.	Oxide Total	MgCO ₃	SrCO ₃	SO ₄ ²⁻
1685	53.49	1.09	1.04	1.03
1785	54.69	0.93	1.14	1.00
18/1	54.42	0.88	1.11	0.84
	56.17	1.08	1.01	0.98
	57.81	1.10	1.17	1.18
	57.98	1.04	1.01	1.16
18/2	56.64	0.99	0.96	1.27
	58.86	0.78	1.26	0.86
	58.13	0.65	1.08	1.20
	56.53	0.99	1.22	1.42
	58.03	0.69	1.17	0.77
	57.24	0.59	1.01	0.49
	56.14	(0.40)	1.31	0.28
18/3	56.65	0.76	1.18	1.19
18/4	53.70	5.25	0.38	1.30
2085	57.11	1.29	1.16	1.18
	56.97	0.69	1.00	0.94
	56.37	0.97	0.97	0.68
	56.05	2.31	0.30	0.26
	57.59	0.90	0.78	1.00
	56.99	0.89	1.08	1.36
	56.42	1.13	1.28	1.12
	55.58	0.98	1.15	1.08
	57.05	1.55	0.93	0.77
	55.19	0.80	1.11	1.18

SOLUTION CAVITY FILL CALCITE (CONT.)

Expt. No.	Oxide Total	MgCO ₃	SrCO ₃	SO ₄ ²⁻
2085	58.00	1.24	0.78	(0.12)
2185	55.35	1.33	1.25	0.45
2785	56.66	1.30	0.81	0.82
	58.15	2.87	0.63	1.34
	56.32	1.81	0.79	1.05
28/2	54.22	4.38	1.13	1.26
28/3	55.95	3.47	0.69	0.45
2985	*59.84	1.02	1.07	0.98
	*59.83	2.63	0.60	0.89
	*60.72	3.19	0.80	0.98
	*60.08	2.49	0.68	0.98
30/1	53.96	1.82	0.94	0.96
	55.15	1.63	0.86	0.89
30/2	55.98	0.95	0.71	1.06
	58.94	2.05	0.58	0.91
	57.46	2.67	0.60	1.06
30/3	55.71	1.01	0.90	1.32
	56.19	1.50	0.82	1.20
3586	53.03	0.75	1.17	0.61
3686	58.85	1.40	0.95	1.23
	58.84	1.58	0.72	1.78
37/1	58.72	2.47	0.78	1.23
	57.42	2.02	0.80	1.35
	57.61	2.01	0.75	1.25
4086	56.96	2.01	0.64	0.97
4186	58.71	2.71	0.65	1.48
	55.39	1.79	1.02	0.77
	58.97	3.02	0.67	0.76
	57.72	0.92	1.01	1.13
	58.22	1.33	1.15	1.45

*Oxide totals are too high for general use. Data has only been used in Section 6.4 where no other data was available.

NEOMORPHIC SPAR

Expt. No.	Oxide Total	MgCO ₃	SrCO ₃	SO ₄ ²⁻
2085	57.66	1.06	1.22	1.10
	56.58	0.87	0.49	0.74
2185	55.81	0.52	0.94	0.24
	56.66	0.60	0.69	0.22
	57.01	0.40	0.42	(0.10)
	55.12	(0.09)	0.28	(0.15)
	56.87	0.44	0.35	(0.03)
	57.64	0.48	0.23	(0.16)
2485	56.67	(0.42)	0.86	(0.20)
	56.90	0.64	0.90	0.42
	57.68	(0.41)	0.76	0.72
	58.23	(0.30)	0.67	0.42
2585	*59.87	(0.18)	0.17	(0.06)
	*59.79	(0.13)	0.34	(0.22)
	58.09	(0.12)	0.22	(0.18)
	*60.28	(0.10)	0.27	0
2785	57.48	0.89	0.62	0.64
2985	57.59	1.79	1.05	1.17
	57.60	1.82	1.03	1.46
	58.97	1.03	1.08	1.08
	54.37	0.56	0.94	N/D
	57.72	1.13	1.23	1.13
	55.91	0.52	1.03	0.95
	54.65	0.44	0.13	(0.10)
	54.66	0.88	1.12	0.95

NEOMORPHIC SPAR (CONT.)

Expt. No.	Oxide Total	MgCO ₃	SrCO ₃	SO ₄ ²⁻
2985	*61.19	1.28	0.95	1.03
	*61.27	2.76	0.61	1.12
	*62.85	2.33	0.97	1.32
	*59.04	1.26	0.99	0.93
	*60.20	1.38	0.94	1.42
30/3	57.48	1.69	0.61	1.18
	58.22	0.46	1.03	0.26
	55.87	0.52	0.99	N/D
	54.40	0.88	1.01	(0.20)
	54.43	(0.32)	0.97	0.41
3186	57.46	2.42	0.60	0.40
32/4	58.84	(0.18)	0.27	(0.16)

*Oxide totals are too high for general use. Data has only been used in Section 6.4 where no other data was available.

METHOD FOR CALCULATING THE MOLE % MgCO_3 , SrCO_3 AND SO_4^{2-}

ELMT.	% ELMT.	ATOMIC %	% OXIDE
K	0.00	0.00	
Na	0.15	0.14	
Mg	0.00	0.00	
Ca	39.12	20.66	
Mn	0.00	0.00	
Fe	0.00	0.00	
Sr	0.92	0.22	
			56.03
S	0.22	0.15	
O	59.59	78.83	

The data above were collected during the analysis, using the microprobe, of a shell fragment. The method by which the mole % MgCO_3 , SrCO_3 and SO_4^{2-} was calculated is shown below.

Summing the cation atomic % (substituting for Ca^{2+}) and multiplying the value of K^+ and Na^+ to account for charge differences, a total of 21.16 is obtained.

The molecular proportion of MgCO_3 is therefore:

$$\frac{0.00 \times 100}{21.16} = 0.00 \text{ mole } \%$$

The molecular proportion of SrCO_3 is therefore:

$$\frac{0.22 \times 100}{21.16} = 1.04 \text{ mole } \%$$

The calculation of mole % SO_4^{2-} is more complex.

S^{6+} is believed to be present in the precipitated calcite lattices as SO_4^{2-} , substituting for CO_3^{2-} (Busenberg and Plummer, 1985).

The formula that was used for the calculation was as follows:

$$\text{mole } \% \text{SO}_4^{2-} = \frac{(\text{S}^{6+}/32) \times 100}{(\text{S}^{6+}/32) + (\text{O}^{2-} - 2\text{S}^{6+}/60)}$$

where all values are in Eimt. %.

This was derived in the following manner:

$$\text{wt. } \% \text{SO}_4^{2-} = \frac{\text{S}^{6+} \times \text{molecular weight } \text{SO}_4^{2-}}{\text{molecular weight } \text{S}^{6+}}$$

$$\text{molecular weight } \text{S}^{6+} = 32.06$$

$$\text{molecular weight } \text{SO}_4^{2-} = 96.06$$

$$\therefore \text{wt. } \% \text{SO}_4^{2-} = 3\text{S}^{6+} \quad \text{--- --- --- --- --- --- --- --- (1)}$$

$$\text{No. of moles } \text{SO}_4^{2-} = \frac{\text{wt. } \% \text{SO}}{\text{molecular weight } \text{SO}_4^{2-}} \quad \text{--- --- --- --- (2)}$$

Substituting equation (1) into (2):

$$\begin{aligned} \text{No. of moles } \text{SO}_4^{2-} &= \frac{3\text{S}^{6+}}{96.06} \\ &= \frac{\text{S}^{6+}}{32} \quad \text{--- --- --- --- --- --- --- --- (3)} \end{aligned}$$

If we then assume that all the oxygen is in CO_3^{2-} or SO_4^{2-} then:

$$\text{wt.}\% \text{CO}_3^{2-} = \text{O}^{2-} - 2/3 \text{ wt.}\% \text{SO}_4^{2-}$$

as molecular weight of the oxygen in SO_4^{2-} is 2/3 the total molecular weight of SO_4^{2-} .

$$\begin{aligned} \text{No. of moles CO}_3^{2-} &= \frac{\text{wt.}\% \text{CO}_3^{2-}}{\text{molecular weight CO}_3^{2-}} \\ &= \frac{\text{O}^{2-} - 2/3 (3\text{S}^{6+})}{60} \\ &= \frac{\text{O}^{2-} - 2\text{S}^{6+}}{60} \quad \text{--- (4)} \end{aligned}$$

$$\therefore \text{Mole \% SO}_4^{2-} \text{ in carbonate} = \frac{\text{No. of moles SO}_4^{2-} \times 100}{\text{No. of moles CO}_3^{2-} + \text{SO}_4^{2-}}$$

Using equations (3) and (4):

$$\text{Mole \% SO}_4^{2-} = \frac{\text{S}^{6+}/32}{\text{S}^{6+}/32 + ((\text{O}^{2-} - 2\text{S}^{6+})/60)} \quad \text{--- (5)}$$

In the worked example:

$$\begin{aligned} \text{mole \% SO}_4^{2-} &= \frac{0.22/32}{0.22/32 + ((59.59 - 0.45)/60)} \\ &= \underline{\underline{0.70}} \end{aligned}$$

APPENDIX V - X-RAY DIFFRACTION DATA

All analyses in wt. %.

Starting Sediment	Aragonite	Calcite	High-Mg Calcite	Quartz	Feldspar
BSO	96	2	2		
ADDO	98	0.5	1.5		
ADBO	80	9	5	5	1
AKSO	86	4	3	7	
AKDO	87	5	2	6	
AKS4	89	4	5	2	
SBSO	75	6	11	10	
SBDO	70	8	12	10	
28/1 *	75	2	2	20	1
28/2 *	85	2	2	10	1
28/3 *	90	2	2	5	1
28/4 *	83	7	2	7	1

* All sediment AKDO - different size fractions.

Expt. No.	Aragonite	Calcite	High-Mg Calcite	Quartz	Feldspar	% Aragonite Conversion *
1384	63	19	7	10		15
1584	62	25	8	3		10
1685	74	26				23
1785	78	15	5	1	1	2
18/1	76	24				25
18/2	70	30				28
18/3	80	20				19
18/4	94		6			4
2085	52	46		1	1	40
2185	65	34		1		25
2385	76	12	6	5	1	6
2485	86	9	3	1	1	0
2585	79	12	6	1	2	2
2685	75	13	5	5	2	5
2785	79	14	3	3	1	1
28/1	70	13	4	13		7
28/2	78	20	1	1		11
28/3	68	30		2		25
28/4	58	39		3		30
2985	51	45		4		41
30/1	86	14				10
30/2	77	20	2	1		15
30/3	77	21		2		17
30/4	83	10	4	3		7
3186	5	86		9		94
32/1	78	17	3	2		10
32/2	87	11	1	1		3

Expt. No.	Aragonite	Calcite	High-Mg Calcite	Quartz	Feldspar	% Aragonite Conversion *
32/3	85	8	4	3		5
32/4	88	6	5	1		0
3386	58	24	9	9		22
34/2		100				100
34/3	77	13	10			20
34/4	68	15	7	10		1
3586	96	2	2			0-1
3686	74	26				24
37/1	78	20	2			19
37/2	87	8	3	1	1	0
37/3	70	29		1		18
37/4	68	30		2		22
3886	98	2				0
4086	84	15	1			12
4186	68	28	2			28

$$* \% \text{ Aragonite Conversion} = \frac{(\text{Wt. \% Initial Aragonite} - \text{Wt. \% resultant Aragonite}) \times 100}{\text{Wt. \% Initial Aragonite}}$$

APPENDIX VI - LIST OF TERMS AND ABBREVIATIONS USED

APPENDIX VI - LIST OF TERMS USED AND ABBREVIATIONS

DEFINITIONS

Definitions have been given as used in this thesis.

Baton Cement: Cement crystals which in two dimensions are bladed but which under three dimensional examination show an approximately equal width-breadth ratio.

Bladed Cement: Cement crystals with a length-width ratio of between 1.5:1 and 6:1 (Scholle, 1978).

Cement: Crystals (of variable composition) which bind sediment grains together or which have been precipitated on the outer surface of sediment grains.

Coated Grains: A general term for grains with coatings or rims of calcium carbonate; includes ooids and superficial ooids (Scholle, 1978).

Equant Cement: Cement crystals with a length-width ratio of less than 1.5:1 (Scholle, 1978). Generally larger than the granular cement crystals precipitated during these experiments and usually show crystal faces.

Granular Cement: Small cement crystals which show no defined crystal faces and have a length-width ratio less than 1.5:1. Generally are smaller than equant cement crystals.

Micro-porosity: Secondary porosity created by the removal of micrite leaving an organic meshwork.

Neomorphic Spar: Calcite which has replaced the original aragonite during the experiments across a micron-sized alteration front.

Oomoldic Porosity: Secondary pore spaces formed by the dissolution of cortical aragonite in coated grains.

Overgrowth: Calcite which is in optical continuity with calcitic fragments.

Peloid: A grain formed of cryptocrystalline or microcrystalline carbonate, irrespective of size or origin (Scholle, 1978).

Secondary Porosity: Any porosity created in the sediments during the experiments.

Solution Cavity Fill Calcite: Calcite which infills

secondary porosity created during the experiments.

Vuggy Porosity: Secondary porosity, usually formed in micritic grains during these experiments, where the organic meshwork has been removed along with micrite, forming an irregular pore space.

ABBREVIATIONS

S.D.: Standard deviation

BSO: Bahaman Subtidal Ooids

ADDO: Abu Dhabi Dune Ooids

ADBO: Abu Dhabi Beach Ooids

AKSO: Kuwait Subtidal Ooids

AKDO: Kuwait Dune Ooids

AKS4: Kuwait Shell fragments

SBSO: Shark Bay Subtidal Ooids

SBDO: Shark Bay Dune Ooids

SBO: Shark Bay Ooids